MASS TRANSFER EFFECTS IN SUBCOOLED NUCLEATE BOILING

A THESIS

Presented to

The Faculty of the Graduate Division

by

Theodore Tydings Robin, Jr.

In Partial Fulfillment

of the Requirements for the Degree

Doctor of Philosophy

in the School of Nuclear Engineering

Georgia Institute of Technology

November, 1966

In presenting the dissertation as a partial fulfillment of the requirements for an advanced degree from the Georgia Institute of Technology, I agree that the Library of the Institute shall make it available for inspection and circulation in accordance with its regulations governing materials of this type. I agree that permission to copy from, or to publish from, this dissertation may be granted by the professor under whose direction it was written, or, in his absence, by the Dean of the Graduate Division when such copying or publication is solely for scholarly purposes and does not involve potential financial gain. It is understood that any copying from, or publication of, this dissertation which involves potential financial gain will not be allowed without written permission.

3/17/65
b

MASS TRANSFER EFFECTS IN SUBCOOLED NUCLEATE BOILING

Approved: _____

_____

_____

Date approved by Chairman: Nov 18, 1966

ACKNOWLEDGMENTS

The author is deeply grateful to Dr. Nathan W. Snyder, his advisor for this study. His helpful suggestions and encouragement are sincerely appreciated. The comments and advice of Dr. Thomas W. Jackson and Dr. Henderson C. Ward, who served as members of the thesis committee, are gratefully acknowledged. The author is also indebted to Dr. William B. Harrison and to Dr. Carlyle J. Roberts of the School of Nuclear Engineering for their support during the course of this work.

The author also thanks Mr. C. L. King, Sr., Mr. J. W. Biddy, and Mr. F. W. Shue for their assistance in the construction of the experimental equipment. Mr. F. C. Apple contributed valuable comments concerning the mechanical equipment design. The cooperation of Mr. R. E. Meek concerning electronics was also appreciated. Thanks are also due to Miss Martha Shoemaker and Mr. Pete Matrangos of the Georgia Tech Photo Lab, whose excellent work on the figures added considerable quality to this thesis presentation. Also, Mr. L. C. Prowse of the Georgia Tech Photo Lab deserves considerable credit in obtaining the high speed motion pictures and the photographs which were required in this work. Sincere appreciation is extended to Mrs. Lydia Fisher for the excellent typing of this manuscript.

The author appreciated the National Science Foundation Graduate Traineeship he received. This project was also supported by NASA Grant No. NsG-657.

Finally, the sacrifice by his wife and children is deeply appreciated.

TABLE OF CONTENTS

TABLE OF CONTENTS (Concluded)

LIST OF TABLES

LIST OF ILLUSTRATIONS

LIST OF ILLUSTRATIONS (Continued)

LIST OF ILLUSTRATIONS (Continued)

LIST OF ILLUSTRATIONS (Continued)

LIST OF ILLUSTRATIONS (Continued)

LIST OF ILLUSTRATIONS (Concluded)

SUMMARY

In 1952 Snyder (33) proposed a mass transfer mechanism which appeared to be the most important method of removing heat from a heated surface in boiling heat transfer. This mechanism was thought to be the major reason for the large increase in the heat transfer coefficient observed in a boiling situation over a non-boiling one. The essential features of this mechanism are: (A) the evaporation of liquid from a thin liquid film located between the vapor in the bubble and the heated plate and (B) the simultaneous condensation of vapor on the liquid surface surrounding the bubble cap. This simultaneous evaporation and condensation resulted in a transfer of latent heat from the heated plate to the cooler liquid. The broad objective of this research effort was to investigate the effects of mass transfer in highly subcooled nucleate boiling in a forced convection system.

Three major investigations were made:

1. An experimental determination of the amount of latent heat deposited by condensation on the surface of a single bubble which grew on the surface of a heated plate, through a thermal and laminar boundary layer, and into a turbulent subcooled stream of water flowing parallel to the heated surface.

2. An experimental observation of the thermal effects in the turbulent liquid surrounding a bubble by means of a schlieren optical system.

3. The derivation of two theoretical models, one of which describes

in detail the dynamics of the single bubble observed in the experimental work and the second describes in detail the bubble dynamics for a bubble in real boiling in forced convection.

Single Bubble Experiment

The primary purpose of this experimental work was to demonstrate the ability of a turbulent subcooled stream to remove large quantities of latent heat deposited by condensation on the surface of a single bubble. This result would indicate the possibility of a significant role for a mass transfer mechanism in subcooled nucleate boiling. A similar result was reported by Bankoff (7). However, in his experiment the turbulent subcooled stream impinged down onto the bubble instead of from the side as in real boiling in forced convection. Also, his bubble did not grow through a thermal boundary layer as it would have in real boiling. Bankoff's experiment was repeated here except that the vapor bubble grew on the surface of a heated plate, through a thermal boundary layer and into a turbulent subcooled stream of liquid flowing parallel to the heated surface. The bubbles were formed at a single site by passing steam through a 0.0135 inch hole in a heated plate. The measurement of the heat removal rate from the bubble was accomplished by determining the vapor flow rate into the bubble and by obtaining high speed photographs of its growth and collapse. The water velocity was varied from 0.2 to 38 ft/sec (Reynolds numbers from 900 to 2×10^5) and the inlet water temperature was varied from 80 °F to 140 °F. The results of this experiment showed that a large amount of heat was removed from the bubble surface, permitting a large amount of condensation. The ratio of the actual amount of heat

removed from the bubble to the amount of latent heat necessary to form a volume of steam equal to the maximum observed volume of the bubble varied from approximately 10 to 100. The bubble heat transfer coefficient varied from approximately 4×10^4 to 4×10^5 BTU/hr ft^2 °F.

Schlieren Experiment

In this experiment, schlieren photographs were obtained of bubbles in forced convection boiling. This was an effort to observe thermal effects in the liquid surrounding individual bubbles. The observation of these thermal effects should produce an understanding of the mechanism of heat removal from the bubble surface. Schlieren photographs were obtained at several values of the heat flux while the velocity and inlet temperature of the cooling stream were held constant. Turbulence could be observed in these photographs which extended up to the bubble surface. The resolution of the schlieren system was not sufficient to permit detailed measurements.

Theoretical Developments

Two theoretical models were derived: one describes in detail the single bubble dynamics observed in the experimental work and the second describes in detail the bubble dynamics for a bubble in real boiling. In the first model, by adjusting the value for the effective thermal diffusivity (which is the sum of the molecular thermal diffusivity and the turbulent diffusivity) the resulting value of the maximum bubble radius as predicted by the model could be made to agree with the value observed in the experiment. In this manner, the model served as a tool by which

the effective thermal diffusivity with respect to a single bubble was determined. As the cooling stream velocity was varied from 1.9 to 25.5 ft/sec, the effective thermal diffusivity varied from 0.06 to 3.00 ft^2/hr. However, while varying the temperature from 80 °F to 140 °F and keeping the velocity constant, the effective thermal diffusivity was reasonably constant.

The same procedure was used with the second model. Here Gunther's data (15) were used for comparison. Several observations were made. First, for those model cases in which the thin liquid film was allowed to completely dry up, the resulting radius versus time curve was not similar to those observed by Gunther. This indicated that complete thin liquid film dry up does not occur for the experimental boiling case in question. However, in some cases for which an unlimited supply of liquid was available for evaporation from the thin liquid film, the bubble did not completely collapse. Because complete bubble collapse is observed in this regime of boiling, it was concluded that some thin liquid film dry up does occur. Secondly, the predicted maximum bubble radius was a strong function of the local effective thermal diffusivity and of the local cooling fluid temperature. Small changes in either of these two quantities resulted in a large change in the value of the predicted maximum bubble radius. Thus, in a turbulent stream in which the local values of the effective thermal diffusivity and the local temperature are statistical variables, some variation in the observed maximum bubble radius is expected even under the same bulk fluid conditions (velocity, temperature, and pressure). This effect was experimentally observed by Gunther (15). The value of the effective thermal diffusivity which produced

a theoretical curve of the bubble radius as a function of time which reasonably agreed with the experimental curves obtained by Gunther (15) was approximately 0.1 ft^2/hr. This value is about one-tenth the value of the eddy diffusivity of fully developed pipe flow turbulence at a distance of approximately one bubble radius from the heated wall. It appears that the full effect of pipe flow turbulence is not available for removing heat deposited on a bubble surface. A final observation concerned the ratio of the amount of heat removed from the heated plate, as calculated by the model, to that required to form one volume of steam equal to the maximum bubble volume. This ratio was approximately 30, which substantiated the importance of Snyder's mass transfer mechanism.

The clumsy nomenclature used in the text corresponds to that used in the computer codes. Thus, minimum effort is required in relating the computer code to the text while a slight inconvenience may be experienced in reading the text.

CHAPTER I

INTRODUCTION

Background

The importance of boiling heat transfer arises from its ability to remove large quantities of heat from small surface areas. Thus, the use of this mode of heat transfer has become of value in cooling rocket nozzles and in removing heat produced in nuclear reactors. The general subject of boiling heat transfer has been reviewed by several authors: Tong (37) and Rohsenow (30). In the boiling heat transfer process, there is danger of surface damage. This is best illustrated by the familiar plot of the heat flux as a function of the difference between the wall temperature and the bulk fluid temperature, shown in Figure 1. When the wall temperature is equal to the fluid bulk temperature, the heat flux is zero. In the region from point A to point B, heat is transferred from the plate by forced convection. At point B, the fluid next to the heated surface has become slightly superheated and some boiling has started. As the heat flux is increased beyond point B, the level of boiling increases. The region between points B and C is known as the nucleate boiling regime. However, as the heat flux is increased beyond point C, the surface temperature experiences a sudden increase to point E in the film boiling regime. If the temperature at point E is greater than the melting point of the wall material, then "burnout" will occur. In most applications, this event is extremely undesirable. However, since the most economical situation is

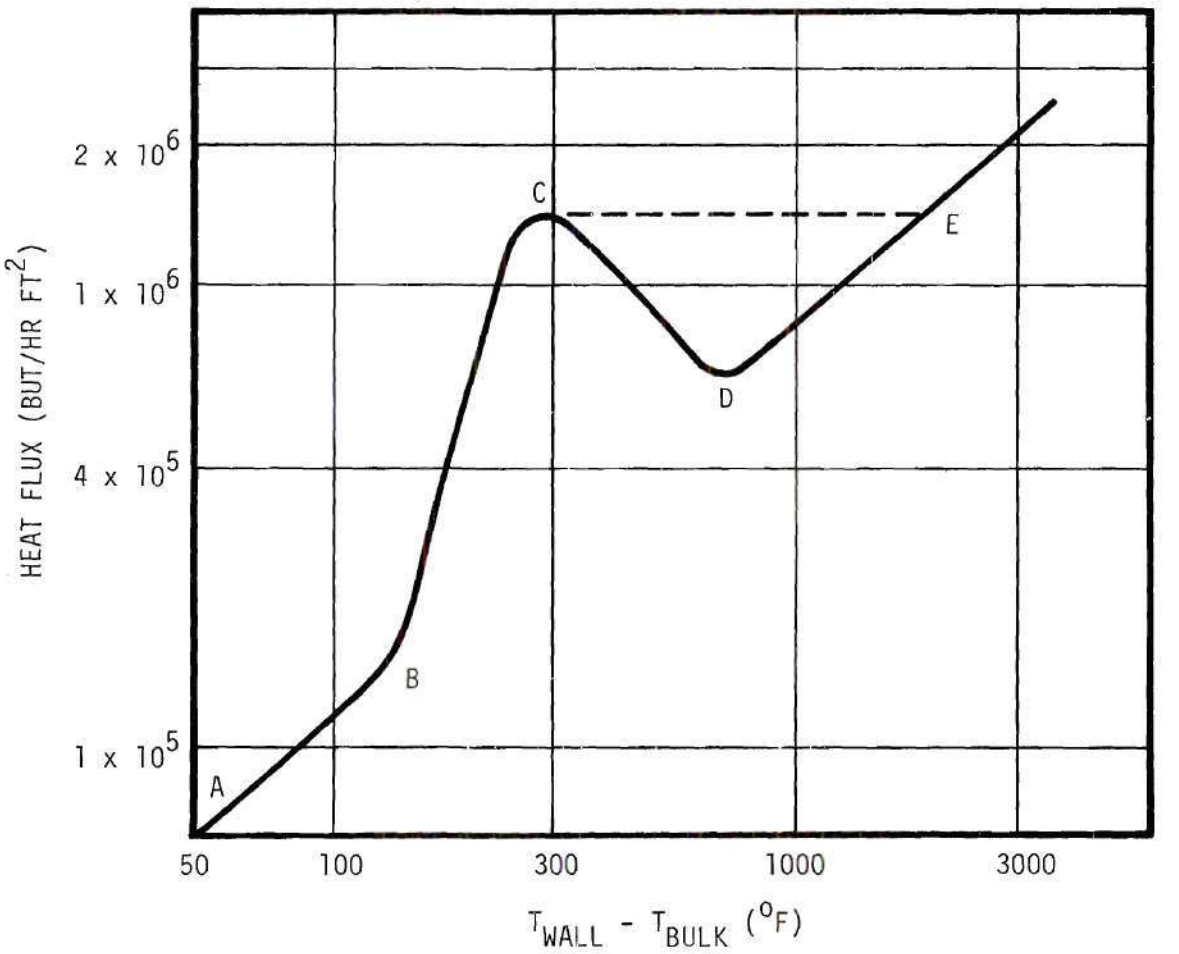

Figure 1. Characteristics of Boiling.

usually in the nucleate boiling regime near point C, designers would like to approach the so called burnout point as closely as the situation will allow. The uncertainty in the location of point C for any given situation is, however, quite large. This in turn requires that the operating point be located a safe distance below the predicted burnout heat flux.

The region between points C and D is known as the partial film boiling regime and beyond point D is the film boiling regime. If the bulk fluid temperature is below the saturation temperature corresponding to the system pressure, the boiling is termed subcooled; however, if the bulk temperature is equal to the saturation temperature, it is termed saturated. If the fluid is being forced over the heated surface, the boiling process is termed forced convection; whereas, in pool boiling, the only fluid motion is that due to the bubbles and natural convection.

In the forced convection region, A to B, the heat flux is directly proportional to the temperature difference. In this region, the heat transfer mechanism is characterized by conduction through a thermal boundary layer. However, in the nucleate boiling regime, B to C, the heat flux depends on approximately the fourth power of the temperature difference. Obviously the heat transfer mechanism in this regime is extremely powerful. Several theories explaining this powerful mechanism have been investigated. The work presented here investigates the mass transfer mechanism which is described and analyzed in the next section. It is believed that studies investigating the mechanism of nucleate boiling will lead to a better understanding of this physical phenomenon and perhaps reduce the large uncertainties now present in burnout predictions. Also, once the boiling process is fully understood, ways to improve the heat transfer performance

may become apparent.

In this thesis, only highly subcooled nucleate boiling in forced convection will be considered. In this case, the bubbles grow and collapse on the heated surface. It is noted for clarity that no net production of vapor occurs for this case because the vapor produced condenses in the subcooled liquid.

The Mass Transfer Mechanism

The mass transfer mechanism as proposed by Snyder around 1952 (33) and presented in 1956 (34) for the case of highly subcooled nucleate boiling in forced convection is as follows. The bubble cycle begins with nucleation on the heated surface at an active bubble site (see Figure 2). The wall temperature is greater than the saturation temperature based on the liquid pressure near the bubble site. Also, there is a thin superheated layer of liquid that extends from the heated wall into the laminar sub-layer and buffer layer. This superheated liquid is required for initial bubble growth. As the bubble grows through the buffer layer, mass evaporates from the liquid surfaces into the bubble vapor. As growth continues, a thin liquid film is left on the surface of the heated plate beneath the bubble vapor. This thin liquid film forms because viscous forces in the liquid very close to the wall prevent movement of this liquid. The temperature in this film is almost as high as the wall temperature and thus is the highest liquid surface temperature surrounding the bubble. Therefore, a large percentage of the mass evaporating into the bubble vapor comes from this thin liquid film.

As the bubble grows through the buffer layer, the bubble cap extends

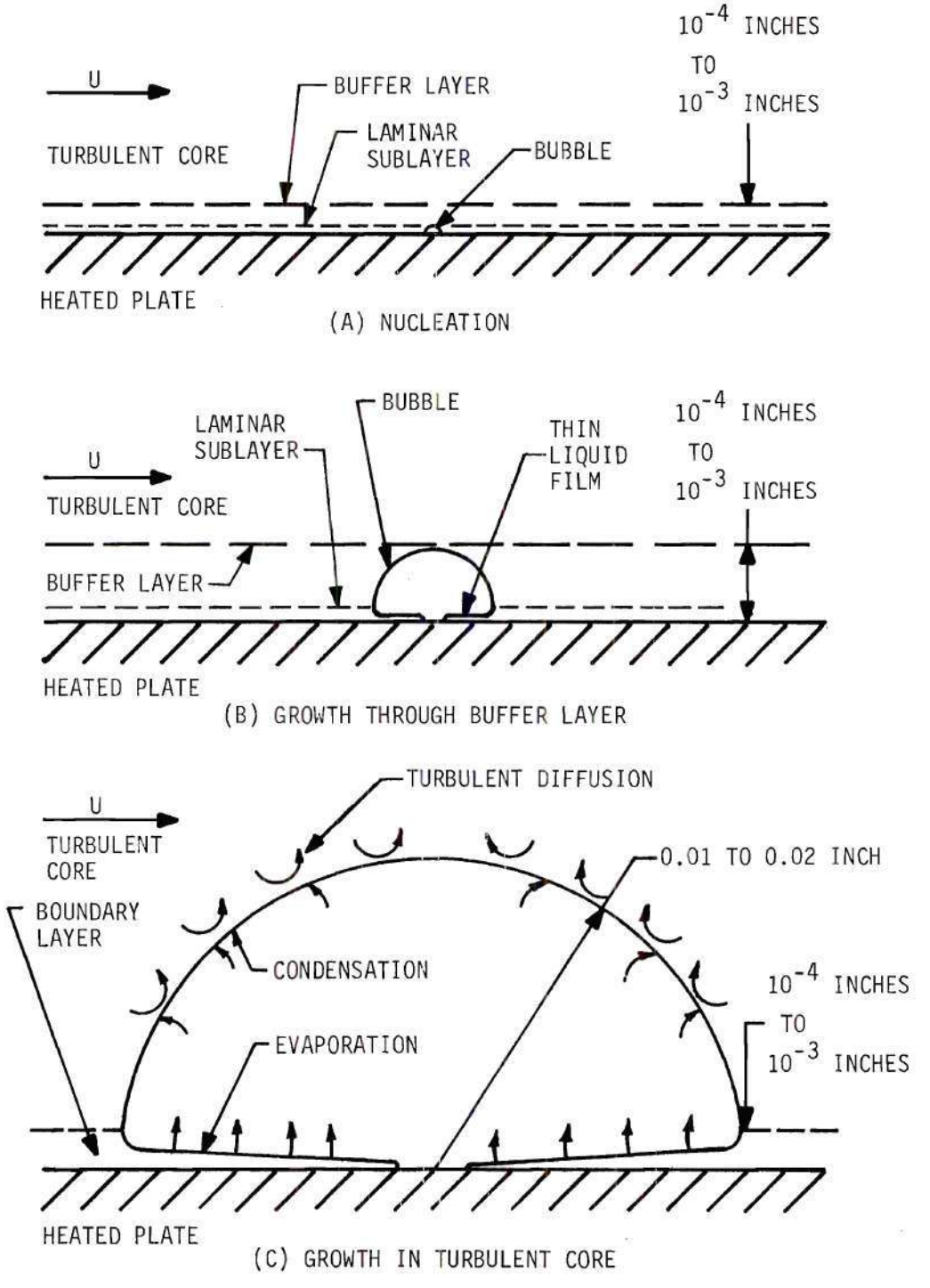

Figure 2. The Mass Transfer Mechanism.

into the turbulent core. Since the buffer layer is of the order of 10^{-4} to 10^{-3} inches thick, the time required to grow through it is small compared to the total lifetime of the bubble. Also, since the bubble grows to a radius of approximately 0.02 inch, nearly all of the bubble surface is surrounded with the turbulent core for a period of time just short of the bubble lifetime. During this stage, the velocity distribution in the liquid near the bubble interface is different from that near a liquid-solid interface. In the latter case, the familiar boundary layer forms, since the relative velocity of the fluid with respect to the wall is zero, at the interface. However, for a liquid-vapor interface, the vapor molecules have a negligible shear effect on the liquid molecules, and thus, no laminar boundary layer forms. This implies that at the vapor-liquid interface which extends into the turbulent core, there can be high turbulence.

The turbulent effect of the subcooled liquid will begin to remove heat rapidly from the interface where condensation of the vapor will provide a latent heat source. The amount of condensation will depend on the effectiveness of the turbulent diffusion of heat from the bubble surface. This turbulent diffusion is an important part of the overall mechanism!

As condensation takes place at the bubble cap, a simultaneous evaporation will be occurring from the thin liquid film at the base of the bubble. With evaporation occurring from this film, the latent heat required is supplied, primarily, by the plate material which, subsequently, experiences a drop in temperature. This transfer of mass from the thin liquid film to the turbulent core by simultaneous evaporation and condensation is the mass transfer mechanism for the case under consideration.

As part of the phenomena associated with this model, Snyder predicted (33, 34) that because of the high latent heat flux from the thin film of liquid at the base of the bubble, a very rapid temperature decrease would occur in the hot solid wall supporting the bubble. This effect was experimentally demonstrated recently (26, 29, 16, 9, 24).

In order to obtain an insight as to the magnitude of the mass transfer effect, consider Gunther's experiment (15). For a burnout condition with a heat flux of 3.75 BTU/in^2 sec, Gunther observed 8×10^5 bubbles/in^2 sec on the heated plate, and the average bubble radius was 0.013 inch. Now, assuming that all the heat transferred from the wall at this condition was through the mass transfer mechanism, the amount of heat which must have been removed by one bubble was

$$\frac{3.75 \text{ BTU/in}^2 \text{ sec}}{8 \times 10^5 \text{ bubbles/in}^2 \text{ sec}} = 0.469 \times 10^{-5} \frac{\text{BTU}}{\text{bubble}}$$

Also, the volume of a bubble was approximately 7.98×10^{-9} ft^3. Assuming the density of the steam to be 0.0373 lb/ft^3 (corresponding to saturated vapor at the system pressure), the mass required to form one bubble volume was $0.373 \times 7.98 \times 10^{-9} = 2.88 \times 10^{-10}$ pounds. Assuming a latent heat of 970 BTU/lb, the latent heat required to produce this mass of vapor would be 2.79×10^{-7} BTU. Thus, the ratio of the heat removed by the mass transfer mechanism to the heat required to form one bubble volume of steam would be approximately

$$\frac{0.469 \times 10^{-5}}{2.79 \times 10^{-7}} = 16.8$$

This number will be shown to be a reasonable value.

Historical Review of the Mechanism of Nucleate Boiling

During the last thirty years, the mechanism of nucleate boiling has been the subject of many investigations. It is of interest to consider a brief historical review of some of these proposed boiling mechanisms. This sketch will not be limited to the case which was the subject of this research since some physical phenomena are similar for the various boiling cases (pool, forced convection, saturated or subcooled).

In 1949, McAdams (23) made a study of subcooled nucleate boiling in forced convection. From some photographs taken in this study, he observed that for the conditions investigated the vapor bubbles broke away from the heated surface and condensed in the cooling stream. In analyzing the results, he did not consider simultaneous evaporation and condensation associated with a single bubble. He considered the boiling of degassed water to be a two-step process involving nucleate boiling at the heated surface and condensation of the vapor in the subcooled liquid after the bubbles broke away from the surface. This may be called the latent heat transport mechanism.

Another nucleate boiling mechanism which was under consideration was the bubble agitation or stirring mechanism. Jakob (20,21) analyzed pool boiling data under the assumption that the vapor bubbles were surrounded with a very thin boundary layer of liquid across which the temperature decreased from a high value existing in the superheated liquid to the saturation value. He concluded that only a small part of the heat produced in a heater is directly transferred to the interior of bubbles

adhering on the surface, and that the main part of the energy makes a detour through the liquid. He also stated that at high rates of heat flow the vapor bubbles, rising in more or less permanent columns, exert a stirring effect upon the liquid which increases the heat transfer enormously.

In 1949 Poppendiek (28) offered the following:

> The increased rate of heat transfer which arises in the case of local boiling is visualized to be due to a lowering of the thermal resistances in the laminar and buffer layers. These resistances are usually the controlling resistances in the thermal circuit. Two possible ways in which these thermal resistances may be lowered in the laminar and buffer layers are (1) the formation of vapor bubbles which provide low resistance heat flow paths and (2) the creation of additional fluid turbulence by the vapor bubbles resulting in a reduction of the thickness of the laminar and buffer layers and higher values of eddy diffusivity in the buffer layer.

The simplified model that he considered is shown in Figure 3. However, Poppendiek did not state the physical processes which would make the vapor bubbles a low resistance heat flow path nor did he suggest the relative effectiveness of the two paths that he visualized.

Around 1952, Snyder (33) visualized an additional boiling mechanism. He proposed a mechanism in which mass would evaporate from a thin liquid film on the heated surface below the bubble vapor and, simultaneously, condensation would occur on the cap of the bubble. On the basis of approximate calculations, he found that this mass transfer through the bubbles could account for a large percentage of the high heat flux which was observed in subcooled nucleate boiling in forced convection.

Thus, in the early fifties, three of the proposed mechanisms for nucleate boiling which were being investigated were latent heat transport, bubble agitation or stirring, and mass transfer. Gunther (15) investigated the highly subcooled nucleate boiling region in forced convection. In dis-

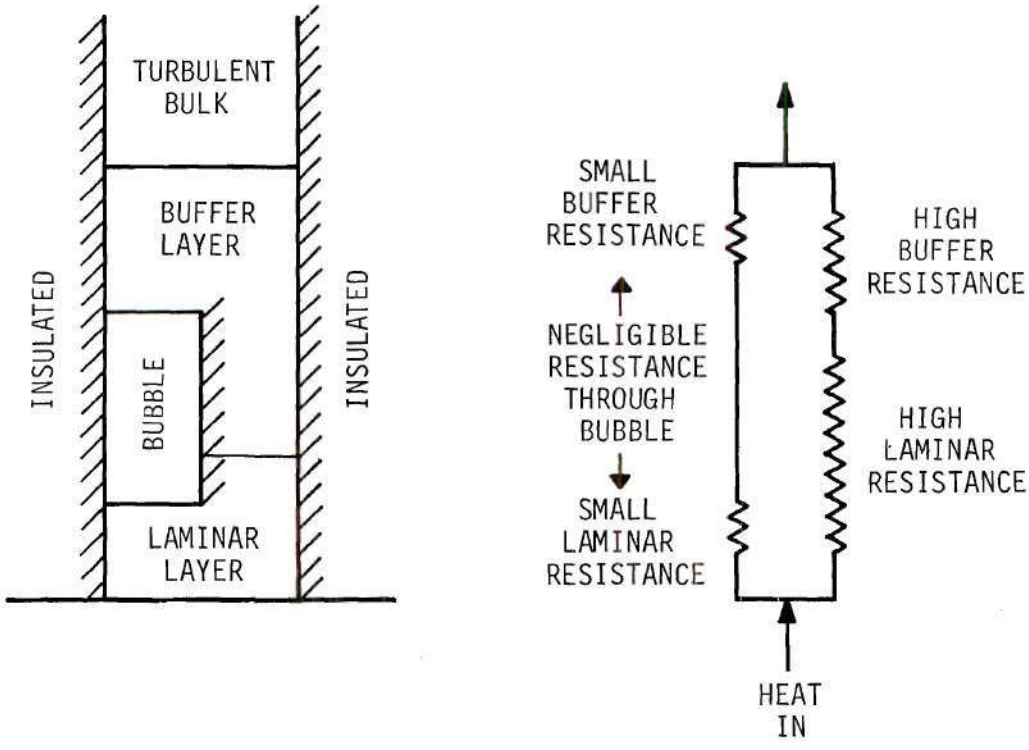

Figure 3. Poppendiek's Thermal Circuit Model for Boiling Heat Transfer.

cussing his results, Gunther stated: "Turbulent mixing adjacent to the heating surface, excited by boundary-layer boiling, makes possible the high heat-transfer rates observed experimentally. The sliding of bubbles observed on the heating surface should add to the turbulence caused by the action of bubble growth and collapse."

Another investigation was reported in 1951 by Rohsenow and Clark (31). The abstract for their paper is:

> An analysis of the heat quantity required to form a vapor bubble in a liquid is presented. High-speed motion pictures of boiling heat transfer in forced convection showing bubbles departing from a heated surface are analyzed and the net heat transferred to the bubbles is compared with the total heat transferred from the heated surface. It is found that the heat transferred to the moving liquid by the condensation of the bubbles is a negligible part of the total convective heat transfer. Therefore it is proposed that the high rate of heat transfer associated with surface boiling in a subcooled liquid is due primarily to the violent agitation of the quiescent layers of liquid adjacent to the heated surface resulting from the motion of vapor bubbles being generated there. From the literature two examples of similar processes are cited as evidence supporting the proposed agitation mechanism.

However, in the discussion of this paper, Zmola (see reference 31, page 618) commented on the conclusions reached about the mechanism of boiling:

> The high oscillatory velocities that exist in the boundary layer as a result of bubble growth and collapse certainly must contribute to the manifold increase of heat transfer when phase change accompanies the ordinary convection process. On the other hand, the assumption that the only role of the bubble is to provide this mechanical action does not seem entirely justified. As a bubble grows on the heater surface, the liquid-vapor interface passes through a region of high-temperature gradient. It seems plausible that, for at least part of the bubble lifetime, evaporation would be taking place at that section of the interface in the high-temperature region (near the heating surface), while vapor would condense at the interface at the low temperature. This mass transfer would provide a low-resistance heat path. Under these conditions a calculation which would evaluate the heat transferred by the bubble as the latent heat of the vapor at maximum volume would underestimate the role of bubble formation as a means of reducing the thermal resistance through the boundary layer.

> Poppendiek[28] [reference number changed to correspond to that of this thesis] performed calculations* for an idealized system which indicated that the heat transferred as a result of mass transfer within the bubble exceeded by several times the latent heat of the vapor at maximum bubble size. There is also some further evidence that the phase change processes take place with sufficient speed under the conditions experienced in subcooled boiling that an appreciable mass transfer could take place even during the lifetime of the bubble.[14]

In the authors' closure, Rohsenow and Clark reminded the reviewer that they had stated that their analysis accounted for only the net heat transferred to the bubble and could not distinguish between bubble and surface exchange and bubble and liquid exchange. They further stated that even if the effect studied by Poppendiek was included, this heat quantity would still be small and the conclusion the same.

Another investigation was reported in 1954 by Ellion (13). He acknowledged the probable existence of a thin film of liquid at the base of the bubble. Ellion stated that the viscous and adhesion forces in the liquid prevent the bubble from wiping the wall clear of water and the evaporation rate may not be sufficiently large to evaporate any appreciable thickness of liquid at the bubble base. He also said that calculations by the use of Plesset equations (27) indicated that the flow of vapor through the bubble may be eliminated as a prime source of heat transfer. In conclusion, Ellion stated that it seems likely that the induced turbulence in the liquid boundary layer is the basic mechanism by which heat is transferred in the nucleate boiling region. However, at the JPL con-

---

*The calculations by Poppendiek referred to by Zmola are not shown in reference 28. Poppendiek's estimation apparently was based on a modified form of the Boelter-Martinelli-Jonassen equation for the Nusselt number which attempted to account for the parallel heat flow path shown in Figure 3 and given in reference 28.

ference noted below, Snyder specifically stated (34) that his calculations showed a large amount of latent heat transfer was possible in using Plesset's equations.

It was thus tentatively concluded by most investigators in the mid-fifties that the mechanism which causes high heat transfer rates in boiling was the additional turbulence near the heated surface caused by bubble stirring or agitation. However, at a JPL conference, Snyder (34) presented strong arguments for the mass transfer mechanism with his comments dispersed through the proceedings of this seminar. His hypothesis led to much discussion which is recorded therein. Arguments against this mechanism were given by Zwick, Zuber, Rohsenow, Sebersky, Ellion, and Bankoff. (Although Bankoff reversed this in his final comments and did some follow up research noted below.) The two main points which supported the belief that mass transfer was negligible were (a) the accommodation coefficient which relates the actual amount of evaporation (or condensation) to that predicted by kinetic theory was too low for an appreciable amount of mass transfer to occur and (b) the thermal conductivity of the liquid was too low to remove the latent heat deposited by condensation around the bubble surface; thus allowing the surface temperature to rise and dampen the condensation process. This last objection presupposed a stagnant thermal layer surrounding the bubble.

The accommodation coefficient had been reported to be 0.04 for water (1). This result was obtained in an experiment during which the water surface was not disturbed and in which the bulk water temperature was measured rather than the surface temperature. Snyder stated that the value for fresh surfaces such as those of a vapor bubble should be much

closer to unity. Hickman and Trevoy (17) measured the rate of evaporation into a vacuum from a liquid surface being stirred. They showed that the condition or "freshness" of the surface had a profound effect on the accommodation coefficient. Returning to the second objection to the mass transfer mechanism, Zwick (39) had shown that pure conduction would not transfer the heat at a sufficient rate to keep the temperature of the bubble cap near that of the bulk temperature. Snyder postulated that the heat flow from the top of the bubble did not occur by pure conduction but rather the turbulent mixing of the bulk fluid would be the predominant effect.

Also at this conference, Snyder described an experiment which would help prove the existence of the thin liquid film vaporization. During the growth of the bubble, the latent heat required to vaporize the hypothesized thin film was believed to come from the heated surface under the thin film. Thus, by losing heat in this manner, the surface should experience a rapid drop in temperature during bubble growth. Snyder believed that an observation of such temperature drops would confirm the existence of the thin film. He also reported that one of his students, D. K. Edwards (12), had attempted to observe the temperature fluctuations of a thermocouple placed on the under side of a heated gold strip and beneath a growing bubble. However, some difficulty was experienced in having a bubble form over the thermocouple. Next, Edwards (12) investigated the effect of mass transfer by varying the thickness of the heated plate. However, this only showed in an indirect manner the effect of mass transfer.

In 1959, Bankoff and Mikesell (8) helped support Snyder's belief

concerning turbulent cooling of the bubble top. They postulated that the heat flux from the portion of the bubble projecting into the turbulently-flowing core depended primarily upon turbulent and convective heat flow rather than laminar heat conduction. They also repeated the suggestion that mass transfer* may be an important mode of heat transfer in subcooled nucleate boiling. In this paper, an interesting experiment was suggested. This was to supply a metered flow of saturated steam through one, two, or more small holes in a heating surface and to compute the condensation rates from photographs of the growing and collapsing bubbles.

Later Bankoff (2, 3, 4) reported another series of analytical investigations. First, he analyzed Gunther's data (15) on the basis of a model which divided the heat flow into three sequential steps: (a) from the heating surface to the inner portion of the two-phase wall layer, (b) from the inner to the outer portion of the two-phase layer, and (c) from the outer portion of the two-phase layer to the single-phase turbulent core liquid. In this analysis he considered a combination of several mechanisms including mass transfer. However, he stated that the contribution of mass transfer was not known, although it was probably significant. Next, using an equation developed by Plesset (27) for the flow of vapor between two liquid surfaces, Bankoff was able to correlate the maximum heat flux as a function of pressure which was experimentally determined by Cichelli and Bonilla (10). Bankoff admitted that the correlation might have been coincidental; however, it seemed to indicate the importance of mass transfer particularly near the burnout point.

---

*Bankoff used the term latent heat transport for what has been called the mass transfer mechanism in this work.

In 1962, Bankoff and Mason (7) presented results of an experiment that Bankoff had suggested earlier. Turbulent heat transfer coefficients were measured at the surface of single bubbles formed by injecting steam into a subcooled water stream at atmospheric pressure. However, in this experiment the stream of water impinged head on with the bubble instead of from the side as in forced convection boiling in a pipe. Also, the bubbles did not grow through a thermal and laminar boundary layer as they would in forced convection. The heat transfer coefficients determined from his measurement ranged from 13,000 to 320,000 (BTU/hr sq ft °F). After analyzing Gunther's data (15) on the basis of the measured bubble heat transfer coefficients, Bankoff concluded that this mechanism accounted for a significant fraction of the total heat flow.

In 1958 Mesler and Banchero (25) reported temperature fluctuations of a thermocouple which monitored wall temperatures during a boiling heat transfer investigation. Apparently these observations led Mesler to the investigation reported by Moore and Mesler (26) in 1961. In this investigation, a special surface thermocouple with a time response of approximately one microsecond was monitored with an oscilloscope during saturated pool boiling. Temperature changes of from 20°F to 30°F were observed to occur in about two milliseconds. They argued that nothing in the bubble agitation hypothesis predicted these temperature drops. Moore and Mesler cited Snyder's 1956 hypothesis (34) that a thin liquid film was present at the base of the bubble from which evaporation would take place and result in a rapid drop in the surface temperature. They also acknowledged Snyder's suggestion of an experiment such as they performed as a method to prove his hypothesis. Then they stated that the only hypothesis that appeared to be

consistent with their observation was the one which proposed vaporization at the base of the bubble. Thus, the results of this experiment offered strong evidence that Snyder's hypothesis was correct.

In 1964, Rogers and Mesler (29) reported an experiment which correlated the surface temperature fluctuations to the bubble cycle. It was found that the beginning of the temperature drop occurred at the same time as bubble initiation and that the temperature continued to drop sharply as the bubble grew. Only after the bubble broke away from the surface did the temperature start to rise. It was in this paper that the claim was made that Moore and Mesler (26) had postulated that the temperature drops were due to thin liquid film evaporation. However, reference 26, pages 622-623, seems to discredit this claim and thus the hypothesis seems to have been originally presented by Snyder in 1956 (34) and 1952 (33).

Also in 1964, Hendricks and Sharp (16) reported an independent effort to correlate surface temperature fluctuations with the bubble cycle. They also observed that the temperature dropped as the bubble grew. They concluded that this gave strong support to the evaporating thin liquid film hypothesis of Snyder. Similar results have been obtained by Bonnet et al. (9) and Marcus (24). Sharp (36) has also reported an optical observation of the thin liquid film in which the initial thickness was found to be approximately 1.5×10^{-5} inches. Also, Hospeti and Mesler (19) have recently obtained a measure of the thickness of the thin liquid film through use of a radioactive tracer. It was estimated to be of the order of 10^{-5} to 10^{-4} inches. Thus, the existence of a thin liquid film from which evaporation takes place as postulated by Snyder seems to have been proven.

Only one study (7) has been reported in which the condensation of vapor on the bubble cap was investigated. It should be noted that vapor condensation is not expected to be very significant in all boiling cases. For example, in saturated boiling, the bulk liquid is at such a high temperature that a large amount of condensation is not expected. Also, for liquid metals, the situation is probably similar because of the high thermal conductivity which allows only small temperature gradients. This presents a situation not favorable to a large amount of condensation. For the case of highly subcooled nucleate boiling of water and other liquids with a $Pr > 1$ in forced convection, the situation is different. Here the fluid temperature is much less than the wall temperature and thus condensation of vapor is very important.

CHAPTER II

PURPOSE AND DESCRIPTION OF THE RESEARCH EFFORT

The general objective of the work presented here was to investigate the role of mass transfer in subcooled nucleate boiling in forced convection. The region investigated was that of large subcooling in which the bubbles grow and collapse while attached to the heated surface. The phenomenon of evaporation into the bubble from a thin liquid film adjacent to the heated surface has been demonstrated.* Also, some results have been presented by Bankoff on the heat transfer from a single bubble growing and collapsing in a subcooled turbulent stream flowing down onto the top of the bubble. The primary purpose of this thesis was to extend the results of Bankoff's experiment to the case of bubble growth through a thermal boundary layer and into a subcooled turbulent stream of water flowing parallel to the heated plate. A second phase of the experimental effort was to obtain schlieren photographs of actual boiling in subcooled forced convection to determine, if possible, whether a high temperature gradient occurred next to the bubble surface. Two theoretical efforts were also made. The first was to derive a model of bubble dynamics which would predict the single bubble experimental results and the second was to derive a model of bubble dynamics including thin film evaporation as

---

*These were for both saturated and subcooled liquids in pool boiling. It has been assumed throughout this work that the same general phenomenon of thin film evaporation will occur in subcooled forced convection boiling.

in real boiling.

Single Bubble Experiment

The object of this part was to determine the effectiveness of a turbulent subcooled stream of liquid in removing heat deposited on the surface of a bubble by condensation. The geometry for this experiment was similar to real boiling in that the bubble was required to grow through a laminar as well as a thermal boundary layer and into a turbulent stream flowing parallel to a heated plate. The effectiveness of the turbulent subcooled stream was expressed as a bubble heat transfer coefficient which is defined below. High values of this heat transfer coefficient will indicate a large amount of condensation and help confirm the importance of the mass transfer mechanism.

The bubble heat transfer coefficient, h_b, is defined in the following relation:

$$Q_{IN} = h_b A_b \Delta T_{sub} \qquad (2.1)$$

Normally the heat transfer coefficient is defined for a steady state operation. However, in the present case the heat transfer process is in a purely transient state. Even with this limitation in the definition, h_b still provides a convenient way to compare the physical process under different conditions. This comparison is the sole purpose in defining the heat transfer coefficient for a single bubble.

An average area over the bubble lifetime might have been a more appropriate quantity to use in equation 2.1 rather than the maximum area.

Likewise, the temperature difference between the steam in the bubble and the fluid centerline might have been more appropriate in equation 2.1 instead of ΔT_{sub}. However, ΔT_{sub} and A_b were used since these were easily determined and had a much smaller uncertainty than their similar quantities of the alternate representation mentioned. Due to the inherent limitation of equation 2.1 in this transient case, the use of ΔT_{sub} and A_b is not expected to detract from the usefulness of h_b.

The first task in measuring h_b in equation 2.1 was to produce a rapidly growing and collapsing bubble under the desired conditions. This was accomplished by generating steam, passing it through a small hole in a stainless steel heated plate, and into a turbulent subcooled stream. The quantities measured, in order to calculate h_b, were the heat flow rate represented by the steam flow in BTU per hour, the bubble lifetime, the maximum radius of the bubble, the cooling water temperature, and the absolute pressure near the bubble site.

To obtain the amount of heat per hour going into the bubbles, an energy balance was made on the steam generator. The power input to the steam generator was measured by determining (a) the current through the steam generator resistance heater and (b) the applied voltage. During the measurements, the steam generator was in a steady state condition. Thus, by subtracting from the power input to the steam generator the rate of heat loss by the generator to the room, the heat rate represented by the steam flow was obtained. The heat loss by the generator was obtained by calibration before the actual runs were made.

The maximum radius of the bubble and the bubble lifetime were obtained from high speed motion pictures of the bubble. Also, the cooling

water temperature and the absolute pressure were determined with a thermometer, a thermocouple, two pressure gauges, and a barometer.

The bubble heat transfer coefficient was determined for various cooling stream velocities with its temperature held constant. Other runs were made with the velocity held constant while varying the stream temperature. Initially an attempt was made to keep the energy input to the bubbles constant from run to run. However, this was not possible, as under certain conditions the bubbles were unacceptably small or nonexistent. Thus, to obtain reasonable size bubbles, the power input was adjusted. Also, during these runs power was applied to the heated plate to develop a thermal boundary layer and thus produce a condition more in keeping with actual boiling. Under one set of conditions, in addition to the normal run, a second run was made without heating the stainless steel strip. This was done in order to determine the effect of the thermal boundary layer. Another set of constant temperature runs was made with the velocity ranging from a condition of laminar flow to a condition of turbulent flow. This was done to determine the effect of the type of turbulence characteristic of pipe flow.

Schlieren Experiment

The object of the schlieren experiment was to observe the process of actual subcooled nucleate boiling in forced convection. If the mass transfer mechanism is powerful, then the heat input to the bubble surface will be large. This large heat input should cause large temperature gradients at the bubble surface depending on the effectiveness of the turbulent stream in removing heat from the bubble surface. Both the temperature

gradients and the nature of the heat transfer process around the bubble cap should be visible in the schlieren photographs. These observations were made by taking photographs of the schlieren image with a short duration light source. The duration of the light source was five microseconds and this was short enough to stop both the motion of turbulence and the motion of the bubbles. The runs were made with constant velocity and constant inlet temperature while varying the heat input from zero up to a substantial fraction of the burnout value.

Bubble Dynamics for the Single Bubble Experiment

This theoretical effort consisted of deriving a mathematical model which would allow the prediction of the maximum bubble radius and the bubble lifetime. The major input variables were the bulk cooling fluid temperature, the cooling fluid flow rate, the fluid pressure near the bubble site, and the mass flow rate of steam into the bubble.

Another important input number was the effective thermal diffusivity in the liquid which is the sum of the molecular thermal diffusivity and the eddy diffusivity at and near the bubble interface for heat flow. The molecular thermal diffusivity is known; however, the eddy diffusivity for this case was unknown. Initially it was thought that, since the bubbles were growing inside a square channel, the eddy diffusivity should be the value for (normal) pipe flow without boiling. Closer examination indicates this to be incorrect.

One reason why a bubble does not experience the full effect of pipe turbulence is thought to be the finite lifetime of the bubble surface. In characterizing any quantity such as velocity in a turbulent field,

the average value is usually used:

$$\overline{U} = \lim_{\tau \to \infty} \frac{1}{2\tau} \int_{-\tau}^{+\tau} U \, d\tau$$

where τ represents time and U represents velocity. To make this definition reasonable for actually determining the average value, the limit on the integral, τ, is usually made finite. The actual magnitude of τ depends on the physical conditions under study. For example, τ should be made small compared to slow periodic or semi-periodic variations imposed on the turbulent fluctuations which are not considered to be part of the turbulence proper. For the case of normal pipe flow turbulence in a steady flow condition, there are no physical phenomena which restrict the upper limit of τ. In considering the turbulent transport of heat from a solid wall, this means that all fluctuations, regardless of how long they are in time, will contribute to the transport process. For the case of heat transport from a bubble surface, only those fluctuations whose lifetimes are of the order of the bubble lifetime or shorter can be completely effective in the transport process.

Turbulent temperature fluctuations in mercury and ethylene glycol in pipe flow have been reported by Rust and Sesonske (32). The measurements indicated that the mean energy of the fluctuations was at frequencies of the order of 8 to 23 cycles per second. At frequencies of the order of 1000 cycles per second, the magnitude of the fluctuations was found to be reduced by approximately four orders of magnitude. This indicates that a substantial portion of the effect of pipe flow turbulence

lies below a frequency of 1000 cycles per second. Since the bubble frequency for subcooled nucleate boiling in forced convection of water is of the order of 2000 cycles per second, the effect of pipe flow turbulence can be expected to be somewhat modified with respect to a single bubble.

Also, the flow situation with respect to a single bubble is different from normal pipe flow. For the bubble case, the motion of the fluid due to bubble growth interacts with the mean fluid motion and induces more intense high frequency turbulence. Even for very low or zero mean flow (corresponding to pool boiling), it is possible that the motion of the liquid due to bubble growth could cause additional turbulence at the top of the bubble which would be effective in removing heat from that (bubble) surface.

Thus, since the effective thermal diffusivity was unknown, various values were assumed in the process of solving the bubble dynamics model. For conditions tested experimentally, this diffusivity could be adjusted until reasonable agreement existed between the experimental values for the maximum bubble radius and the bubble lifetime, and those predicted by the theoretical model. In this manner, the model actually served as a tool by which the effective diffusivity was determined.

Bubble Dynamics in Real Boiling

Once a proper description of the mode of heat transfer from the top of the bubble to the subcooled stream had been established, it was then possible to consider a complete description of bubble dynamics for subcooled nucleate boiling. This description consisted of a model based on the first principles of the physical phenomena occurring during the bubble

lifetime. The object of this exercise was to demonstrate that a bubble model based on thin liquid film evaporation and subsequent condensation on the bubble top surface could predict bubble radius versus time curves that were reasonably close to those obtained experimentally. Once this was accomplished, a relatively high degree of confidence could be placed in the model, and then a very important effect could be observed in the solution of the model: the total amount of heat removed from the heated surface by a single bubble.

CHAPTER III

THEORETICAL DEVELOPMENTS

General Considerations in Bubble Dynamics

The rate of evaporation from a liquid surface into a vapor whose density is less than the saturation density corresponding to the surface temperature is given as (27):

$$MP = \alpha' \left(\frac{R_{GAS}\, T_{SUR}}{2\Pi M} \right)^{\frac{1}{2}} (\rho_{sat} - \rho_{vap}) \qquad (3.1)$$

where MP is the rate of evaporation, lb/sec ft^2

T_{SUR} is the surface temperature, °R

ρ_{sat} is the saturation density at T_{SUR}, lb/ft^3

ρ_{vap} is the density of the vapor into which evaporation is occurring, lb/ft^3

M is the molecular weight of the fluid

R_{GAS} is the universal gas constant, 49,690 ft^2/sec^2 °R

α' is the accommodation coefficient.

If ρ_{vap} is greater than ρ_{sat} then condensation will occur and the magnitude will be

$$MP = \alpha' \left(\frac{R_{GAS}\, T_{SUR}}{2\Pi M} \right)^{\frac{1}{2}} (\rho_{vap} - \rho_{sat}) \qquad (3.2)$$

The liquid surfaces associated with growing and collapsing bubbles are believed to be new and clean; thus, an accommodation coefficient of 1.0 was used in these calculations. The value of $\alpha' = 1.0$ is supported by recent work of Hickman (18). A value of 0.04 was supported for many years in the literature (1); however, Hickman points out that this value was based on measurements in which heat transfer effects were neglected. Also, the measurements were made on undisturbed surfaces.

Dynamic Equation for Bubble Radius

The Rayleigh equation for the growth of an isothermal bubble is given as (22):

$$\rho_l \left\{R\ddot{R} + (3/2)(\dot{R})^2\right\} = P_{VAP} - P_\infty \qquad (3.3)$$

where ρ_l is the liquid density

R is the bubble radius

$\dot{R}$ is the derivative of R with respect to time

$\ddot{R}$ is the derivative of $\dot{R}$ with respect to time

P_{VAP} is the pressure of the vapor in the bubble.

In some cases an additional pressure term due to surface tension forces is subtracted from the right hand side of equation 3.3 (see reference 37, pp. 11-12). This term is $2\sigma/R$ where σ is the surface tension. The smallest value of R considered in this work was 0.001 inch and for the case of water, the missing term has a value of approximately 1.0 psi. As R increases, this value decreases. Thus, neglecting the surface tension term was acceptable.

General Scheme of Bubble Dynamics

In the two models which were developed, use was made of a control volume concept. The bubble was considered to be a hemisphere with its base on a flat surface. One boundary of the control volume was the interface between the liquid and the vapor at the surface of the hemisphere. For the single bubble experimental case, the other boundary was the vapor-metal interface at the base of the hemisphere while for the real bubble case, the other boundary was the vapor-thin liquid film interface at the base.*

At the top of the bubble, mass was allowed to cross the control surface by condensation or evaporation. (Evaporation at the top was allowed during the initial growth through the superheated layer near the wall.) Only the mass taken from or added to the control volume was actually considered in the mass balance. That is, if an amount of mass was condensed on the liquid surface during a time interval, the total amount of mass in the control volume was made smaller by that amount. However, the actual mass added to the liquid stream was neglected with respect to the total amount of mass in the stream and with respect to the dynamic motion of the stream (i.e., momentum effects were neglected). Also, heat conduction between the vapor and the liquid across the interface at the top of the bubble was neglected. However, the latent heat of condensation or evaporation was included as a source or sink in the heat balance of the liquid surrounding the bubble. The value for the latent heat was taken

*Thin liquid film dry up was possible during the bubble lifetime. If this occurred, the vapor-metal interface at the dry up spot became the boundary of the control volume.

to be the saturation value corresponding to the density of the vapor in the bubble.

During most of the bubble lifetime, condensation at the bubble top provided a mass output from the bubble. In the experiment, a mass input was provided by forcing a flow of steam through a tiny hole in the plate. The average value of the mass input over the life of the bubble was experimentally determined. Thus, in the model for this case, the mass input to the control volume consisted of a constant amount of steam per unit time. However, for the real bubble case, the situation was different. The mass input occurred at the vapor-thin liquid film interface at the base of the bubble. Again, during a time interval the amount of mass added to the control volume was counted as an increase in the total mass in the control volume. Also, the amount of mass removed from the thin liquid film was counted as a loss from the total amount of liquid in this film. The temperature drop across the film was neglected and the temperature of the film was assumed to be that of the metal surface of the heated plate. The heat required for vaporization was assumed to come solely from the heated plate.

Thus, the control volume was mainly concerned with the total amount of mass inside the bubble while the surroundings were mainly concerned with the thermal effect of the latent heat. The state of the vapor in the bubble was assumed to be saturated, corresponding to a saturation density equal to the vapor mass present in the control volume divided by the volume. The entire mass in the control volume was assumed to be at a uniform temperature and pressure. The rate of mass flow across the control volume boundaries was governed by equations 3.1 and 3.2. Also, the rate of growth

of the bubble was determined by equation 3.3 in which the driving pressure differential was a function of time.

Bubble Dynamics for the Single Bubble Case

Description of Bubble History and Assumptions

During the life of the bubble, mass was added at a constant rate and removed by condensation on the top of the bubble. The difference between the mass input and the mass output determined the change in mass of the bubble and, in turn, affected the bubble pressure. During the growth stage, the pressure in the bubble was greater than the local liquid pressure and this caused the bubble to grow. However, as the surface area of the bubble grew larger, the mass output also increased. Eventually, the mass output exceeded the mass input and the total mass in the bubble started to decrease. Also, as the bubble volume increased, the pressure in the bubble tended to decrease. At some point, the pressure became less than the local fluid pressure. These effects coupled with the dynamics expressed in equation 3.3 then led to a decreasing bubble radius and thus bubble collapse.

At any point during the bubble lifetime, the rate of mass output was controlled by the vapor density in the bubble and the liquid surface temperature. The liquid surface temperature was controlled by the rate of condensation at the surface and the transfer of heat to the cooling stream. The liquid surface temperature determined the value for ρ_{sat} in equation 3.2.

The assumption that the bubble was hemispherical during all of its lifetime is not completely correct. However, the high speed photographs

show that it is not too bad over most of the bubble lifetime. The shape of the bubble was not that of a hemisphere during the initial and final stages of the bubble lifetime. Since the steam input to the bubble came through a hole approximately 0.0135 inch in diameter, the initial interface between the liquid and the vapor was a flat circular disk. This was transformed into a roughly hemispherical surface at some later time. Due to the mathematical complexity of describing such a transformation, the initial bubble radius was assumed to be 0.013 inch. This led to the requirement of establishing the state of the vapor in the bubble and the temperature distribution around the bubble at the initial time.

The most critical item concerning the state of the vapor in the bubble was the pressure. For a bubble in real boiling, the initial radius is usually small and the initial pressure is usually high (possibly as much as 20 to 30 psia higher than the pressure in the ambient liquid). However, as the bubble grows, the bubble pressure approaches the pressure of the ambient liquid. In the experimental case, 0.013 inch was usually within 50 percent of the maximum radius. Thus, the pressure of the bubble was chosen slightly larger than the local stream pressure. The actual procedure was to first determine the local liquid pressure near the bubble site for the run under consideration and then to obtain the corresponding saturation temperature. Next, a temperature slightly greater than this value was chosen as the vapor temperature in the bubble and the vapor was assumed saturated at this temperature. This made the pressure in the bubble slightly larger than the local liquid pressure.

As a first approximation to the temperature distribution around the bubble at the beginning of the solution, a step distribution was assumed.

That is, the temperature of a thin shell of liquid around the bubble was assumed to be equal to the temperature of the vapor in the bubble at that time. The remainder of the liquid was assumed to be equal to the inlet temperature of the cooling fluid as determined in the experiment. The thickness of this shell was chosen so as to account for the heat input to the bubble wall during the growth from the flat disk interface to the hemispherical interface with a radius of 0.013 inch. This was done by first assuming the time required to grow from a flat disk to a hemisphere. Next, the heat input during this time was calculated by multiplying the time interval by the rate of heat input which was a constant. Next, the mass of liquid which would experience a temperature rise corresponding to the difference in temperature of the thin shell and the inlet temperature was calculated from $Q = m\, C_p \Delta T$. Knowing the density of the liquid, the volume was then calculated from the known mass. Finally, since the surface area of the bubble was known, the shell thickness was obtained.

The initial values for $\dot{R}$ and $\ddot{R}$ were also required. $\ddot{R}$ was assumed to be zero and then $\dot{R}$ was calculated using equation 3.3.

The stream in which the bubble was growing was assumed to have a uniform velocity profile. In reality it was that corresponding to fully developed turbulent flow for the high velocity cases. In those cases, the boundary layer was of the order of 10^{-3} to 10^{-4} inches and, since the bubble radius was usually large compared to this value, the uniform velocity assumption was justified. The experimentally determined mean velocity was used as the magnitude of the uniform velocity. However, for the low velocity cases, the velocity profile was probably far from uniform. Nevertheless, a uniform velocity, equal to the mean velocity, was assumed here.

Heat Diffusion from Bubble Surface

By making the bubble spherical rather than hemispherical and making the mass input rate twice as great as the actual rate, the mathematical heat diffusion problem is similar to a case considered by Wittke (38). In his case a uniform flow of liquid impinged on a spherical bubble as shown in Figure 4. Since no heat flow occurred in the ψ direction, the case under consideration here and his case were similar under the changes stated above. For example, the wall of the heated plate might be considered to be the X-Z plane. (Note that the heat transfer from the heated plate to the fluid by convection was neglected.) The heat diffusion equation to be solved was that derived by Wittke plus a heat generation term.

$$\frac{\partial T}{\partial t} + \left[- U\left(1 - \frac{R^3}{r^3}\right) \cos\theta + \frac{R^2 \dot{R}}{r^2} \right] \frac{\partial T}{\partial r} + \frac{U}{r}\left(1 + \frac{1}{2}\frac{R^3}{r^3}\right) \sin\theta \frac{\partial T}{\partial \theta} \qquad (3.4)$$

$$= \alpha \left(\frac{\partial^2 T}{\partial r^2} + \frac{2}{r}\frac{\partial T}{\partial r} + \frac{1}{r^2}\frac{\partial^2 T}{\partial \theta^2} + \frac{\cot\theta}{r^2}\frac{\partial T}{\partial \theta} \right) + \frac{Q'}{\rho_l C_P}$$

where $T = T(t, r, \theta)$

U is the magnitude of the velocity

R is the radius of the bubble

$\dot{R}$ is the time derivative of R

α is the equivalent thermal diffusivity of the liquid

Q' is the heat generation rate associated with condensation or evaporation

ρ_l is the liquid density

C_P is the specific heat of the liquid

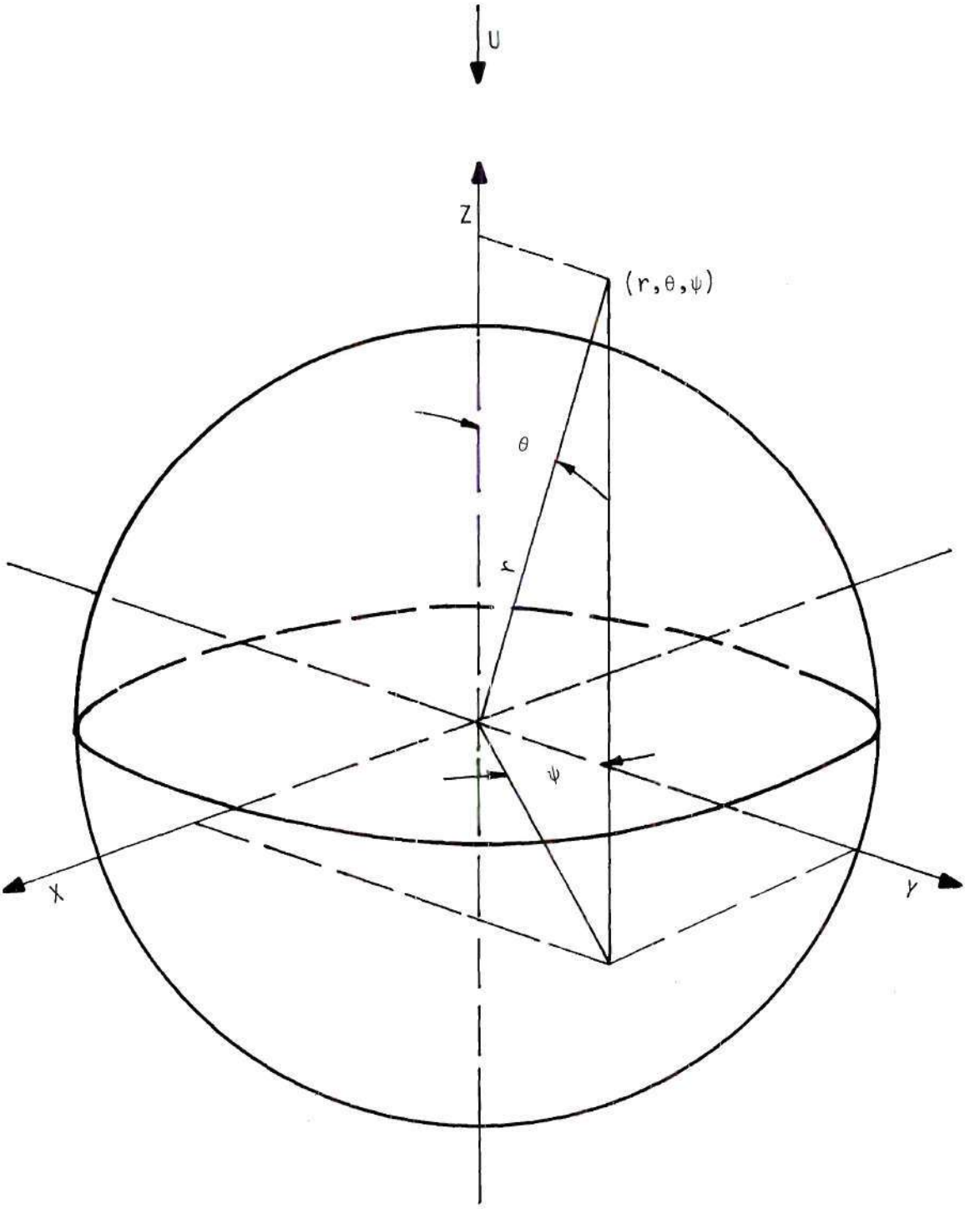

Figure 4. Equivalent Coordinate System for the Single Bubble Case.

t is the time

r and θ are defined in Figure 4.

The heat generation rate will be zero everywhere except in a thin shell surrounding the bubble. Here the latent heat of condensation (or vaporization) will be considered a heat source (or sink) uniformly distributed throughout the shell. The numerical approach here is similar to one considered by Dusinberre (11) for radiant heating (see Appendix B). Under this procedure the boundary condition for the vapor liquid interface is

$$\left.\frac{\partial T}{\partial r}\right|_{r = R} = 0$$

The other boundary condition is

$$\left.\frac{\partial T}{\partial r}\right|_{r = R_{MAX}} = 0$$

where R_{MAX} is a substantial distance from the bubble surface. The boundary conditions in the θ direction are

$$\left.\frac{\partial T}{\partial \theta}\right|_{\theta = 0} = 0 \quad \text{and} \quad \left.\frac{\partial T}{\partial \theta}\right|_{\theta = 180^\circ} = 0$$

The initial temperature distribution is described on page 33. Now let

$$\Phi = (T - T_{BL})/(T_{SAT} - T_{BL}) \tag{3.5}$$

where T_{BL} is the temperature of the cooling fluid and T_{SAT} is the saturation temperature corresponding to the local fluid pressure. Also let

$$t' = \frac{4\alpha}{(DIA)^2}\, t \tag{3.6}$$

where DIA is the equivalent hydraulic diameter of the channel. Let

$$r' = \frac{2r}{DIA} \qquad \text{and} \qquad \gamma = \frac{2R}{DIA} \tag{3.7}$$

Also define a Peclet number

$$P_E = DIA\ U/\alpha \tag{3.8}$$

Now using equations 3.5, 3.6, 3.7, and 3.8, equation 3.4 becomes:

$$\frac{\partial\Phi}{\partial t'} - \frac{P_E}{2}\left(1 - \frac{\gamma^2}{r'^3}\right)\cos\theta\,\frac{\partial\Phi}{\partial r'} + \dot{\gamma}\,\frac{\gamma^2}{r'^2}\,\frac{\partial\Phi}{\partial r'} \tag{3.9}$$

$$+ \frac{P_E}{2}\,\frac{1}{r'}\left(1 + \frac{1}{2}\,\frac{\gamma^3}{r'^3}\right)\sin\theta\,\frac{\partial\Phi}{\partial\theta} = \frac{\partial^2\Phi}{\partial r'^2} + \frac{2}{r'}\,\frac{\partial\Phi}{\partial r'}$$

$$+ \frac{1}{r'^2}\,\frac{\partial^2\Phi}{\partial\theta^2} + \frac{\cot\theta}{r'^2}\,\frac{\partial\Phi}{\partial\theta} + \frac{Q'(DIA)^2}{4\alpha\,\rho_l\,C_P\,(T_{SAT} - T_{BL})}$$

where $\dot{\gamma} = d\gamma/dt'$.

Also with the transformations

$$y = r' - \gamma \qquad \text{and} \qquad \mu = -\cos\theta \tag{3.10}$$

equation 3.9 becomes:

$$\frac{\partial\Phi}{\partial t'} - \dot{\gamma}\left[1 - \frac{1}{(1+\frac{y}{\gamma})^2}\right]\frac{\partial\Phi}{\partial y} + \frac{P_E}{2}\mu\left[1 - \frac{1}{(1+\frac{y}{\gamma})^3}\right]\frac{\partial\Phi}{\partial y} \tag{3.11}$$

$$+ \frac{P_E}{2}\frac{(1-\mu^2)}{\gamma(1+\frac{y}{\gamma})}\left[1 + \frac{1}{2(1+\frac{y}{\gamma})^3}\right]\frac{\partial\Phi}{\partial\mu} = \frac{\partial^2\Phi}{\partial y^2} + \frac{2}{\gamma(1+\frac{y}{\gamma})}\frac{\partial\Phi}{\partial y}$$

$$+ \frac{(1-\mu^2)}{\gamma^2(1+\frac{y}{\gamma})^2}\frac{\partial^2\Phi}{\partial\mu^2} - \frac{2\mu}{\gamma^2(1+\frac{y}{\gamma})^2}\frac{\partial\Phi}{\partial\mu} + \frac{Q'(DIA)^2}{4\alpha\,\rho_l\,C_P\,(T_{SAT} - T_{BL})}$$

The numerical approximation to equation 3.11 is developed in Appendix B. It should be noted that the first transformation of equation 3.10 required the y coordinate to have the same absolute velocity as the bubble wall.

Method of Advancing the Numerical Solution

After the solution had been advanced up to a time t, the following quantities were known:

1. the state of the steam in the bubble (density and pressure)
2. R, $\dot{R}$, $\ddot{R}$, and the bubble volume
3. the amount of mass in the bubble

4. the liquid temperature at the vapor-liquid interface

5. the liquid temperature distribution.

To advance the solution an increment of time, the following procedure was used.

1. Since R, $\dot{R}$, $\ddot{R}$ and the bubble vapor pressure were known, the change in R, $\dot{R}$, $\ddot{R}$ was calculated with the aid of equation 3.3 and a Taylor series expansion for R and $\dot{R}$ (see Appendix B).

2. Next, equation 3.2 was used to calculate the amount of vapor condensed. This involved calculating the saturation vapor density corresponding to the known liquid surface temperature. Using this value and the known value of the bubble vapor density, the amount condensed was calculated.

3. Next, the new total mass in the bubble was calculated by adding to the old total mass the difference between the amount condensed and the amount added due to the constant rate of mass addition.

4. Then the volume was calculated using the new value of R found in step one. This was divided into the new mass found in step three and the result was the new density. Under the assumption that the vapor in the bubble was saturated, the new pressure was determined.

5. The latent heat represented by the condensed steam was then used along with the numerical approximation to equation 3.11 to calculate the new surface temperature and the new liquid temperature distribution. Following this procedure, the variables were determined over the life of the bubble.

Bubble Dynamics in Real Boiling

Description of Bubble History and Assumptions

During the lifetime of the bubble, the mass removed due to condensation on the liquid stream was similar to the case of the experimental bubble as just discussed. However, the mass input, rather than having a constant rate, was controlled by the heat capacity and temperature of the heated plate, the density of the bubble vapor, and the amount of liquid in the thin liquid film. Again, the initial growth of the bubble was due to a higher pressure in the bubble relative to the local liquid pressure. As the bubble grew, the mass output increased because of the increased surface area. Also, as the size increased, the pressure had a tendency to decrease. As evaporation occurred from the thin liquid film, the latent heat required was supplied from the heated plate with a subsequent drop in the plate temperature. The mass rate of input was proportional to the square root of the surface temperature as shown in equation 3.1 and thus, the mass input rate tended to decrease as the surface temperature dropped. Also, since only a given amount of fluid was contained in the thin liquid film, the total mass input tended to decrease as dry up occurred. (This of course reduced the total area from which evaporation was occurring and thus reduced the total amount evaporating.) Again the above effects combined with equation 3.3 to yield a decreasing radius and thus bubble collapse.

The major assumptions for this case in addition to those previously mentioned are:

1. The initial bubble radius was assumed to be of the order of the thickness of the buffer layer as calculated from the general velocity dis-

tribution using the desired stream velocity and hydraulic diameter.

2. The initial temperature distribution in the heated plate was assumed uniform.

3. The initial temperature of the liquid was assumed equal to the center line temperature except for a thin shell of liquid surrounding the bubble the temperature of which was assumed equal to the plate temperature.

4. The initial state of the vapor in the bubble was assumed to be saturation corresponding to the plate temperature.

5. The bubble was assumed to be stationary with respect to the heated plate. The relative velocity between the stream and the bubble surface was assumed zero. Thus, the fluid moved only in the r direction and also the temperature distribution was a function of r and t only. Figure 5 shows the coordinate system for this problem.

6. The heat generation rate in the plate was assumed uniform and the opposite side of the plate was insulated.

Heat Diffusion from Bubble Surface

The equation to be solved for this case can be obtained from equation 3.4 by letting U equal zero and removing the θ dependence of the temperature:

$$\frac{\partial T}{\partial t} + \frac{R^2 \dot{R}}{r^2} \frac{\partial T}{\partial r} = \alpha \left(\frac{\partial^2 T}{\partial r^2} + \frac{2}{r} \frac{\partial T}{\partial r} \right) + \frac{Q'}{\rho_l C_P} \qquad (3.12)$$

where $T = T(t, r)$

By using the definitions of γ, r', t', and Φ introduced for the experi-

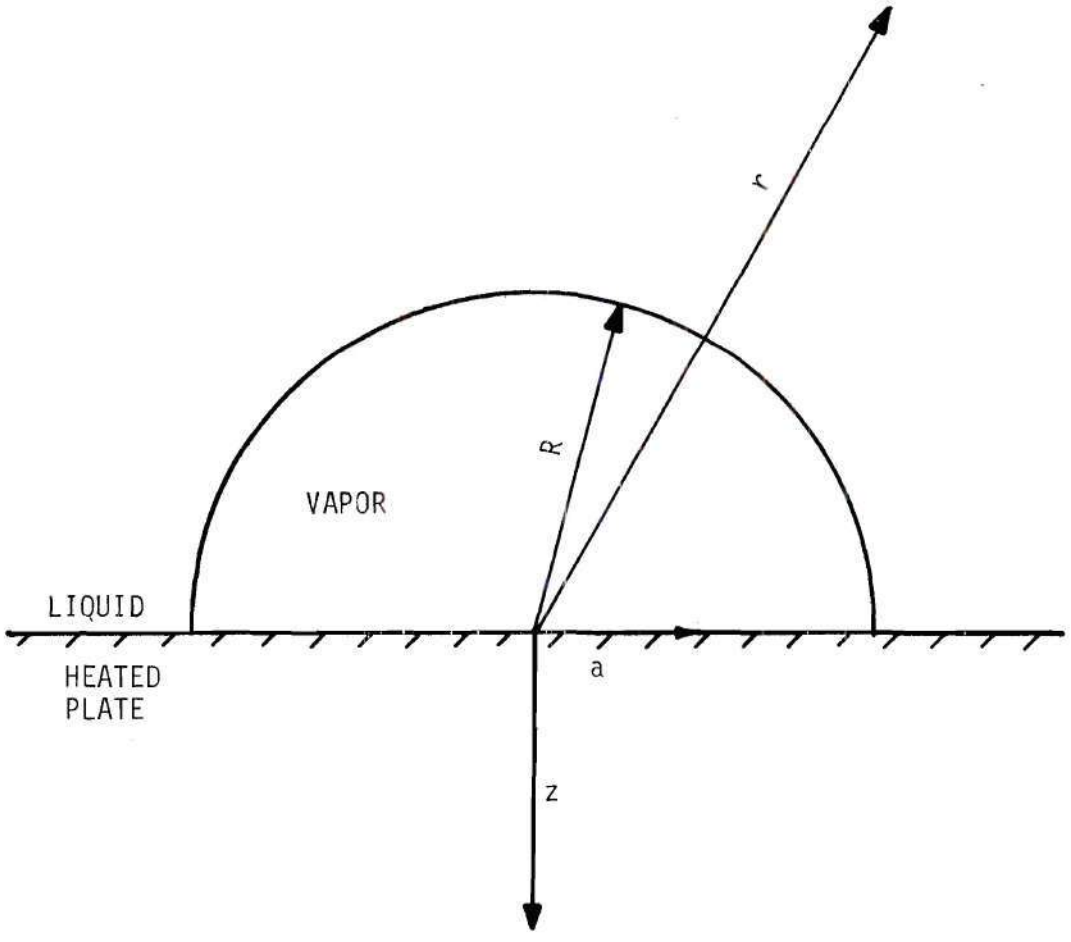

Figure 5. Coordinate System for Real Boiling Case.

mental bubble case, this becomes:

$$\frac{\partial \Phi}{\partial t'} + \frac{\gamma^2}{r'^2}\,\dot{\gamma}\,\frac{\partial \Phi}{\partial r'} = \frac{\partial^2 \Phi}{\partial r'^2} + \frac{2}{r'}\,\frac{\partial \Phi}{\partial r'} + \frac{Q'(DIA)^2}{4\alpha\,\rho_1\,C_P\,(T_{SAT} - T_{BL})} \qquad (3.13)$$

Also, with the transformation $y = r' - \gamma$, equation 3.13 becomes:

$$\frac{\partial \Phi}{\partial t'} - \dot{\gamma}\left[1 - \frac{1}{(1 + \frac{y}{\gamma})^2}\right]\frac{\partial \Phi}{\partial y} = \frac{\partial^2 \Phi}{\partial y^2} + \frac{2}{\gamma(1 + \frac{y}{\gamma})}\,\frac{\partial \Phi}{\partial y} \qquad (3.14)$$

$$+ \frac{Q'(DIA)^2}{4\alpha\,\rho_1\,C_P\,(T_{SAT} - T_{BL})}$$

The numerical approximation for this equation is developed in Appendix B.

Heat Diffusion in Heated Plate

The coordinate system chosen for the heated plate was cylindrical for which $T = T(a, z)$. The z axis was placed so that it passes through the center of the bubble. For this case, the heat diffusion equation is:

$$\frac{\partial T}{\partial t} = \alpha_p\left(\frac{\partial^2 T}{\partial a^2} + \frac{1}{a}\,\frac{\partial T}{\partial a} + \frac{\partial^2 T}{\partial z^2}\right) + \frac{Q}{\rho_p\,C_P'} \qquad (3.15)$$

Since this equation was solved simultaneously with 3.14, the same time scale was used here. This is $t' = \frac{4\,t\,\alpha}{(DIA)^2}$. Also, the following definitions were made:

$$\Phi' = \frac{T - T_{INV}}{T_{DROP} - T_{INV}} \tag{3.16}$$

$$z' = z/Z$$

$$a' = a/A_{MAX}$$

where

T_{INV} is the initial plate temperature

T_{DROP} is the lowest temperature to which the plate drops (usually selected as the saturation temperature of the cooling stream at the system pressure)

Z is the thickness of the plate

A_{MAX} is a value for the radius (a) beyond which the bubble was assumed to have no effect.

With the above definitions, equation 3.15 becomes:

$$\frac{\partial \Phi'}{\partial t'} = \frac{\alpha_p}{4\alpha} \frac{(DIA)^2}{(A_{MAX})^2} \left(\frac{\partial^2 \Phi'}{\partial a'^2} + \frac{1}{a'} \frac{\partial \Phi'}{\partial a'} \right) \tag{3.17}$$

$$+ \frac{\alpha_p}{4\alpha} \frac{(DIA)^2}{Z^2} \frac{\partial^2 \Phi'}{\partial z'^2} + \frac{Q(DIA)^2}{4\alpha \rho_p C_P' (T_{DROP} - T_{INV})}$$

The numerical approximation to this equation is developed in Appendix B.

Method of Advancing the Numerical Solution

After the solution had been advanced up to a time, t, the following quantities were known:

1. the state of the steam in the bubble (density and pressure)

2. R, $\dot{R}$, $\ddot{R}$, and the bubble volume

3. the amount of mass in the bubble

4. the liquid temperature at the surface of the bubble

5. the temperature of the thin liquid film

6. the temperature of the surface of the heated plate

7. the temperature distributions in both the liquid and the heated plate

8. the amount of liquid in the thin liquid film.

To advance the solution an increment of time, the following procedure was used:

1. Since R, $\dot{R}$, $\ddot{R}$, and the bubble vapor pressure were known, the changes in R, $\dot{R}$, $\ddot{R}$, were calculated with the aid of equation 3.3 and a Taylor series expansion for R and $\dot{R}$ (see Appendix B).

2. Using equation 3.2, the amount of vapor condensed was calculated by first finding the saturation vapor density corresponding to the known liquid surface temperature. This value and the known bubble vapor density were then used in equation 3.2 and thus, the amount of condensation calculated.

3. Next, the amount of liquid which would evaporate from the thin liquid film during the time increment was calculated. First the saturation vapor corresponding to the temperature of the thin liquid film was obtained. Then the evaporation rate was calculated and from this the amount which evaporated was obtained.

4. Next, the new total mass in the bubble was calculated by adding to the old total mass the difference between the mass evaporated and the mass condensed.

5. Next, the new volume was calculated using the results of step one. This volume was divided into the new mass found in step three and the result was the new density. Since the vapor in the bubble was assumed saturated, the new pressure was also fixed.

6. The latent heat represented by the condensed steam was then used along with the numerical approximation to equation 3.14 to calculate the new liquid surface temperature and the new temperature distribution in the liquid.

7. The latent heat represented by the evaporated liquid from the thin liquid film together with the numerical approximation to equation 3.17 was used to calculate the new plate surface temperature and the new temperature distribution in the heated plate.

8. Finally, the amount of mass evaporated was subtracted from the total mass in the thin liquid film to give the new total mass in the film.

CHAPTER IV

INSTRUMENTATION AND EQUIPMENT

Basic System

Flow System Components

The basic heat transfer system is shown in Figure 6 and a schematic diagram is shown in Figure 7. The system was designed to provide a maximum water velocity of 50 ft/sec flowing over a 3/8 inch × 3/8 inch × 6 inch stainless steel heater strip. To accomplish this, a five horsepower Goulds' pump was used which drew water from the storage tank and forced it through the remainder of the system. The storage tank was obtained from a Scanlan-Morris sterilizing unit and it housed a 7500 watt resistance heater plus a copper cooling coil. A Pall-Trinity filter was placed in the line to keep the water clean. To remove the heat input by the stainless steel heater strip, an American-Standard heat exchanger was provided. An Ilco-Way ion exchanger was provided on the distilled water fill line. A distilling capacity was also provided by the second tank of the Scanlan-Morris unit which also contained a 7500 watt resistance heater. Since schlieren photographs and high speed motion pictures were to be attempted, the test section was mechanically isolated from the pump in order to avoid any test section vibration. This was accomplished by means of flexible rubber hoses and stainless steel flexible couplings. The test section, along with the steam generator, will be discussed in detail in another section (see page 52).

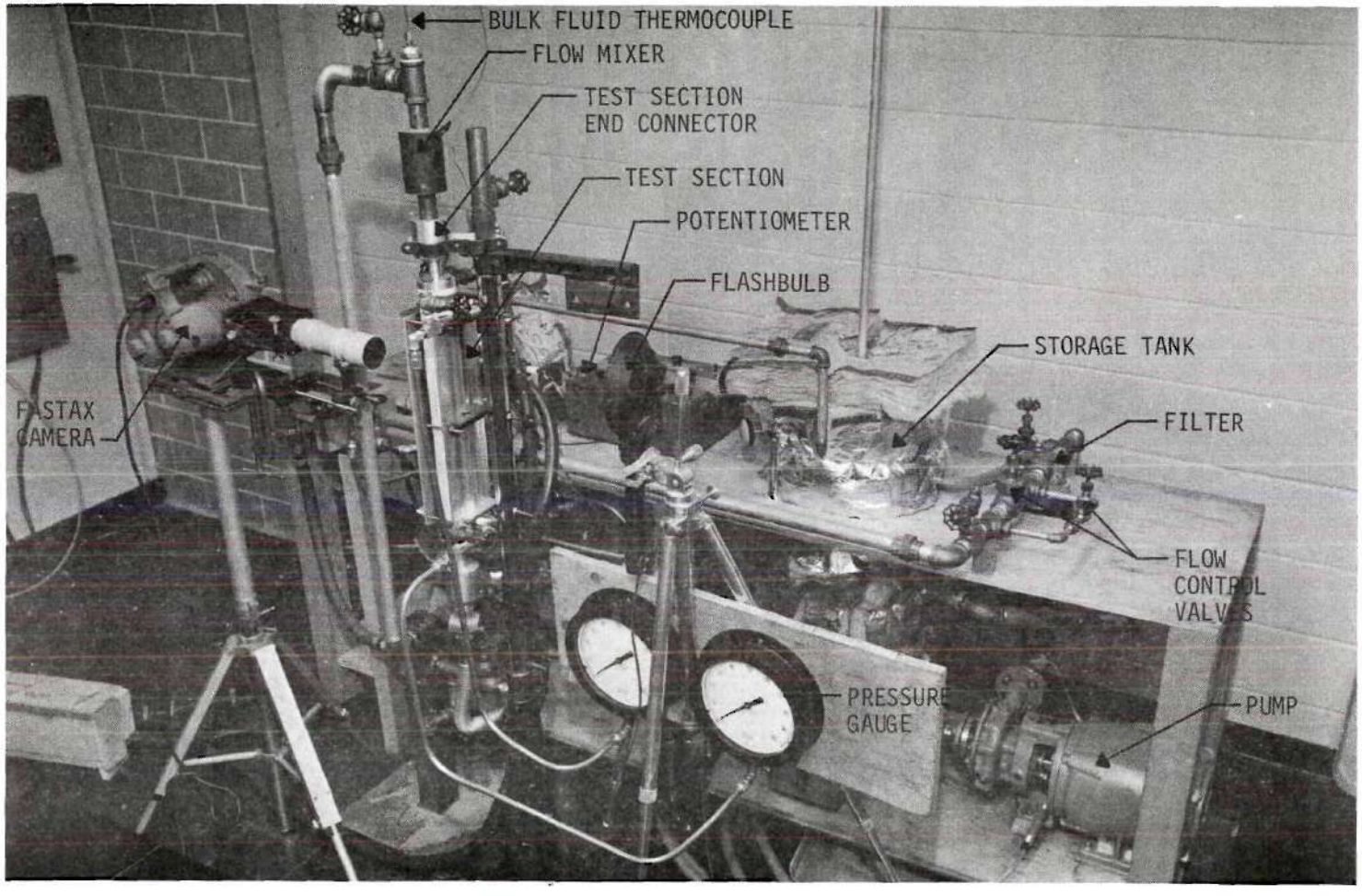

Figure 6. Overall View of Equipment.

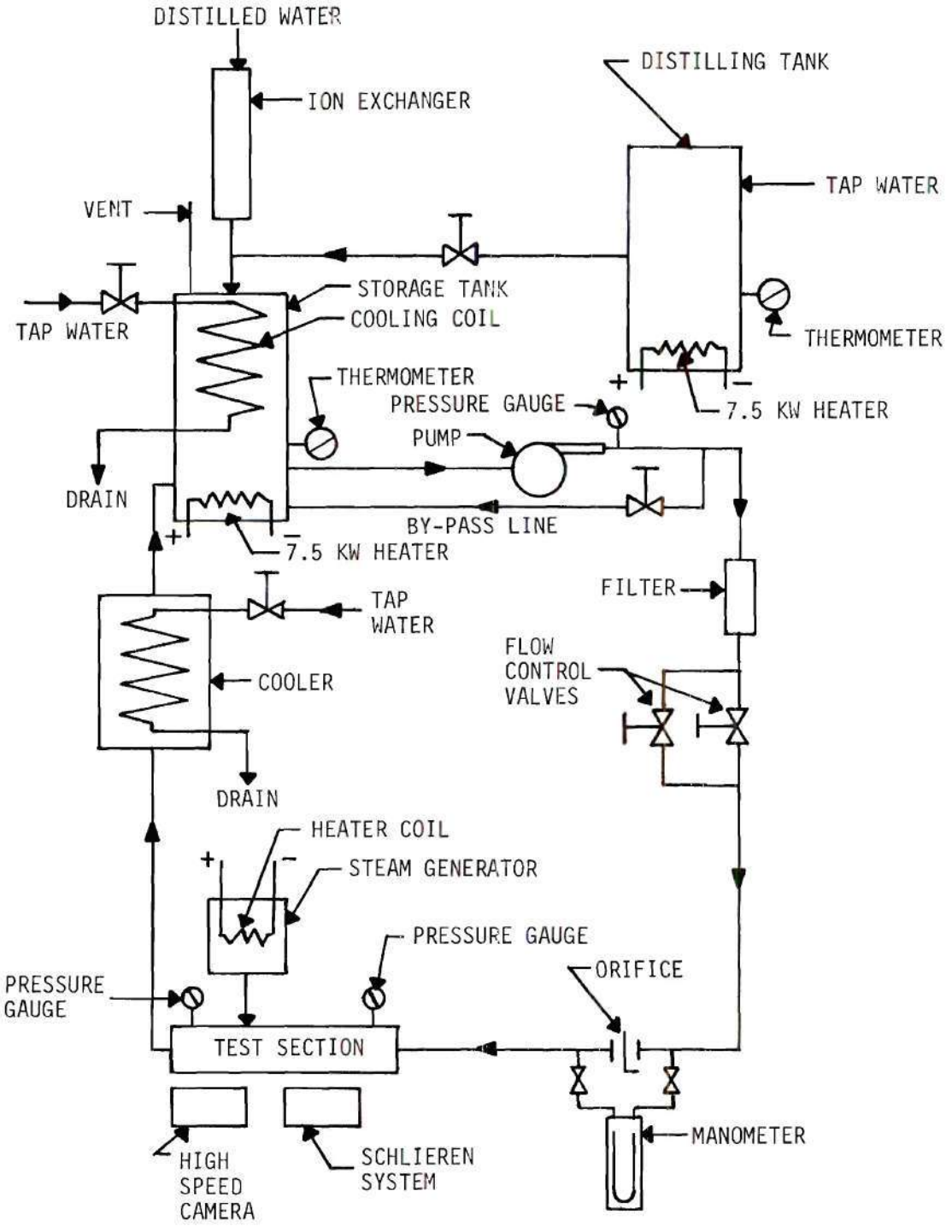

Figure 7. Flow System Schematic.

Electrical Equipment

The purpose of the electrical equipment was to provide power to the stainless steel heater strip. This equipment consisted of a modified Rectodyne DC power supply in combination with a three phase adjustable autotransformer. This combination could provide a maximum input of approximately 20 kilowatts of DC power with a voltage ripple of about 12 percent peak to peak. A schematic of the power supply is given in Figure 8.

Instrumentation

In the flow loop, three pressure gauges were used. Two of these were used to obtain the pressure at the inlet and outlet of the test section and had a range of from zero to 100 psi with an accuracy of ± 1/2 percent. The third pressure gauge was placed on the outlet of the pump.

The flow rates were obtained with a Meriam flow rate indicator consisting of an orifice and a 13 inch manometer. The bulk temperature of the fluid leaving the test section was indicated by a chromel-alumel thermocouple whose voltage was obtained with a Leeds and Northrop precision potentiometer. The temperature in the storage and distilling tanks was indicated by thermometers provided in the original Scalan-Morris sterilizing system.

Dissolved oxygen in the system water was measured with a YSI model 51 dissolved oxygen meter. Power input to the strip was obtained by measuring the voltage drop across (a) the heater strip and (b) a precision shunt in series. These measurements were made with a DC-AC differential voltmeter.

High speed pictures were taken with a Fastax camera with a Goose control unit and these were analyzed with an analyzer projector.

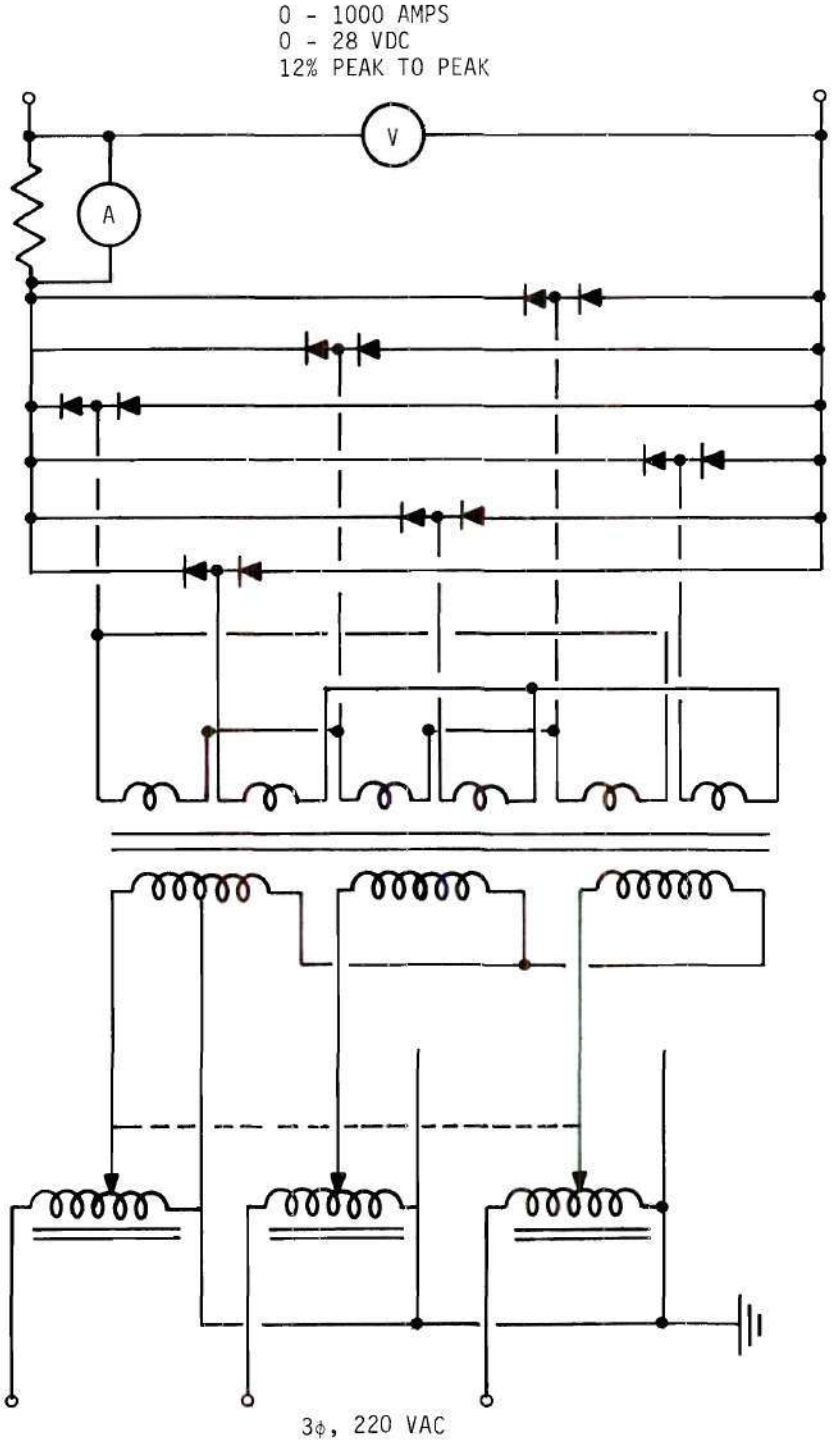

Figure 8. Power Supply.

Test Section and Steam Injection System

The purpose of the test section and steam injection system was to produce a rapidly growing and collapsing steam bubble on the surface of a heater strip over which flowed a turbulent stream of subcooled water. To accomplish this, a steam generator was constructed from which steam was led to the under side of the stainless steel heater strip which was 27 mils thick. The steam then passed through a hole in the heater strip, made with a No. 80 drill, and into the turbulent, subcooled stream.

The details of the bleed line are shown in Figure 9. The steam first passed through a Yale number 23 hypodermic needle which was passed through a rubber end cap which was placed over the end of the inner steam passage tube (see Figure 10). The purpose of this needle was to provide a high resistance in the steam flow path. This made the total pressure drop from the generator to the cooling stream large in comparison to that across the final hole in the heater strip. Without this needle, the steam flow consisted of an intermittent stream of bubbles. After passing through the inner steam passage tube, the steam then entered the hole in the heater strip. The purpose of the outer steam tube was twofold: (a) it provided a blanket of steam around the inner tube which insured that only dry saturated steam entered the hole in the heater strip and (b) it formed one of the two electrodes. The second electrode was formed with a 1/4 inch diameter copper rod whose connecting tip was separated from the body of the electrode by a flexible length of grounding wire capable of carrying 1000 amps (see Figure 10). The resulting electrode allowed a downward force to be put on the heater strip, thus keeping it snug against the wall; however, it also allowed for thermal expansion along the length of the strip. The

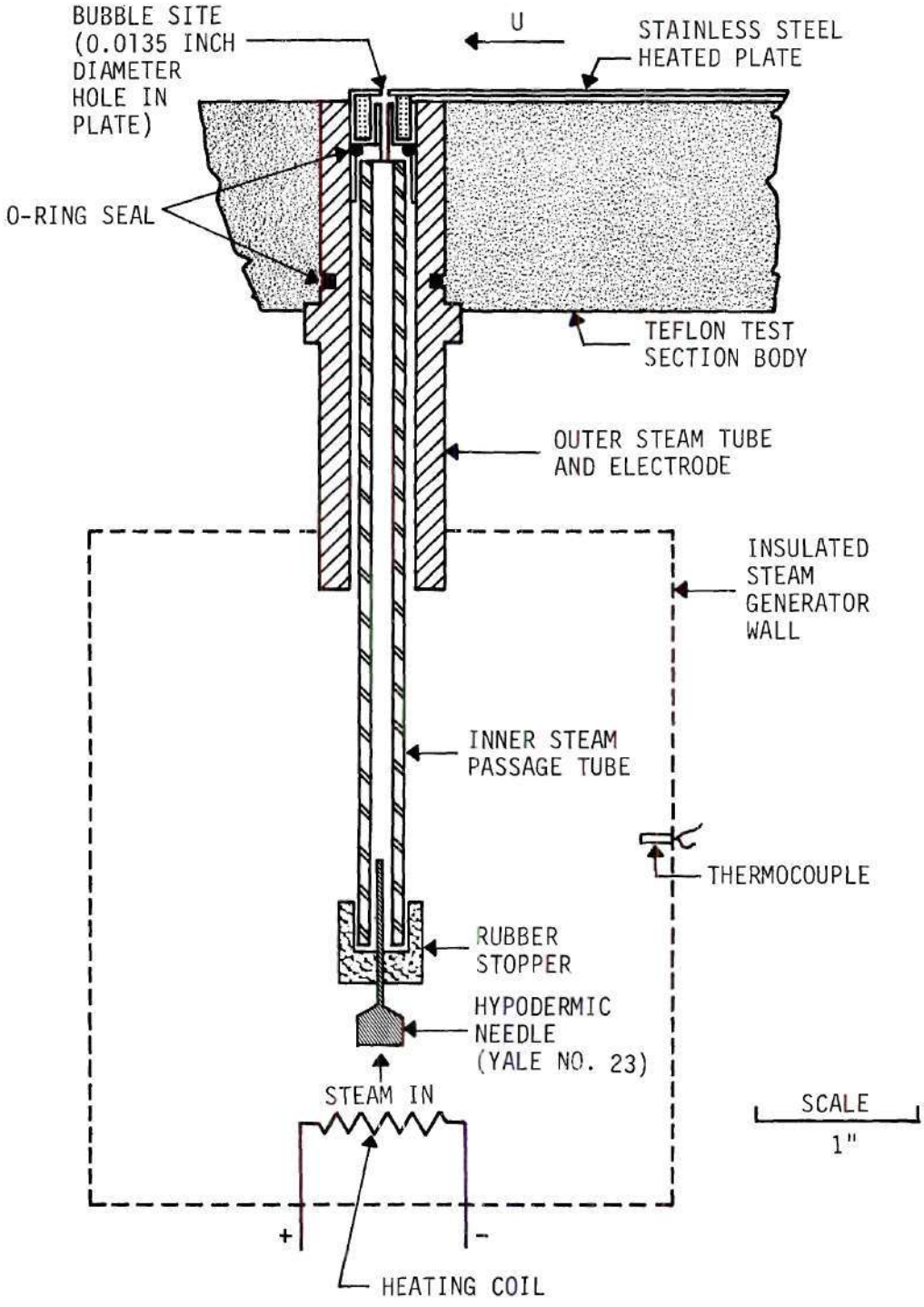

Figure 9. Steam Line From Generator to Bubble Site.

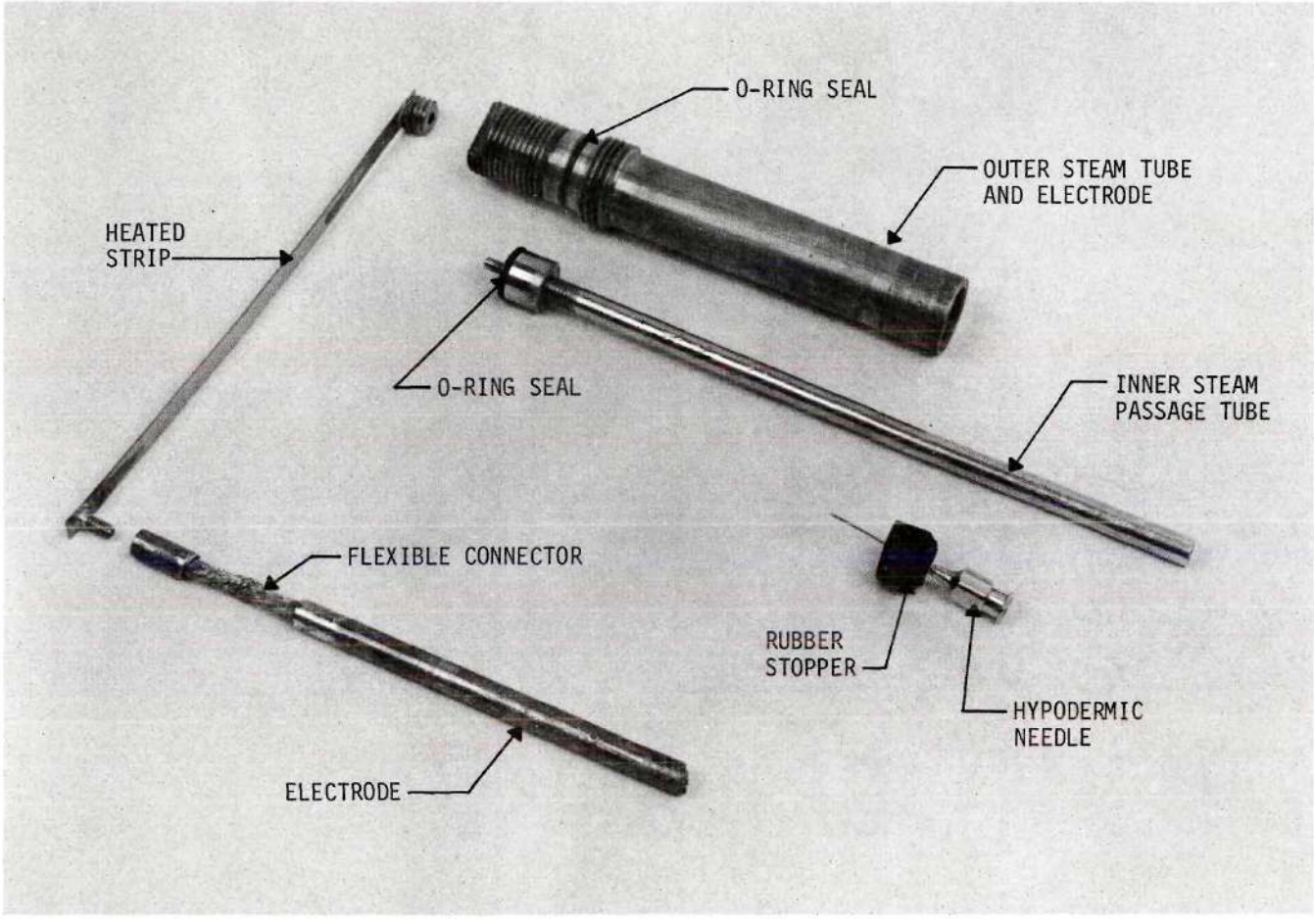

Figure 10. Details of Steam Bleed Line and Electrodes.

test section body was made of Teflon which provided electrical insulation. Other parts of the test section are shown in Figure 11.

The steam generator is shown in Figures 12 and 13. The body was constructed of standard copper pipe fittings using Teflon tape as a sealing agent. The electrodes were made of 1/4 inch diameter copper rods which were electrically insulated by Swagelock male connectors made of Teflon. These connectors also served as pressure seals for the electrodes. A nichrome electrical resistance heating coil was placed between the electrodes. A copper constantan thermocouple was placed in the generator through a Conax transducer gland. A valve was provided for filling the generator with water and also for allowing a blowdown from a pressurized condition. During the calibration of the generator and during the test runs, glass wool was packed around the generator in an effort to minimize the heat loss to the room.

The two connectors which were used to change the cooling fluid flow geometry from one inch pipe to a 3/8 inch by 3/8 inch square channel are shown in Figure 14.

Schlieren System

The schlieren system is shown in Figure 15. It consisted of two Kodak lenses, a Sylvania c300 high intensity continuous light source, a razor as a knife edge, and a ground glass image plate. For the present application, the continuous light source was replaced with a General Radio strobe light which could provide a short duration flash. Also, the image plate was replaced with a Nikon 35 millimeter camera to record the schlieren image.

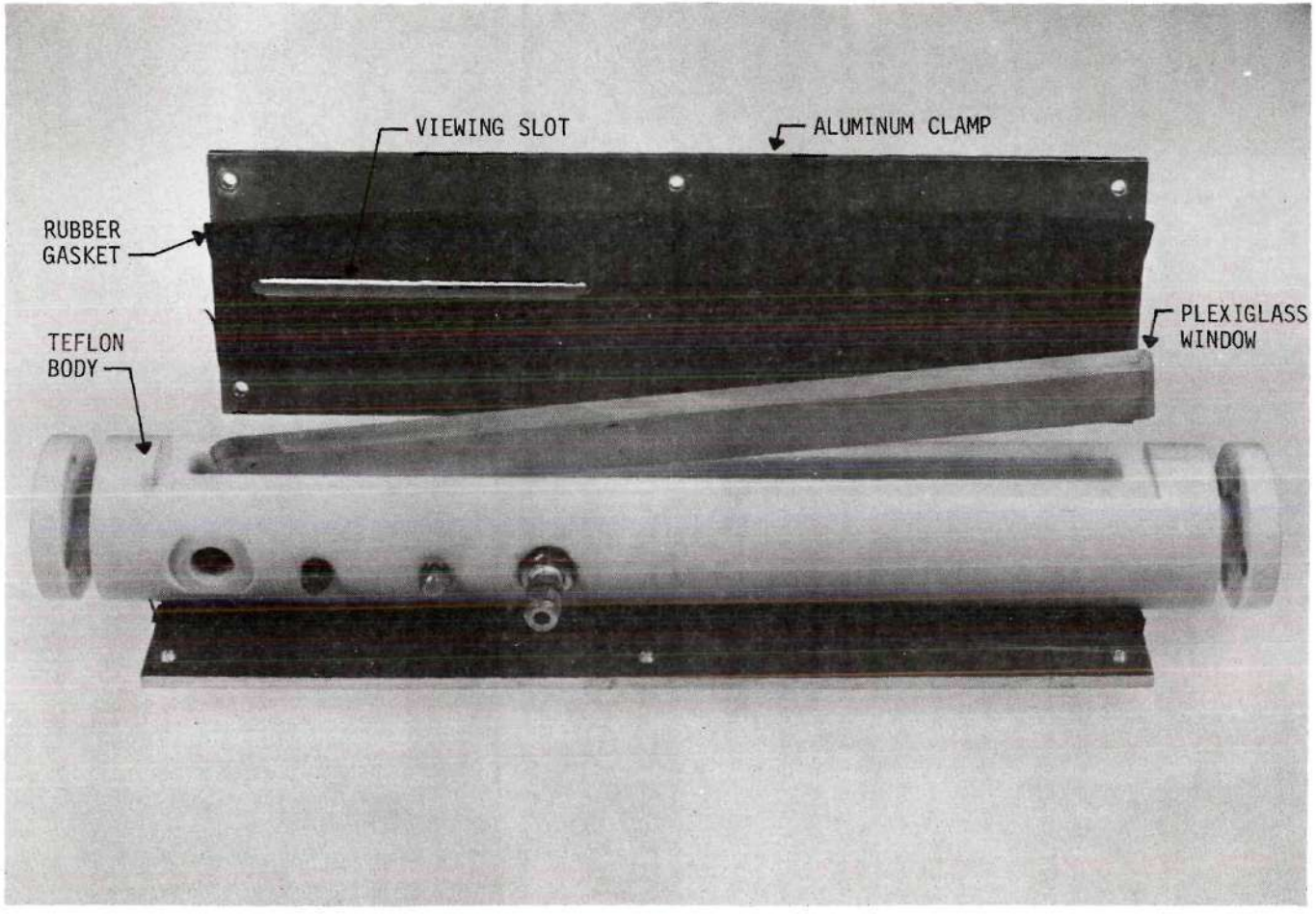

Figure 11. Test Section Components.

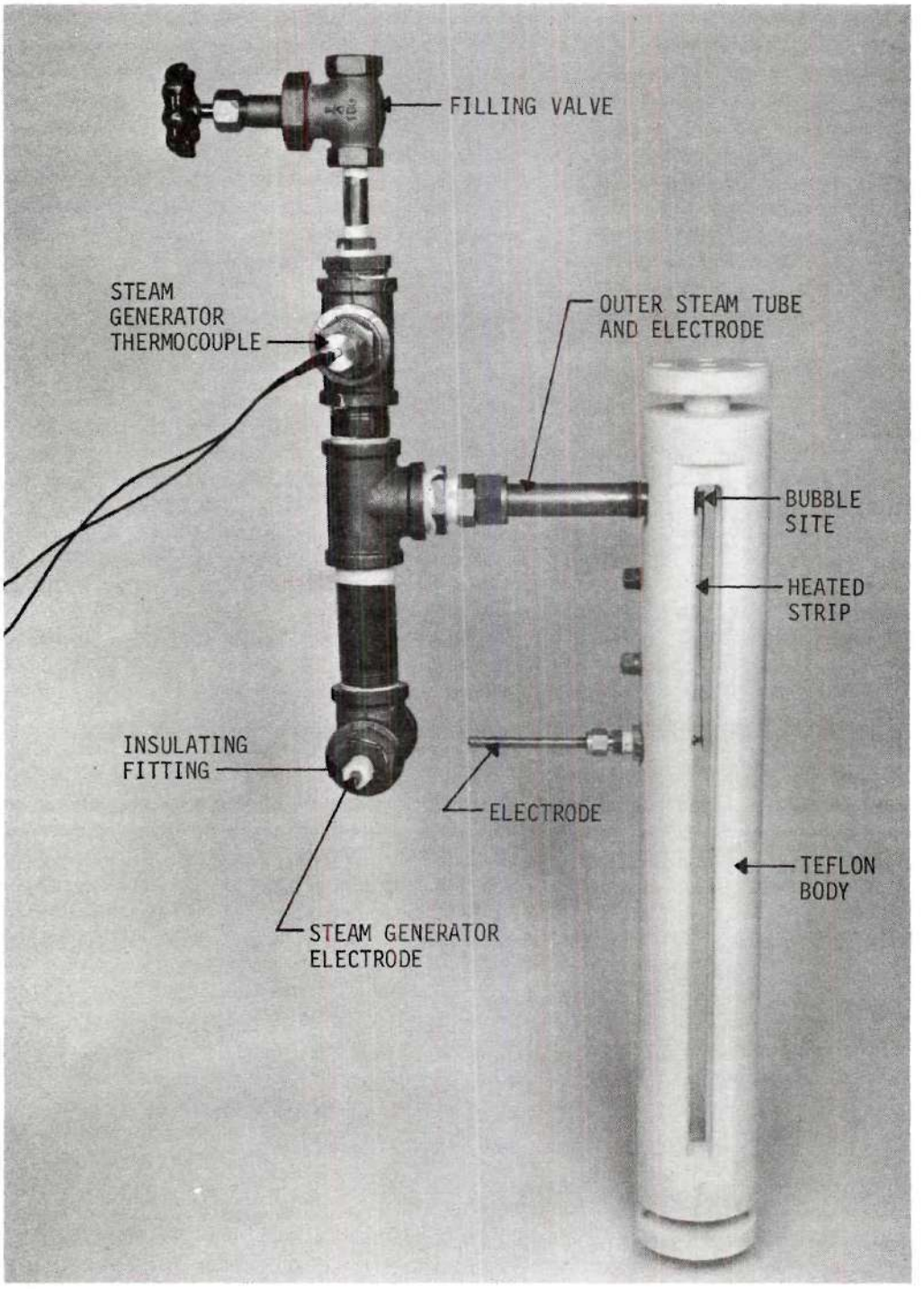

Figure 12. Steam Generator and Test Section.

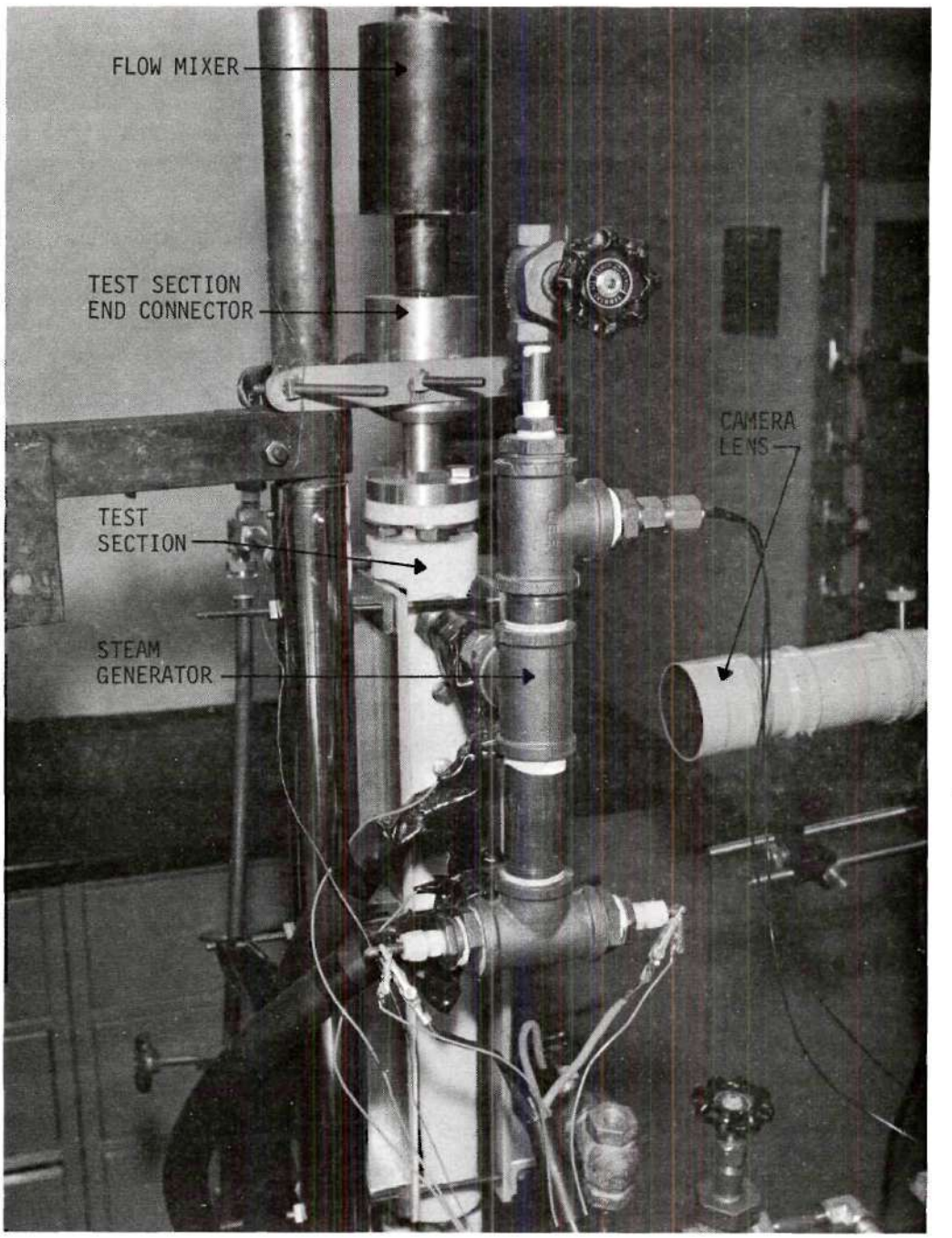

Figure 13. Steam Generator.

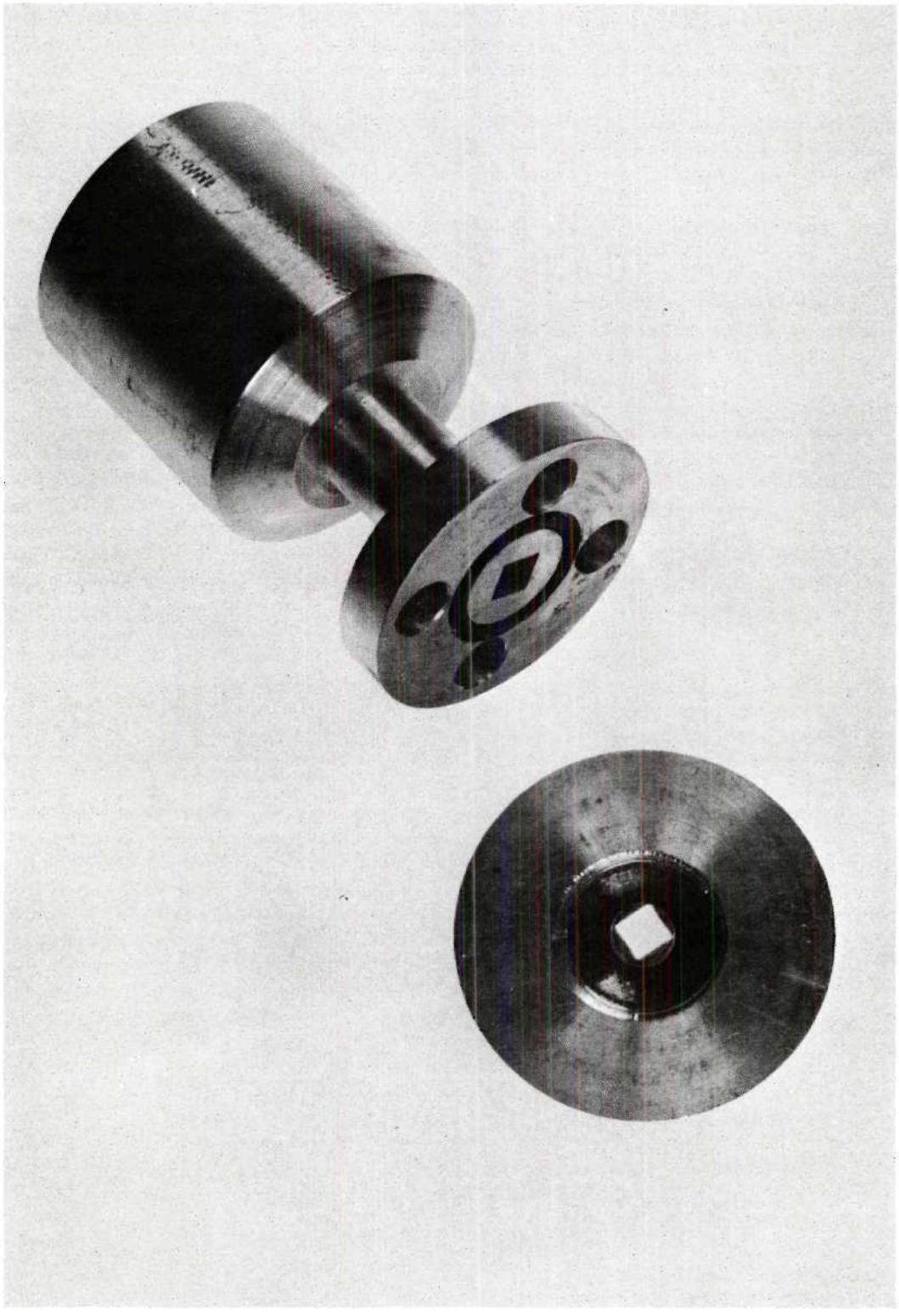

Figure 14. Test Section End Connectors.

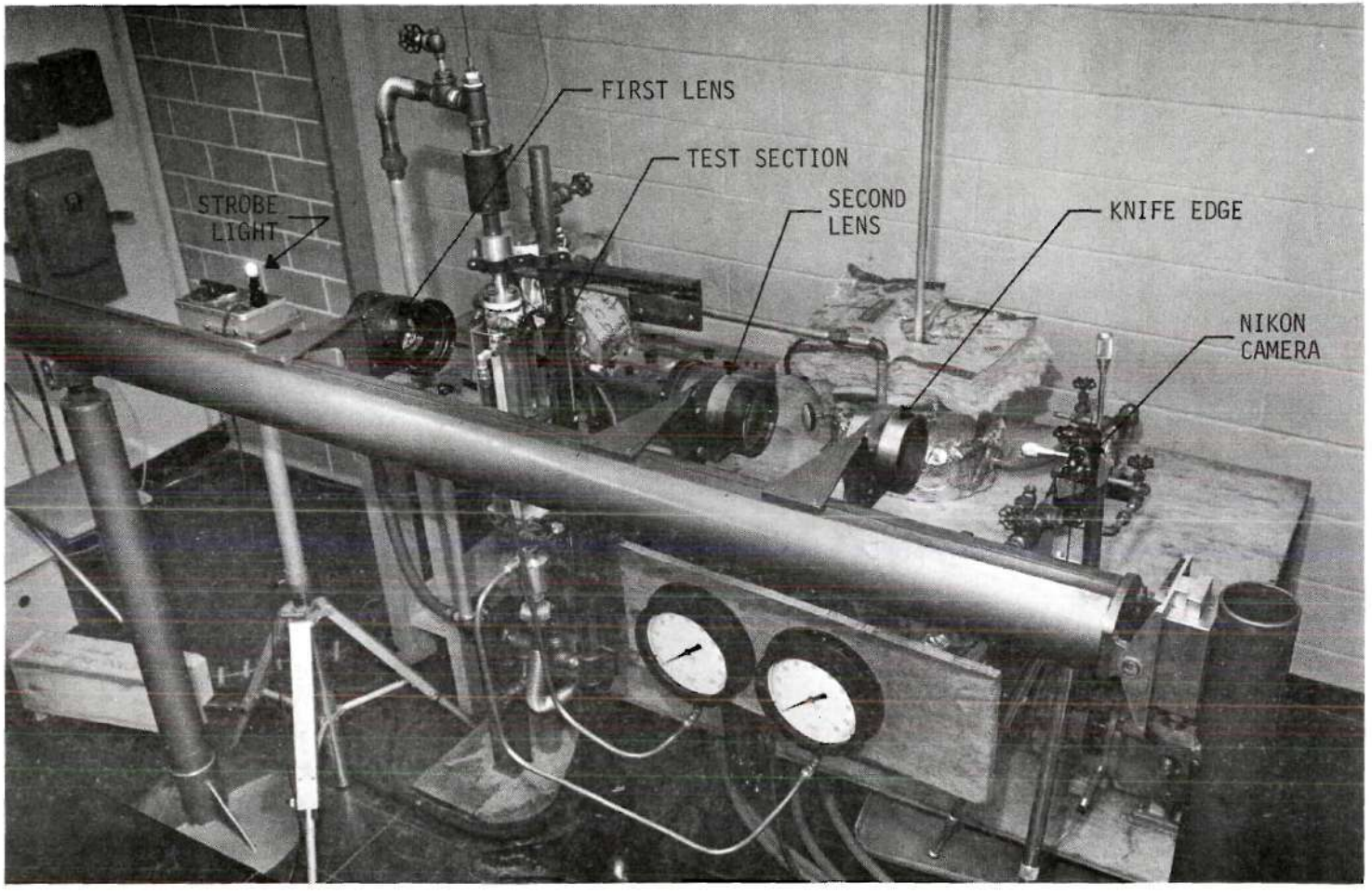

Figure 15. Schlieren System.

CHAPTER V

EXPERIMENTAL PROCEDURE

Single Bubble Experiment

Data Run

The loop was prepared for the test runs by first filling the system with distilled water and then draining it. This was done several times in an effort to clean out any foreign matter which might have accumulated. Next, distilled water was passed through an ion exchanger and then into the loop storage tank. After the system was filled, power was applied to the storage tank heater until the water began to boil. This was done in an effort to degas the water. The time required to boil the water was several hours since the power available to the tank heater was only two kilowatts. The resulting dissolved oxygen content was then of the order of six parts per million as indicated by the YSI model 51 oxygen meter.

Next, water was prepared for the steam generator by boiling 1000 cubic centimeters of distilled-deionized water down to a volume of approximately 500 cubic centimeters. This procedure reduced the dissolved oxygen content to less than one part per million. The steam generator was then slowly filled with this water making sure that no air was trapped. Then the steam generator valve was closed.

Next, the desired electrical power input was applied to the steam generator. The current input was determined by measuring the voltage drop across a precision shunt in series with the resistance heater. The

voltage drop across the resistance heater was also measured and from these two values the power input could be determined. During the initial heating period, a small jet of hot liquid came from the injection hole in the heated strip. (This was observed during the preliminary runs with the aid of the schlieren system.) After approximately 30 minutes, depending on the power input, the hot liquid jet was replaced with a steady stream of rapidly growing and collapsing vapor bubbles.

At this point, the by-pass valve and the test loop valves were shut off and the pump was started. In this condition, the pressure gauge at the pump outlet indicated approximately 80 psi. This was reduced to approximately 40 psi by opening the by-pass valve an appropriate amount. At this point any velocity (up to approximately 35 ft/sec) could be obtained in the test section by adjusting the test loop valves. To obtain velocities above 35 ft/sec, the by-pass valve had to be closed an appropriate amount. The velocity in the test section was obtained by noting the pressure drop across the orifice and using the calibration curves. Orifice plate No. Y63931 was used in the high velocity runs while No. Y63933 was used in the low velocity runs.

After adjusting the velocity to the desired value for a particular run, it was noted that the bubbles had stopped forming. This was due to an increase in the system pressure when the pump was on. At this point, another waiting period (approximately 30 minutes) was necessary while the pressure in the steam generator built up enough to again cause bubbles to form. During this period, the temperature in the storage tank was adjusted to the desired value by running hot or cold city water through the copper coil in the tank. Next, for runs which required the presence of a thermal

boundary layer, the DC rectifier was turned on. Power was slowly applied to the heater strip by turning the dial on the three phase Variac in small increments. At each step, the heating strip was observed for surface boiling. Once boiling was visually observed, the power input was reduced slightly to suppress the boiling. (It was decided not to allow actual boiling during the run as this might have interferred with photographing the artificial bubble.) Following this procedure, a temperature distribution which approximated the real boiling case was produced.

After adding power to produce the thermal boundary layer, it was necessary to readjust the temperature in the storage tank. By allowing a continuous flow through the copper coil, a steady state was obtained. The cooling capacity of the cooling coil was large enough that, for the runs made, the cooling capacity of the heat exchanger was not required.

While power was applied to the steam generator, the voltage output of the steam generator thermocouple was monitored with the potentiometer. This yielded the inside temperature and, since the condition inside the generator was saturation, the corresponding inside pressure was available. For quick determinations, a plot of thermocouple voltage output versus pressure was prepared. During equipment check-out and preliminary test runs, the steam generator pressure was not allowed to exceed 100 psia. During the test runs, it was not necessary to exceed 50 psia.

After the steam generator temperature had reached a steady value, the following quantities were observed and recorded: voltage across the heater strip shunt, voltage across heater strip, voltage across the steam generator resistance heater shunt, voltage across the steam generator resistance heater, pressure drop across the orifice, absolute pressure at

the inlet to the test section, absolute pressure at the exit of the test section, room temperature, and barometric pressure. At this point, the temperature in the storage tank was readjusted to the desired value, if required. This value was then recorded.

Next, high speed motion pictures of the artificial bubbles were obtained. This was accomplished using a Fastax camera with a 152 millimeter Bell and Howell lens set at f/11. A bellows extension was used between the lens and the camera. The film used was Dupont 931A-Reversal, perforated for the Fastax camera, which was processed as reversal. The framing rate was set at 8,000 frames per second. The actual framing rate was determined from timing marks produced at 60 cycles per second. The bubble was silhouetted by means of a cloudy plastic sheet placed behind it and a Sylvania high speed flash bulb pointed directly into the camera through the plastic sheet.

After the high speed motion pictures were obtained, the voltage output from the thermocouple, which indicated the bulk temperature of the fluid at the exit of the test section, was recorded. Then the voltage output from the steam generator thermocouple was recorded. Next, the inlet water temperature or the velocity was changed to the desired value for the next run. After two runs were completed, the power inputs were stopped and the pump turned off. It was found during preliminary test runs that, if a third run was attempted without refilling the steam generator with water, the generator would run dry and the resistance heater would burn out.

Five runs were made in this manner with a thermal boundary layer present. The first three were with a velocity of 25.5 ft/sec and tempera-

tures of 80°F, 110°F, and 140°F. The other two runs were made with a water temperature of 110°F and the velocities were 12 ft/sec and 39 ft/sec. Four runs were made without a thermal boundary layer present. These were made with a water temperature of 110°F and at velocities of 0.25, 0.75, 1.80, and 27.0 ft/sec.

Steam Generator Calibration

The object of the steam generator calibration was to relate the heat loss from the steam generator to its operating conditions. The first method tried was to measure (a) the electrical power input and (b) the energy output associated with the steam leaving the generator system. The latter measurement was attempted by a direct measurement of the volume increase of the steam condensate. The difference in these two quantities was the heat loss to the surroundings. These measurements were performed with the steam generator and test section in normal configuration with the rest of the system. One exception was a graduated glass tube which was inserted into the flow line above the cooling fluid mixer (see Figure 6). The top end of this glass tube was open to the atmosphere. With the steam generator in operation, the change in water level in the glass tube was observed over a period of time. From this measurement, the volume rate of condensed steam being produced could be calculated. However, since this method did not allow forced flow through the test section, the calibration did not account for the change in the heat transfer mechanism on the heated strip in going from free convection (calibration condition) to forced convection (test condition). Thus, a second method was used which allowed the calibration to be made with forced flow in the test section. This was accomplished by stopping up the steam bleed line from the generator to the

heater strip with a rubber stopper. Thus, since there was no steam output, the heat loss was equal to the heat input (at steady state). These runs were made by first applying power to the generator. Next, the power input was measured by obtaining the voltage drop across (a) the heater coil and (b) the precision shunt in series with it. The voltage output from the steam generator thermocouple was monitored and when steady state was obtained this value plus the room temperature were recorded. Next, the power input was changed and the procedure repeated. The heat transfer conditions in the test section were free convection for one set of runs and forced convection (with a velocity of 35 ft/sec and a bulk temperature of 70°F) for another. These two conditions represented the extremes of the heat removal rate from the generator by the cooling fluid. The resulting curves of heat loss versus difference in temperature between the steam generator and the room are shown in Figure 16. For the test runs made in measuring the bubble heat transfer coefficient, the heat loss from the generator was between the values indicated by the two limiting curves.

Schlieren Experiment

In obtaining schlieren photographs, the first step was to adjust the location of the light source. It was placed at the focal point of the first lens. This was done with the light source pulsing at about 10,000 cycles per minute and the position could be checked by observing the light leaving the lens to see if it was parallel. Next, the position of the second lens was adjusted so that the image would be in focus roughly at the location of the camera. The knife edge was then placed at the focal

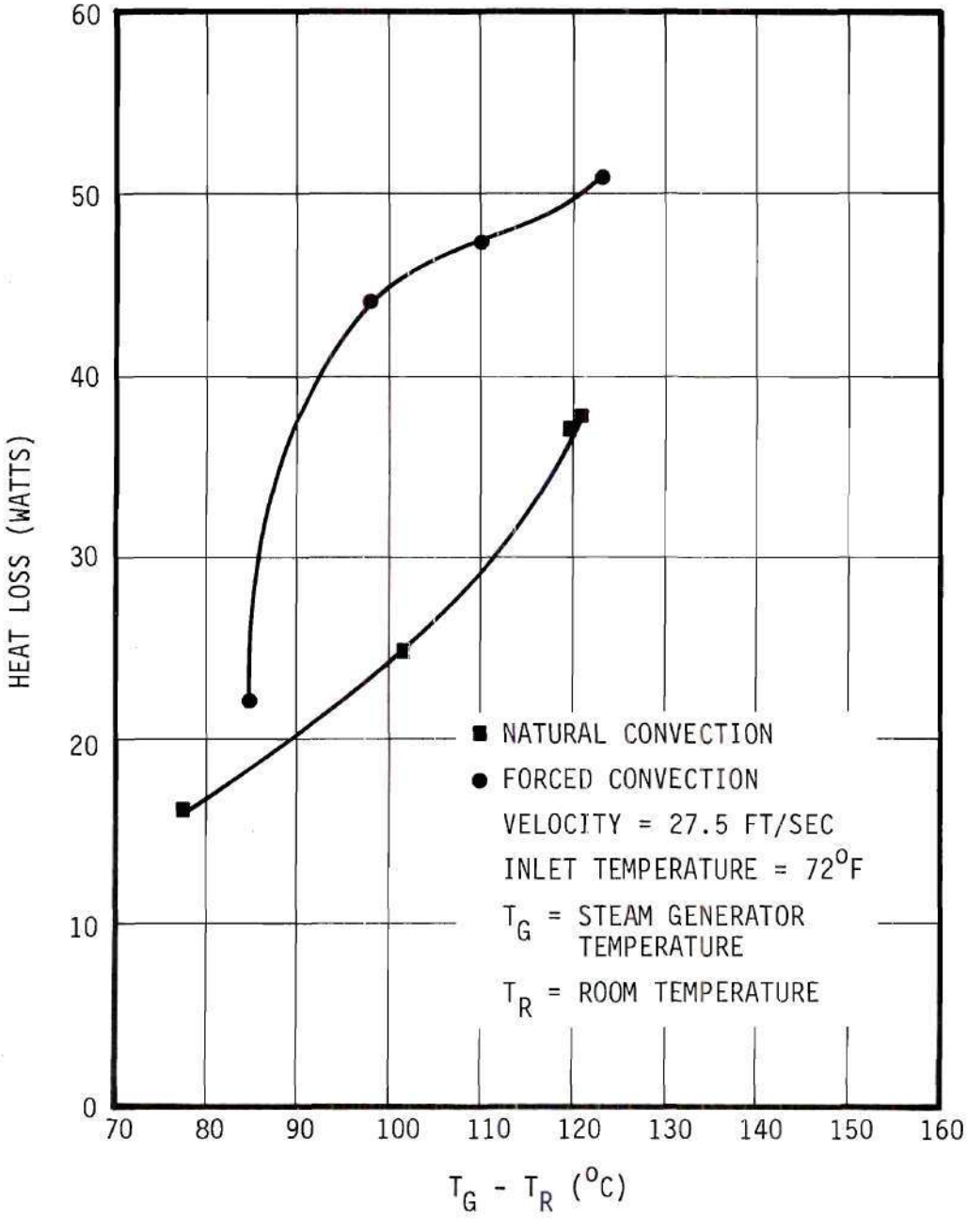

Figure 16. Steam Generator Calibration.

point of the second lens so as to cut off approximately one-half of the beam. Next, the power supply to the heater strip was energized and a small amount of power was applied to the strip until small air bubbles began to appear on the heater surface. Next, the camera was adjusted by varying its distance from the knife edge until these bubbles were in focus. At this time, the pump was started and the velocity and temperature of the water were adjusted to the desired values. The heat input was then increased until the desired degree of boiling was obtained. Next, the room was darkened and the strobe light was put in the single flash mode. A series of shots was then obtained by opening the camera shutter, flashing the strobe light, and then closing the shutter.

CHAPTER VI

DISCUSSION OF RESULTS

Single Bubble Experiment

Figure 17 shows a typical series of high speed photographs taken during this phase of the experiment (see Appendix A for others). From such photographs and other recorded data, the bubble heat transfer coefficient was calculated. The recorded data along with the calculated data are given in Appendix A, while sample calculations are presented in Appendix D. The results are summarized in Figure 18, which gives h_b as a function of velocity with temperature held constant and in Figure 19, which gives h_b as a function of temperature with velocity held constant.

Figure 19 shows that h_b decreases as temperature increases. This result is logical since, as the temperature is lowered, the ability to condense is increased, thus increasing the heat transfer. Figure 18 implies that, as the velocity is increased, h_b increases. This result seems logical, since an increase in velocity results in a faster removal of hot fluid from around the bubble due to bulk fluid transport. Since this fluid is replaced with colder fluid from upstream of the bubble, the average temperature around the bubble is reduced. Also, an increase in the velocity might increase the level of turbulence around the bubble which would result in faster heat removal and an increase in h_b. Figure 18 also shows that, when the velocity is below two ft/sec, the effect of the velocity becomes negligible. This effect seems probable as the motion of the

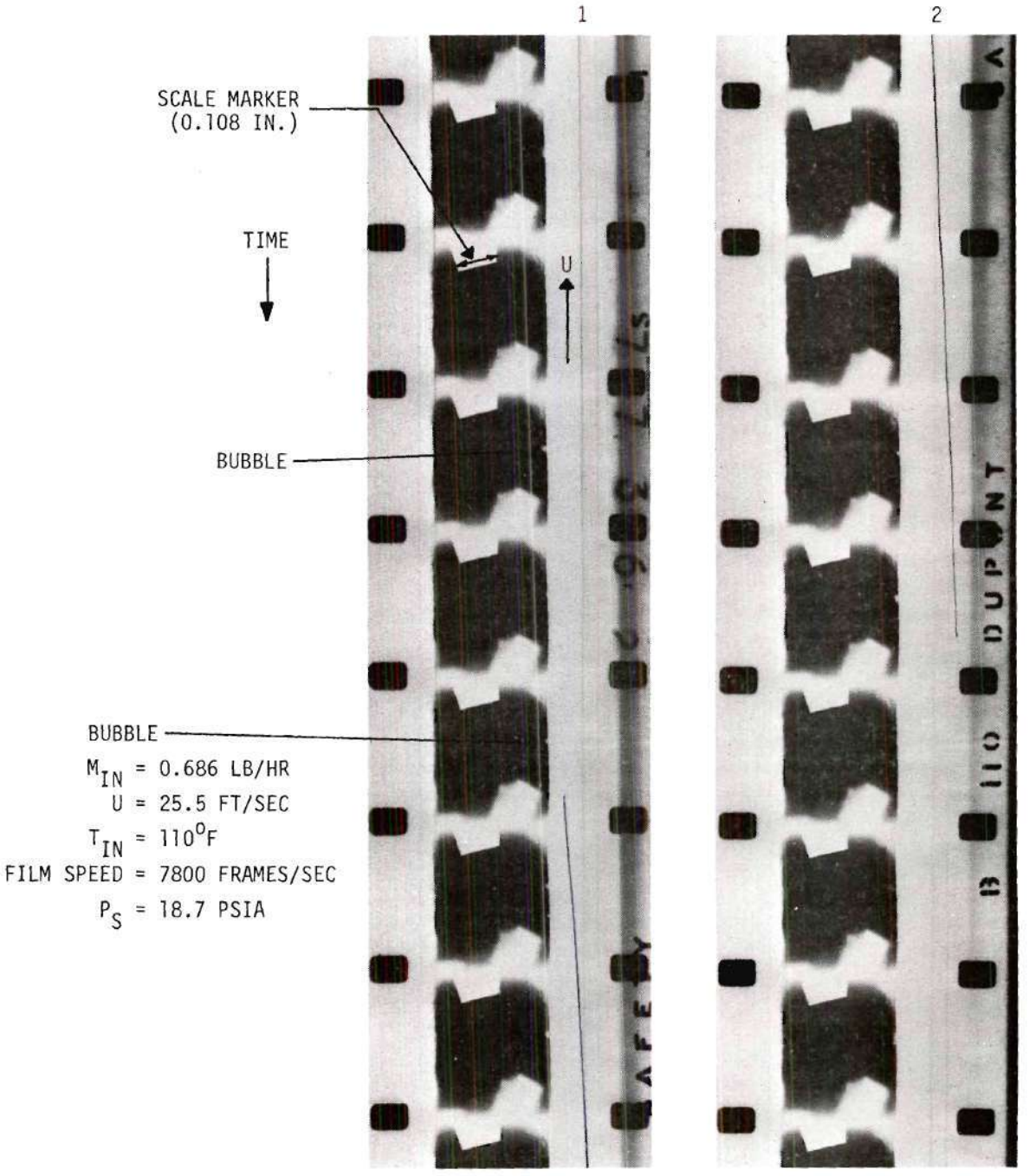

Figure 17. High Speed Photographs of Run No. 5.

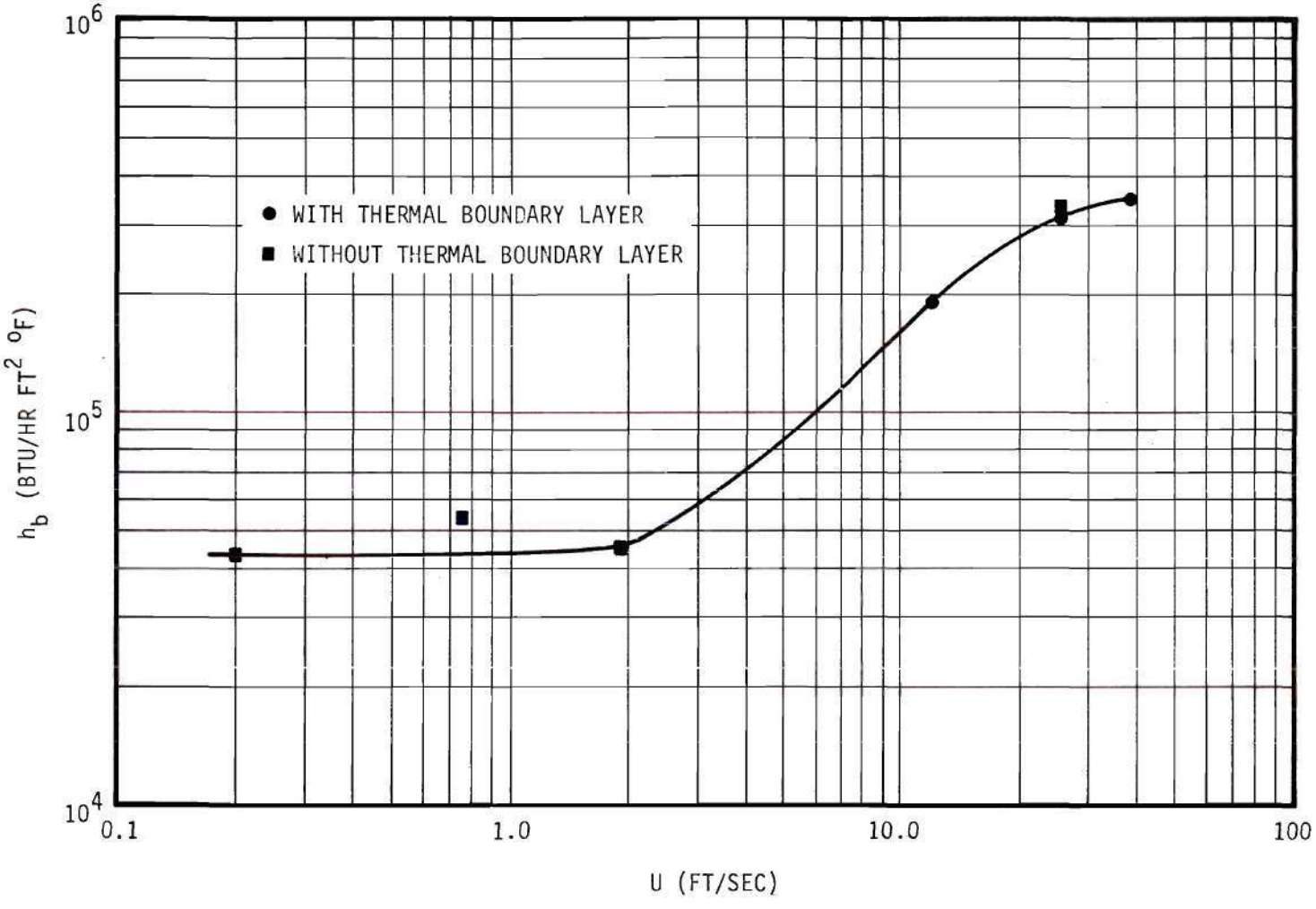

Figure 18. Bubble Heat Transfer Coefficient as a Function of Cooling Stream Velocity with a Bulk Temperature of 110°F.

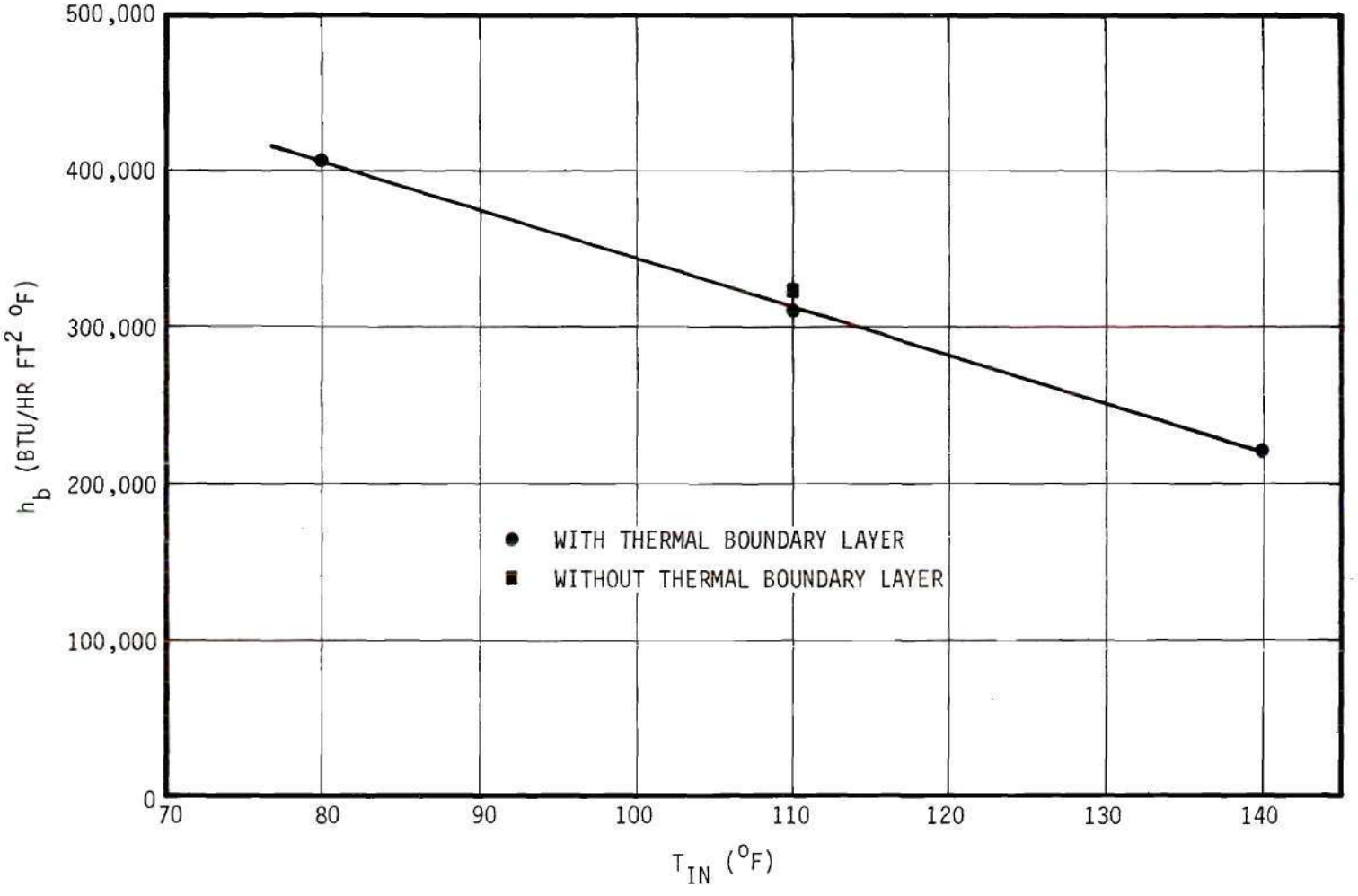

Figure 19. Bubble Heat Transfer Coefficient as a Function of Cooling Stream Temperature with a Velocity of 25.5 ft/sec.

fluid due to the bubble motion during growth and collapse might cause turbulence which would be independent of bulk fluid motion.

In Figure 18, the experimental point for a velocity of 0.75 ft/sec indicates a higher value of h_b than the two adjacent points. Inspection of the recorded data indicates that the water inlet temperature was 110°F for all three runs; however, the indicated outlet fluid bulk temperature for the 0.75 ft/sec run is, at approximately 108°F, two degrees lower than the other runs. Figure 19 shows that a two degree decrease in bulk temperature yields an increase in h_b of roughly 10^4 BTU/hr ft^2 °F. Since this value is approximately the difference between h_b for a velocity of 0.75 ft/sec and h_b for the adjacent data points, the recorded value for the inlet water temperature is probably in error for the case in question.

The Reynolds number for the 0.2 ft/sec run was approximately 892 and that for 1.9 ft/sec was 8,460. Thus, the first run was probably in the laminar flow regime and the second in the turbulent flow regime. However, h_b for each case was approximately the same value. This seems to indicate that the presence of normal pipe turbulence has a negligible effect on the heat removal from a single bubble.

Two runs were made with a velocity of 25.5 ft/sec and a bulk temperature of 110°F. The first was made using the normal procedure of providing a thermal boundary layer through which the bubble grew. The second was made without the presence of this thermal boundary layer. The resulting values of h_b were approximately the same. This indicates that the presence of the thermal boundary layer had a negligible effect. It has been argued that, because of a thin layer of hot fluid (whose origin could have been the thermal boundary layer) surrounding the bubble, a large amount

of condensation would not occur. However, this did not prove to be the case.

In some boiling heat transfer investigations in the past (31), it has been assumed that the total heat associated with a single bubble may be obtained from the observed volume of the bubble and by assuming that the state of the steam in the bubble is saturation corresponding to the system pressure.* To investigate the validity of this assumption, the heat associated with a single bubble was calculated in the manner just described. These results along with the known amount of heat input to the bubble are tabulated in Table 1. It was observed that the actual input varied from about 10 to 100 times more than that calculated with the simplifying assumption. Thus, any conclusions based on this simplifying assumption are certainly questionable.

For the case of real boiling, Gunther (15) reported that the relative velocity between the stream and the bubble wall was 0.2 times the stream velocity. In this experiment the bubbles were stationary with respect to the wall. Thus, the stream velocities in this experiment must be divided by 0.2 in order to obtain an equivalent stream velocity for real boiling. This equivalent velocity was used in a comparison of Q_{IN}/A versus the product of the one-half power of the velocity and the subcooling for the single bubble data of this experiment and the burnout data of Gunther (see Figure 20). For this experiment, the A represents the maximum surface area of the bubble (A_b) while for Gunther's data, the A refers to the

---

*See Appendix D for sample calculation.

Table 1. BTU Per Bubble: As Measured and As Based on Maximum Bubble Volume

Run No.	T_{IN} (°F)	U (ft/sec)	BTU/BUBBLE $\times 10^5$ (As Measured)	BTU/BUBBLE $\times 10^5$ (Max Bubble Vol)
5	110	25.50	4.49	0.0443
7	110	12.00	4.42	0.0974
8	110	25.50	4.40	0.0422
9	80	25.50	5.54	0.0305
10	140	25.50	5.49	0.1620
11	110	38.20	5.00	0.0494
12	110	0.20	1.11	0.1040
13	110	0.75	1.13	0.0758
14	110	1.90	1.12	0.0985

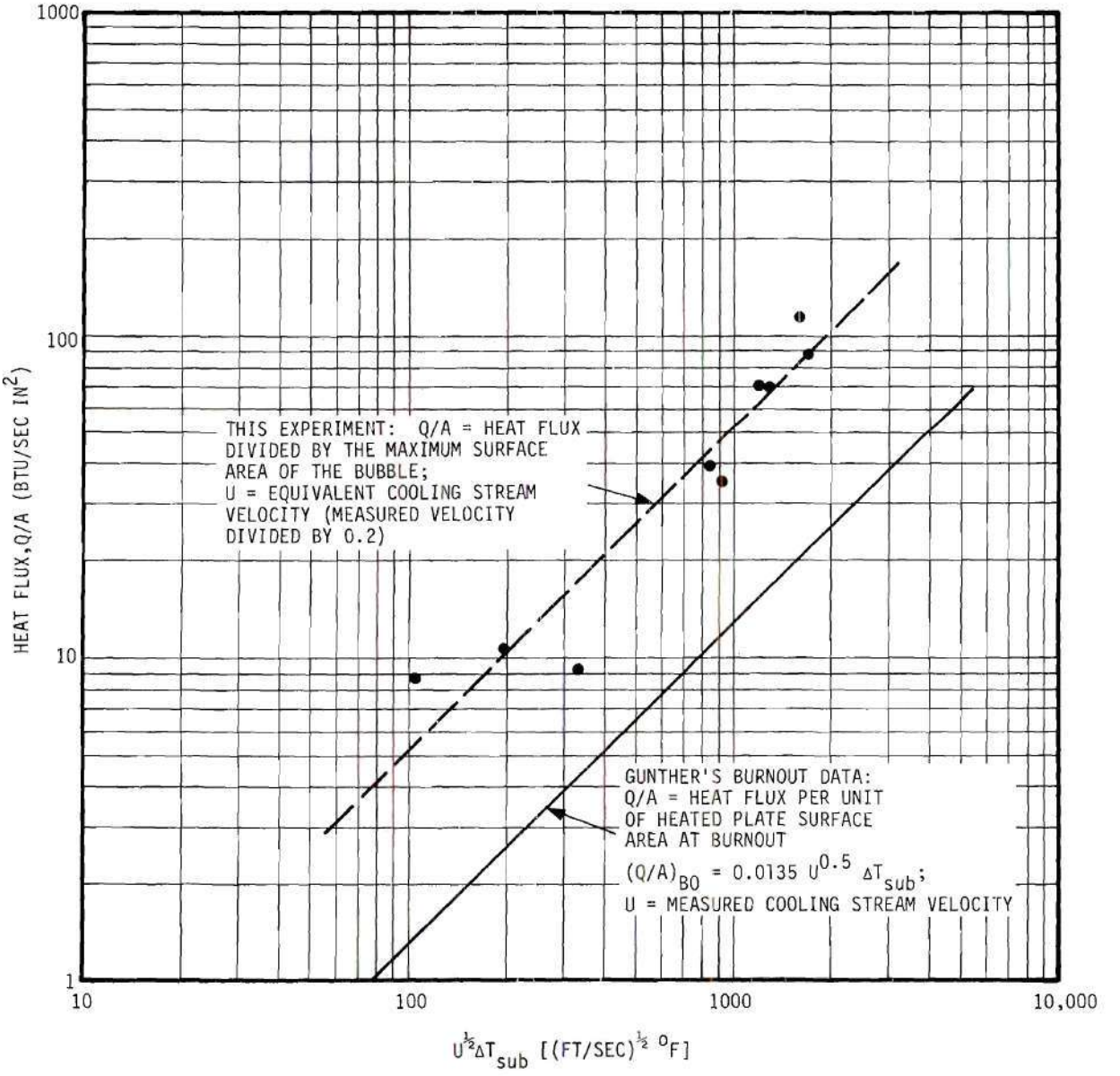

Figure 20. Heat Flux as a Function of Subcooling Times the One-Half Power of the Velocity: Gunther's Burnout Data (15) and this Experiment.

surface area of the heated plate. The solid line in Figure 20 represents Gunther's burnout data, while the dashed line was drawn through the data points of this experiment. Figure 21 represents the same comparison with Bankoff's (7) single bubble experimental results except that A represents the average surface area of the bubble. The ordinate for the experimental points in Figure 20 and in Figure 21 is about a factor of four greater than Gunther's data. This number could be a reasonable value for the ratio of the plate surface area to the time averaged surface area of the bubble population. One is led to the conclusion that the mechanism of heat transfer at the critical heat flux (burnout) is that of mass transfer across the bubbles.

Schlieren Experiment

Figures 22 through 28 show the results of the schlieren experiment. These photographs were obtained with a velocity of 20 ft/sec and an inlet water temperature of 125°F. In Figure 22 the power input was zero which resulted in no temperature differences; thus, the turbulence is not visible. However, in Figures 23 and 24, the heat input was 1.28×10^5 BTU/hr ft^2 and boiling had not started. The level of turbulence is visible in these photographs. In Figures 25 and 26, the heat flux had been increased to 9.86×10^5 BTU/hr ft^2. Subcooled nucleate boiling was taking place since a high frequency crackling sound was coming from the test section. The heat flux was approximately 34 percent of the burnout value, which was calculated as suggested by Gunther (15). The level of turbulence here seems to be much higher than in the non-boiling case. However, this is not a positive conclusion, since as the heat flux is increased the ability

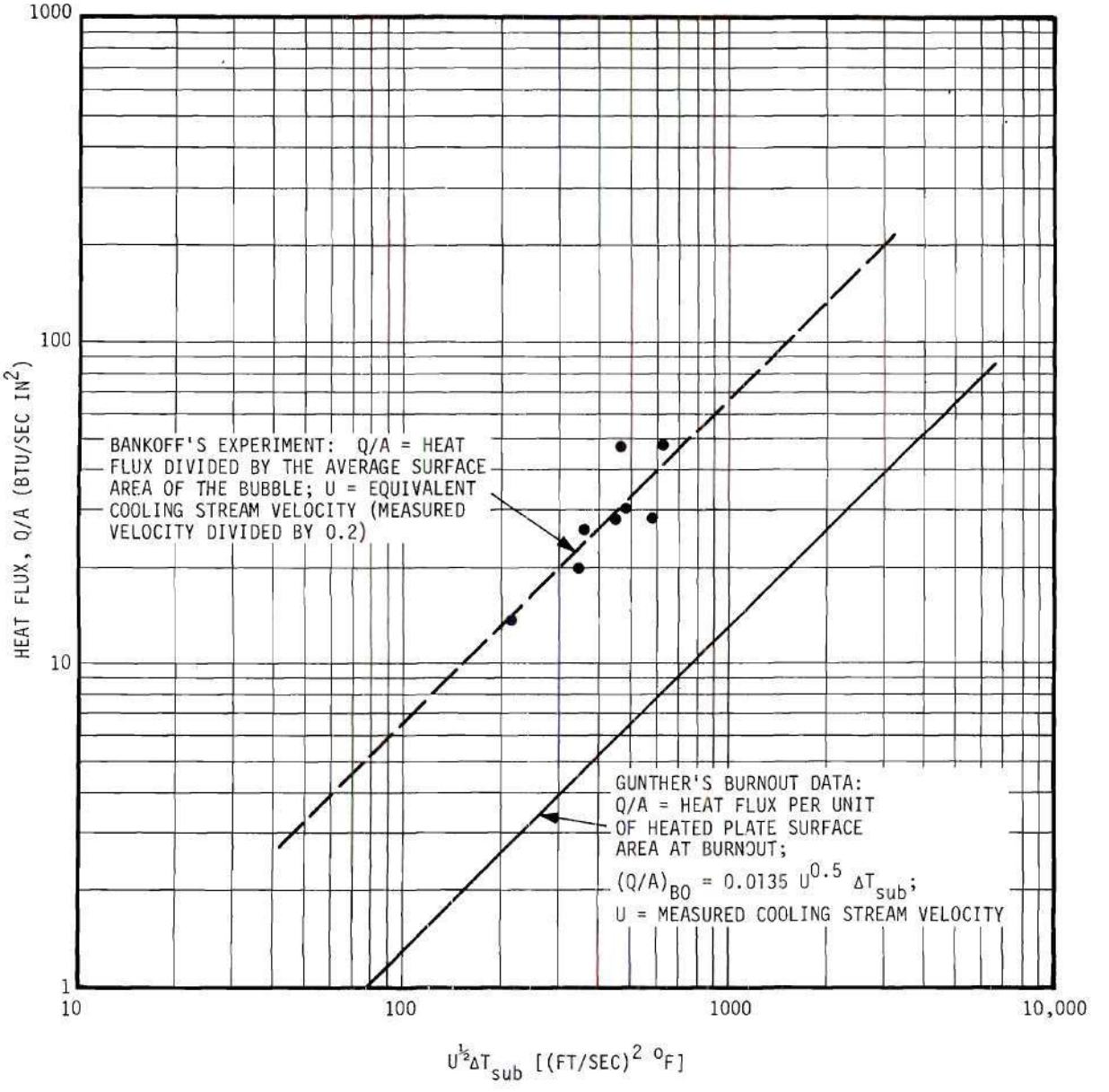

Figure 21. Heat Flux as a Function of Subcooling Times the One-Half Power of the Velocity: Gunther's Burnout Data (15) and Bankoff's Experiment (7).

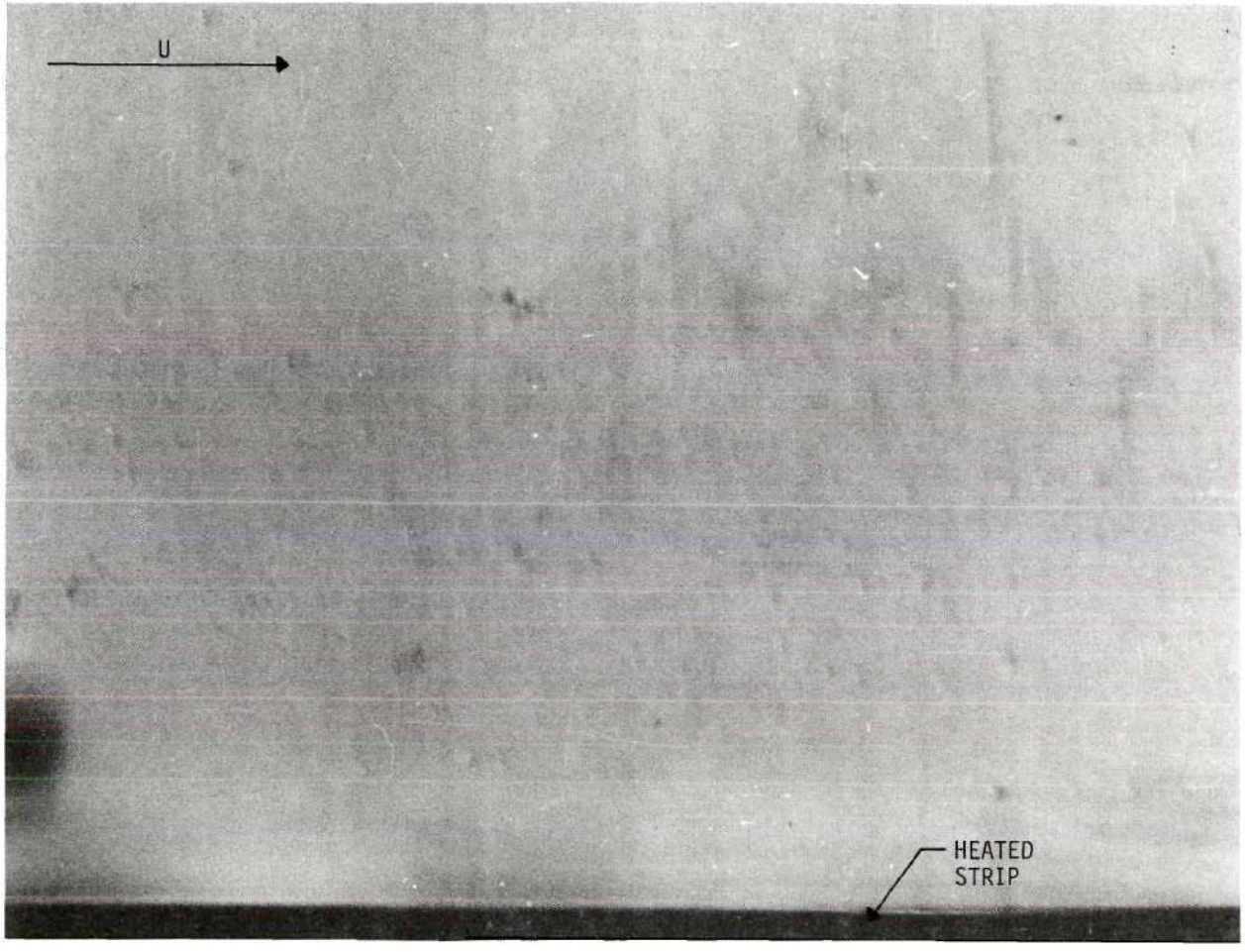

Figure 22. Schlieren Picture No. 3: Velocity, 20 ft/sec; Inlet Temperature, 125°F; Heat Flux, 0 BTU/hr ft^2.

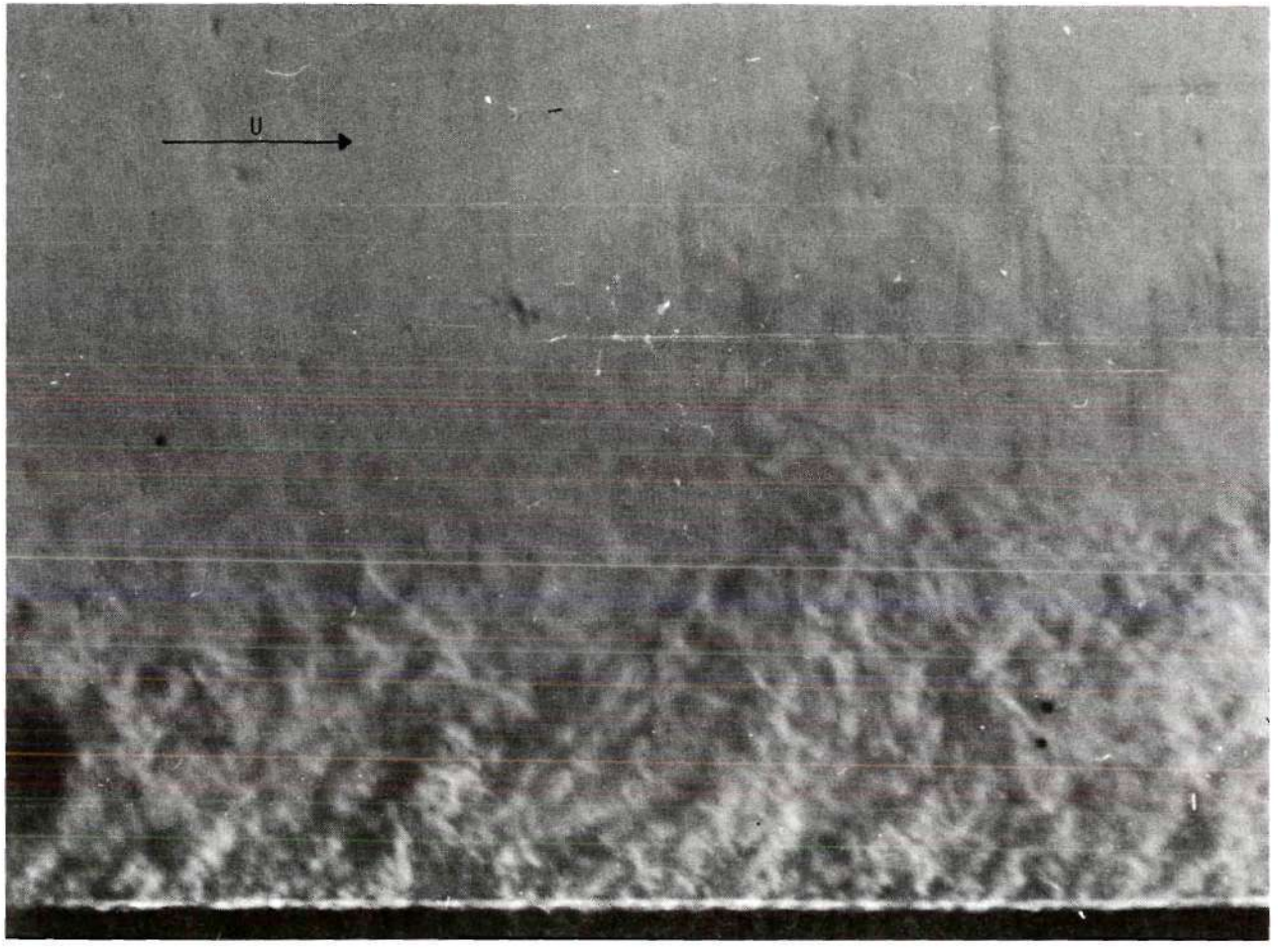

Figure 23. Schlieren Picture No. 4: Velocity, 20 ft/sec; Inlet Temperature, 125°F; Heat Flux, 1.28 X 10^5 BTU/hr ft^2; Heated Surface Temperature, 242°F.

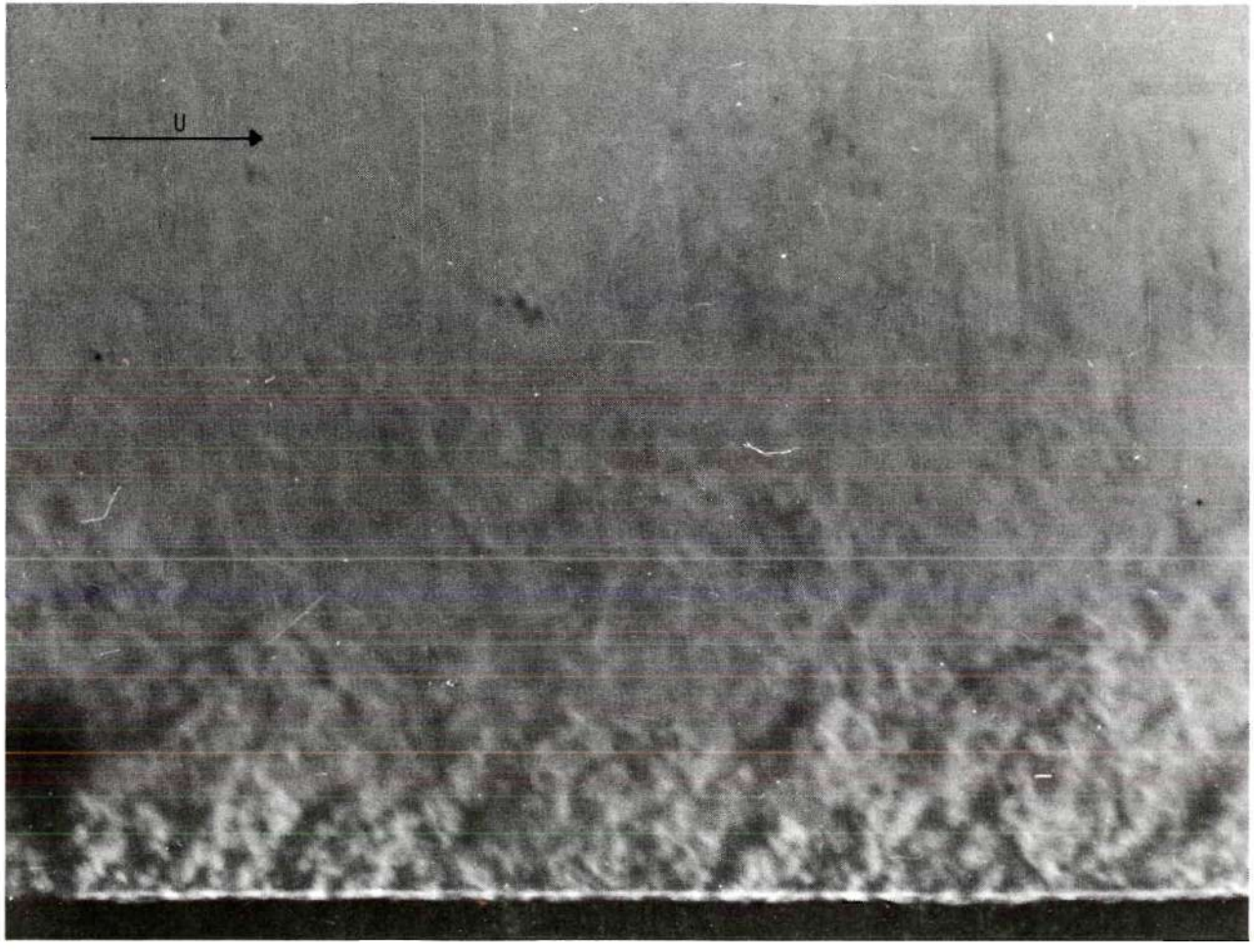

Figure 24. Schlieren Picture No. 5: Velocity, 20 ft/sec; Inlet Temperature, 125°F; Heat Flux, 1.28 X 10^5 BTU/hr ft^2; Heated Surface Temperature, 242°F.

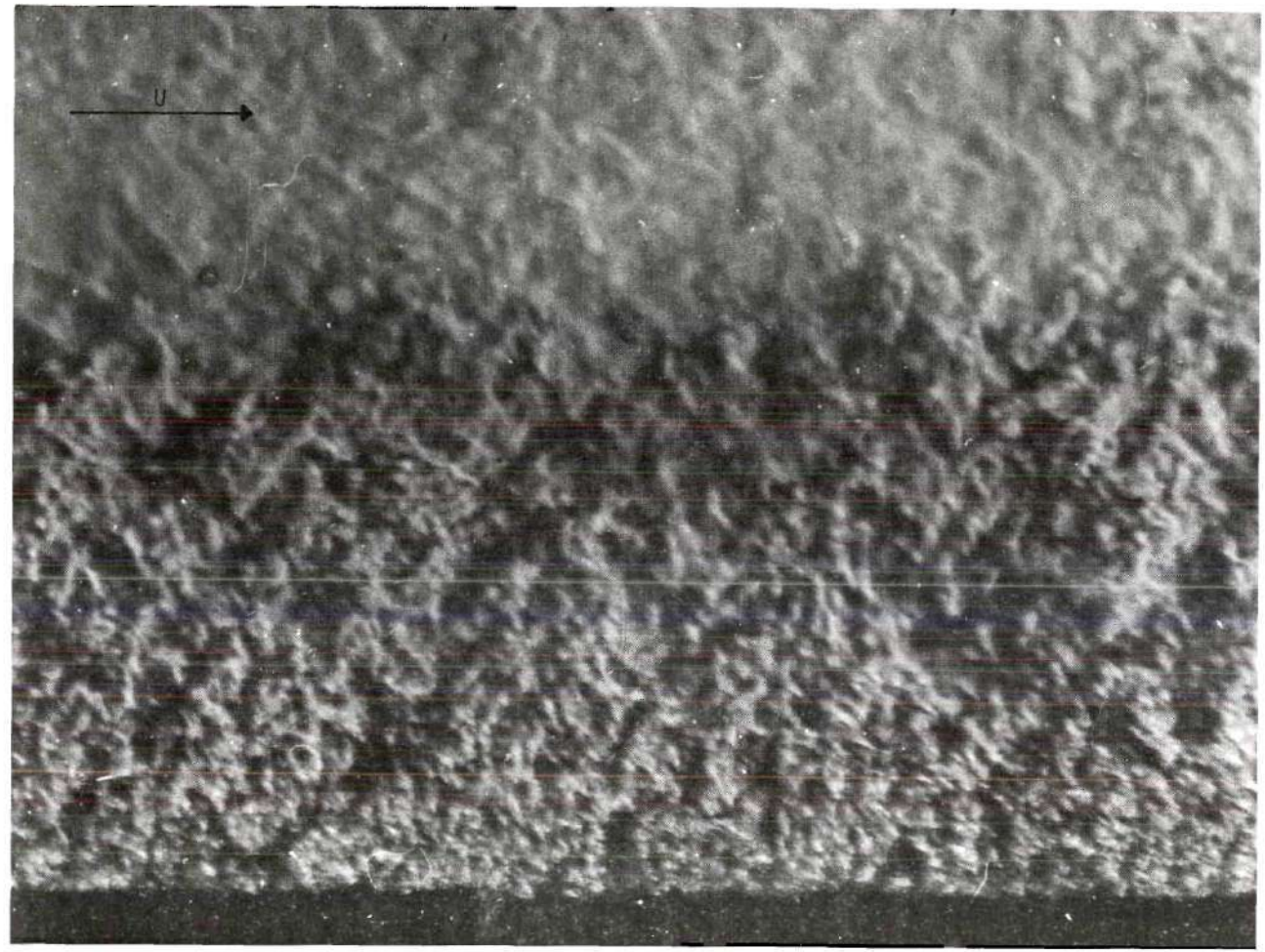

Figure 25. Schlieren Picture No. 7: Velocity 20 ft/sec; Inlet Temperature, 125°F; Heat Flux, 9.86 X 10^5 BTU/hr ft^2; Heated Surface Temperature, 330°F.

Figure 26. Schlieren Picture No. 8: Velocity, 20 ft/sec; Inlet Temperature, 125°F; Heat Flux, 9.86 X 10^5 BTU/hr ft^2; Heated Surface Temperature, 330°F.

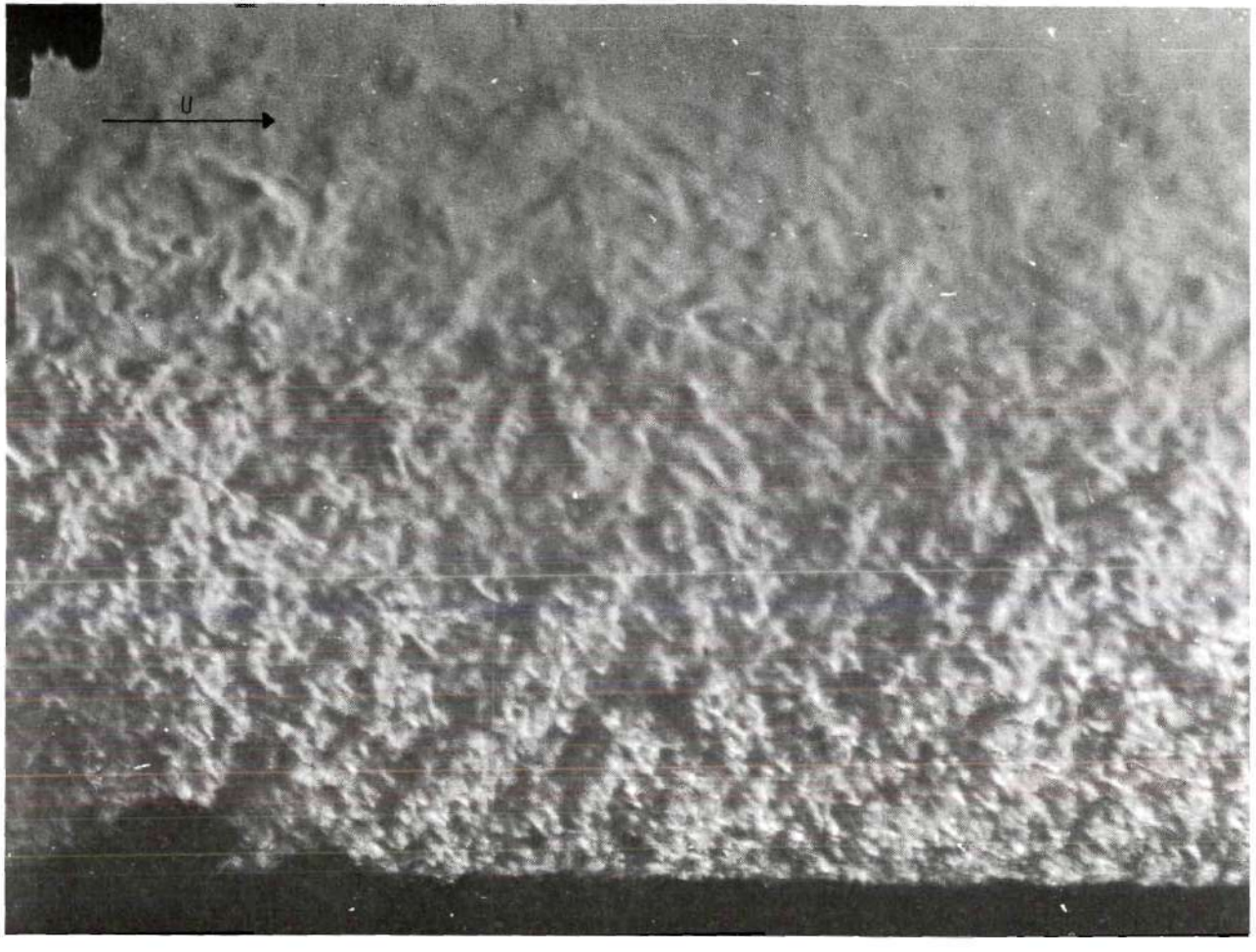

Figure 27. Schlieren Picture No. 16: Velocity, 20 ft/sec; Inlet Temperature, 125°F; Heat Flux, 19.3 X 10^5 BTU/hr ft^2; Heated Surface Temperature, 384°F.

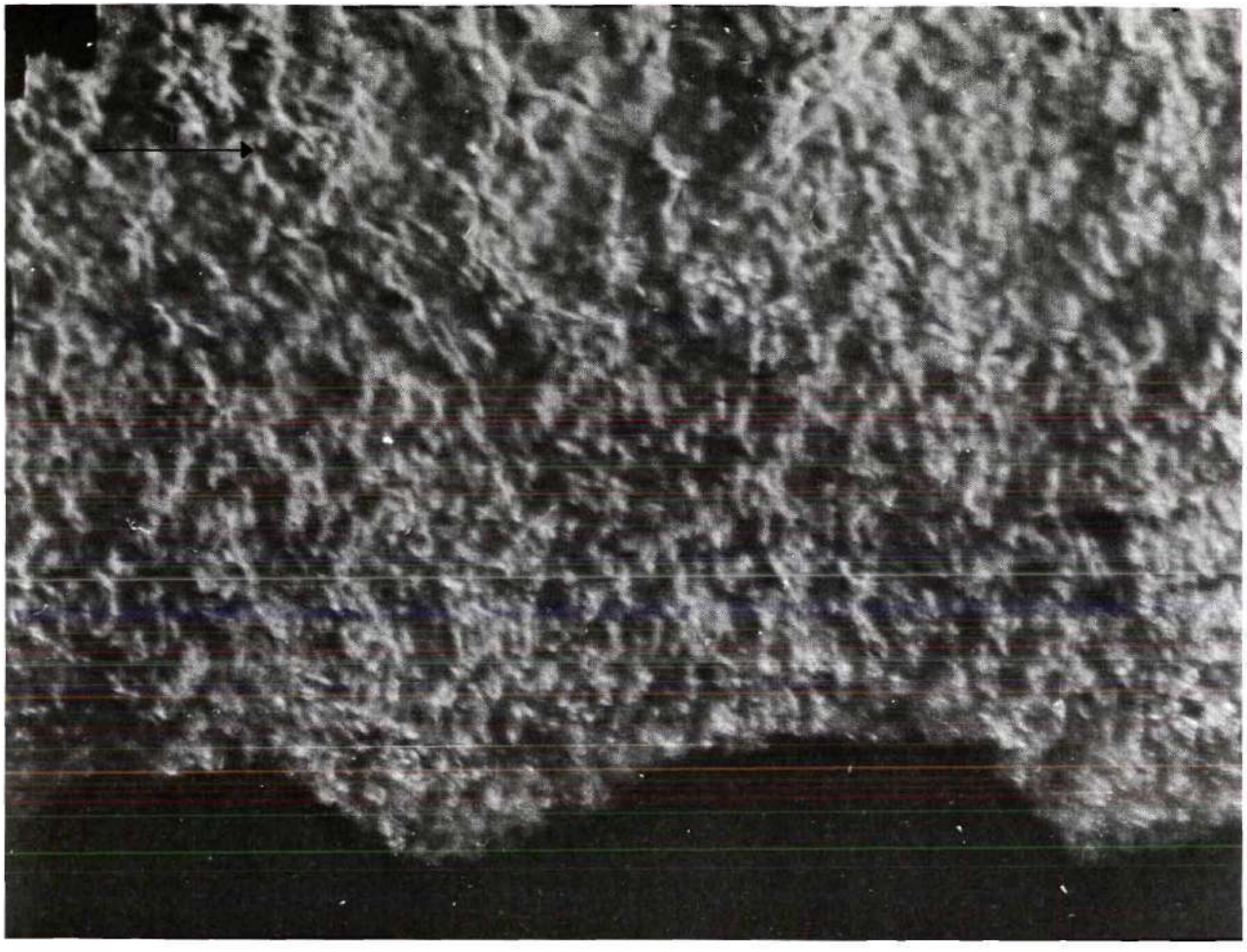

Figure 28. Schlieren Picture No. 17: Velocity, 20 ft/sec; Inlet Temperature, 125°F; Heat Flux, 19.3 X 10^5 BTU/hr ft^2; Heated Surface Temperature, 384°F.

to distinguish turbulence increases. This increase in ability occurs, since the temperature gradients are larger. Figures 27 and 28 show the schlieren effect with the heat flux at 1.93×10^6 BTU/hr ft^2 or approximately 67.0 percent of the burnout point.

Figure 29 shows the result of an early attempt to develop the method of obtaining schlieren photographs. The situation was that of pool boiling. It is not believed that this was a true schlieren effect. However, it appears that some effect of the temperature distribution was present. Figures 30 and 31 show the results of other attempts to develop the method. Here the boiling was occurring under forced convection. Since these runs were aimed at perfecting the technique of obtaining schlieren photographs, no measurements were made. However, in obtaining these photographs, the procedure was to increase the heat flux until the larger bubble began to appear. It was estimated that this point was of the order of 50 percent of the burnout heat flux. In any event, the size of the bubbles may be estimated, since the width of the channel is known to be 3/8 inch.

The photographs show that there are a substantial number of large bubbles which have a height above the plate of approximately 0.01 inch to 0.04 inch. Also, there are a large number of smaller bubbles visible with a height above the plate of approximately 0.005 inch or smaller. At first it was thought that each of the smaller bubbles grew to the larger size. However, this was shown to be false, since in some cases approximately four small bubbles were seen in the same area as one large one. Of course, since the bubbles were observed only from one side, it might be argued that the smaller bubbles were distributed across the width of the heated strip;

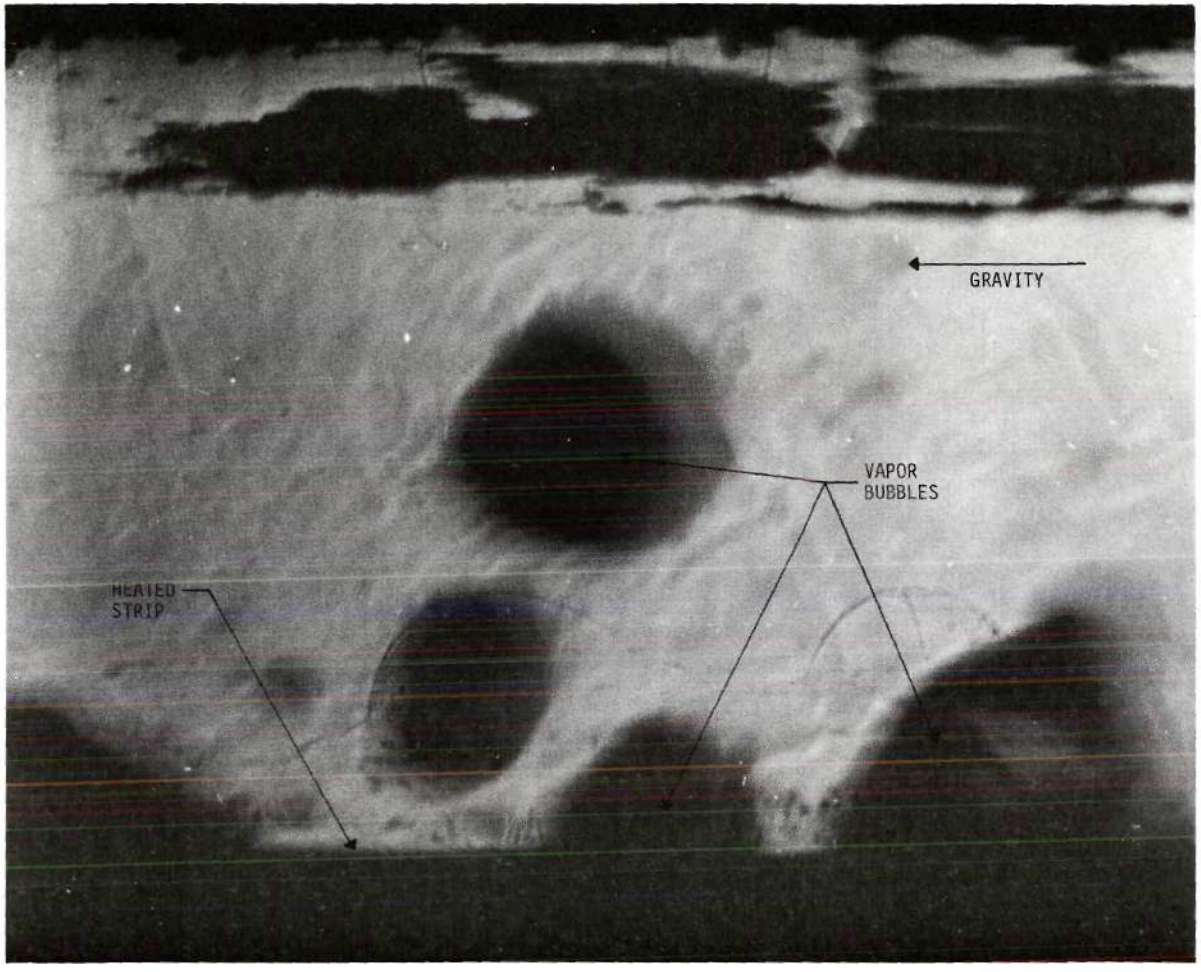

Figure 29. Attempted Schlieren Photograph: Pool Boiling.

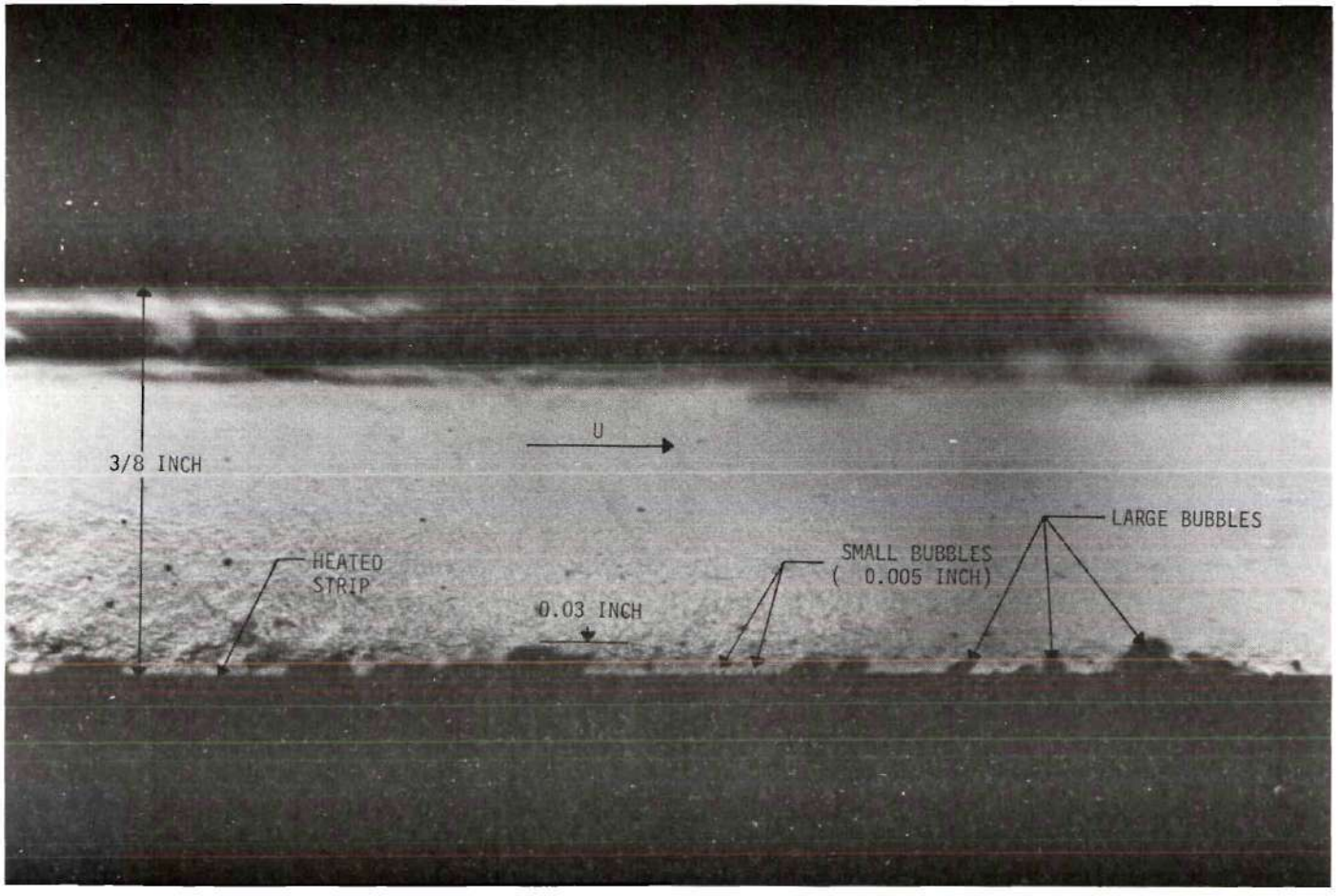

Figure 30. Attempted Schlieren Photograph: Forced Convection Boiling.

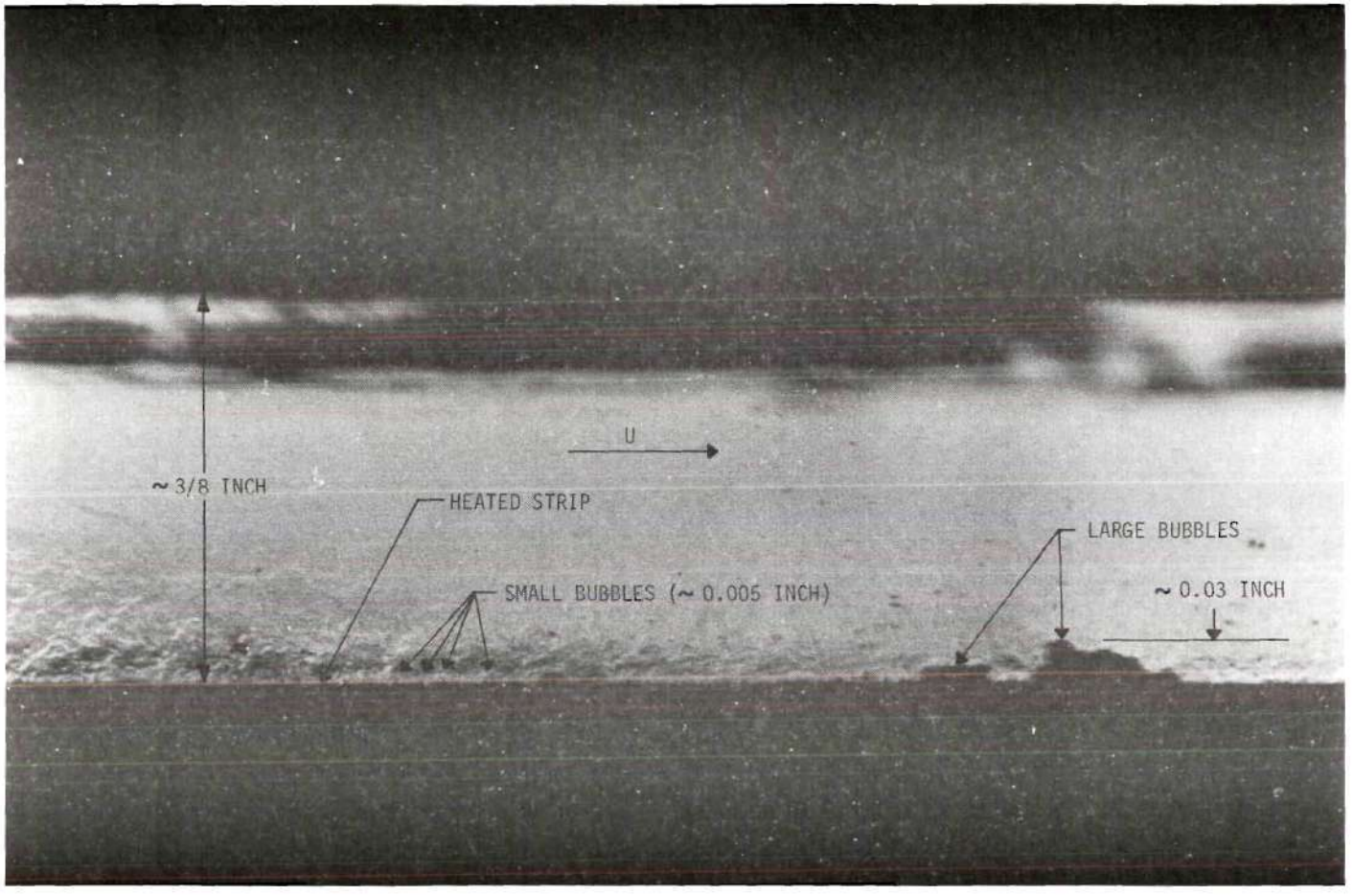

Figure 31. Attempted Schlieren Photograph: Forced Convection Boiling.

thus allowing room for each small bubble to grow into a larger one. However, if each small bubble grew to be a larger one, the population of large bubbles should be the same as the population of the small bubbles. But, the small bubbles out numbered the large bubbles approximately four to one. Thus, it was concluded that not all small bubbles grew to produce large ones.

There seem to be two general sizes of bubbles, and it is believed that this observation has not been made before in other boiling investigations. It is thus in order to try to discredit the existence of one of these general groups of bubbles. First, it may be argued that the smaller bubbles were actually air bubbles. However, this is not believed to be the case for several reasons. In the first place, if these were air bubbles, they would not have collapsed but would have left the heated surface and gone into the cooling stream. However, none were seen leaving the heated surface nor was there an appreciable number observable in the cooling stream near the heated plate. (Some black specks appear in the cooling stream. These are uniformly distributed throughout the stream and if they are air bubbles their origin does not appear to be the heated surface.) Also, if the smaller bubbles were air bubbles, then the source of the crackling sound, which came from the test section at the lower heat fluxes where there were no large bubbles, was unknown. Since the air bubbles would not collapse, the only apparent source for the crackling sound was the growth and collapse of vapor bubbles. Thus, the small bubbles observed here seem to be vapor bubbles.

Next, it might be argued that the larger bubbles could have originated beneath the heated plate where some cooling liquid might have been

trapped between the plate and the Teflon test section wall. Thus, they would not be considered normal vapor bubbles. Also, it must be reported that at very high heat fluxes, it appeared that some vapor was coming from beneath the plate and around the edge. This observation was made with the unaided eye, and since the bubbles lasted only about 1/2 millisecond, the confidence in this observation is extremely low. In any event, the sizes that were observed here may be compared to those observed by Gunther (15). In his experiment, the radii of the bubbles were observed to be in the range of from 0.005 inch up to 0.025 inch. Since the bubbles observed here were in approximately the same range, it seems probable that all the bubbles observed were normal vapor bubbles.

Assuming this to be the case, it is in order to attempt to explain the four to one relationship between the small bubbles and the large ones. First, it seems possible that several small bubbles could combine to form a larger one. Whereas, if a small one is growing by itself, it may remain small. Alternately, Snyder (35) suggested that the presence or absence of a turbulent eddy near the bubble site may affect its ultimate size. Also, the reason for the four to one relationship might be due to the interaction of the small bubble population with the turbulent field of the cooling fluid. Perhaps when some statistical quantity (such as temperature or velocity) is high or low, the bubble grows to be a large one; whereas, if this quantity is at the opposite end of its spectrum, the bubble remains small. These hypotheses are, of course, highly speculative.

It should also be mentioned that after taking the photographs in this part of the experiment, the following trend was observed. As the

heat flux was lowered, the number of large bubbles began to decrease, and a definite heat flux was reached below which no large bubbles were produced. There seemed to be a "quantum jump" in the boiling phenomena at this point. The size of the large bubbles might have decreased as the heat flux was lowered; however, this did not occur. Again, since a detailed investigation of this point was not made, this observation is not definite.

The object of this schlieren experiment was to observe the temperature gradients around individual bubbles. This may be done from Figures 27 and 28. Other photographs taken during the initial attempts to develop the method of taking schlieren photographs are given in Appendix A.

Bubble Dynamics in Single Bubble Experiment

The bubble radius as a function of time as predicted by the theoretical model is shown in Figure 32. This curve is for run No. 7. The value used for α was 1.2 ft^2/hr and this choice resulted in a maximum radius of 0.0266 inch as compared to the experimental value of 0.0266 inch. The predicted value and the observed value of the bubble lifetime are 286 and 256 microseconds, respectively. This comparison is not as good, but it is within experimental error.

Near the beginning and the end of the bubble life, the theoretical model did not correctly predict the physical situation. This result indicates that at these times the theoretical model does not accurately represent the physical phenomena. It was realized that the model developed in Chapter III would be most accurate only when the bubble size is large. Because the bubble size was large during most of its lifetime, the theoretical model is acceptable even with the poor prediction of small bubble

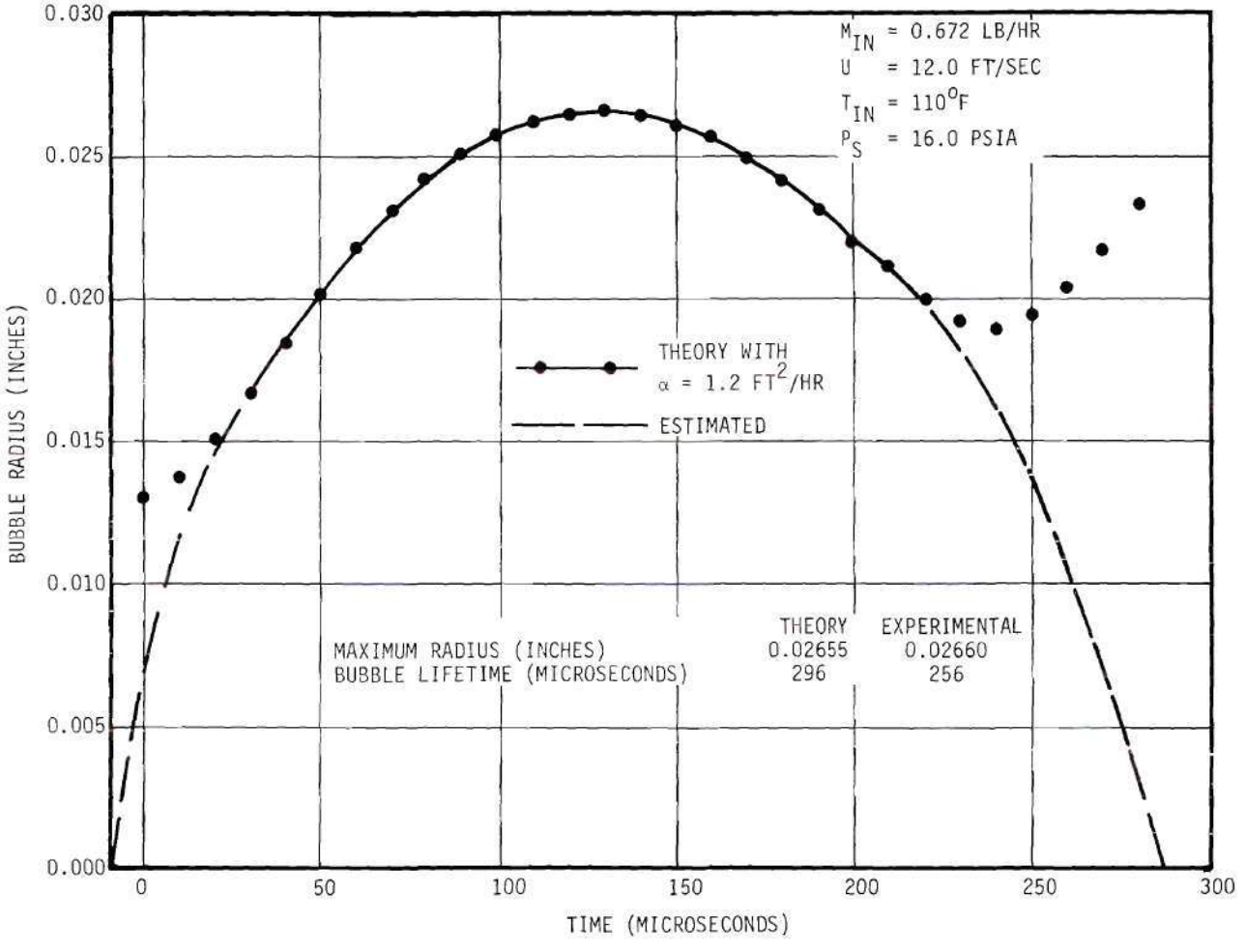

Figure 32. Bubble Radius as a Function of Time for Run No. 7.

radii.

The high value of α necessary to yield agreement between the theoretical and the experimental value of the maximum radius suggests that the level of turbulence with respect to a single bubble may be relatively high. If so, this high turbulence should be optically observable. Figures 33 and 34 are enlarged high speed photographs of runs number 10 and 12, respectively. Upon close examination, the region surrounding the bubble appears hazy, which might indicate a high value of α.

A number of variables were recorded for run No. 7 in order to characterize the theoretical model. Figures 35, 36, and 37 represent the bubble mass, the bubble pressure, and the liquid surface temperature as functions of time, respectively. Figures 38 through 43 represent the temperature distribution in the liquid surrounding the bubble at various times during its life. The liquid surface temperature as a function of μ at various times during the bubble life is shown in Figure 44. To be noted in Figure 44 is the fact that the temperature of the liquid surface varied at times as much as 20°F from $\mu = -1$ to $\mu = +1$. Also, the temperature distribution in the upstream direction (see Figure 39) was much steeper than in the downstream direction (see Figure 43). These results are reasonable; since cold fluid comes from the upstream direction, the surface temperature of the fluid at this end should be coldest. Also, as the fluid moves over the bubble, its temperature should increase due to the latent heat of condensation.

The bubble radius as a function of time for runs number 8, 9, 10, and 14 is shown in Figure 45. Some pertinent information is tabulated in Table 2. Since the velocity for runs 8, 9, and 10 was the same, the value

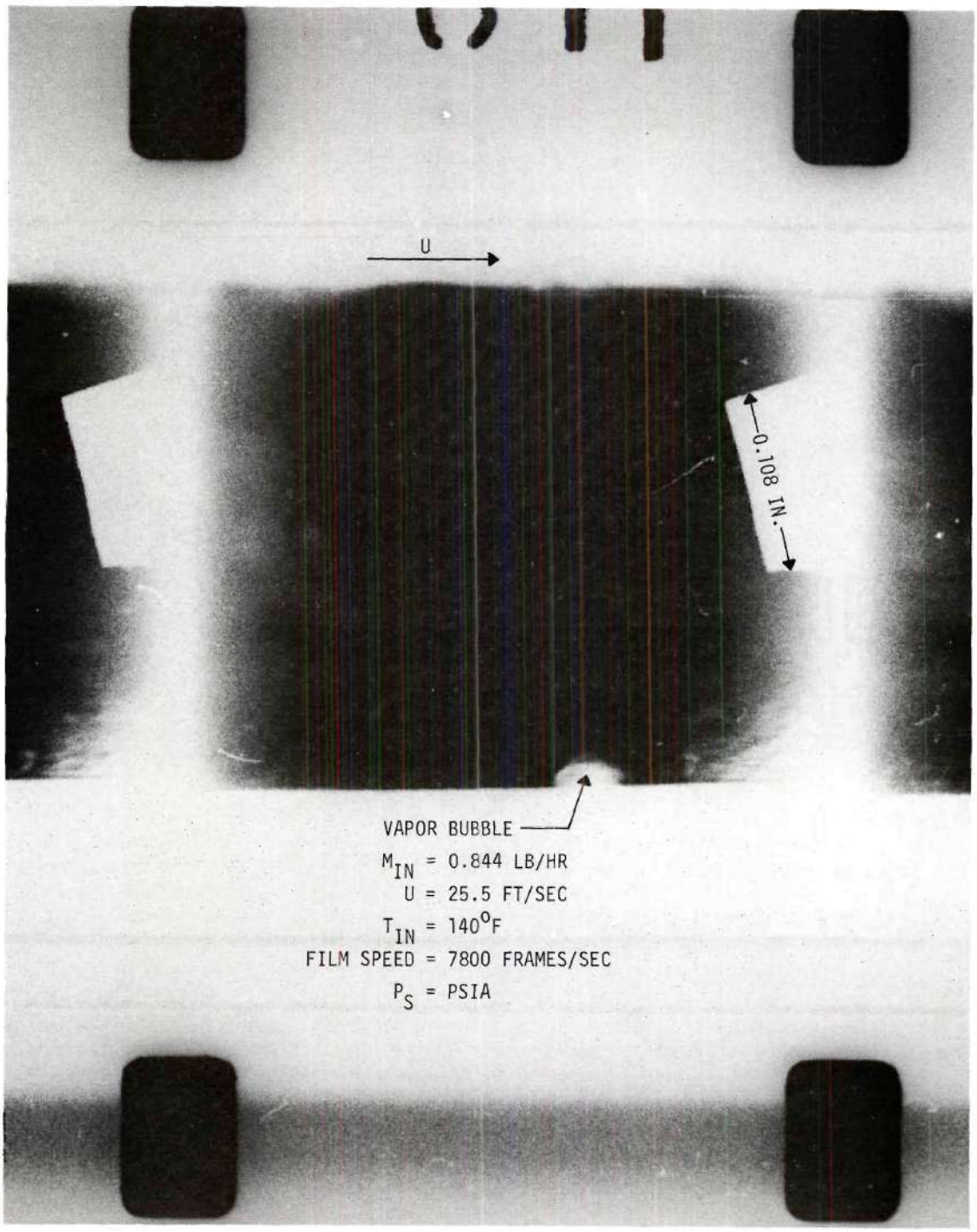

Figure 33. High Speed Photograph of Run No. 10.

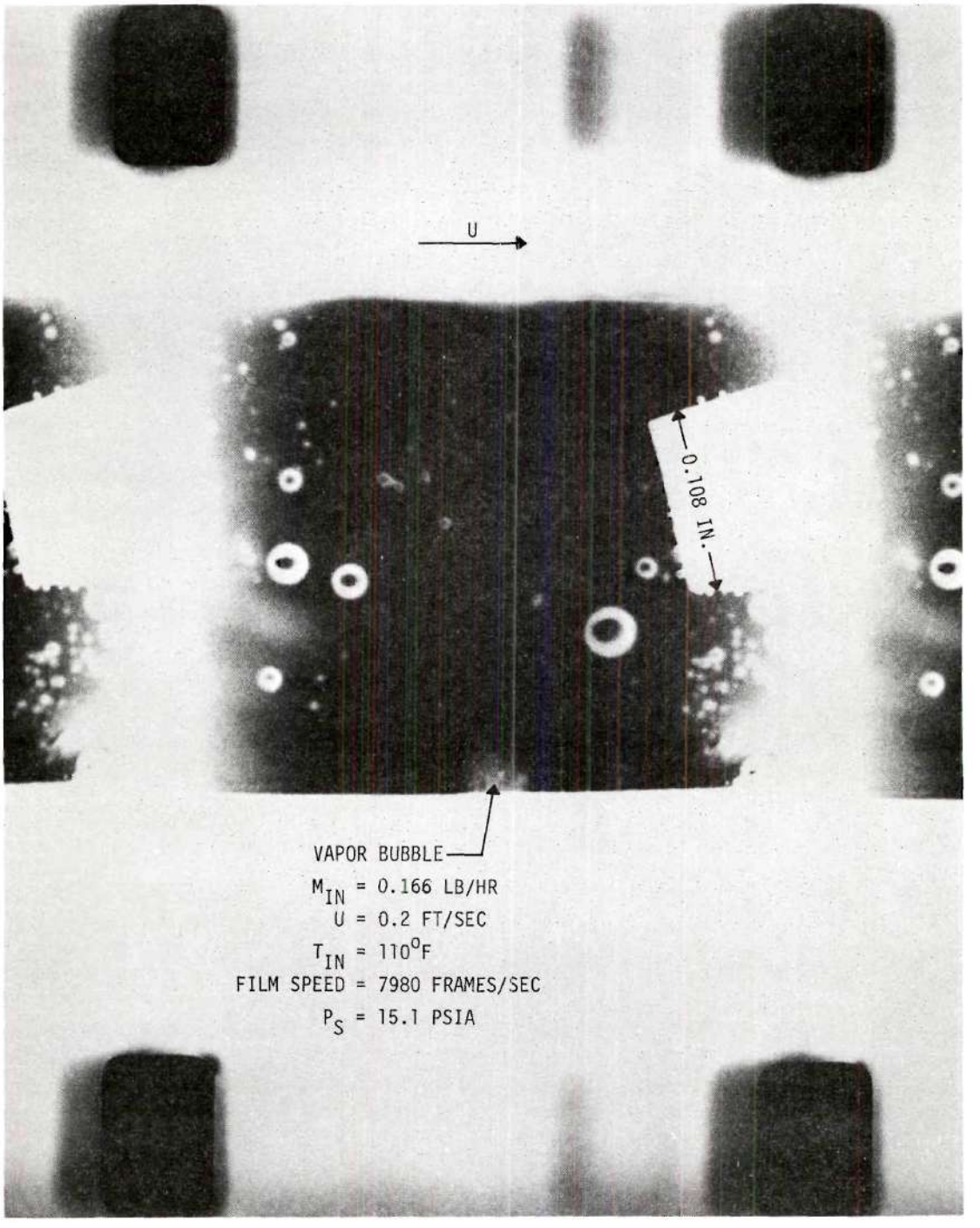

Figure 34. High Speed Photograph of Run No. 12.

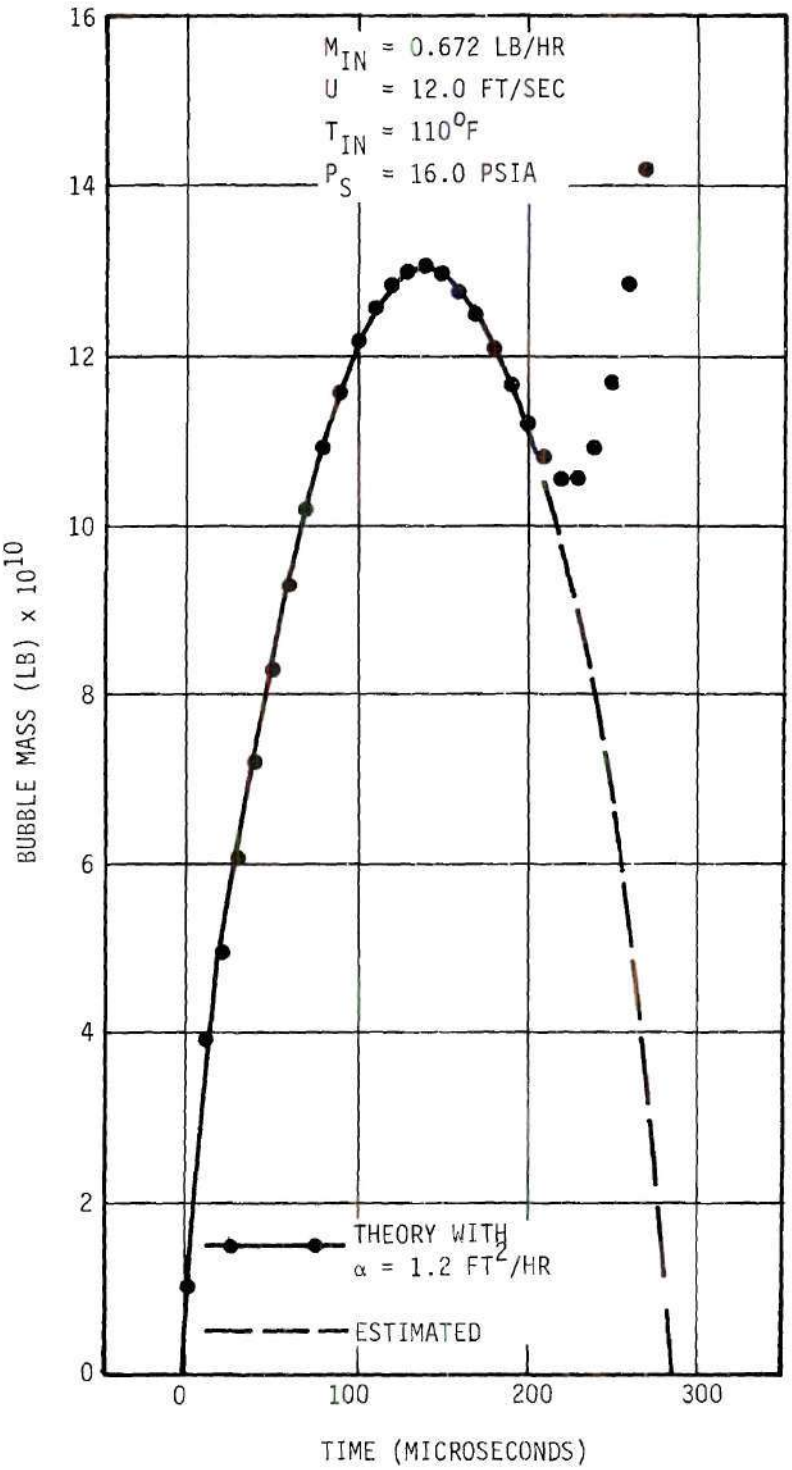

Figure 35. Bubble Mass as a Function of Time for Run No. 7.

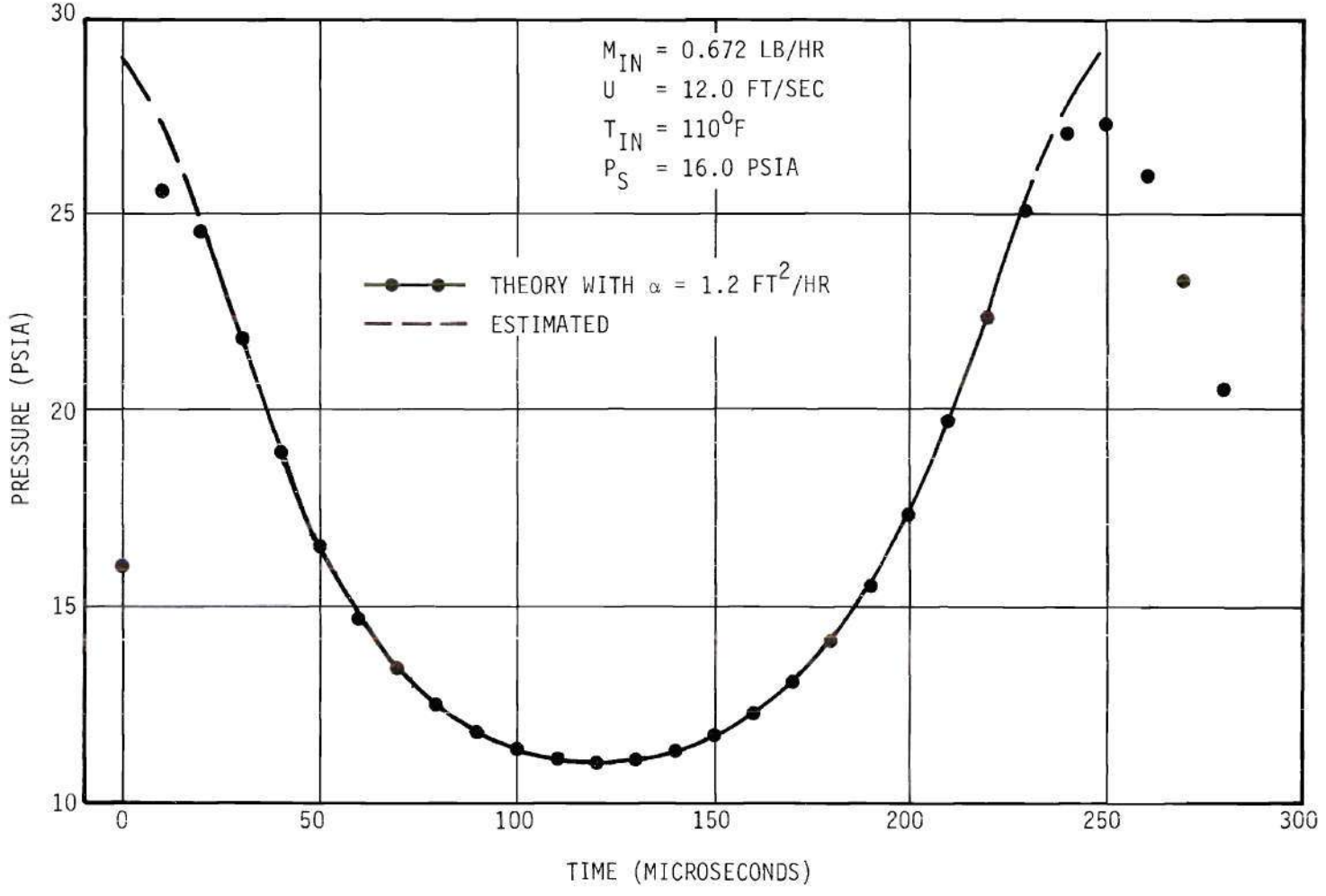

Figure 36. Bubble Pressure as a Function of Time for Run No. 7.

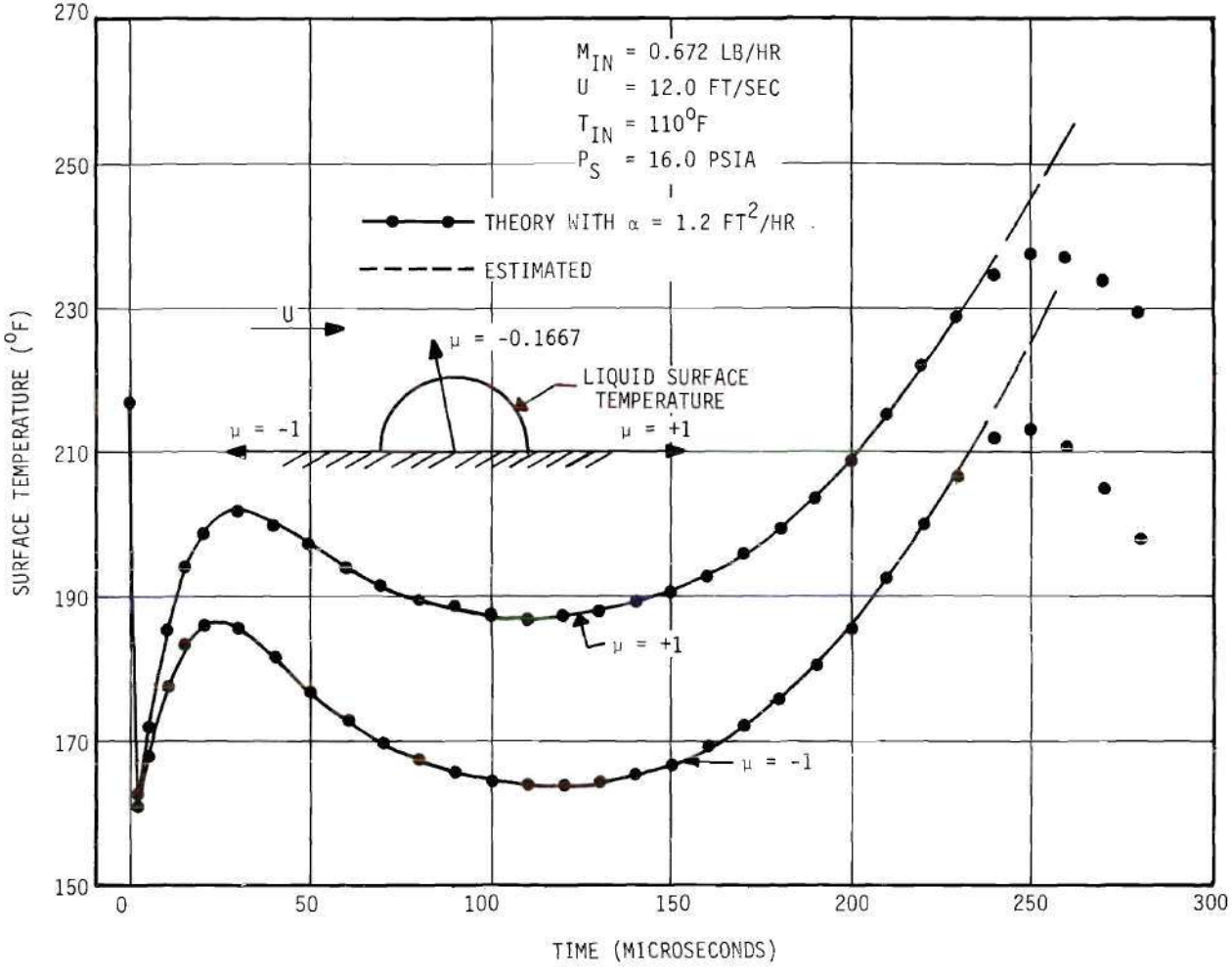

Figure 37. Liquid Surface Temperature as a Function of Time for Run No. 7.

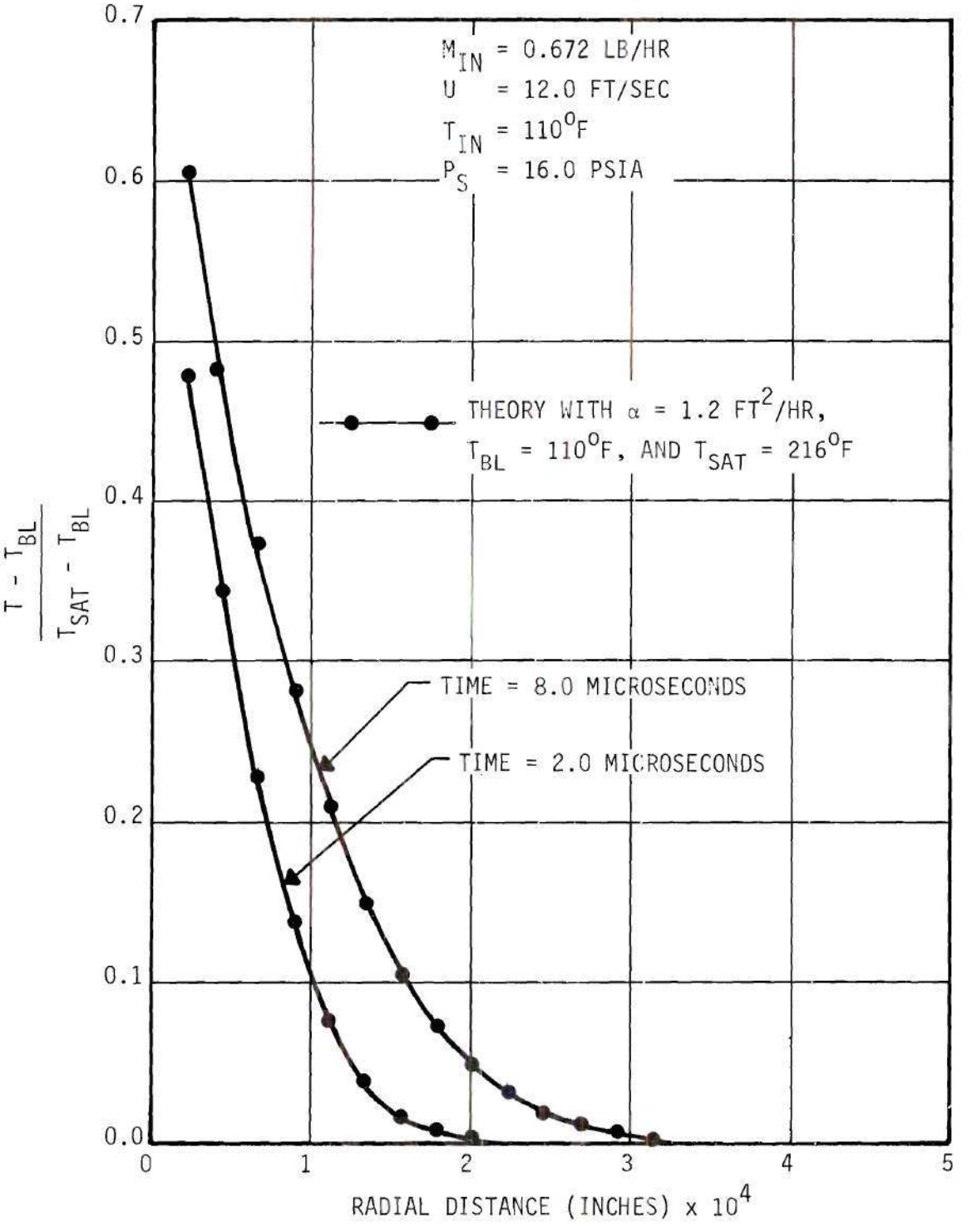

Figure 38. Dimensionless Temperature Difference for the Cooling Liquid as a Function of Radial Distance from the Bubble Surface for $\mu = -1$ (Upstream Direction) for Run No. 7.

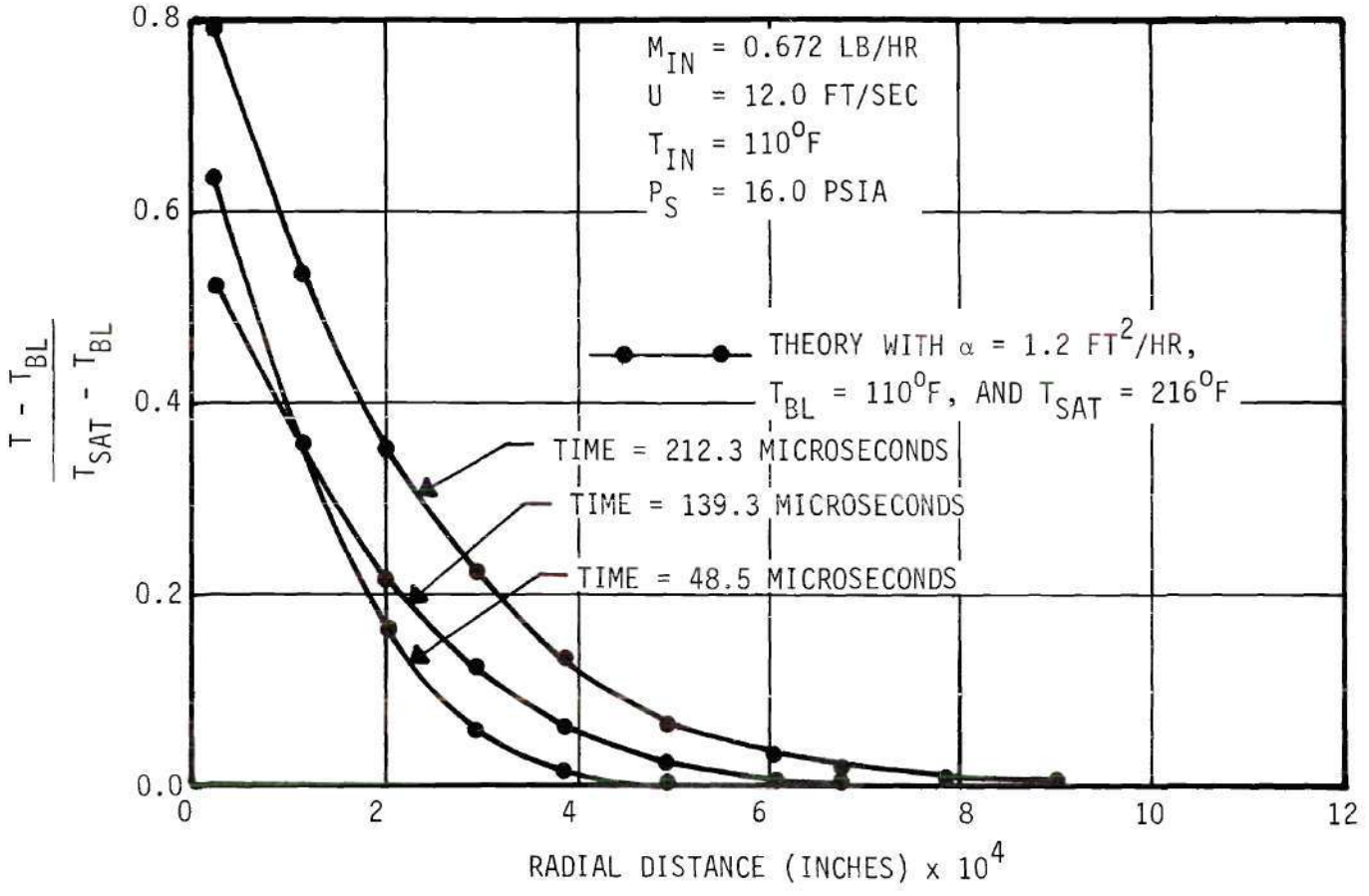

Figure 39. Dimensionless Temperature Distribution for the Cooling Liquid as a Function of Radial Distance from the Bubble Surface for $\mu = -1$ (Upstream Direction) for Run No. 7.

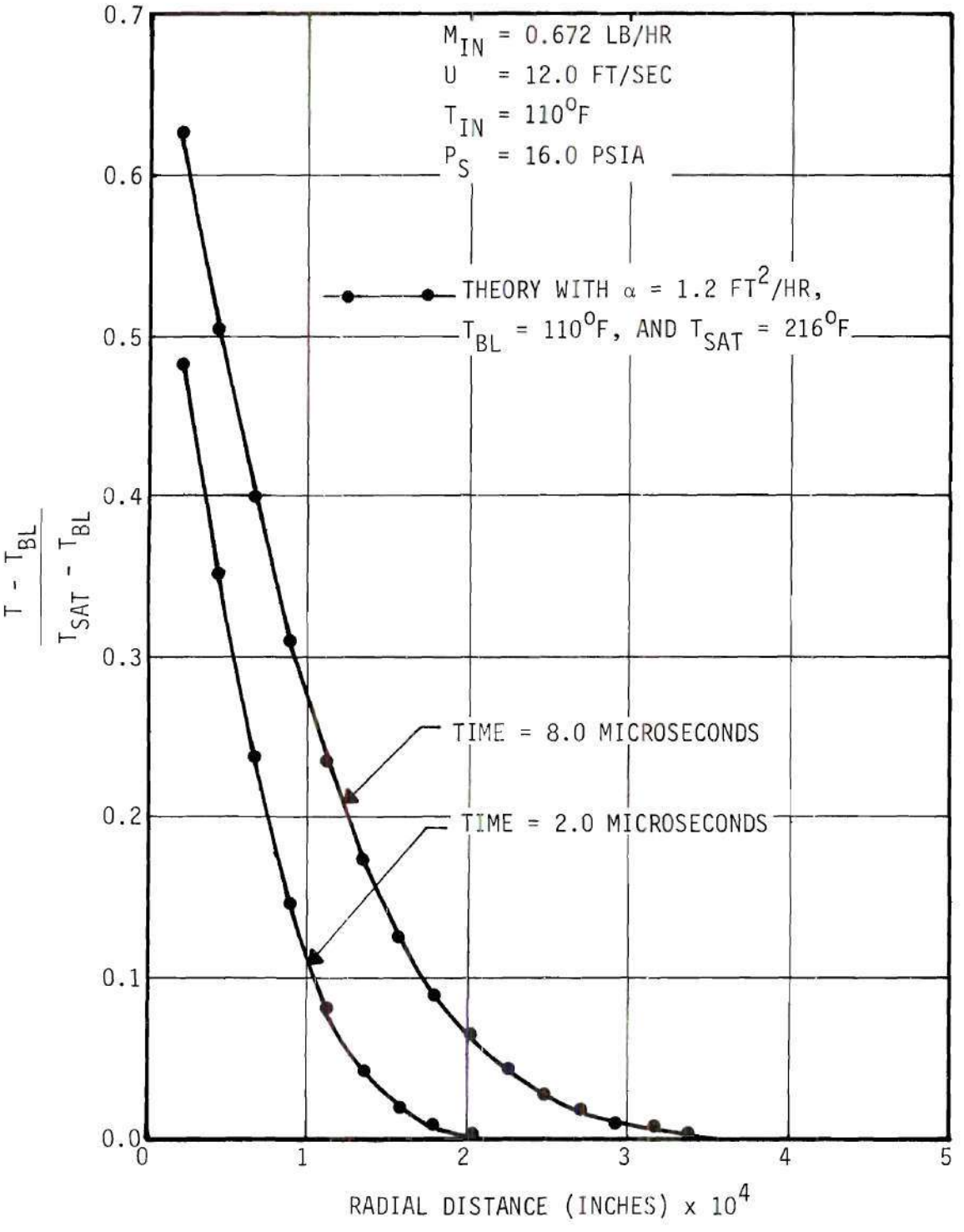

Figure 40. Dimensionless Temperature Distribution for the Cooling Liquid as a Function of Radial Distance from the Bubble Surface for μ = -0.1667 for Run No. 7.

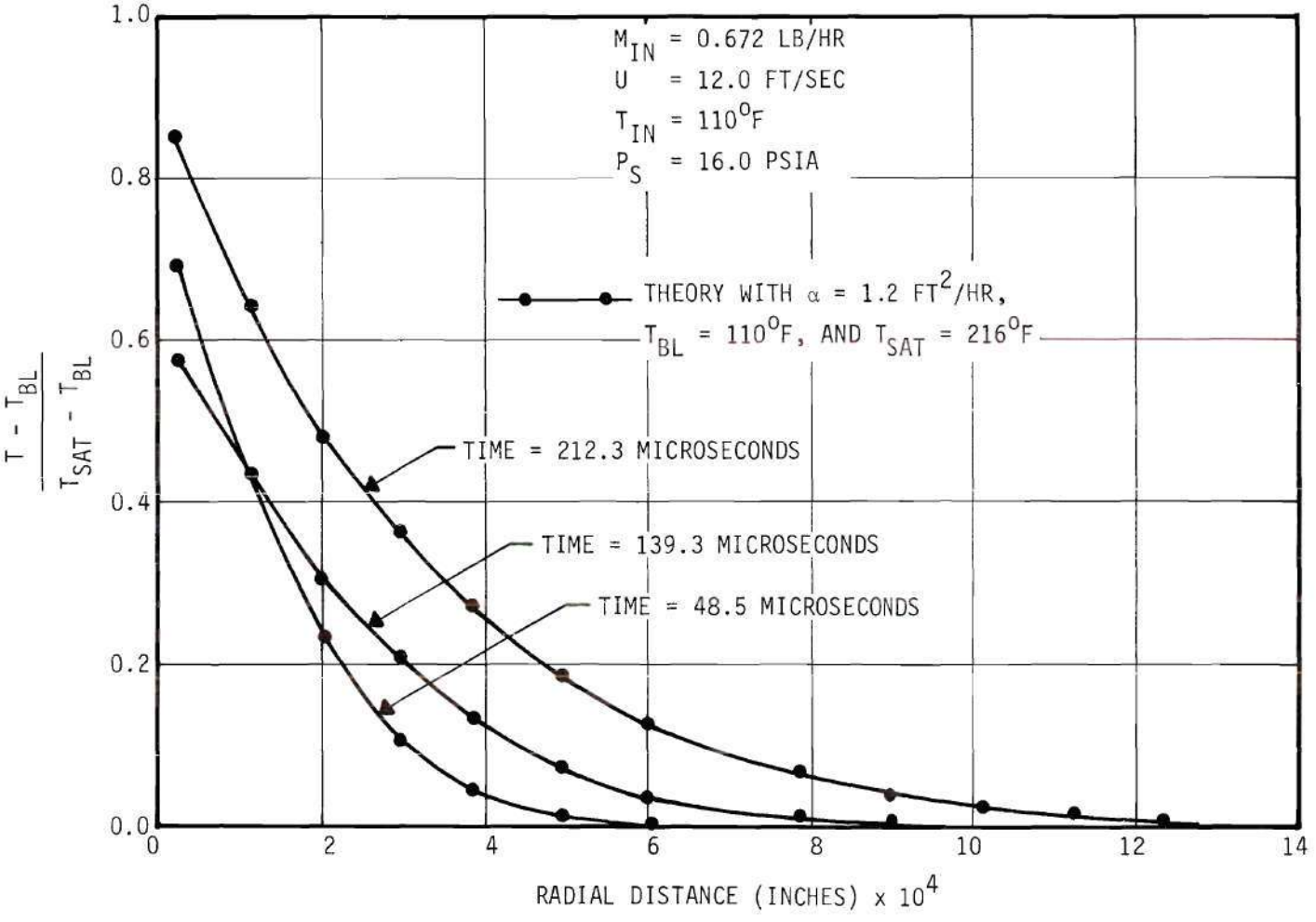

Figure 41. Dimensionless Temperature Distribution for the Cooling Liquid as a Function of Radial Distance from the Bubble Surface for μ = -0.1667 for Run No. 7.

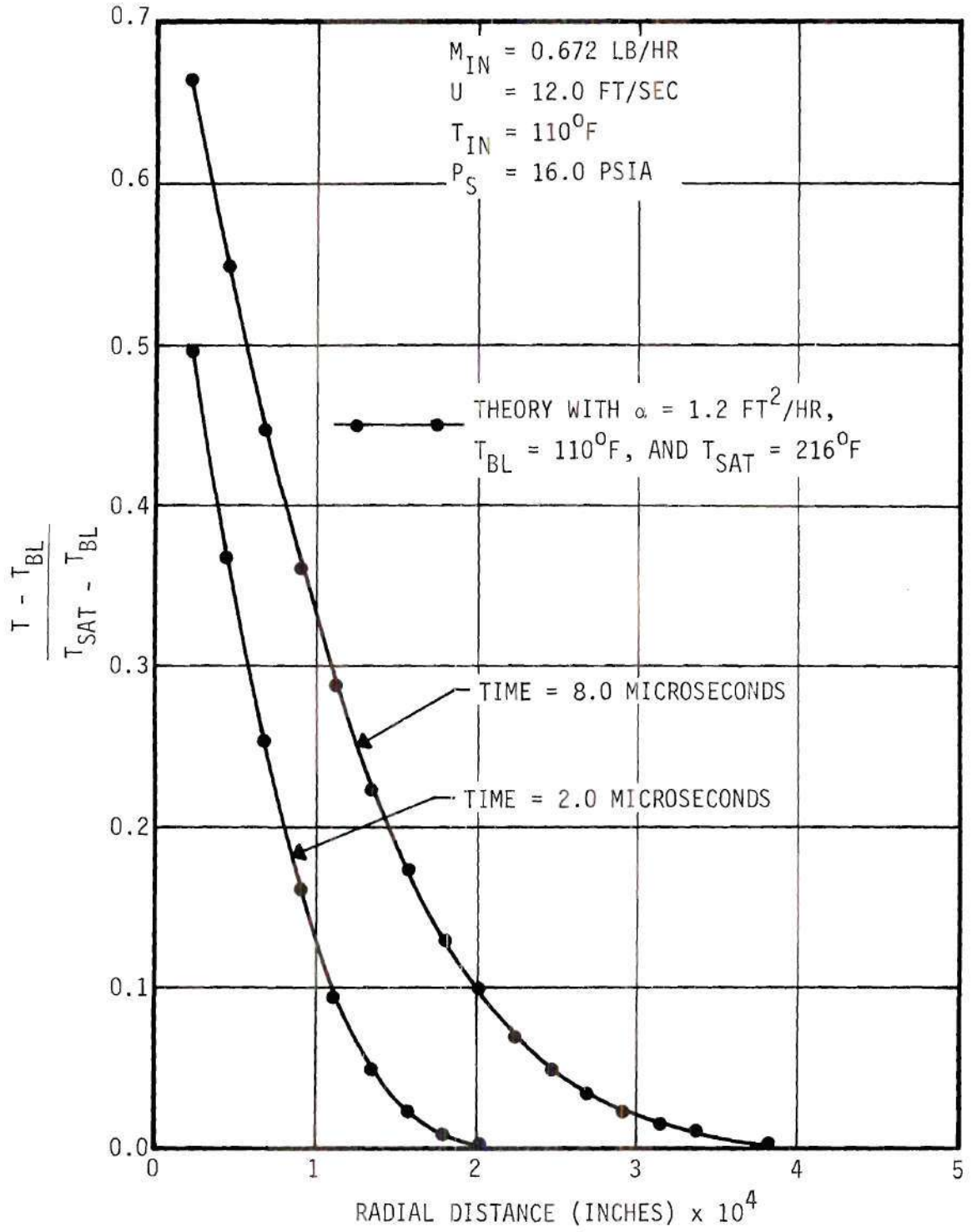

Figure 42. Dimensionless Temperature Distribution for the Cooling Liquid as a Function of Radial Distance from the Bubble Surface for μ = +1 (Downstream Direction) for Run No. 7.

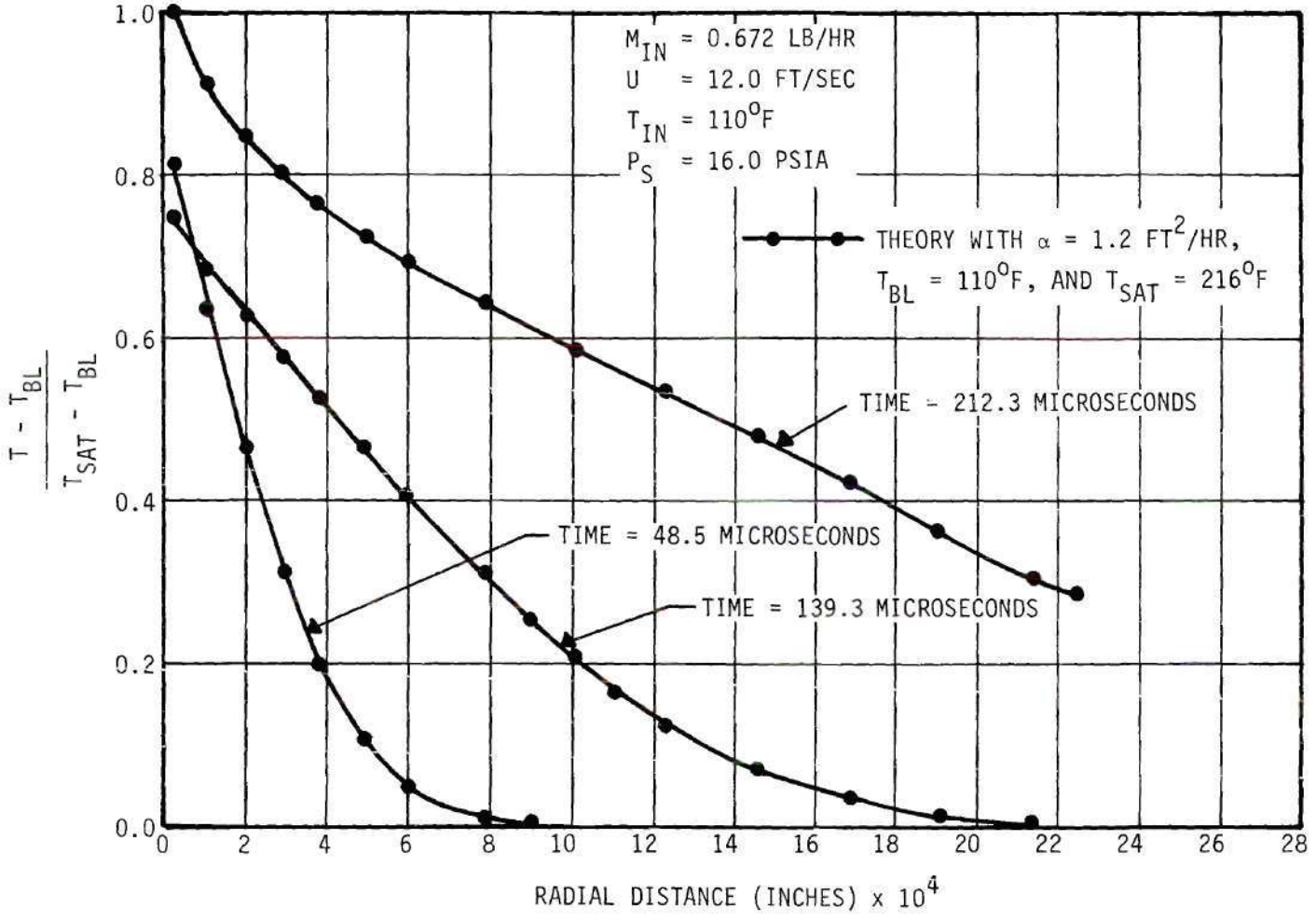

Figure 43. Dimensionless Temperature Distribution for the Cooling Liquid as a Function of Radial Distance from the Bubble Surface for μ = +1 (Downstream Direction) for Run No. 7.

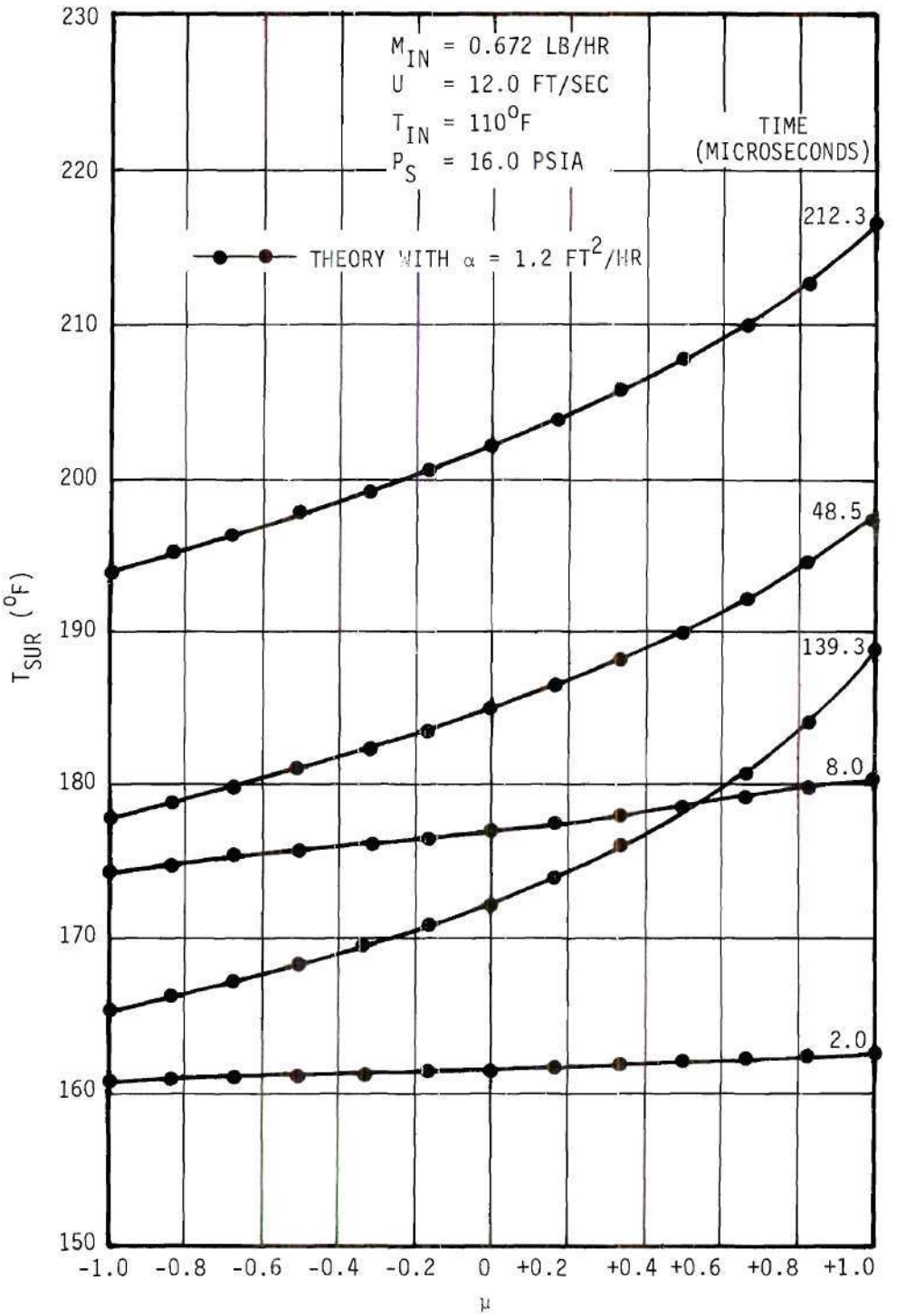

Figure 44. Liquid Surface Temperature as a Function of μ for Run No. 7.

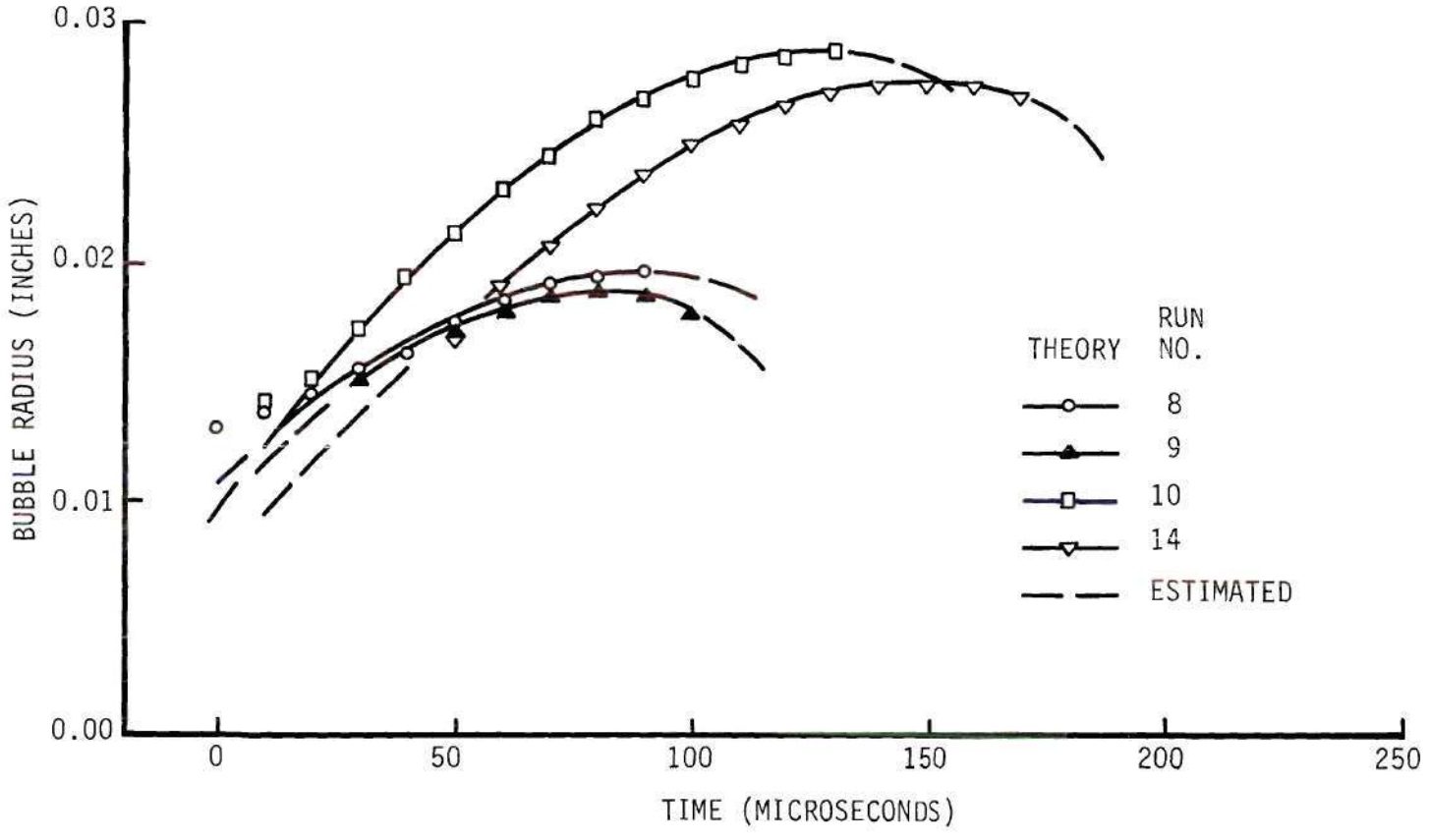

Figure 45. Bubble Radius as a Function of Time for Runs No. 8, 9, 10 and 14.

Table 2. Results of Runs No. 3, 9, 10, and 14

Run	T_{IN} (°F)	U (ft/sec)	α (ft^2/hr)	R_b Model (inches)	R_b Experimental (inches)	Deviation (%)
8	110	25.5	3.00	0.01976	0.0200	- 1
9	80	25.5	3.00	0.01857	0.0172	+ 8
10	140	25.5	3.00	0.02893	0.0314	- 8
14	110	1.9	0.06	0.02763	0.0280	- 1

for the effective thermal diffusivity was expected to be approximately the same value for all three runs. Thus, only the change in the cooling fluid temperature and that in the vapor input rate would change the experimentally observed maximum radius in runs 9 and 10 from the value observed in run 8. Therefore, by using the value of α which yielded agreement between the theoretically predicted maximum bubble radius and that experimentally observed for run 8, in the model for runs 9 and 10, the consistency of the theoretical model with the actual physical phenomenon could be determined. In run 9, the predicted maximum radius differed by only plus eight percent from the observed value, while in run 10 the difference was only minus eight percent.

The values of α which yield agreement between experiment and theory are plotted as a function of the cooling stream velocity in Figure 46. It appears that between 2 ft/sec and 25.5 ft/sec, α is approximately a linear function of U. Also shown is the theoretical value of the eddy diffusivity for fully developed pipe flow turbulence at a distance of 0.02 inch from the wall. These two curves are approximately the same. This result was not expected (see page 23).

The input numbers used in the computer code for the runs mentioned above are tabulated in Table 7 in Appendix A.

Bubble Dynamics in Real Boiling

The theoretical model developed was tested on a situation experimentally investigated by Gunther (see reference 15, p. 119, Figure 9). He experimentally determined the radius versus time curve for several bubbles in subcooled nucleate boiling in forced convection. The fluid was

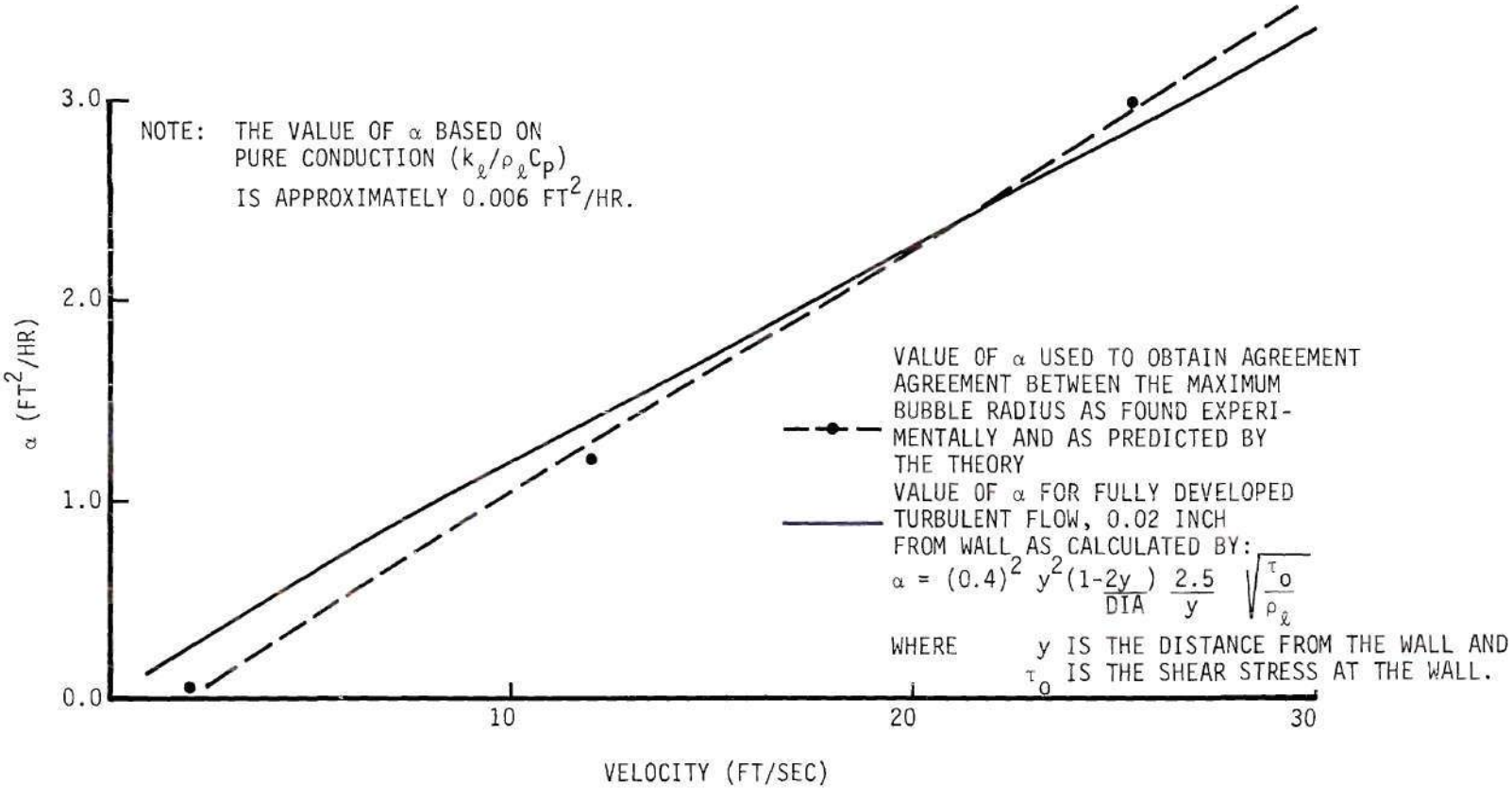

Figure 46. Effective Thermal Diffusivity as a Function of Cooling Stream Velocity.

water and it was assumed that the heated surface was stainless steel. The heated plate was 0.004 inch thick and the heat flux was 2.75 BTU/in^2 sec. The velocity of the fluid was 10 ft/sec at a pressure of 28.8 in Hg. Also, the subcooling was 90°F. Bankoff (2) estimated the wall temperature to be 287°F.

Several preliminary runs were made with an initial liquid temperature of 110°F. The bubble radius versus time curves for these cases are shown in Figure 47. In the cases shown, except for number two, the lower limit for δ, the initial thickness of the thin liquid film, is shown. Any δ larger than this value would yield the same curve using the present model which neglects any temperature drop across the thin liquid film. For run number 2, the initial thickness was fixed at 1.1×10^{-5} inches and at approximately 150 microseconds, this film had dried up near the center of the bubble. As growth continued beyond this point, the thin liquid film continued to dry up. This resulted in a reduction in the mass input rate and thus initiated bubble collapse. However, the shape of this curve does not compare well with those observed experimentally by Gunther (15). This result seems to indicate that in this region of boiling, complete thin liquid film dry up does not occur. This implies that, during the life of the bubble, the thin liquid film available exceeds the demand. One possible source of fluid for the thin liquid film seems to be the liquid adjacent to the wall just downstream of the bubble. Since Gunther's bubbles move over the plate with a velocity 0.8 times the stream velocity, they are continually exposed to a fresh supply of thin liquid film.

In Gunther's case the actual liquid temperature was approximately

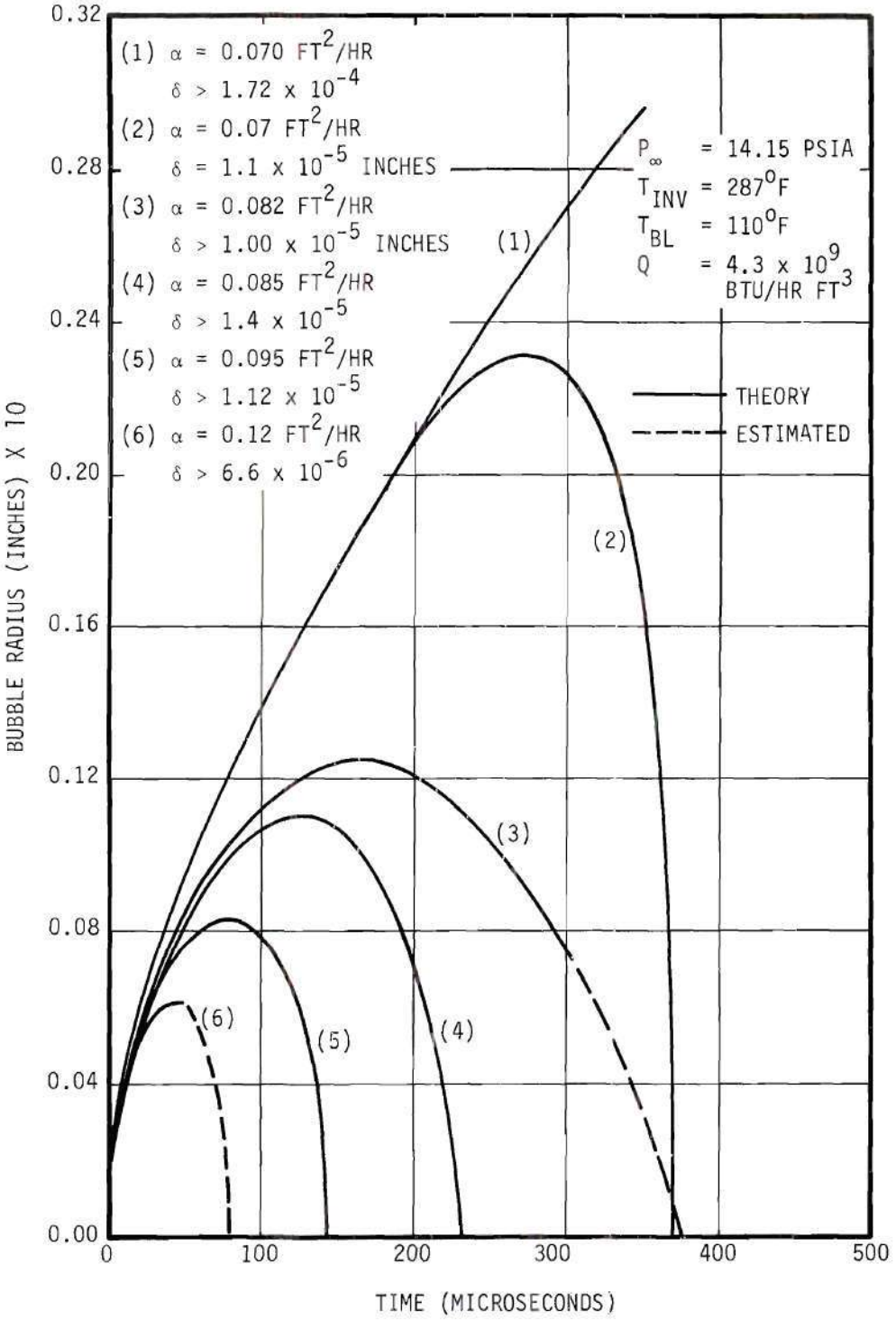

Figure 47. Bubble Radius as a Function of Time for the Real Boiling Model.

122°F. The results of a few cases using the complete physical data for Gunther's case are shown in Figure 48. Curves one through four differ only in the choice of α, and it is observed that the maximum bubble radius is a strong function of α. Curve five has the same value of α as curve three; however, the cooling liquid temperature has been lowered four degrees. This indicates a strong dependence of the maximum bubble radius on the local liquid temperature. The value for the maximum bubble radius observed by Gunther varied from a low of approximately 0.012 inch to a high of approximately 0.026 inch for one set of conditions. A partial explanation for the large range of values for the maximum radius appears to be small variations in the local value of α and in the local temperature which are present in a turbulent stream. This same effect might also be responsible for the small bubble and large bubble populations mentioned on page 86. The shape of curves four and five is reasonably similar to those observed by Gunther. Curve three is also similar except the bubbles observed by Gunther completely collapsed. Curve three would have gone to zero radius if some thin liquid film dry out had occurred. This possibility definitely exists.

An important quantity which was obtained during the solution of this model was the total amount of heat removed from the plate by the bubble and for curve number three of Figure 48 it was 5.17×10^{-6} BTU. In previous investigations, it has been assumed that the total amount of heat removed by the bubble was the latent heat required to form a volume of steam equal to the maximum bubble volume observed. Also, the state of the steam in the bubble was assumed to be saturation at the system pressure. For the theoretical case just mentioned, the maximum volume was

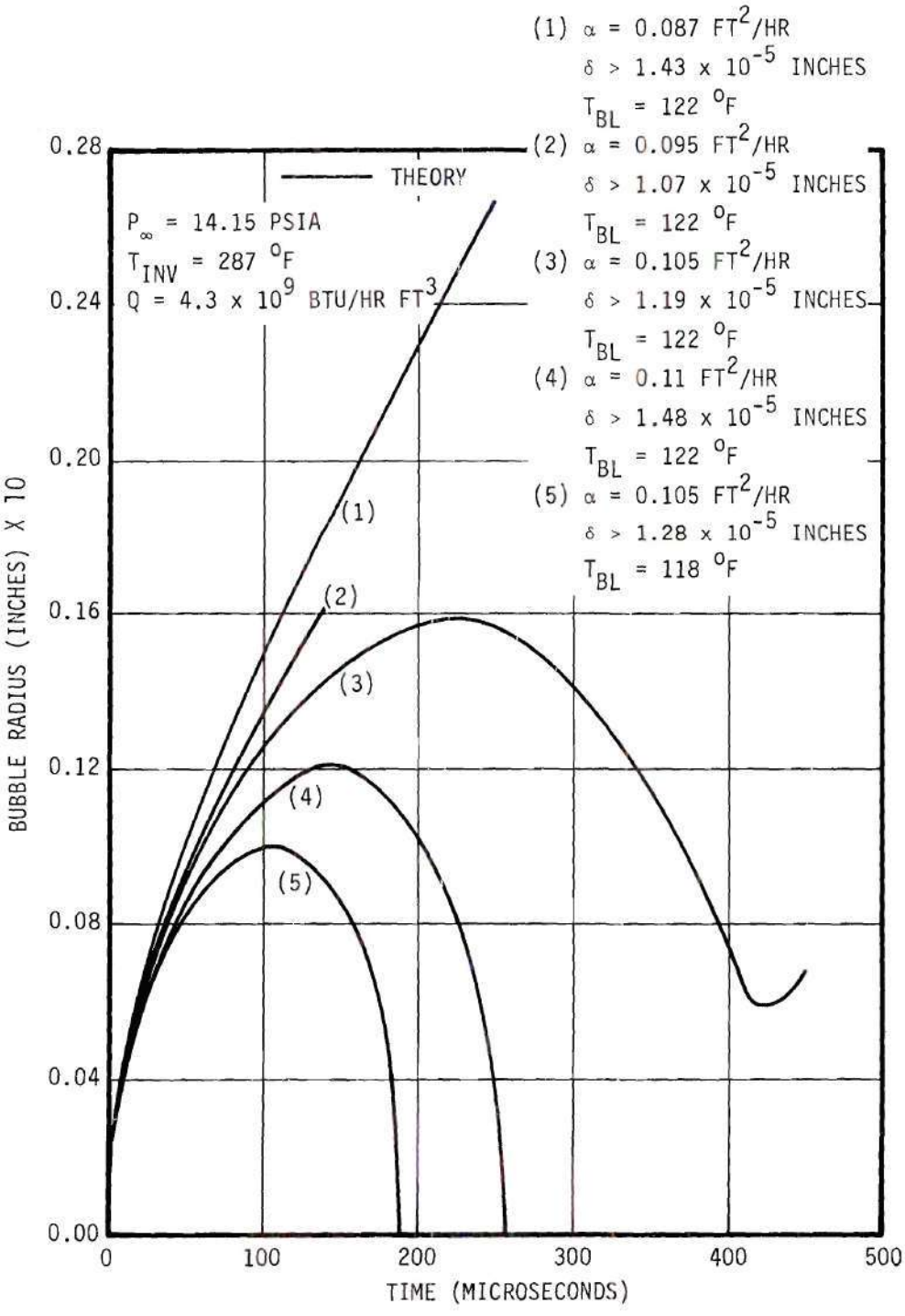

Figure 48. Bubble Radius as a Function of Time for the Real Boiling Model for Conditions as in Gunther's Experiment (See Reference 15, p. 119, Figure 9).

4.79×10^{-9} ft^3. Also, since the system pressure was approximately 14.7 psia, the specific volume was assumed to be 26.8 ft^3/lb and the latent heat was assumed to be 970 BTU/lb. Thus the latent heat associated with one bubble volume of vapor is

$$4.79 \times 10^{-9} \text{ ft}^3 \times \frac{970 \text{ BTU/lb}}{26.8 \text{ ft}^3/\text{lb}} = 1.73 \times 10^{-7} \text{ BTU}$$

and the ratio of the actual heat removed compared to that necessary to form one bubble volume of steam is

$$\frac{5.17 \times 10^{-6}}{0.173 \times 10^{-6}} = 29.82$$

This value may be compared to a similar one mentioned on page 7. In this case, the ratio in question was obtained from Gunther's burnout data (15) on the assumption that all the heat removed from the plate was through the mass transfer mechanism. In that case, the value for the heat flux was 3.75 BTU/in^2 sec and the liquid temperature was approximately 90°F. Also, the pressure was 50 inches of mercury. The resulting ratio of the actual heat to that based on one volume of steam was estimated to be 16.8 by assuming that all of the heat removed from the plate was transferred by the mass transfer mechanism. This number and the one predicted by the theoretical model should not be exactly the same since the case considered by the model had a heat flux of 2.75 BTU/in^2 sec, a pressure of 28.8 inches of mercury, and a liquid temperature of approximately

122°F. (Also, the velocities were different for the two cases.) In any case, both estimates of this ratio are of the same order of magnitude. This result indicates that the mass transfer mechanism is the major mechanism for removing heat from the heated surface for the case of highly subcooled nucleate boiling in forced convection near the maximum heat flux.

Figures 49 through 59 are presented in order to further characterize this model. Figures 49 through 52 represent the following at various times during the bubble life: (a) the liquid temperature as a function of the distance from the surface of the bubble; (b) the thin liquid film thickness as a function of a, the radial distance on the plate surface (see Figure 5, p. 42); (c) the plate surface temperature as a function of a; (d) the dimensionless temperature in the heated plate as a function of distance into the plate, z, for a = 0. Figures 53 through 58 represent the bubble mass, the bubble pressure, the density of the vapor in the bubble, the cooling liquid surface temperature, the heated plate surface temperature for a = 0, the thin liquid film thickness for a = 0, respectively, as they vary with time. Figure 59 shows the total amount of heat removed from the plate per unit of time and the heat flux through the bubble base as functions of time.

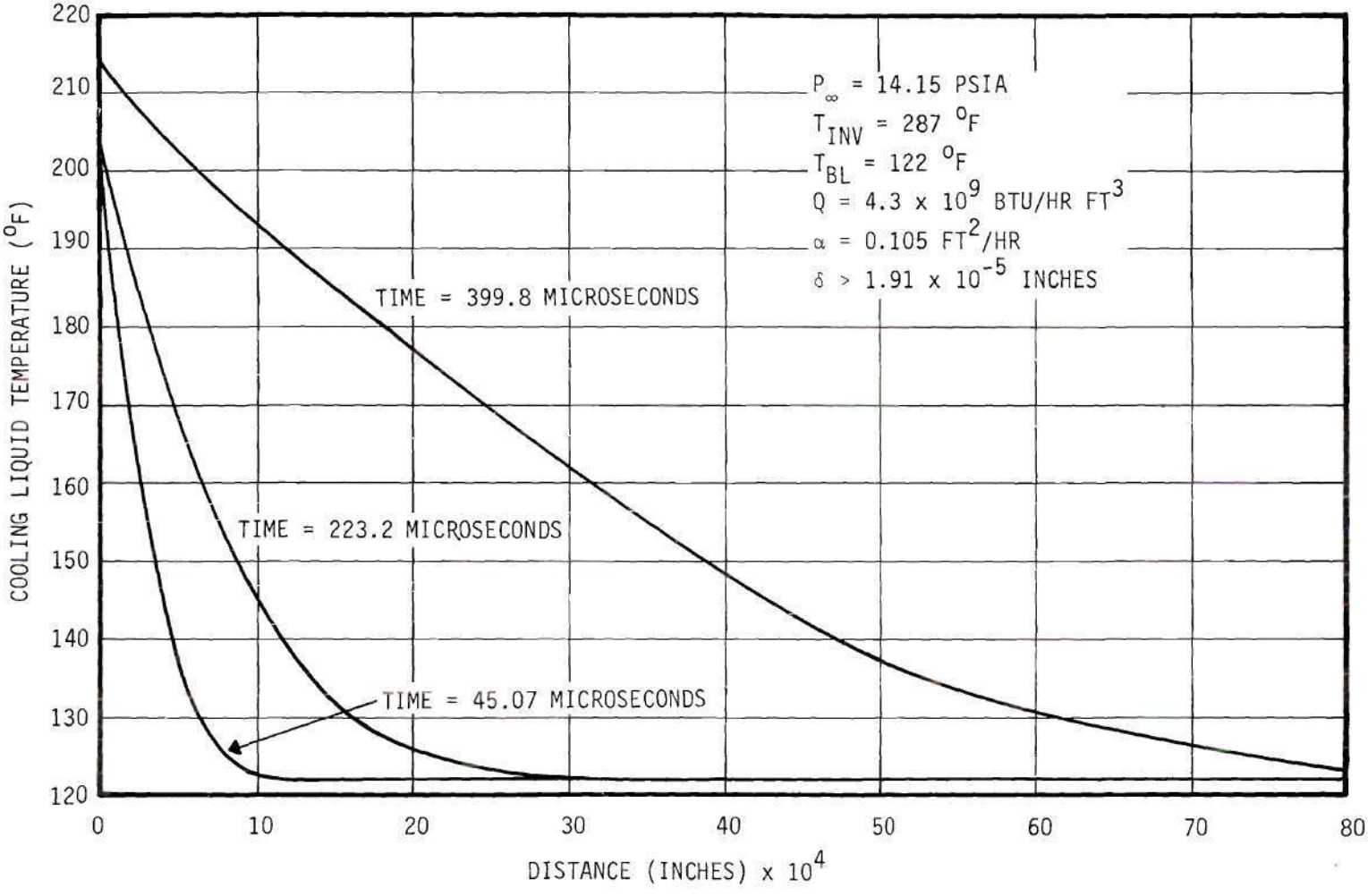

Figure 49. Cooling Liquid Temperature as a Function of Radial Distance from the Bubble Surface for the Real Boiling Model for Conditions as in Gunther's Experiment (See Reference 15, p. 119, Figure 9).

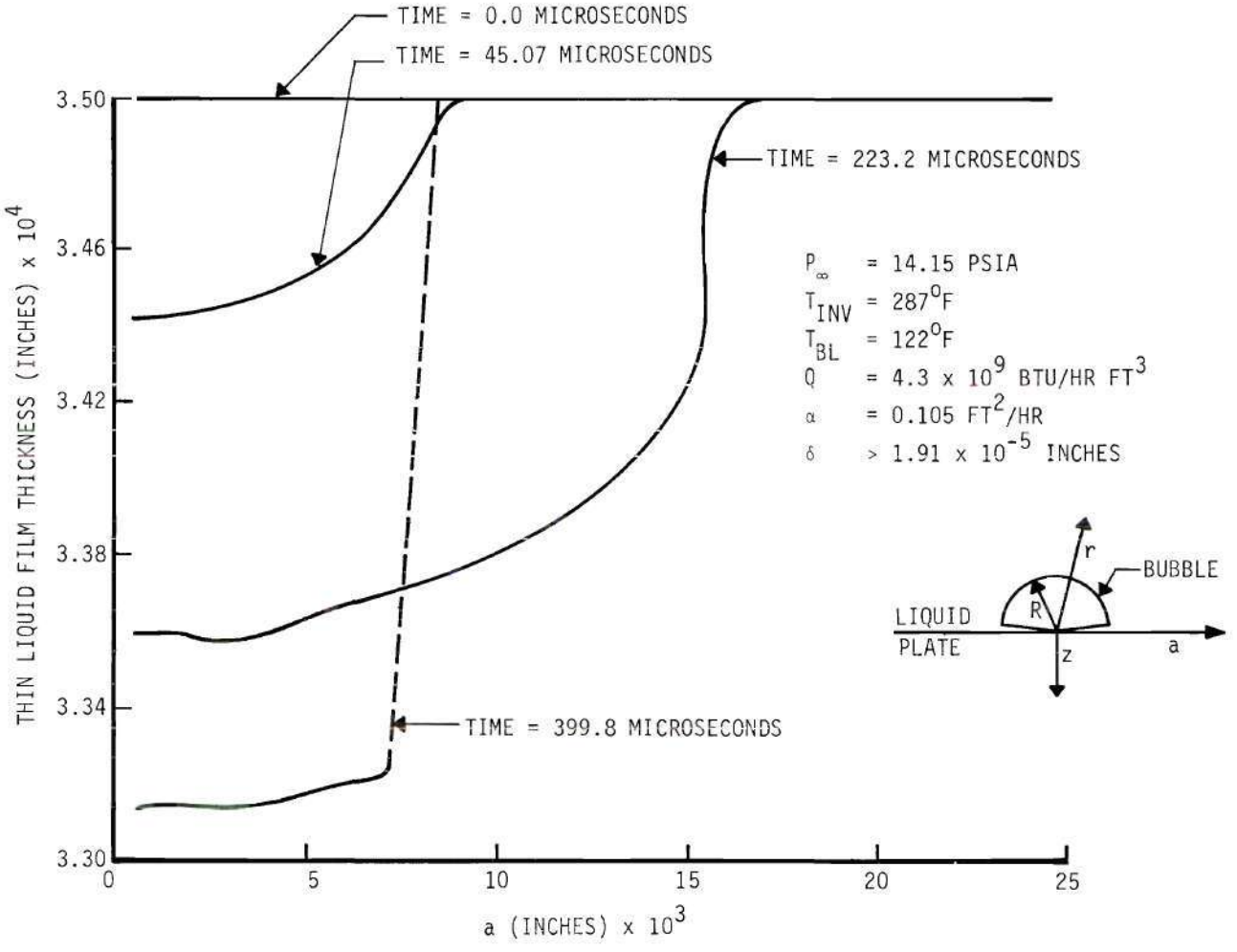

Figure 50. Thin Liquid Film Thickness as a Function of a for the Real Boiling Model for Conditions as in Gunther's Experiment (See Reference 15, p. 119, Figure 9).

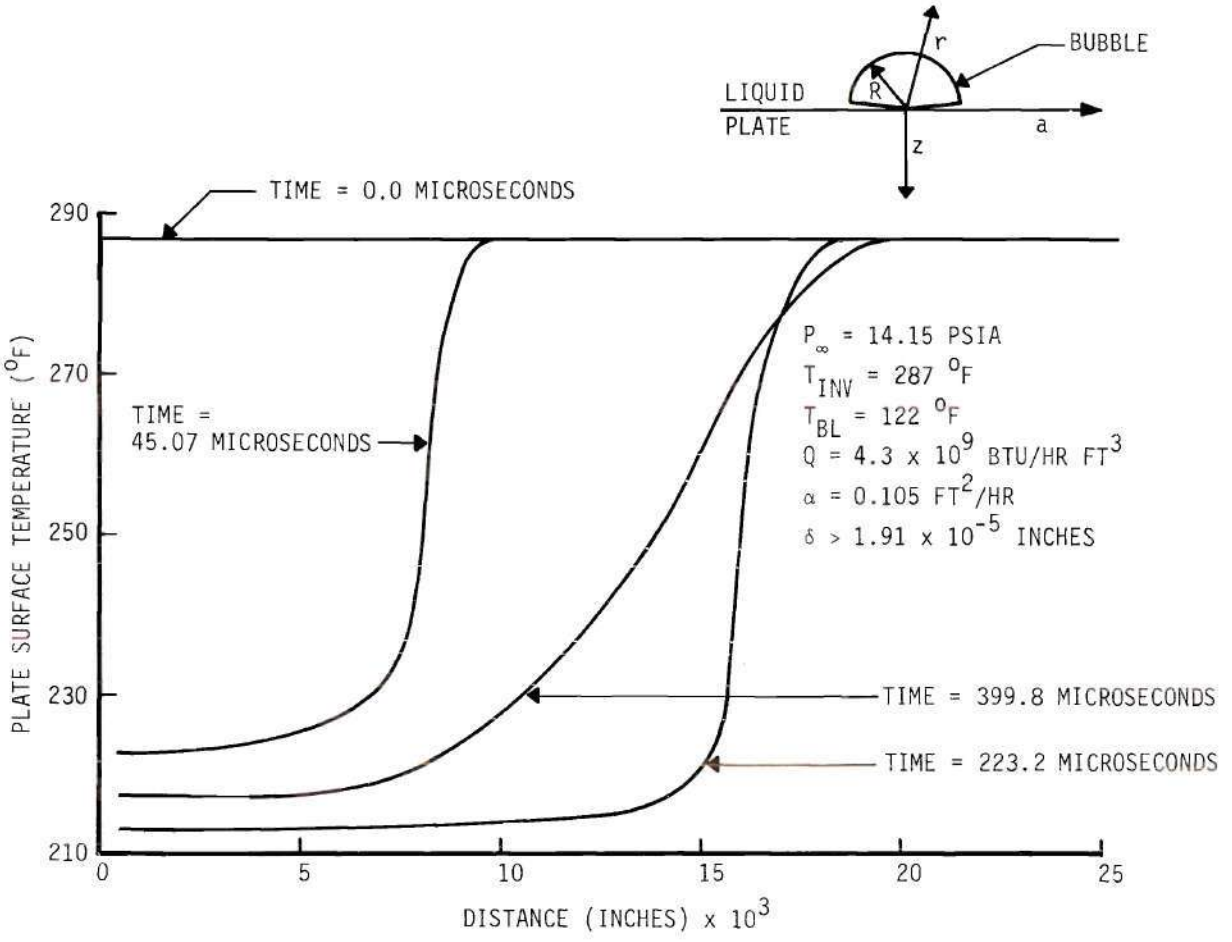

Figure 51. Plate Surface Temperature as a Function of a for the Real Boiling Model for Conditions as in Gunther's Experiment (See Reference 15, p. 119, Figure 9).

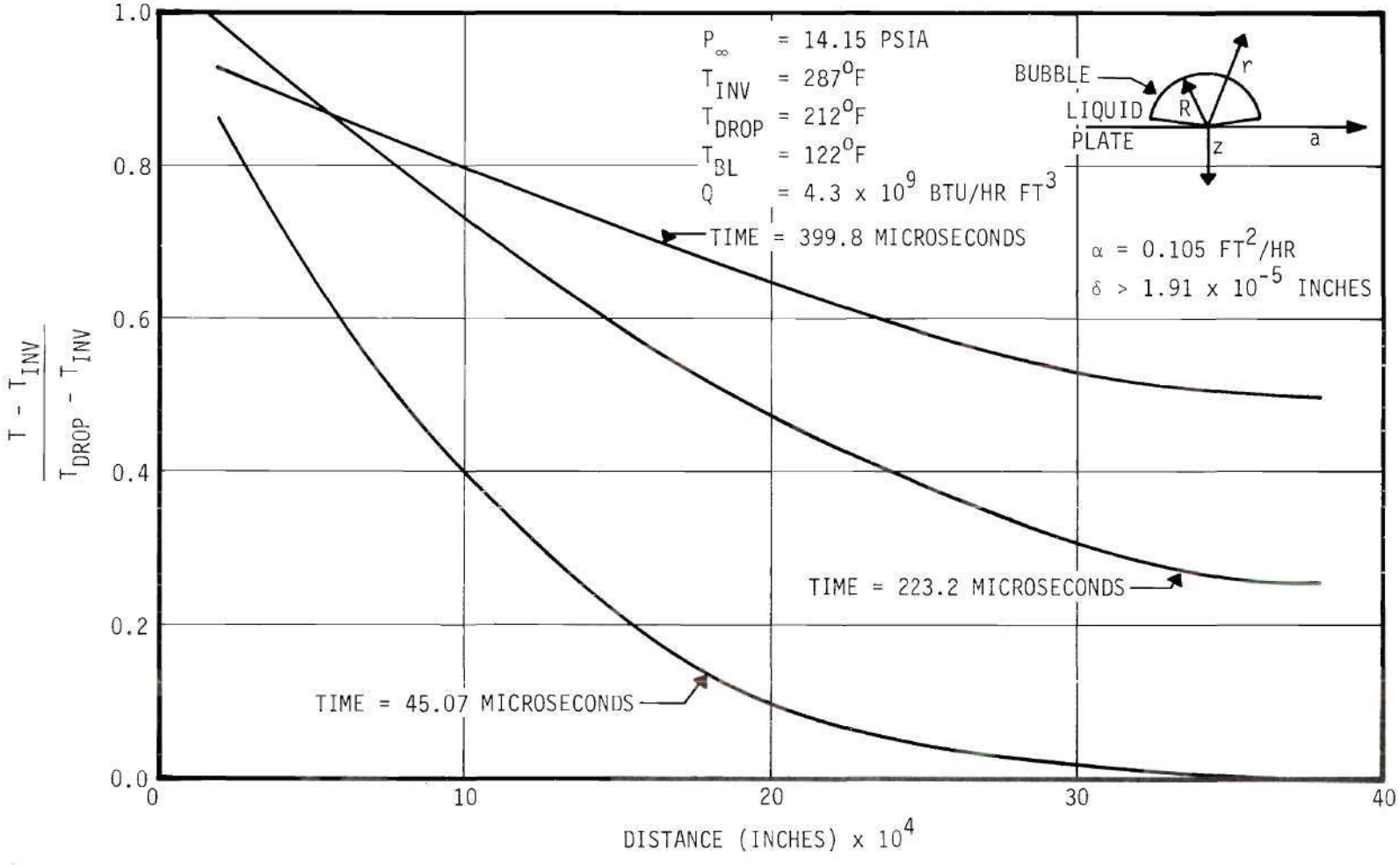

Figure 52. Dimensionless Temperature Difference in Heated Plate for a = o as a Function of z for the Real Boiling Model for Conditions as in Gunther's Experiment (See Reference 15, p. 119, Figure 9).

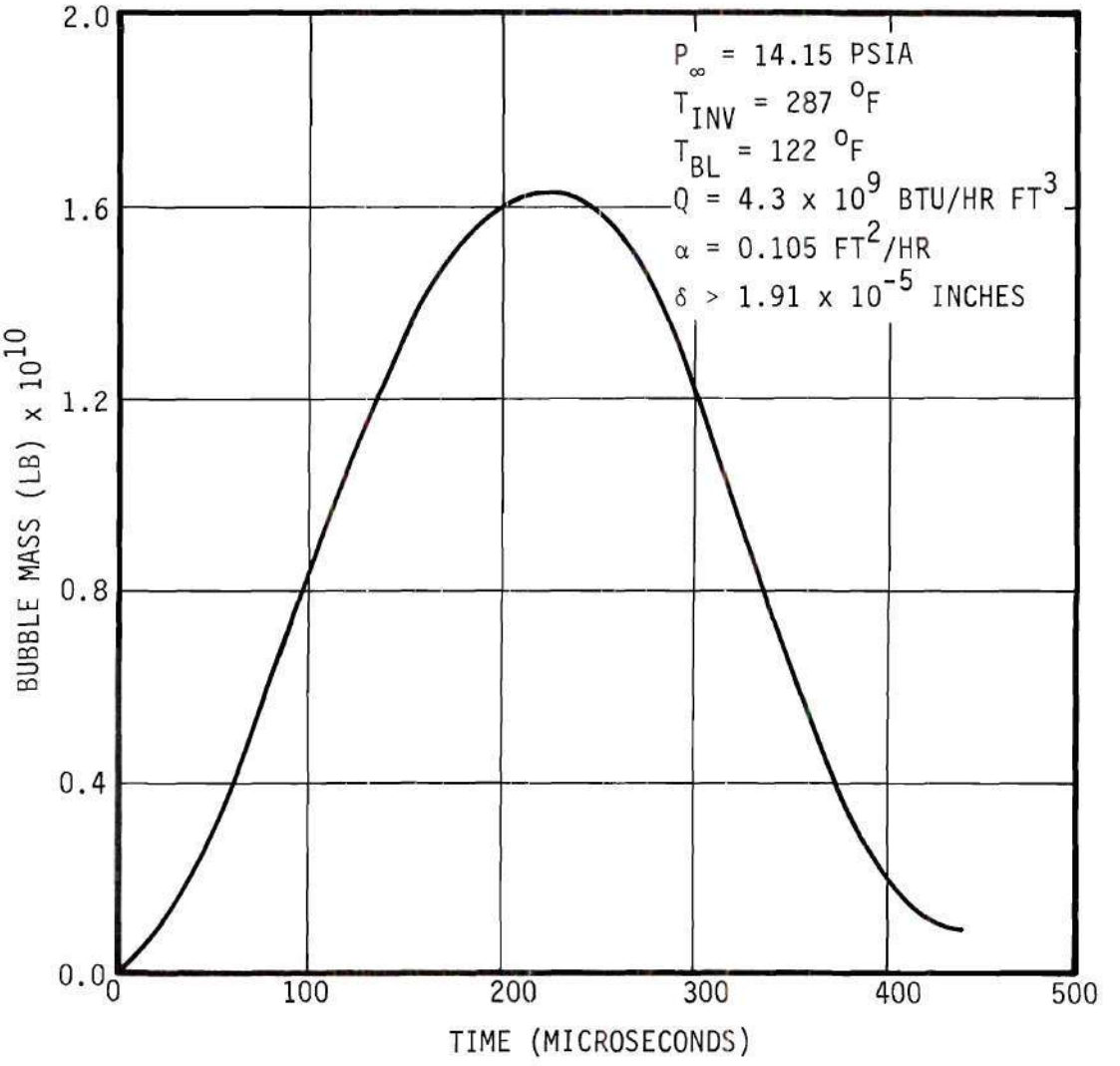

Figure 53. Bubble Mass as a Function of Time for the Real Boiling Model for Conditions as in Gunther's Experiment (See Reference 15, p. 119, Figure 9).

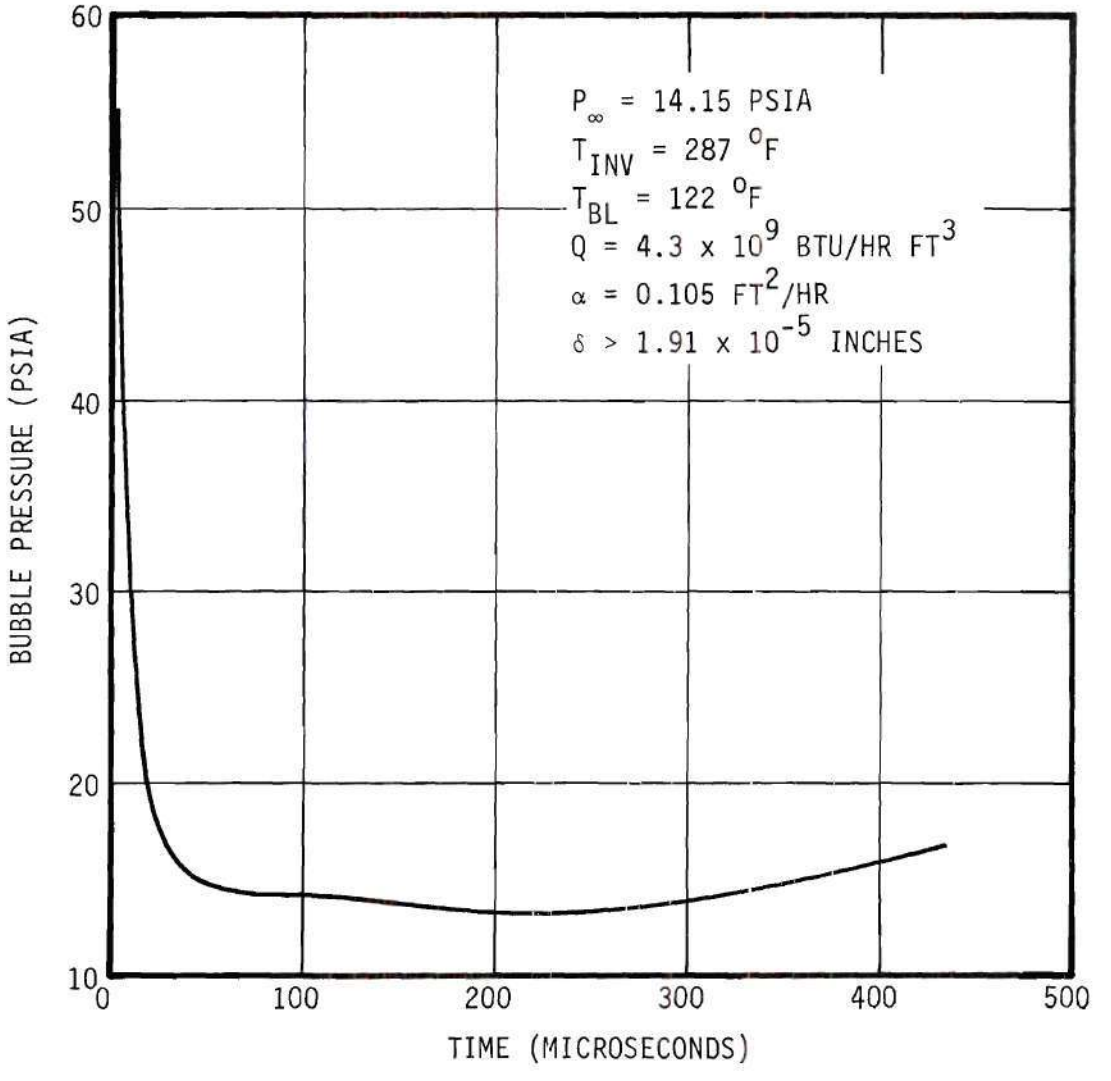

Figure 54. Bubble Pressure as a Funciton of Time for the Real Boiling Model for Conditions as in Gunther's Experiment (See Reference 15, p. 119, Figure 9).

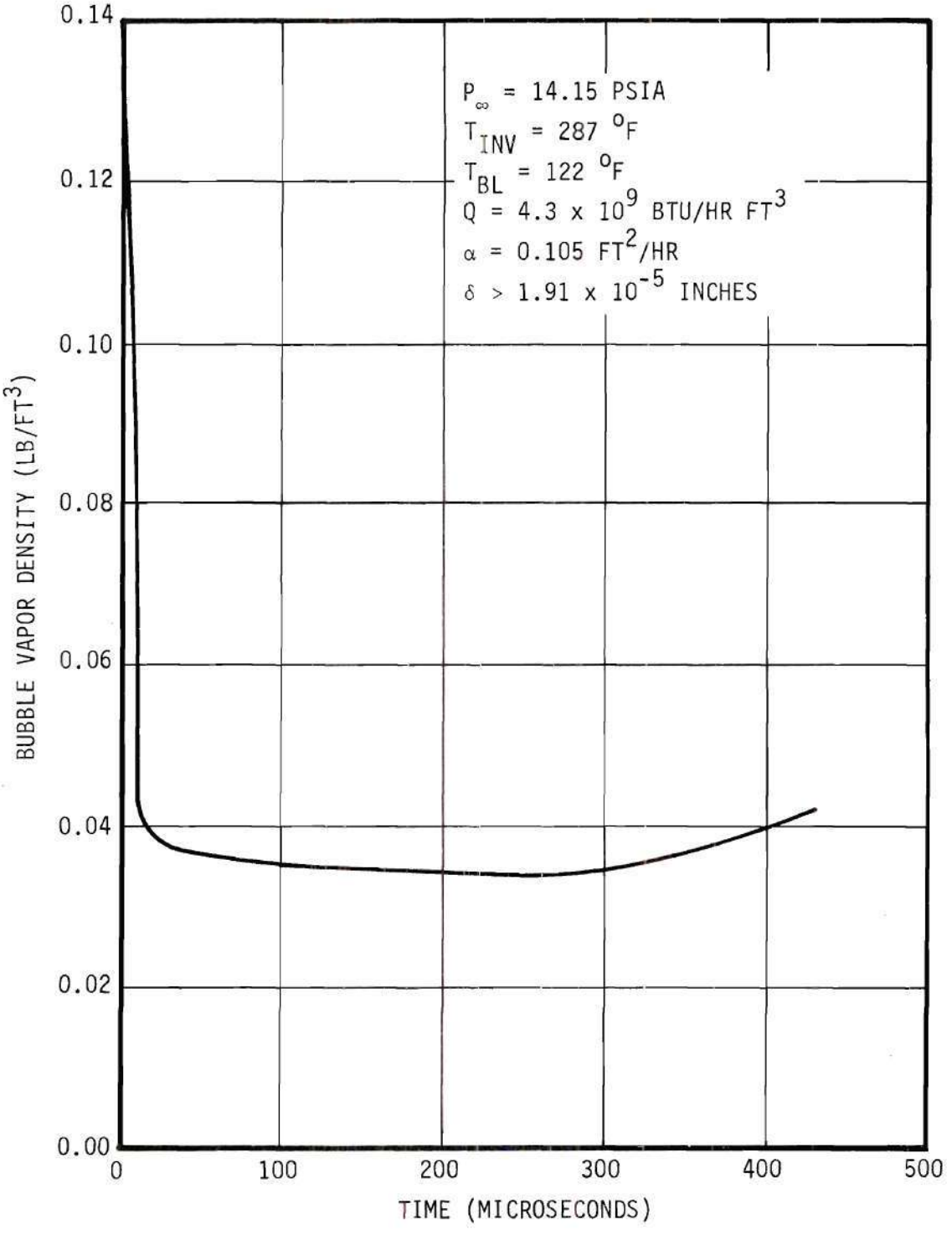

Figure 55. Bubble Vapor Density as a Function of Time for the Real Boiling Model for Conditions as in Gunther's Experiment (See Reference 15, p. 119, Figure 9).

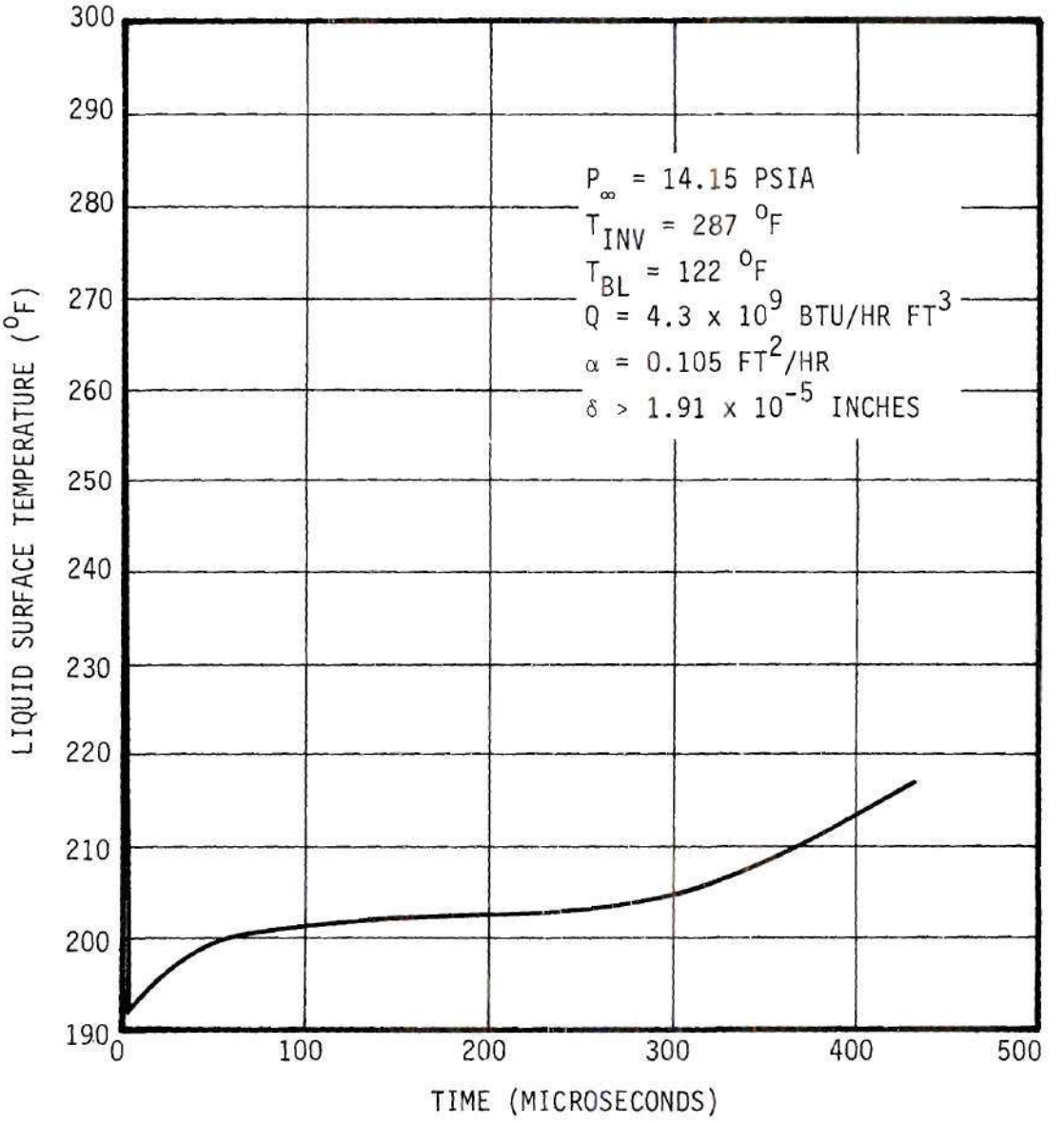

Figure 56. Liquid Surface Temperature as a Function of Time for the Real Boiling Model for Conditions as in Gunther's Experiment (See Reference 15, p. 119, Figure 9).

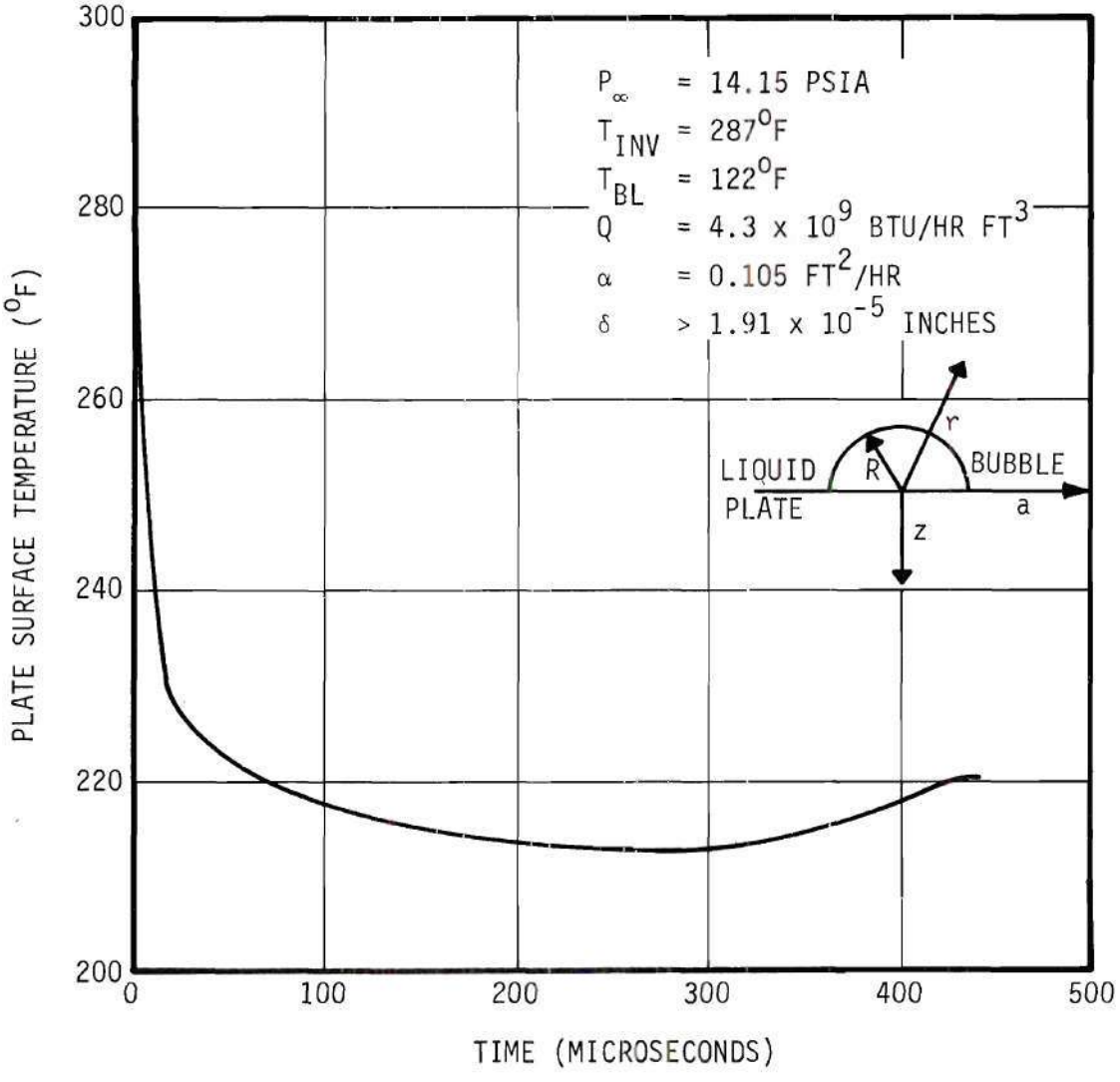

Figure 57. Plate Surface Temperature for a = o as a Function of Time for the Real Boiling Model for Conditions as in Gunther's Experiment (See Reference 15, p. 119, Figure 9).

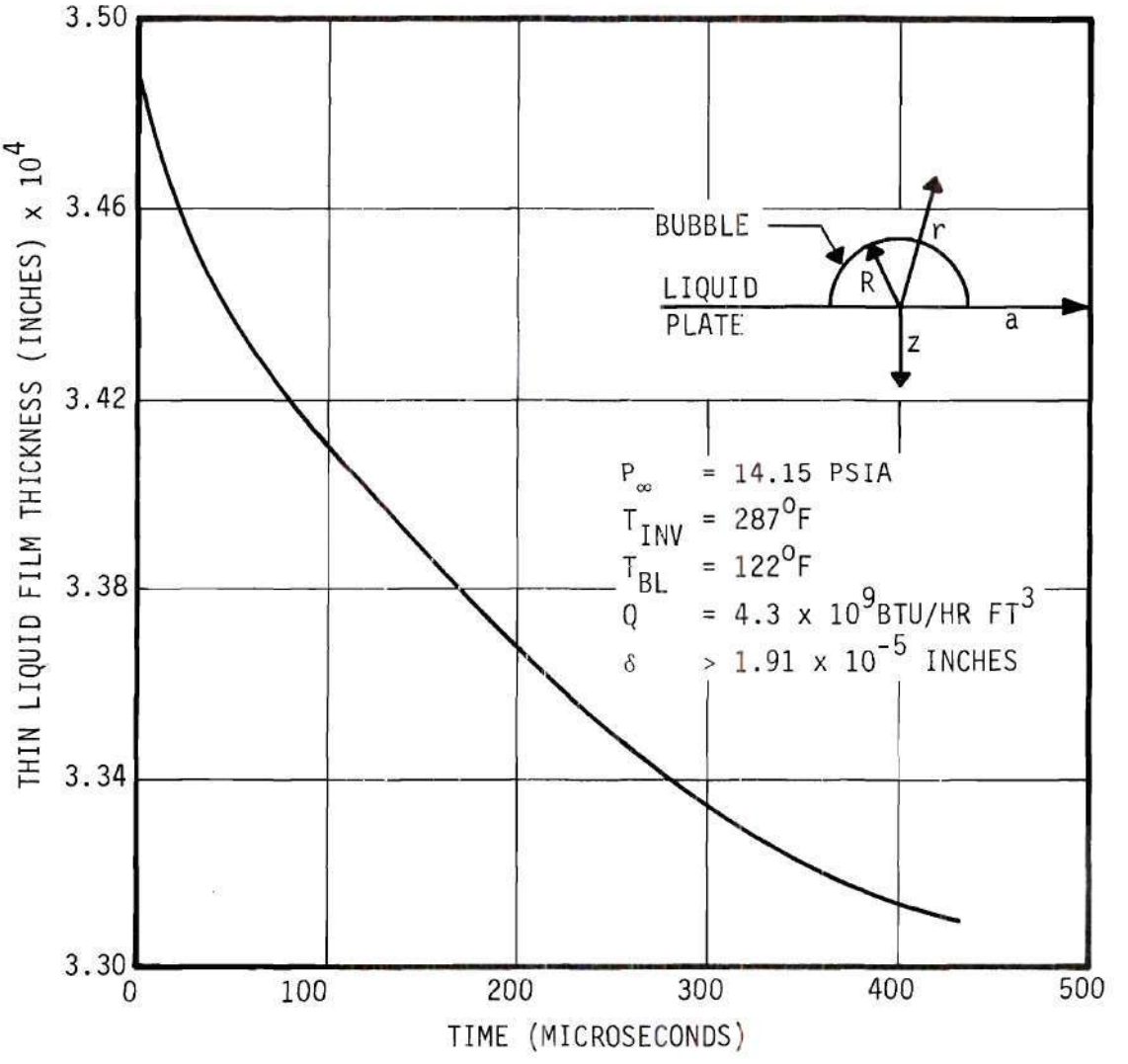

Figure 58. Thin Liquid Film Thickness for a = o as a Function of Time for the Real Boiling Model for Conditions as in Gunther's Experiment (See Reference 15, p. 119, Figure 9).

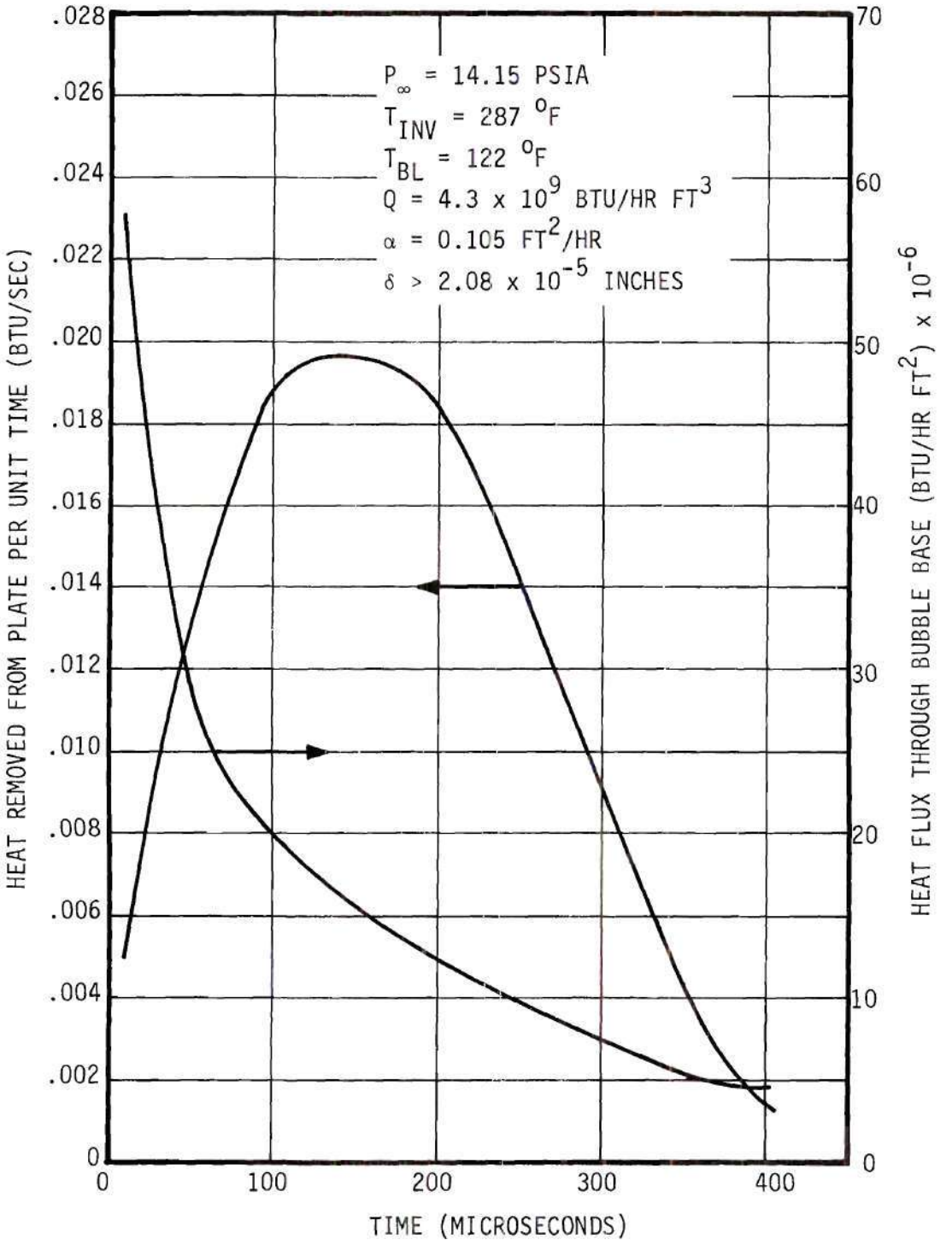

Figure 59. Heat Removed from Plate per Unit of Time and Heat Flux through Bubble Base as Functions of Time for the Real Boiling Model for Conditions as in Gunther's Experiment (See Reference 15, p. 119, Figure 9).

CHAPTER VII

CONCLUSIONS AND RECOMMENDATIONS

Conclusions

Single Bubble Experiment

1. The bubble heat transfer coefficient varied from approximately 4×10^4 to 4×10^5 BTU/hr ft^2 as the cooling stream velocity was varied from 0.2 to 38 ft/sec (Reynolds number varied from approximately 900 to 2×10^5) and as the cooling stream temperature was varied from 140°F to 80°F.

2. The ratio of the actual amount of heat removed from the bubble to the amount of latent heat necessary to form one volume of steam equal to the maximum observed volume of the bubble varied from approximately 10 to 100.

3. The presence (or absence) of a thin thermal boundary layer on the heated plate does not appreciably affect the turbulent diffusion of heat from the bubble surface and, thus, does not appreciably affect the amount of condensation occurring.

4. In the velocity range from approximately 2 ft/sec (Reynolds number equal 8,500) to 0.2 ft/sec (Reynolds number equal 900) the diffusion of heat from the bubble surface is relatively independent of velocity; thus showing that the motion of the fluid at the bubble surface due to the bubble growth motion induces turbulence around the bubble which is effective in removing large amounts of heat.

5. Near "burnout" in the subcooled nucleate boiling regime, it is believed that the mechanism of heat transfer is almost entirely due to mass transfer.

Schlieren Experiment

The surface of a bubble growing in a turbulent subcooled stream is surrounded by turbulent liquid.

Bubble Dynamics in the Single Bubble Case

A model based on first principles can predict the experimental results with a proper choice of the effective diffusivity for heat transfer.

Bubble Dynamics in Real Boiling

A model based on first principles and including a thin liquid film can predict experimental results with a proper choice of the effective diffusivity for heat transfer and this model predicted that the heat removed from the plate due to one bubble was approximately 30 times more than that calculated on the basis of the latent heat associated with the mass required to form one bubble volume.

Recommendations

Four experiments which might prove beneficial in understanding boiling heat transfer are:

1. To determine the frequency spectrum of the temperature fluctuations as a function of velocity and height above the heated surface for both subcooled nucleate boiling and non-boiling for forced convection. The frequency response of the thermocouple should approach 10^6 cycles per second in order to distinguish temperature fluctuations in the bubble boundary layer which arise from individual bubbles.

2. To determine the transient temperature history at various distances around a single bubble as it grows and collapses in subcooled nucleate boiling. This could be compared to theoretical predictions from the computer codes presented in this thesis.

3. To obtain high speed motion picture photograph of a schlieren image with enough resolution to observe the temperature gradients around a single bubble. This might be accomplished with a laser system.

4. To measure the ratio of the heat transferred to the cooling stream by all mechanisms to that transferred by the mass transfer mechanism. This might be accomplished by using two types of radioisotope tracers. The first should freely evaporate with water while the second should not.

The first tracer should be dissolved in a volume of liquid which will be injected into the boundary layer upstream of the boiling section. As the tracer moves onto the boiling surface, the thin liquid films then forming will be made from liquid containing the tracer. If the mass transfer effect is large, a large amount of the tracer will end up in the turbulent stream. A portion of the stream downstream of the boiling section should be removed to determine the tracer concentration. This may be done by standard counting procedures. Another run is then made using the second tracer (which will not evaporate). It is assumed that the amount of tracer reaching the turbulent stream due to diffusion and bubble agitation will be the same in both cases. Thus, the difference in the tracer level for the two cases will be due to the mass transfer mechanism.

Theoretical efforts might be aimed at improving the assumptions made in the constructions of the theoretical models. Also, a computer scheme based on implicit methods might reduce the time required to solve these problems.

APPENDICES

APPENDIX A

RESULTS

Table 3. Recorded Data for Single Bubble Experiment

Run No.	T_{IN}	P_A	P_B	Orifice No.	DP Calibrated Scale	V_G	V_{IG}	f_{60}	f_b
	°F	psi	psi			volts	MV		
5	110	8.60	3.00	Y63691	4.00	29.59	2.58	130	2
7	110	3.50	1.40	Y63691	2.00	29.39	2.53	130	2
8	110	8.70	2.90	Y63691	4.00	29.37	2.53	132	2
9	80	9.00	3.00	Y63691	4.00	31.51	2.86	130	2
10	140	9.00	3.00	Y63691	4.00	31.51	2.86	130	2
11	110	16.10	6.10	Y63691	5.95	30.10	2.81	130	2
12	110	1.25	0.75	Y63693	1.00	19.41	1.23	133	2
13	110	1.25	0.75	Y63693	2.00	19.41	1.23	131	2
14	110	1.40	0.75	Y63693	4.00	19.41	1.23	132	2

Run No.	V_R	V_{IR}	V_{TB}	V_{TG}	A_{cs}*	T_R	P_{ATM}	Dissolved Oxygen
	volts	MV	MV	MV	in^2	°C	mm-Hg	ppm
5	9.71	8.01	1.750	6.050	3.15	22.0	743.6	5.5
7	5.77	4.89	1.760	5.930	5.50	24.0	743.6	5.5
8	0.00	0.00	1.750	5.785	3.10	24.8	743.6	5.5
9	10.54	8.70	1.075	5.995	2.30	23.8	743.6	5.5
10	9.07	7.49	2.490	6.440	7.65	26.0	743.6	5.5
11	12.12	9.93	1.805	5.630	2.89	25.0	743.6	5.5
12	0.00	0.00	1.760	4.550	6.70	21.3	742.2	5.7
13	0.00	0.00	1.680	4.520	5.60	21.3	742.2	5.7
14	0.00	0.00	1.770	4.460	6.05	21.3	742.2	5.7

*This was the observed area under magnification. The scale was 1" observed length = 0.01421" actual length.

Table 4. Calculated Data for Single Bubble Experiment

Run No.	$R_b \times 10^2$ inches	Volume $\times 10^9$ ft^3	θ μ sec	P_S psia	T_{SAT} °F	ΔT_{sub} °F	U ft/sec	M_{IN}
5	2.00	9.85	256	18.7	225	114	25.50	0.686
7	2.66	22.90	256	16.0	216	106	12.00	0.672
8	2.00	9.75	253	17.7	221	111	25.50	0.675
9	1.72	6.12	256	20.6	228	148	25.50	0.845
10	3.14	37.60	256	17.8	221	81	25.50	0.844
11	1.92	8.55	256	24.9	239	129	38.20	0.794
12	2.66	27.90	251	15.1	213	103	0.20	0.166
13	2.56	20.30	254	15.1	213	103	0.75	0.166
14	2.80	26.50	253	15.1	213	103	1.90	0.166

Run No.	Q_{IN} BTU/hr	$h_b \times 10^{-5}$ BTU/hr ft^2 °F	Q_{IN}/A_b BTU/in^2 sec	$(U/0.2)^{\frac{1}{2}} \Delta T_{sub}$ $(ft/sec)^{\frac{1}{2}}$ °F	$H_b \times 10^5$ BTU/BUBBLE	$H_b' \times 10^5$ BTU/BUBBLE	Heated Plate Temperature °F
5	631	3.140	69.3	1278.0	4.49	0.0443	310
7	621	1.900	38.8	840.0	4.42	0.0974	260
8	626	3.230	69.5	1200.0	4.40	0.0422	
9	779	4.060	116.7	1600.0	5.54	0.0305	310
10	771	2.210	34.5	915.0	5.49	0.1620	310
11	740	3.560	88.8	1699.0	5.00	0.0494	320
12	160	0.439	8.7	103.0	1.11	0.1040	
13	160	0.544	10.8	198.5	1.13	0.0758	
14	160	0.454	9.1	316.0	1.12	0.0985	

Table 5. Bankoff's Data

Run No.	U ft/sec	T_{IN} °F	ΔT_{sub} °F	$(U/0.2)^{\frac{1}{2}} \Delta T_{sub}$ $[ft/sec]^{\frac{1}{2}}$ °F	A_{av} $Ft^2 \times 10^6$	Q_{IN} BTU/hr	Q_{IN}/A_{av} BTU/in^2 sec
A-11	1.07	80	132	306	3.53	46.05	25.2
A-12	1.10	120	92	215	5.77	41.35	13.8
A-21	2.45	80	132	463	1.99	48.35	46.8
A-22	2.80	118	94	351	4.73	48.35	19.7
B-31	4.05	82	130	584	3.38	81.00	27.8
B-32	5.00	121	91	454	5.56	80.40	27.8
B-41	4.60	79	133	630	3.29	80.40	47.1
B-42	5.60	120	92	486	5.11	79.60	30.0

Table 6. Recorded and Calculated Data for Schlieren Experiment

Schlieren Picture No.	T_{IN} °F	DP calibrated scale	P_A psi	P_B psi	V_R volts	V_{IR} MV	Heat Flux $\times 10^{-5}$ BTU/hr ft^2	Percent of Burnout heat flux*	Resistance ohm	Average Plate Temp. °F	P_{ATM} mm-Hg
1, 2, 3	125	3.2	6.0	2.1	0.0	0.0	0.0	0.0	---	---	739.0
4, 5, 6	125	3.2	6.0	2.1	3.376	2.89	1.28	4.44	0.02920	242	739.0
7 - 15	125	3.2	6.0	2.1	9.586	7.82	9.86	34.2	0.03065	330	739.0
16 - 26	125	3.2	6.0	2.1	13.64	10.79	19.30	67.0	0.03160	384	739.0

*The burnout heat flux was calculated to be 28.8×10^5 BTU/hr ft^2 with an equation suggested by Gunther (15):

$$Q/A|_B = (0.0135)U^{\frac{1}{2}}\Delta T_{sub}$$

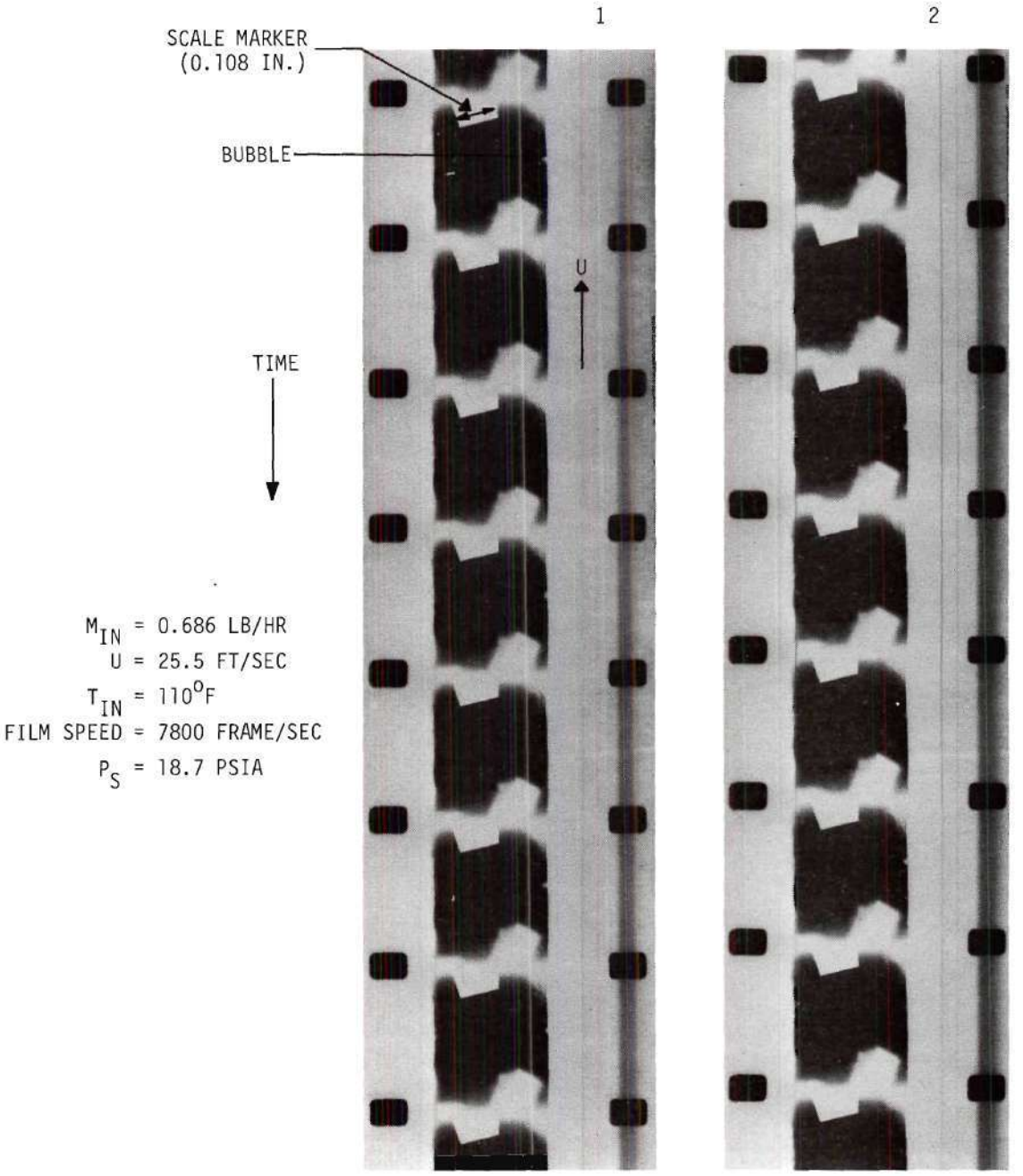

Figure 60. High Speed Photographs of Run No. 5.

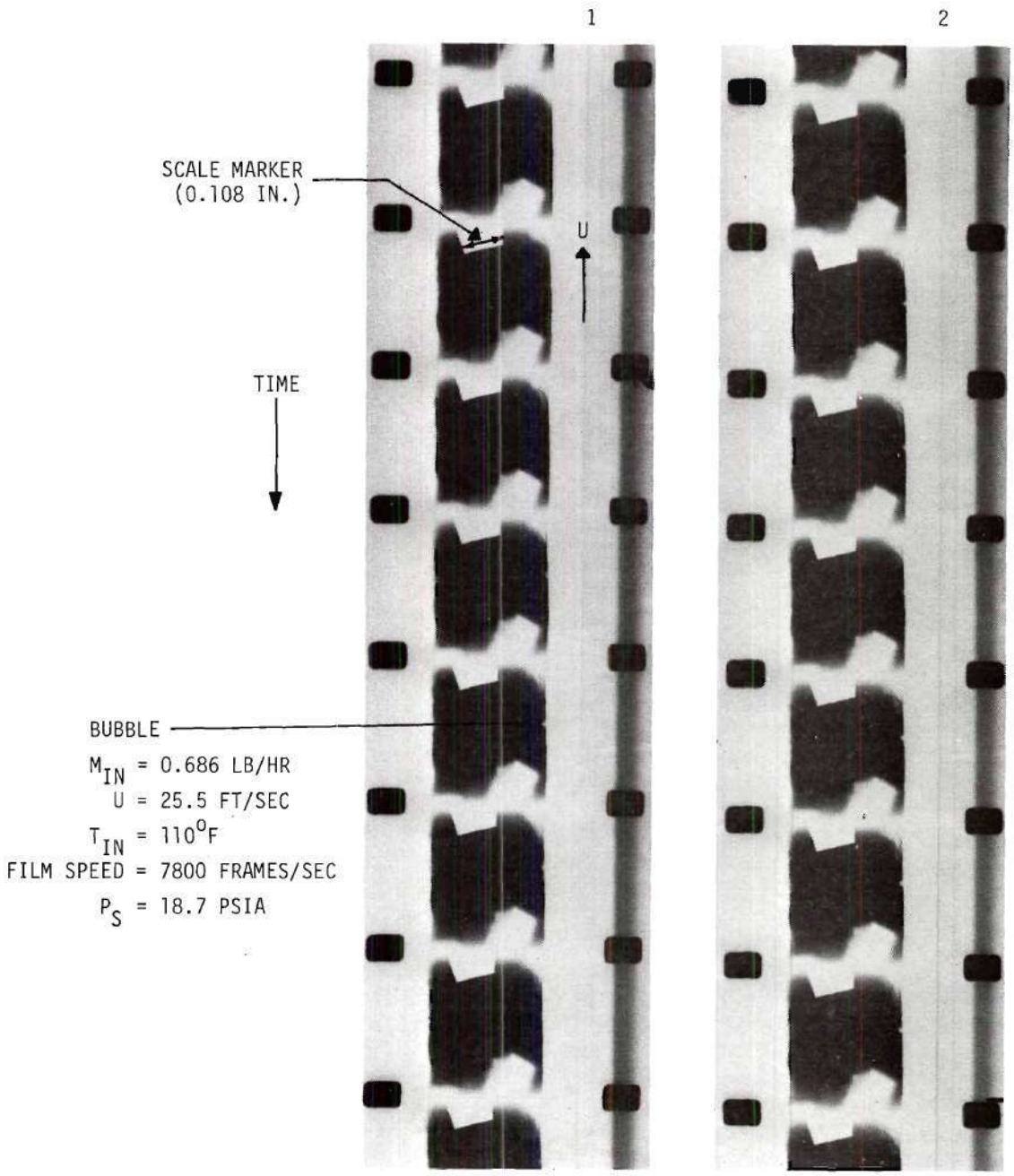

Figure 61. High Speed Photographs of Run No. 5.

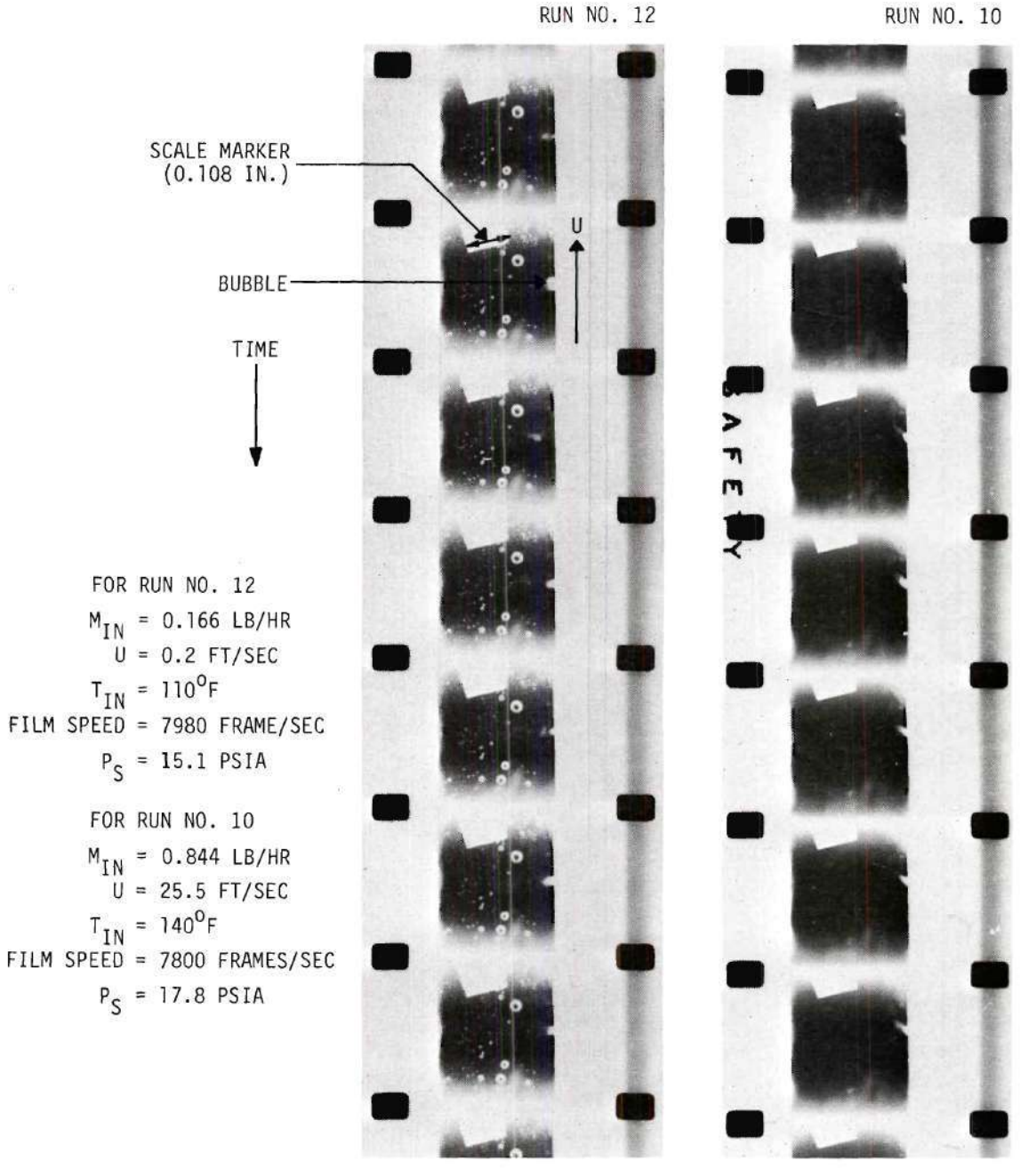

Figure 62. High Speed Photographs of Runs No. 10 and 12.

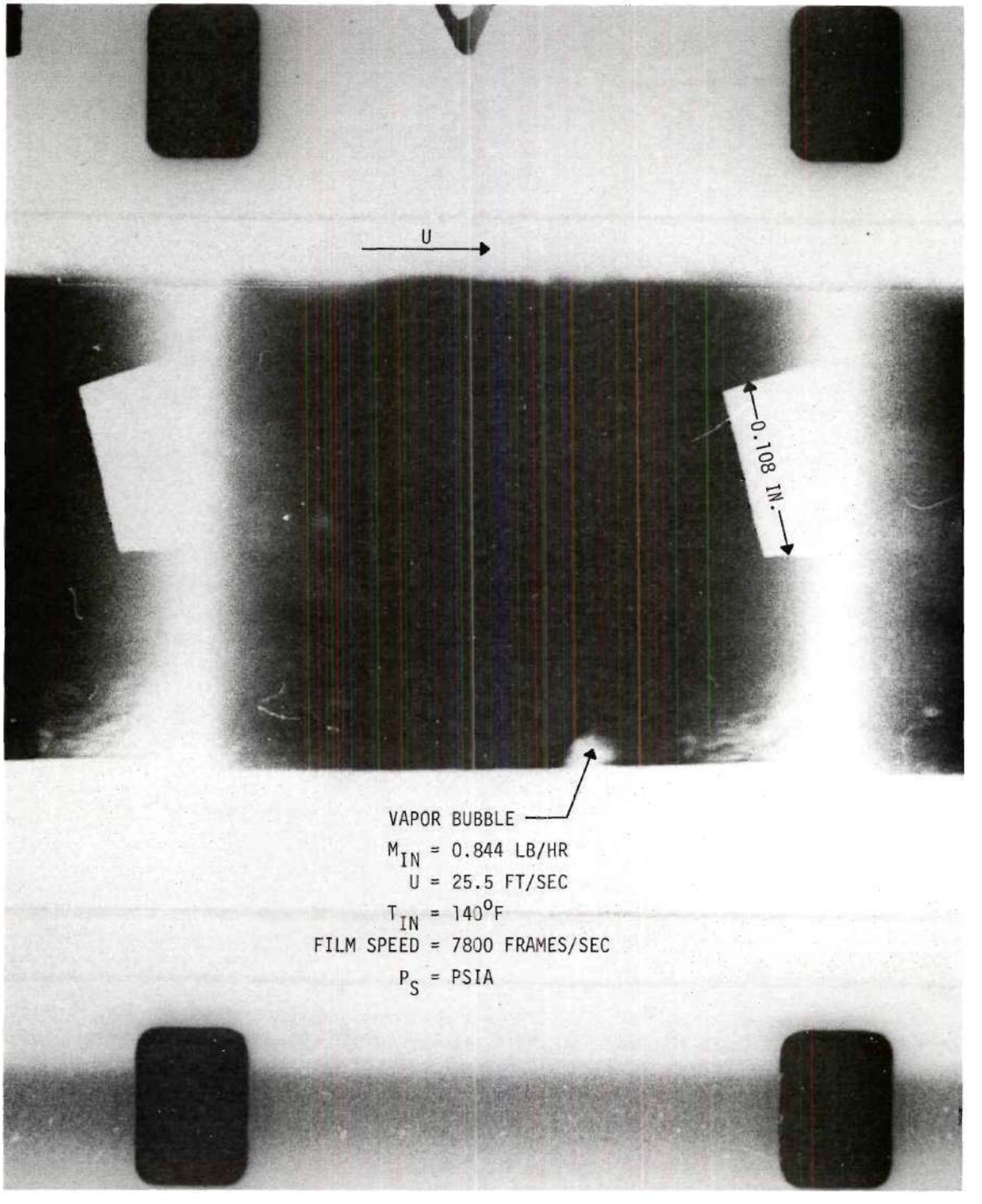

Figure 63. High Speed Photograph of Run No. 10.

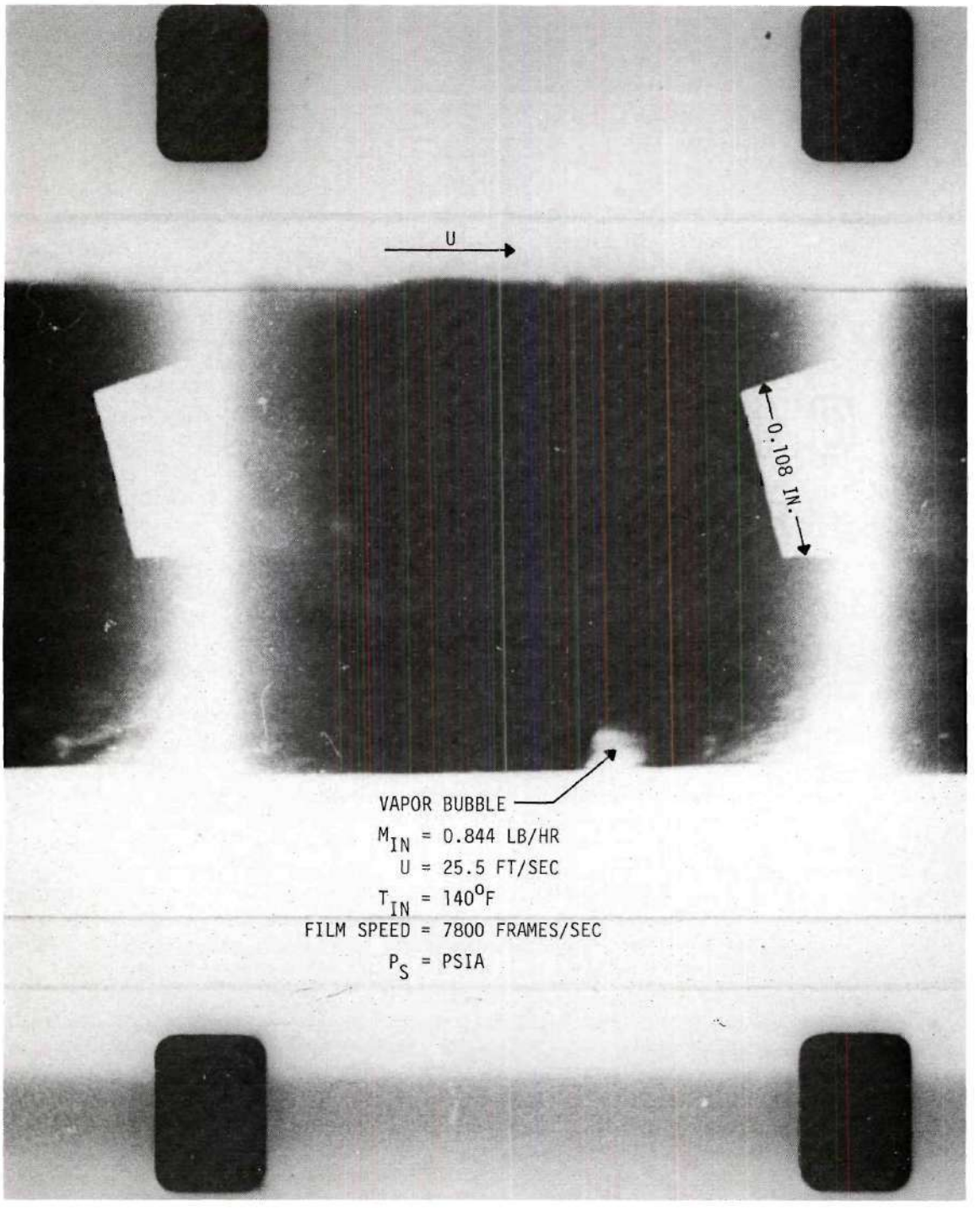

Figure 64. High Speed Photograph of Run No. 10.

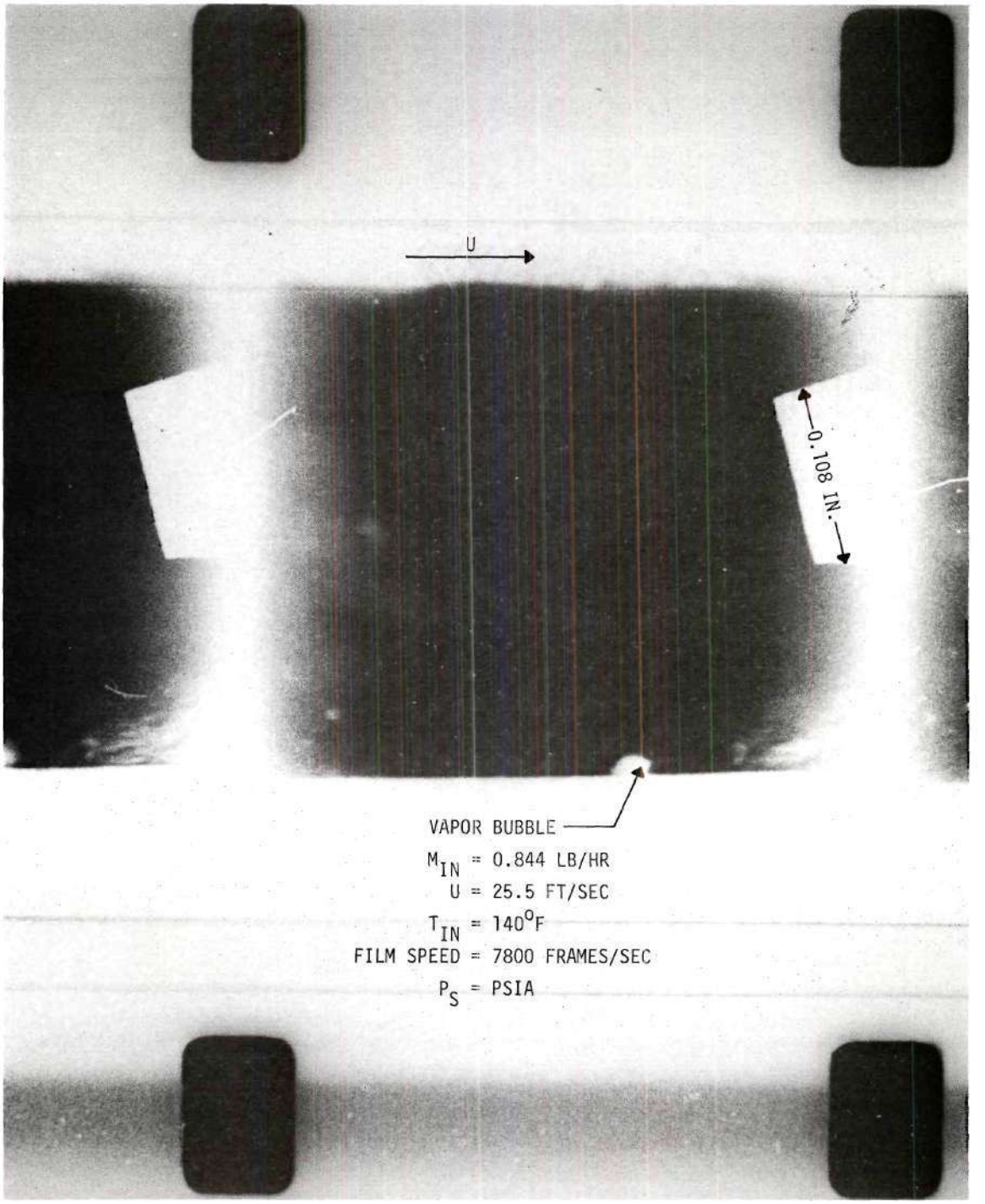

Figure 65. High Speed Photograph of Run No. 10.

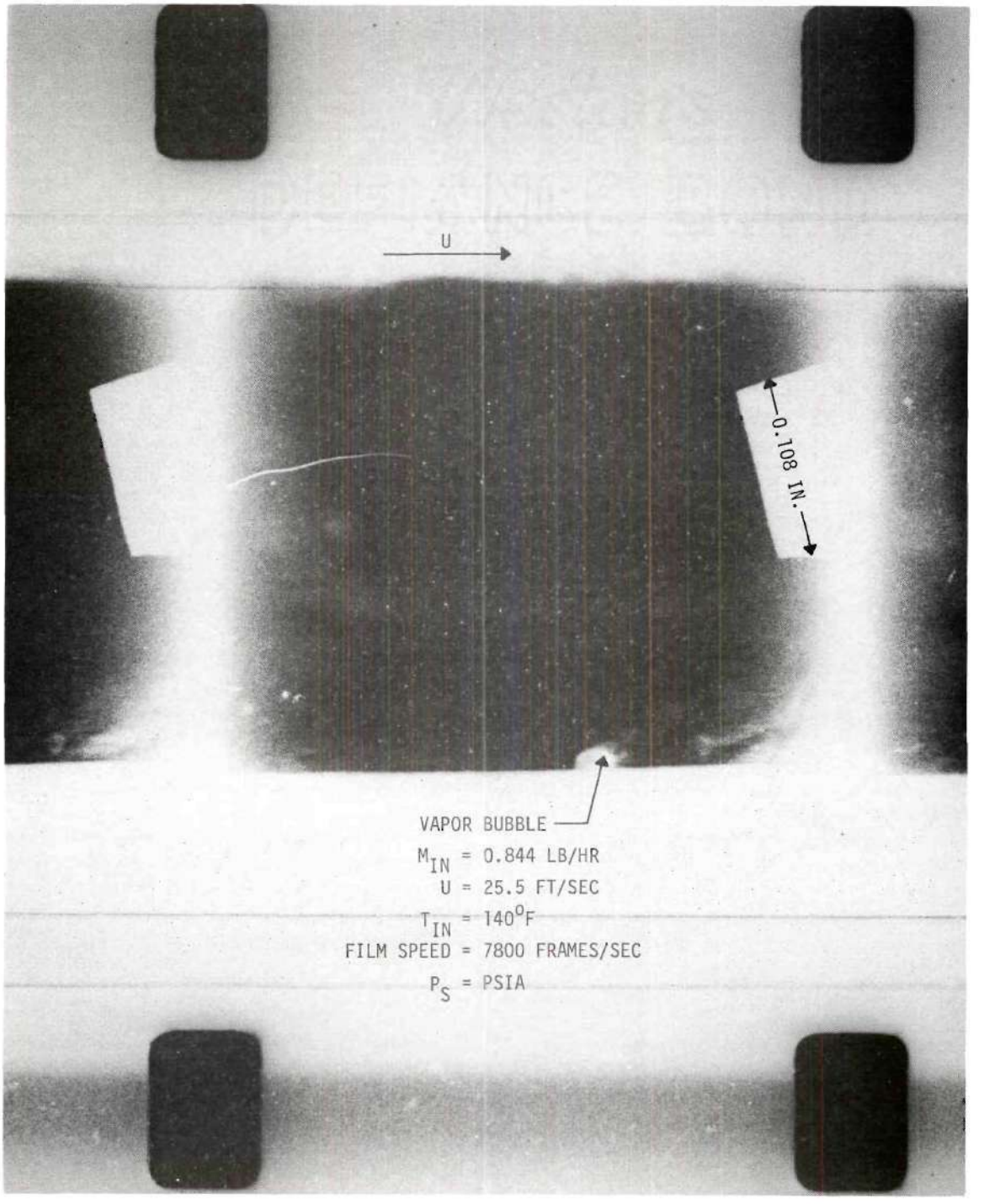

Figure 66. High Speed Photograph of Run No. 10.

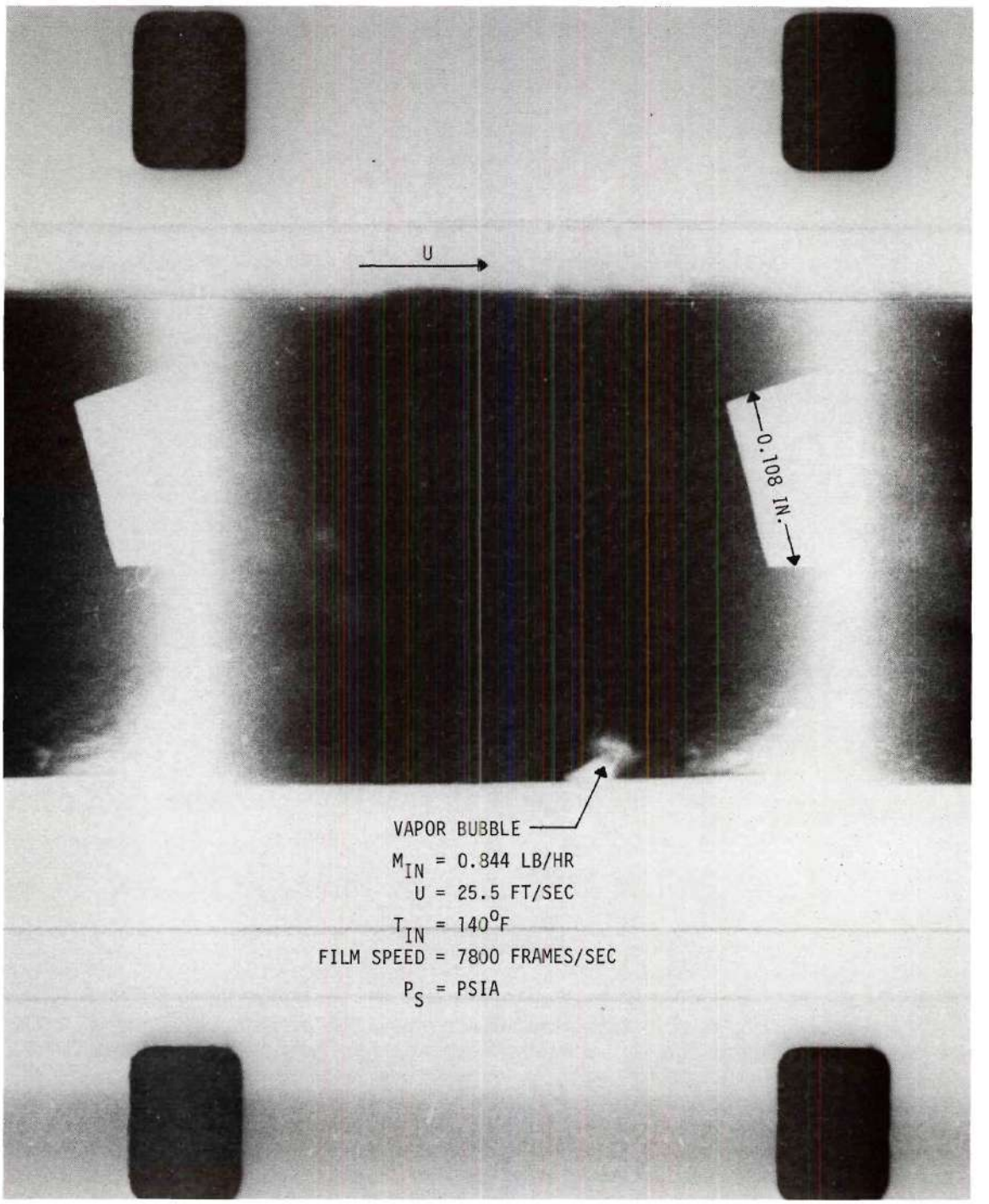

Figure 67. High Speed Photograph of Run No. 10.

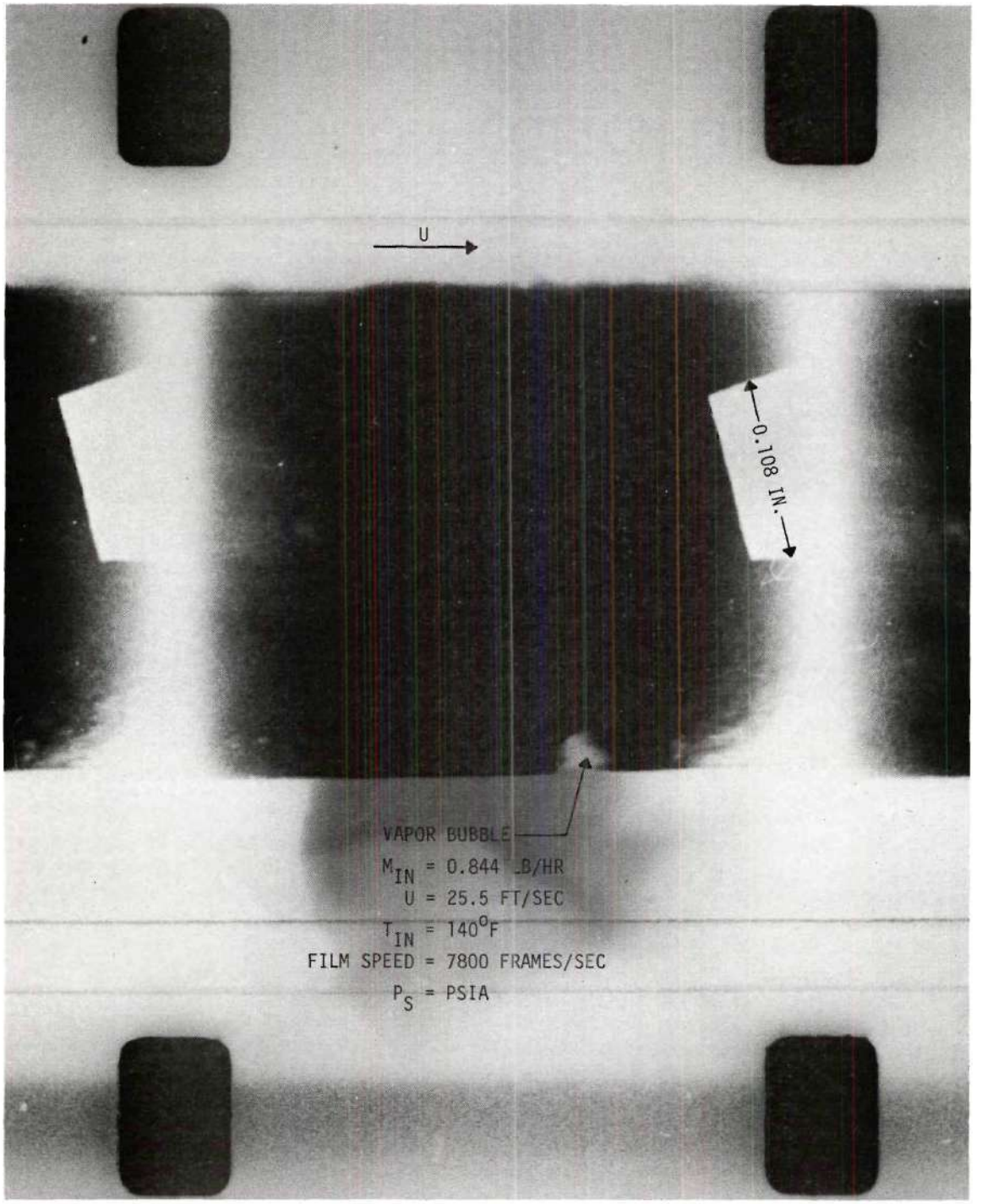

Figure 68. High Speed Photograph of Run No. 10.

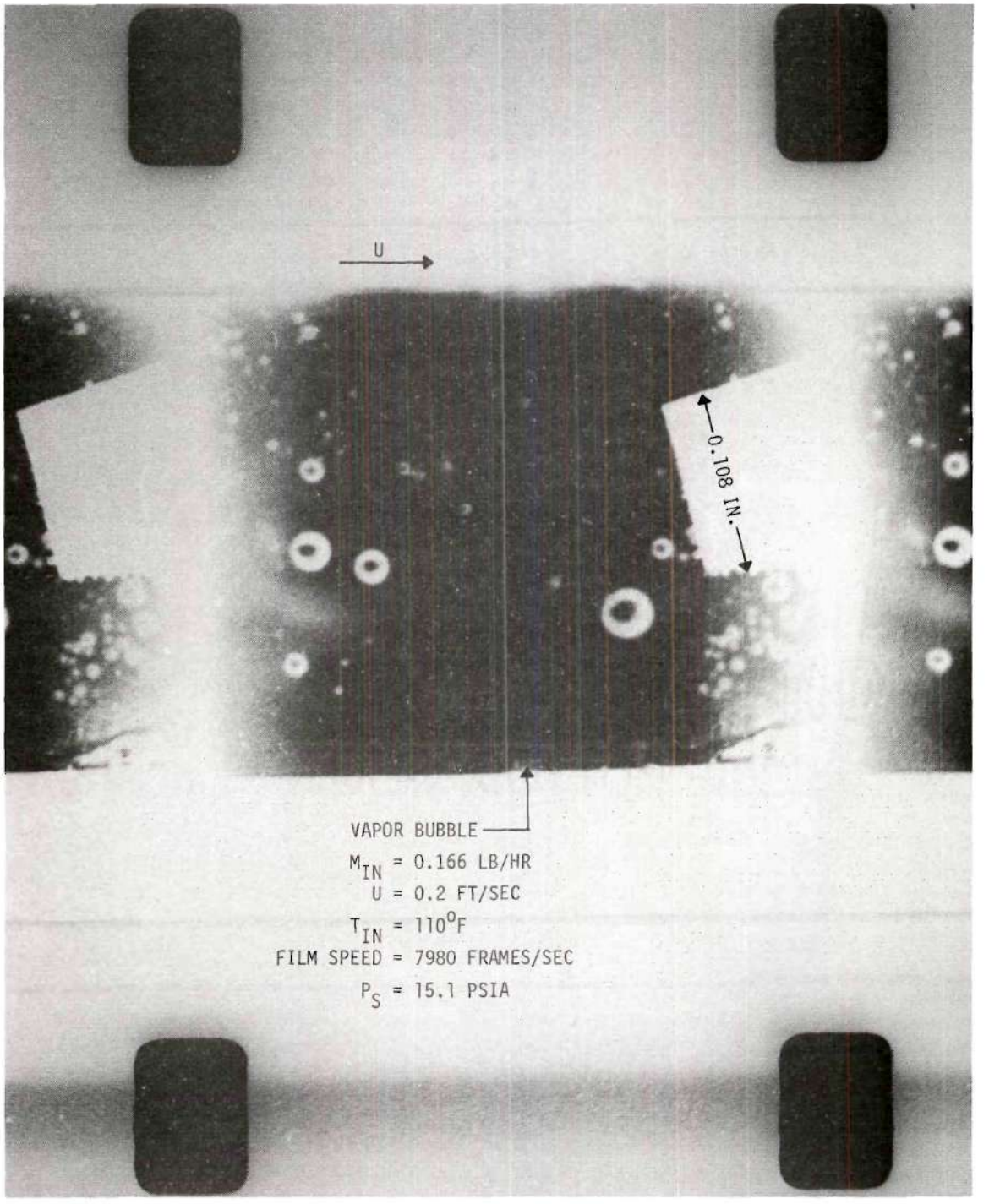

Figure 69. High Speed Photograph of Run No. 12.

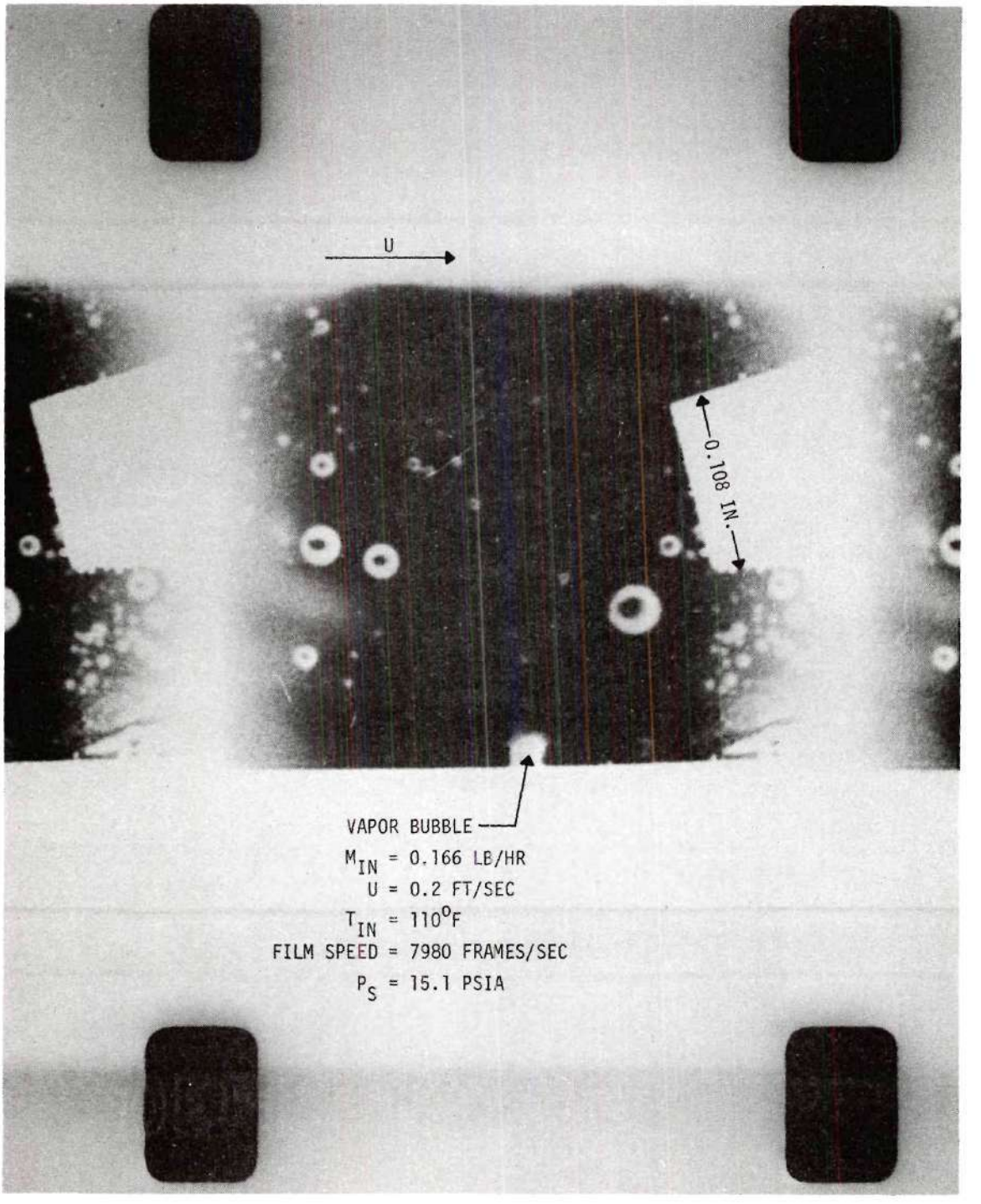

Figure 70. High Speed Photograph of Run No. 12.

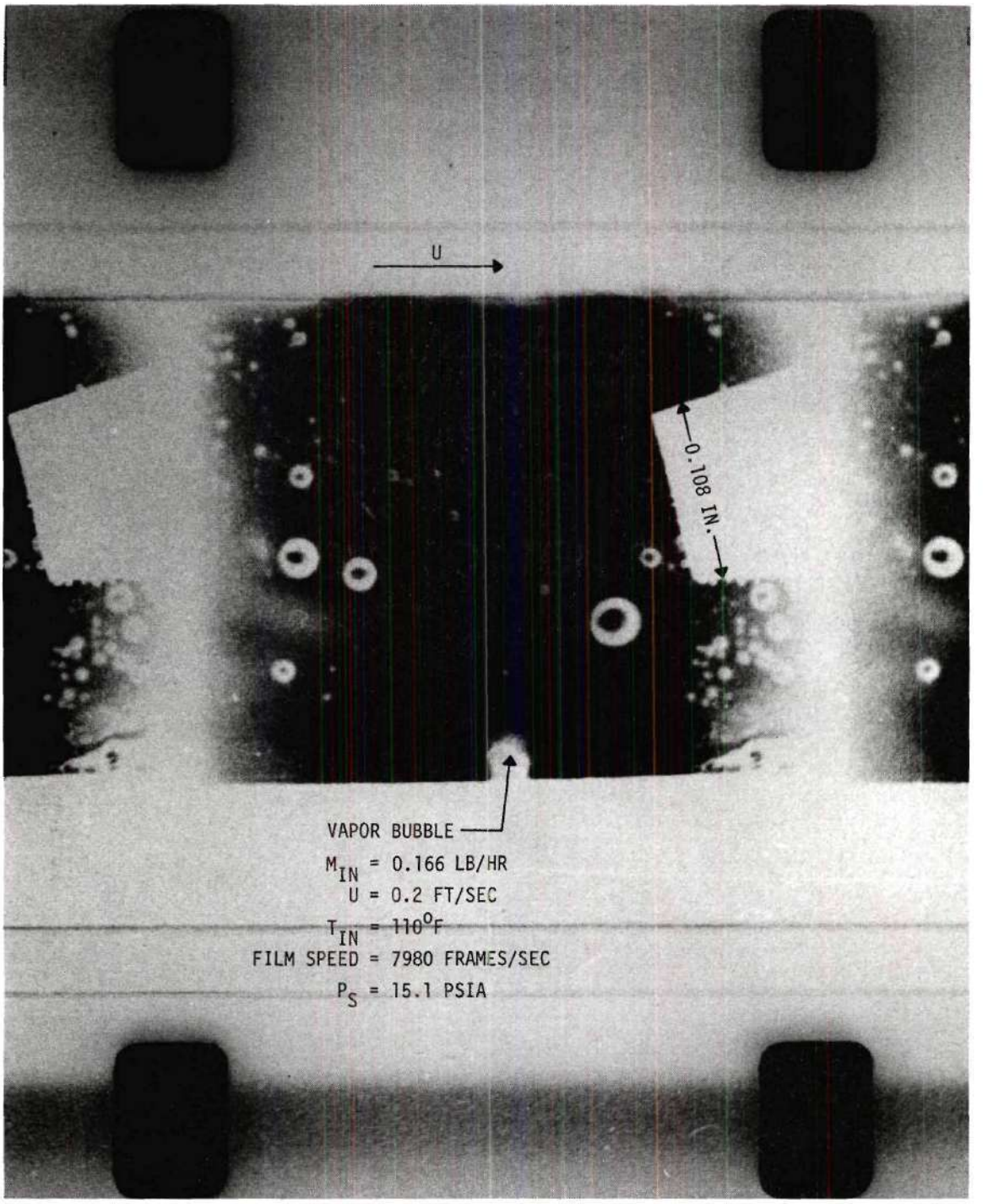

Figure 71. High Speed Photograph of Run No. 12.

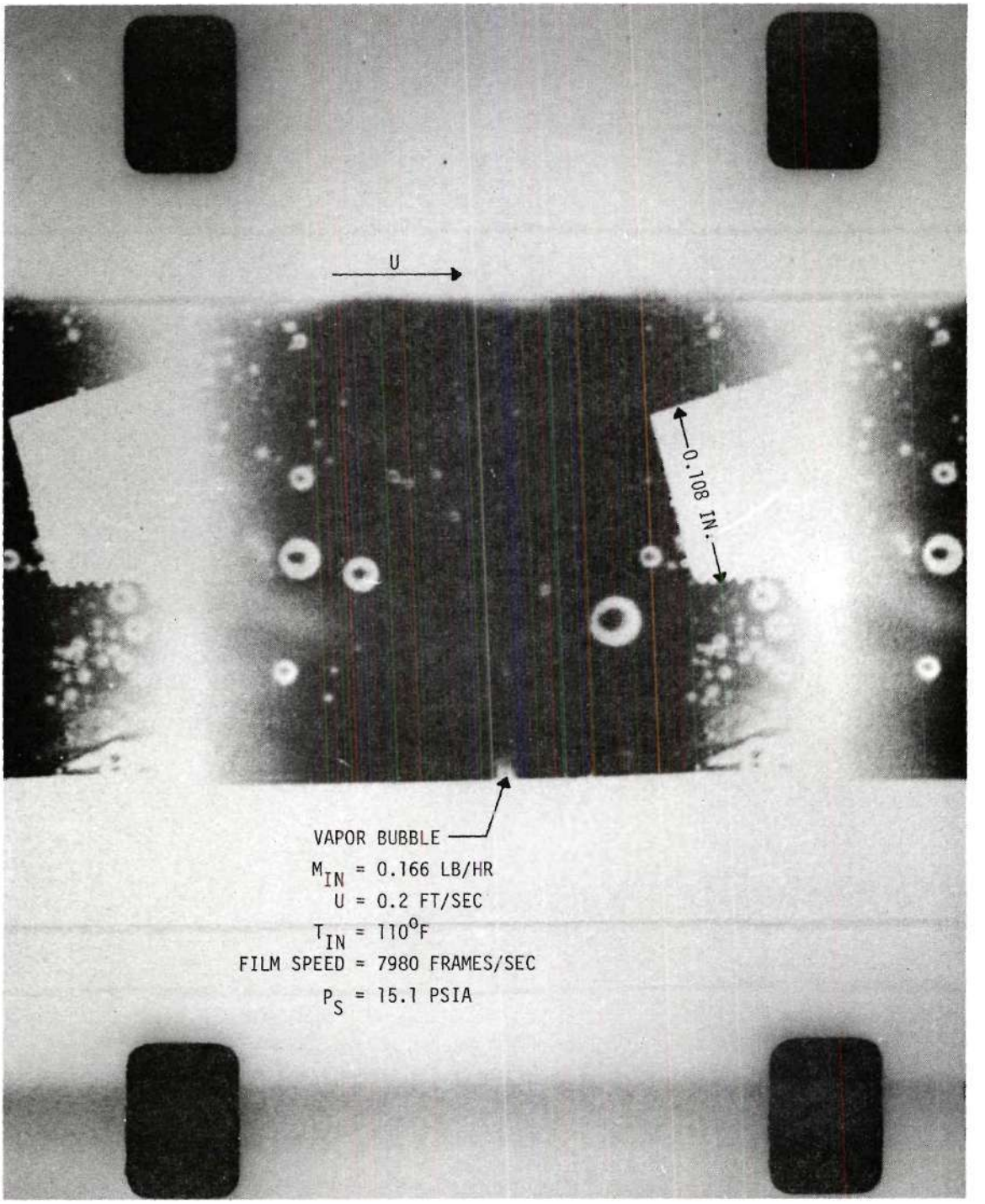

Figure 72. High Speed Photograph of Run No. 12.

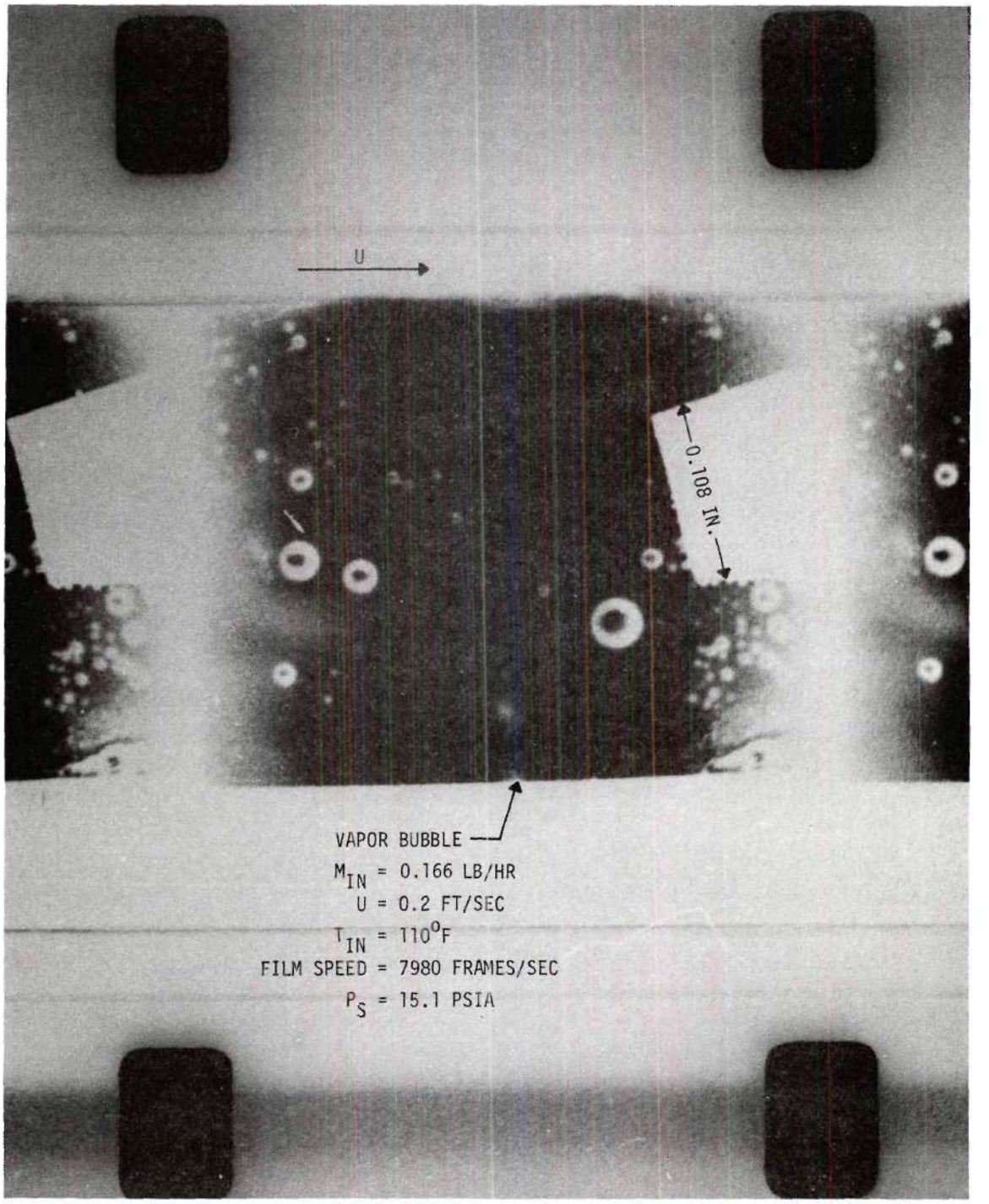

Figure 73. High Speed Photograph of Run No. 12.

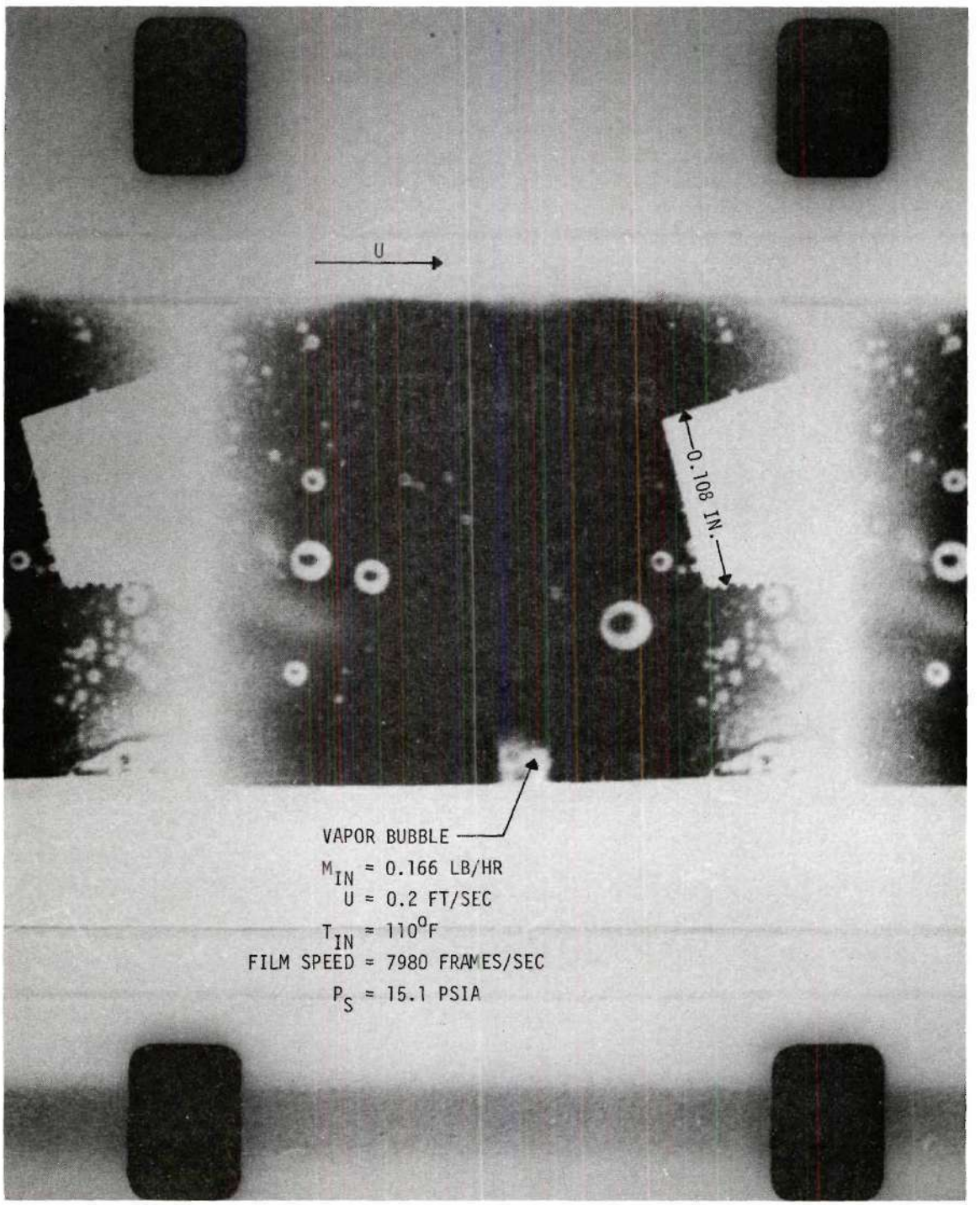

Figure 74. High Speed Photograph of Run No. 12.

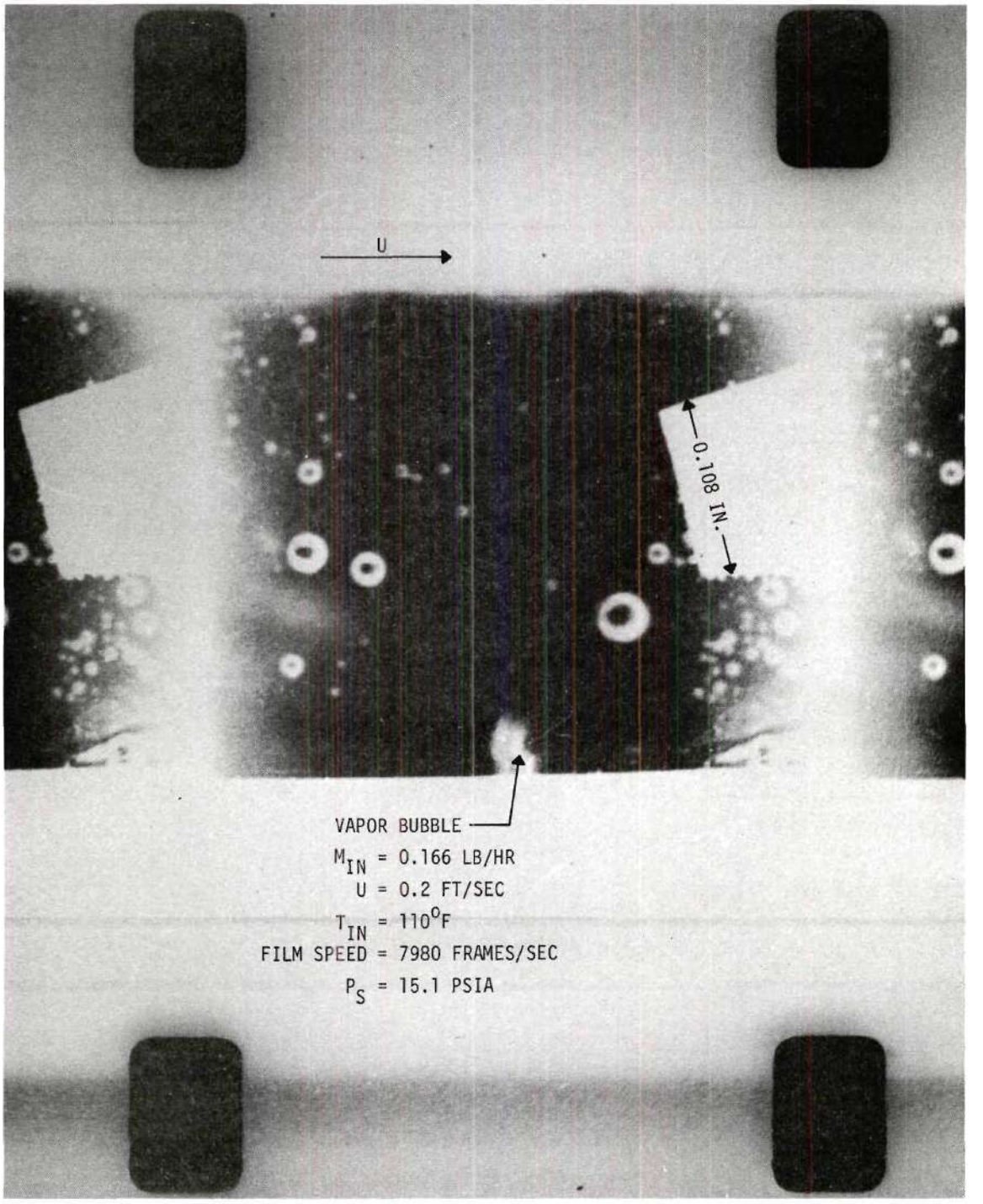

Figure 75. High Speed Photograph of Run No. 12.

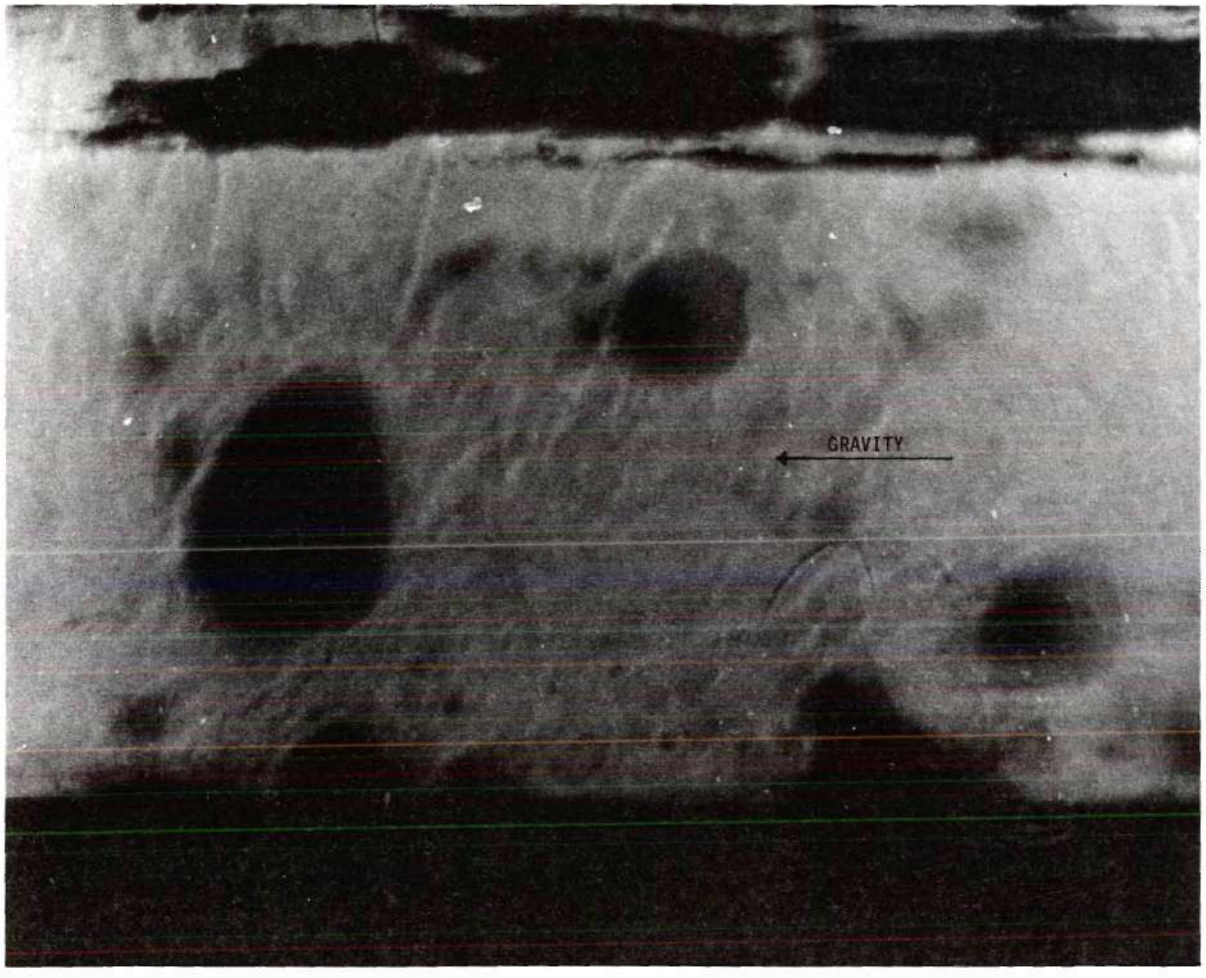

Figure 76. Attempted Schlieren Photograph: Pool Boiling.

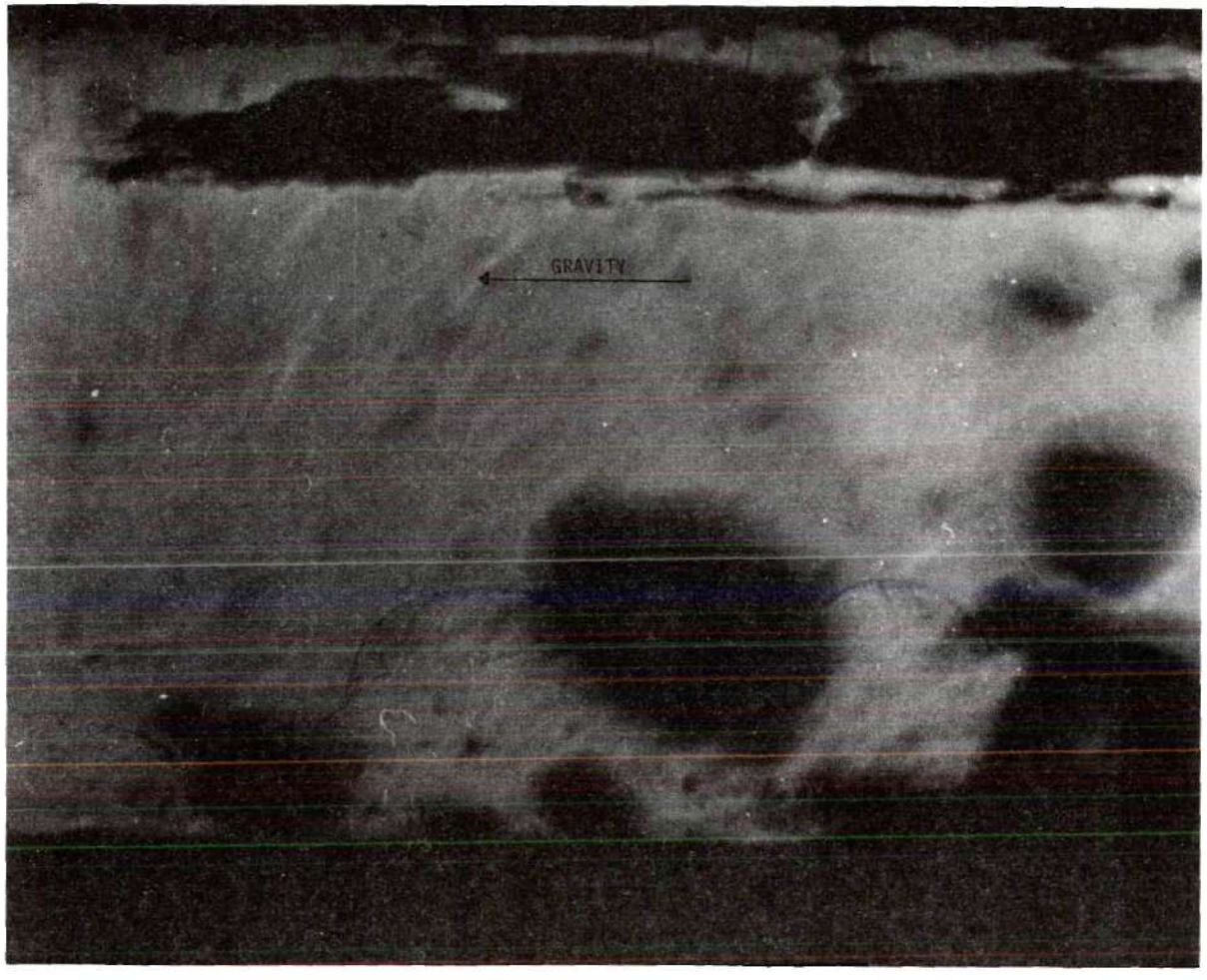

Figure 77. Attempted Schlieren Photograph: Pool Boiling.

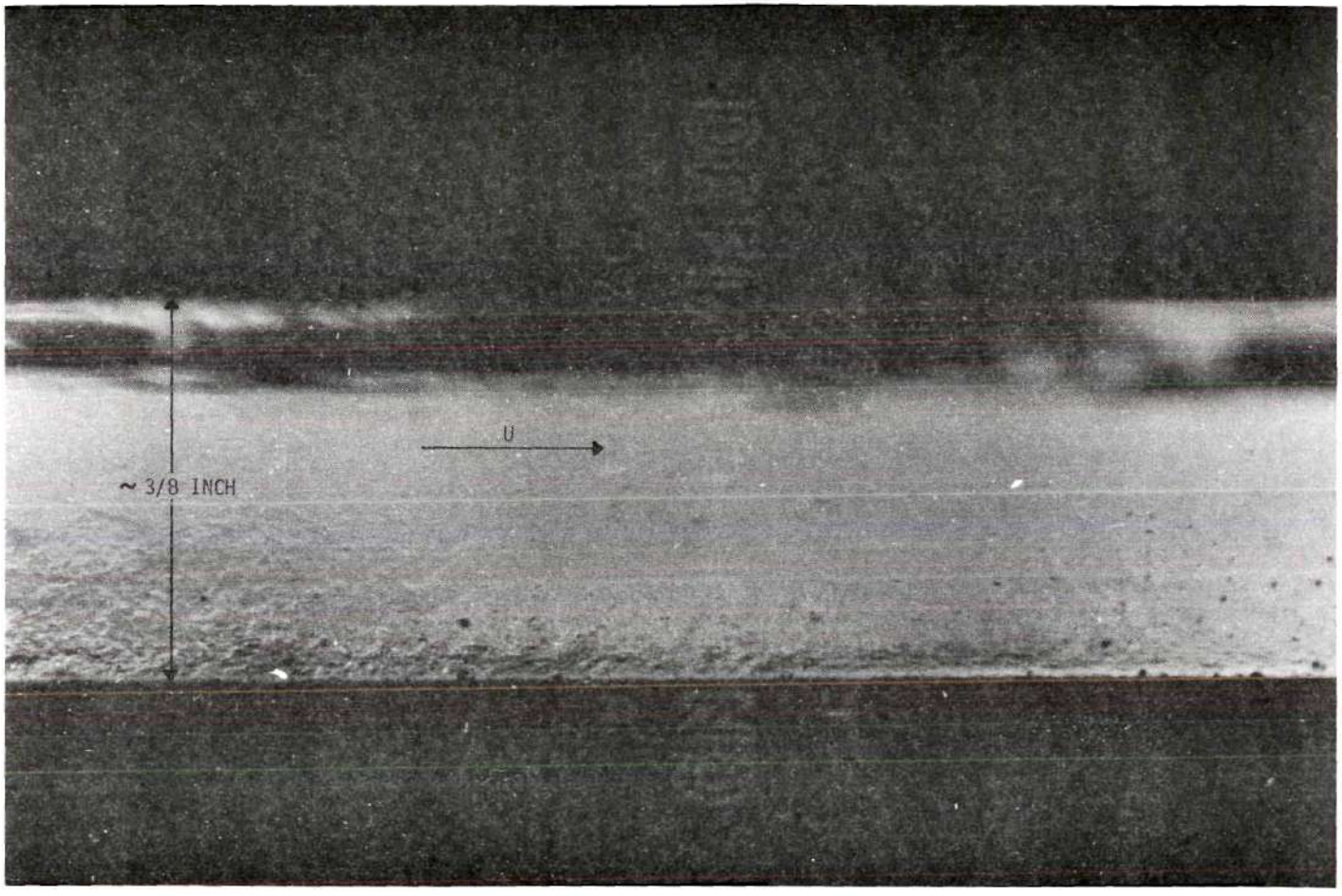

Figure 78. Attempted Schlieren Photograph: Forced Convection Boiling.

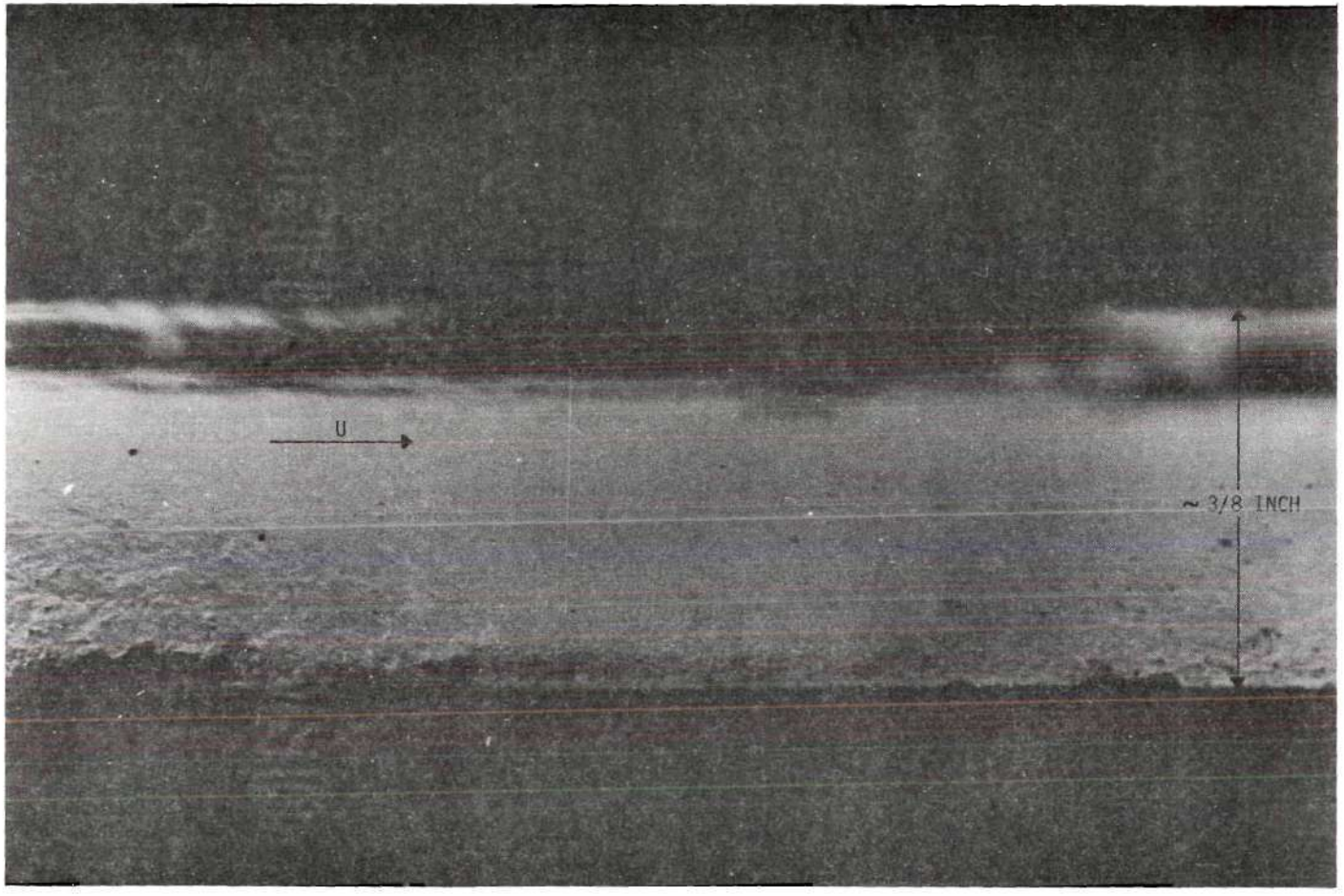

Figure 79. Attempted Schlieren Photograph: Forced Convection Boiling.

Figure 80. Attempted Schlieren Photograph: Forced Convection Boiling.

Table 7. Input Numbers for the Computer Code in the Experimental Case

Run No.	P_∞ psi	T_{BL} °F	U ft/sec	T_{SAT} °F	T_{INV} °F	M_{IN} lb/hr	Dy	α ft^2/hr
7	16.0	110	12.0	216	217	1.343	0.00085	1.2
8	17.7	110	25.5	221	222	1.350	0.00120	3.0
9	20.6	80	25.5	228	230	1.690	0.00075	3.0
10	17.8	140	25.5	221	222	1.690	0.00135	3.0
14	15.3	110	1.9	213	215	0.333	0.00033	0.06

APPENDIX B

NUMERICAL SOLUTIONS OF BUBBLE DYNAMICS MODELS

Single Bubble Experimental Case

Numerical Solution for R, $\dot{R}$ and $\ddot{R}$

Letting R_n indicate the bubble radius at a time n·Dt where Dt is a small increment of time and n is an integer, the following relations for R_{n+1}, $\dot{R}_{n+1}$, and $\ddot{R}_{n+1}$ were used:

$$R_{n+1} = R_n + \dot{R}_n \cdot Dt + \ddot{R}_n \frac{Dt^2}{2} \tag{B.1}$$

$$\dot{R}_{n+1} = \dot{R}_n + \ddot{R}_n \, Dt \tag{B.2}$$

and

$$\ddot{R}_{n+1} = \left(\frac{P_n - P_\infty}{\rho_l} - \frac{3}{2} (\dot{R}_n)^2 \right) \frac{1}{R_n} \tag{B.3}$$

where P_n is the bubble vapor pressure at n·Dt

P_∞ is the ambient liquid pressure.

Equation B.1 is a three-term Taylor series approximation to R and B.2 is a two-term Taylor series approximation to $\dot{R}$. Equation B.3 is equivalent to equation 3.3.

In starting the solution R_o was assumed to be 0.013 inch for the reason given in Chapter III. $\ddot{R}_o$ was assumed to be zero and $\dot{R}_o$ was calculated by:

$$\check{R}_o = \left(\frac{(P^o_{VAP} - P_\infty)}{\rho_l} \frac{2}{3} \right)^{\frac{1}{2}} \qquad (B.4)$$

where P^o_{VAP} is the initial value of the pressure in the bubble which was obtained as discussed on page 32.

Numerical solution of Heat Diffusion in Liquid

This consisted of a numerical solution to equation 3.11 which is repeated here:

$$\frac{\partial \Phi}{\partial t'} - \dot{\gamma} \left[1 - \frac{1}{(1 + \frac{y}{\gamma})^2} \right] \frac{\partial \Phi}{\partial y} + \frac{P_E \mu}{2} \left[1 - \frac{1}{(1 + \frac{y}{\gamma})^3} \right] \frac{\partial \Phi}{\partial y} \qquad (B.5)$$

$$+ \frac{P_E}{2} \frac{(1 - \mu^2)}{\gamma(1 + \frac{y}{\gamma})} \left[1 + \frac{1}{2(1 + \frac{y}{\gamma})^3} \right] \frac{\partial \Phi}{\partial \mu}$$

$$= \frac{\partial^2 \Phi}{\partial y^2} + \frac{2}{\gamma(1 + \frac{y}{\gamma})} \frac{\partial \Phi}{\partial y} + \frac{(1 - \mu^2)}{\gamma^2 (1 + \frac{y}{\gamma})^2} \frac{\partial^2 \Phi}{\partial \mu^2}$$

$$- \frac{2\mu}{\gamma^2 (1 + \frac{y}{\gamma})^2} \frac{\partial \Phi}{\partial \mu} + \frac{Q'(DIA)^2}{4\alpha \rho_l C_P (T_{SAT} - T_{BL})}$$

For the purpose of obtaining a numerical solution to equation B.5, both the y coordinate and the μ coordinate were divided into equal increments; this is illustrated in Figure 81 for a particular value of γ. In denoting a particular cell, the subscripts I and J were used. The center of the cell had coordinates [μ , y] where

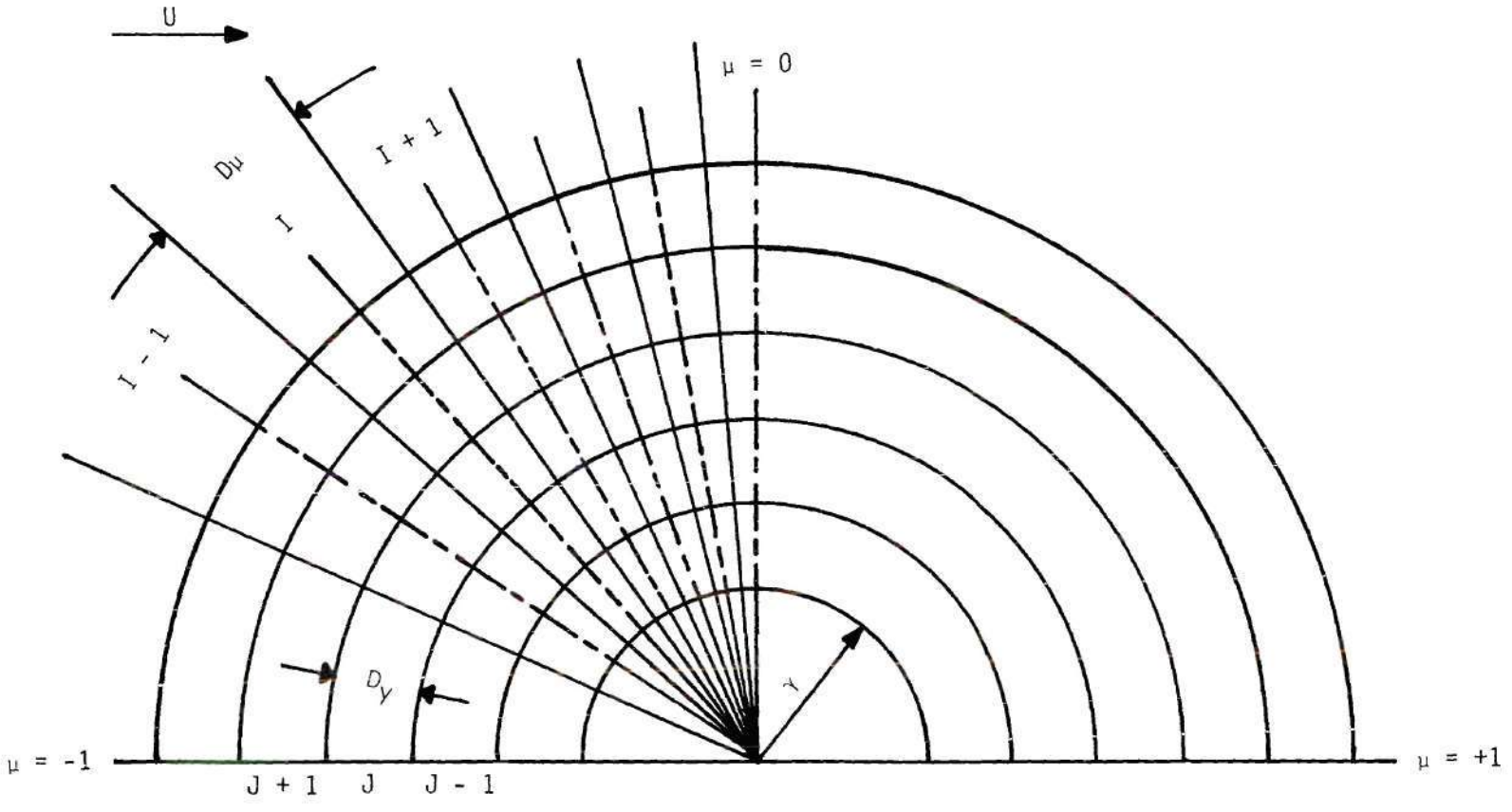

Figure 81. Grid System for the Single Bubble Case.

$$\mu = -1 + (I - 1)D\mu \quad \text{and} \quad y = (J - 1/2)Dy \tag{B.6}$$

J ranged from a value of one at the first cell adjacent to the bubble wall up to a maximum integer of NL and I ranged from one for $\mu = -1$ to a maximum value of IM for $\mu = +1$.

The choice of the value of Dy was governed by the initial temperature distribution which was a step function. This was described in Chapter III. The value of Dy was chosen to correspond to the value of the thickness of the thin shell whose temperature was initially the same as that of the bubble vapor. The choice of $D\mu$ was such as to yield an acceptable approximation to the solution of B.5.

The definition of y was given as:

$$y = r' - \gamma = \frac{2r}{DIA} - \frac{2R}{DIA}$$

Thus,

$$Dy = y_J - y_{J-1}$$

$$= \left[\frac{2r}{DIA} - \frac{2R}{DIA}\right]_J - \left[\frac{2r}{DIA} - \frac{2R}{DIA}\right]_{J-1}$$

$$= 2\,\frac{Dr}{DIA}$$

It should be noted that the thickness of a cell measured in terms of y or r is a constant throughout the life of the bubble. Also, the volume of

any mesh cell [I,J] is given by:

$$\text{Volume} = [2\Pi\ (r)^2\ D\mu]\ Dr$$

$$= 2\Pi\ [R + (J - 1/2)Dy\ \frac{DIA}{2}]^2\ \frac{Dy\ DIA}{2}$$

It should be noted that the volume of any mesh cell is a function of time, since R is a function of time. Another important observation on the coordinate system is that the relative velocity between the fluid radial motion and the radial motion of the coordinate system (equal to $\dot{R}$) is usually not zero and can be either positive or negative. This follows since an increase or decrease in the volume of a mesh cell requires a corresponding amount of mass to flow into or out of the cell.

Now $\frac{\partial \Phi}{\partial y}$ and $\frac{\partial \Phi}{\partial \mu}$ on the left hand side of equation B.5 could not be approximated in the same manner as those quantities on the right hand side. The presence of these derivatives on the right hand side was due to heat conduction, whereas, on the left hand side the reason was fluid motion. The cause which would not allow the two cases to be treated in a similar manner can be explained by considering a simplified one-dimensional problem of the same nature.

Consider one-dimensional flow of liquid in the + x direction (see Figure 82) with a velocity of U ft/sec with respect to the coordinate system. Now the equation under consideration is:

$$\frac{\partial T(x,t)}{\partial t} + \overline{V} \cdot \nabla T(x,t) = \alpha\ \nabla^2 T(x,t) \qquad (B.7)$$

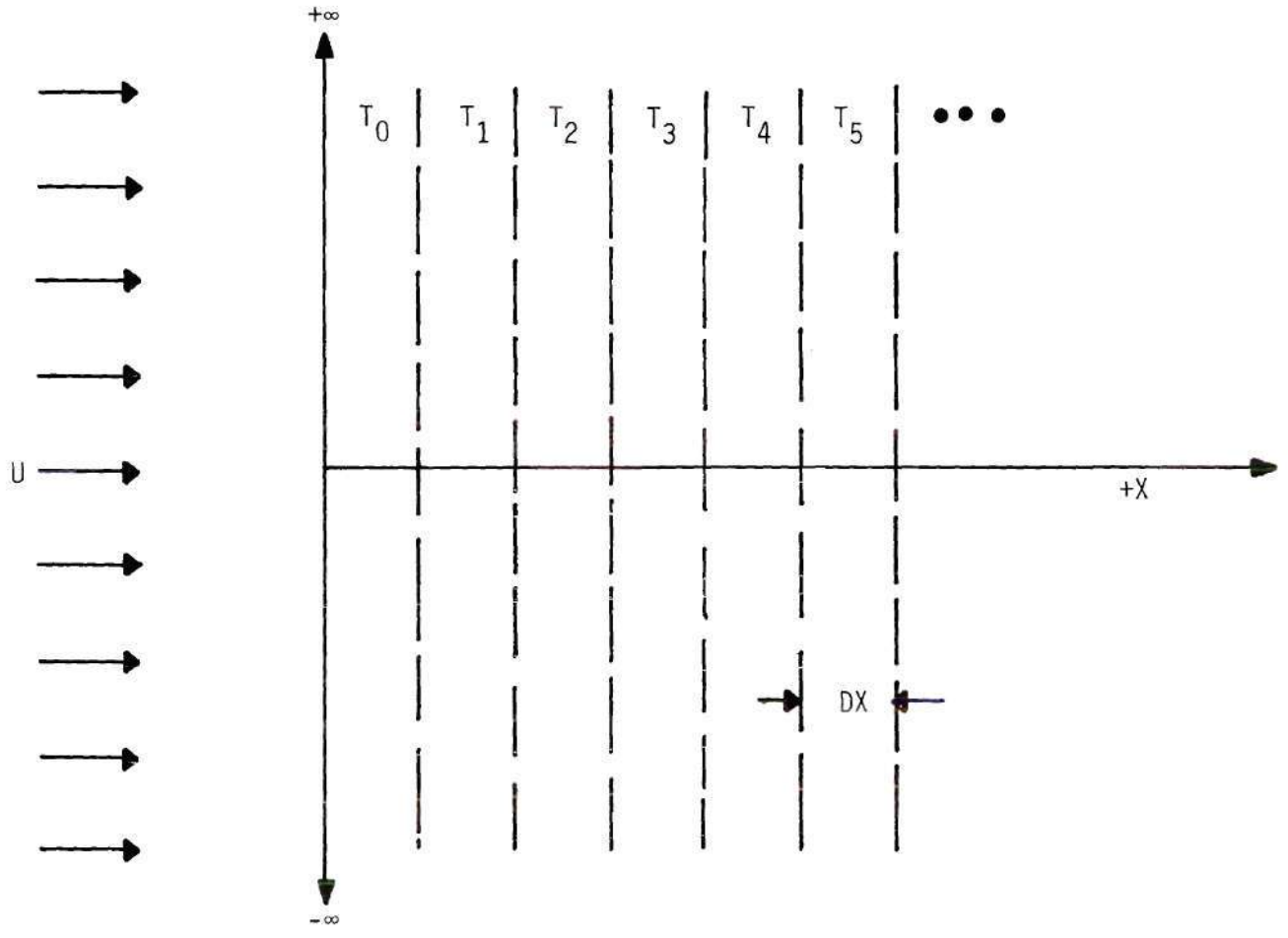

Figure 82. Coordinate System for the One-Dimensional Illustration.

where $\bar{V}$ is the velocity vector. The term $\bar{V}\cdot\nabla T$ is due to bulk fluid transport. Equation B.7 is equivalent to:

$$\frac{\partial T(x,t)}{\partial t} + U\frac{\partial T(x,t)}{\partial x} = \alpha\frac{\partial^2 T(x,t)}{\partial x^2} \qquad (B.8)$$

For this illustration, α is assumed to be zero and equation B.8 becomes:

$$\frac{\partial T(x,t)}{\partial t} + U\frac{\partial T(x,t)}{\partial x} = 0 \qquad (B.9)$$

The usual approximations to these derivatives are:

$$\frac{\partial T}{\partial t} = \frac{T_{J,n+1} - T_{J,n}}{Dt}$$

and

$$\frac{\partial T}{\partial x} = \frac{T_{J+1,n} - T_{J-1,n}}{2Dx}$$

Using these equations B.9 becomes:

$$\frac{T_{J,n+1} - T_{J,n}}{Dt} + U\frac{T_{J+1,n} - T_{J-1,n}}{2Dx} = 0$$

or

$$T_{J,n+1} = T_{J,n} + \frac{U\,Dt}{2Dx}T_{J-1,n} - \frac{U\,Dt}{2Dx}T_{J+1,n} \qquad (B.10)$$

Now assume the initial condition such that $T_{J,0} = T_{J-1,0} \ll T_{J+1,0}$.

In this case, equation B.10 indicates that the higher the value of $T_{J+1,n}$, the lower the temperature at J will be at time $(n+1)\cdot Dt$. Physically, this is impossible. Since U is in the + x direction and since α equals zero, T_{J+1} at any time should have no effect on T_J. The error in the above derivation arises from the approximation of $\frac{\partial T}{\partial x}$. A correct one for this case is:

$$\frac{\partial T}{\partial x} = \frac{T_{J,n} - T_{J-1,n}}{Dx}$$

Using this, the equivalent of B.10 is:

$$T_{J,n+1} = T_{J,n} + U\frac{Dt}{Dx}T_{J-1,n} - U\frac{Dt}{Dx}T_{J,n} \qquad (B.11)$$

Equation B.11 is logically correct. Consider the initial condition: $T_{J,0} \gg T_{J-1,0}$. Then as fluid of high temperature, $T_{J,0}$, leaves cell J to go into cell J + 1 and as fluid of low temperature, $T_{J-1,0}$, leaves cell J - 1 to go into cell J, the resulting temperature of the homogenized fluid in cell J is lower than $T_{J,0}$. Furthermore, the higher the value of $T_{J,0}$ and the lower the value of $T_{J-1,0}$, the lower would be the value of $T_{J,1}$ as predicted by B.11. Thus, derivatives arising due to the transport of bulk fluid must be treated in a non-conventional manner for the present problem.

During the initial attempt to solve equation B.5, several methods were used. All attempts used the conventional numerical approximations to the derivatives $\frac{\partial \Phi}{\partial y}$ and $\frac{\partial \Phi}{\partial \mu}$, regardless of their origin. Implicit, explicit, and a combination implicit-explicit were all tried. However, an

annoying instability in the predicted temperature distribution persisted for several months. Finally, the demon was isolated and identified as the terms arising from bulk fluid transport. Reasoning similar to that illustrated above in the one-dimensional case led to a representation of these terms which produced a stable solution.

The procedure for determining an appropriate approximation to the derivatives $\frac{\partial \Phi}{\partial y}$ and $\frac{\partial \Phi}{\partial \mu}$ which appear on the left hand side of equation B.5 was to first determine the direction of the velocity of the fluid with respect to the coordinate system. The absolute velocity of the fluid in the μ direction is (38):

$$V_\mu = U \left[1 + \frac{1}{2} \frac{R^3}{r^3}\right](1 - \mu^2)^{\frac{1}{2}}$$

The coordinate system has a zero absolute velocity in the μ direction. Thus, the relative velocity is always positive and the approximation was assigned as follows:

$$\frac{\partial \Phi}{\partial \mu} = \frac{\Phi_{I,J,n} - \Phi_{I-1,J,n}}{D\mu} \qquad \text{(B.12)}$$

This assignment follows the logic of the one-dimensional case mentioned above. The absolute velocity of the coordinate system in the r direction is equal to $\dot{R}$; that of the fluid is given by (38):

$$V_r = U \left(1 - \frac{R^3}{r^3}\right) \mu + \dot{R} \frac{R^2}{r^2}$$

which can be positive or negative. Thus, the relative velocity between V_r and $\dot{R}$ can be positive or negative, depending on position and time. It was thus necessary to check the sign of this relative velocity at every point before making the appropriate approximation. In general, the approximation was written as:

$$\frac{\partial \Phi}{\partial y} = \frac{\Phi_{I,S,n} - \Phi_{I,V,n}}{Dy} \tag{B.13}$$

where, if the difference between V_r and $\dot{R}$ were less than zero, then S was equal to J + 1 and V was equal to J or, if the difference between V_r and $\dot{R}$ were greater than zero, then S was equal to J and V was equal to J - 1.

The other numerical representations necessary in equation B.5 are:

$$\frac{\partial \Phi}{\partial t'} = \frac{\Phi_{I,J,n+1} - \Phi_{I,J,n}}{Dt'} \tag{B.14}$$

$$\frac{\partial \Phi}{\partial y} = \frac{\Phi_{I,J+1,n} - \Phi_{I,J-1,n}}{2Dy} \tag{B.15}$$

$$\frac{\partial^2 \Phi}{\partial y^2} = \frac{\Phi_{I,J+1,n} - 2\,\Phi_{I,J,n} + \Phi_{I,J-1,n}}{Dy^2} \tag{B.16}$$

$$\frac{\partial \Phi}{\partial \mu} = \frac{\Phi_{I+1,J,n} - \Phi_{I-1,J,n}}{2D\mu} \tag{B.17}$$

$$\frac{\partial^2 \Phi}{\partial \mu^2} = \frac{\Phi_{I+1,J,n} - 2\,\Phi_{I,J,n} + \Phi_{I-1,J,n}}{D\mu^2} \tag{B.18}$$

Now substituting equations B.12 through B.18 into equation B.5 and rearranging, the expression for $\Phi_{I,J,n+1}$ becomes:

$$\Phi_{I,J,n+1} = \Phi_{I,J,n}\left\{1 - 2\frac{Dt'}{Dy^2} - \frac{2(1-\mu^2)}{\gamma^2(1+\frac{y}{\gamma})^2}\frac{Dt'}{D\mu^2}\right. \tag{B.19}$$

$$\left. - \frac{P_E}{2}\frac{(1-\mu^2)}{\gamma(1+\frac{y}{\gamma})}\left[1 + \frac{1}{2(1+\frac{y}{\gamma})^3}\right]\frac{Dt'}{D\mu}\right\}$$

$$+ \Phi_{I-1,J,n}\left\{\frac{P_E}{2}\frac{(1-\mu^2)}{\gamma(1+\frac{y}{\gamma})}\left[1 + \frac{1}{2(1+\frac{y}{\gamma})^3}\right]\frac{Dt'}{D\mu}\right.$$

$$\left. + \frac{(1-\mu^2)}{\gamma^2(1+\frac{y}{\gamma})^2}\frac{Dt'}{D\mu^2} + \frac{\mu}{\gamma^2(1+\frac{y}{\gamma})^2}\frac{Dt'}{D\mu}\right\}$$

$$+ \Phi_{I+1,J,n}\left\{\frac{(1-\mu^2)}{\gamma^2(1+\frac{y}{\gamma})^2}\frac{Dt'}{D\mu^2} - \frac{\mu}{\gamma^2(1+\frac{y}{\gamma})^2}\frac{Dt'}{D\mu}\right\}$$

$$+ \Phi_{I,J+1,n}\left\{\frac{Dt'}{Dy^2} + \frac{1}{\gamma(1+\frac{y}{\gamma})}\frac{Dt'}{Dy}\right\}$$

$$+ \Phi_{I,J-1,n}\left\{\frac{Dt'}{Dy^2} - \frac{1}{\gamma(1+\frac{y}{\gamma})}\frac{Dt'}{Dy}\right\}$$

$$+ (\Phi_{I,S,n} - \Phi_{I,V,n})\left\{\dot{\gamma}\left[1 - \frac{1}{(1+\frac{y}{\gamma})^2}\right]\right.$$

$$\left. - \frac{P_E}{2}\mu\left[1 - \frac{1}{(1+\frac{y}{\gamma})^3}\right]\right\}\frac{Dt'}{Dy}$$

Equation B.19 is good for $2 \leq J \leq NL - 1$ and $2 \leq I \leq IM - 1$. The equivalent of B.19 for a mesh cell on the boundary was obtained from equation B.19 with the aid of the following:

1. For $J = 1$, an imaginary mesh cell with $J = 0$ was assumed present. It was also assumed that $\Phi_{I,0,n} = \Phi_{I,1,n}$. This made $\frac{\partial \Phi}{\partial y} = 0$ at $y = 0$ for conduction and also provided a proper approximation for bulk fluid transport.

2. For $J = NL$, an imaginary mesh cell with $J = NL + 1$ was assumed present with $\Phi_{I,NL+1,n} = \Phi_{I,NL,n}$. This made $\frac{\partial \Phi}{\partial y} = 0$ at $y = Y_{MAX}$ for conduction and also provided an appropriate approximation for bulk fluid transport.

3. Since node points were placed along the lines $\mu = -1$ and $\mu = +1$, the mesh cells adjacent to these lines were actually half cells with dimensions $D\mu/2$. Thus, to obtain the conditions $\left.\frac{\partial \Phi}{\partial \mu}\right|_{\mu = -1} = 0$ and $\left.\frac{\partial \Phi}{\partial \mu}\right|_{\mu = +1} = 0$, it was required that $\Phi_{0,J,n} = \Phi_{2,J,n}$ and that $\Phi_{IM+1,J,n} = \Phi_{IM-1,J,n}$ where $I = 0$ and $I = IM + 1$ indicate imaginary mesh cells.

4. Also, for the mesh cells on the surface of the bubble, there was a heat generation term which will be mentioned on page 172.

The initial conditions were:

1. $\Phi_{I,1,0} = (T_{INV} - T_{BL})/(T_{SAT} - T_{BL})$ where T_{INV} was a given temperature and $1 \leq I \leq IM$.

2. $\Phi_{I,J,0} = 0$ for $1 \leq I \leq IM$ and $2 \leq J \leq NL$.

Mass and Energy Balance in the Control Volume

For this model, mass was put into the control volume at a constant rate. Thus, the amount of mass added during a small increment of time was

found by multiplying the rate of input by the time interval. The mass output was obtained with the aid of equation 3.2.

First the actual temperature of a surface mesh cell was obtained from the value of $\Phi_{I,1,n}$ and its definition. Next, the saturated vapor density corresponding to this temperature was obtained with the aid of a five-term polynomial that approximated the saturation density as a function of the saturation temperature. The data for this polynomial were obtained from the steam tables and covered the range from 100°F to 300°F. Next, the rate of condensation was calculated with the aid of equation 3.2:

$$MP = \left(\frac{R_{GAS}\, T_{SUR}}{2\pi M}\right)^{\frac{1}{2}} \left(\rho_{vap} - \rho_{sat}\right) \qquad (B.20)$$

Next, this rate was multiplied by the surface area of the cell under consideration, $2\pi(\frac{R}{12})^2 D\mu^*$, and by 3600 seconds per hour to obtain the mass condensed per hour by this cell. Next, the total condensation rate due to all the cells on the surface was obtained by adding the individual contributions. At this point, the new value for the total mass in the bubble was calculated by

$$IBM = BM + (M_{IN} - MOT) \times Dt/3.6 \times 10^9 \qquad (B.21)$$

where IBM is the total mass in the bubble after the time interval Dt, lb

---

*$D\mu$ was replaced by $D\mu/2$ for $\mu = \pm 1$.

BM is the total mass in the bubble, lb

M_{IN} is the mass input rate, lb/hr

MOT is the total mass output rate, lb/hr

Dt is the time interval, microseconds.

Also, by using the new value of the radius as found in the first section of this appendix, the new density of the vapor was calculated by

$$\rho_{vap} = IBM/\left(\frac{4}{3}\,\Pi\left(\frac{R}{12}\right)^3\right)$$

Next, the pressure in the bubble was obtained using the assumption that the state of the bubble vapor was saturated corresponding to ρ_{vap}. This involved the use of a fifth degree polynomial which approximated the saturation pressure as a function of the saturation density over the temperature range of 100°F to 300°F.

Next, the heat generation rate in a surface cell due to the latent heat of condensation was calculated by multiplying the mass rate of condensation by LL, the latent heat of condensation. The value for LL was obtained by using a fifth degree polynomial which approximated the latent heat as a function of the saturation density. This approximation was valid over the range of 100°F to 300°F.

The initial state of the vapor in the bubble was chosen to be saturation at a given temperature. This temperature was chosen so that the initial pressure in the bubble was slightly larger than the local stream pressure near the bubble site.

Real Boiling Case

The calculations for R, $\dot{R}$, and $\ddot{R}$ were the same as illustrated in the previous case and will not be repeated here. Also, the initial conditions were handled in the same manner as those in the previous case. The only exception to this was the initial temperature of the vapor in the bubble which was assumed to be equal to the heated plate temperature.

Numerical Solution of Heat Diffusion in Liquid

Equation 3.14 is:

$$-\frac{\partial \Phi}{\partial t'} - \dot{\gamma}\left[1 - \frac{1}{\left(1 + \frac{y}{\gamma}\right)^2}\right]\frac{\partial \Phi}{\partial y} = \frac{\partial^2 \Phi}{\partial y^2} + \frac{2}{\gamma\left(1 + \frac{y}{\gamma}\right)}\frac{\partial \Phi}{\partial y} \qquad (B.22)$$

$$+ \frac{Q'(DIA)^2}{4\alpha\, \rho_l\, C_p\, (T_{SAT} - T_{BL})}$$

As in the previous case, a numerical solution to this equation was obtained by first dividing the y coordinate into equal increments. The derivatives which arise due to fluid motion were handled in the same manner as in the previous case. Thus, for $\frac{\partial \Phi}{\partial y}$ on the left hand side of B.22, the numerical approximation is:

$$\frac{\partial \Phi}{\partial y} = \frac{\Phi_{S,n} - \Phi_{V,n}}{Dy} \qquad (B.23)$$

where if $\dot{\gamma}$ is positive then S is made equal to J + 1 and V is made equal to J. However, if $\dot{\gamma}$ is negative, the n, S is made equal to J and V is made equal to J - 1.

The other approximations are:

$$\frac{\partial \Phi}{\partial t'} = \frac{\Phi_{J,n+1} - \Phi_{J,n}}{Dt'} \tag{B.24}$$

$$\frac{\partial \Phi}{\partial y} = \frac{\Phi_{J+1,n} - \Phi_{J-1,n}}{2Dy} \tag{B.25}$$

$$\frac{\partial^2 \Phi}{\partial y^2} = \frac{\Phi_{J+1,n} - 2\,\Phi_{J,n} + \Phi_{J-1,n}}{Dy^2} \tag{B.26}$$

Now substituting B.23 through B.26 into B.22 and rearranging, the expression for $\Phi_{J,n+1}$ becomes:

$$\Phi_{J,n+1} = \Phi_{J,n}\left(1 - 2\,\frac{Dt'}{Dy^2}\right) + \Phi_{J+1,n}\left(\frac{Dt'}{Dy^2} + \frac{Dt'/Dy}{\gamma(1 + \frac{y}{\gamma})}\right) \tag{B.27}$$

$$+ \Phi_{J-1,n}\left(\frac{Dt'}{Dy^2} - \frac{Dt'/Dy}{\gamma(1 + \frac{y}{\gamma})}\right) + \left(\Phi_{S,n} - \Phi_{V,n}\right)\left\{\dot{\gamma}\left[1 - \frac{1}{(1 + \frac{y}{\gamma})^2}\right]\frac{Dt'}{Dy}\right\}$$

$$+ \frac{Q'(DIA)^2}{4\alpha\,\rho_l\,C_P\,(T_{SAT} - T_{BL})}$$

Equation B.27 is good for $1 \leq J \leq NL$. Q' is equal to zero for $J > 1$. The boundary conditions are $\frac{\partial \Phi}{\partial y} = 0$ for $y = 0$ and $y = Y_{MAX}$ where Y_{MAX} is a distance beyond which the liquid was assumed unaffected. The boundary conditions were obtained by assuming a fictitious mesh shell at $J = 0$ and $J = NL + 1$ and their temperatures were:

$$\Phi_{0,n} = \Phi_{1,n} \qquad \text{and} \qquad \Phi_{NL+1,n} = \Phi_{NL,n}$$

Using these, equation B.27 was simplified for the case of J = 1 or NL. The initial conditions were:

$$\text{For } J = 1 \qquad \Phi_{1,0} = \frac{T_{INV} - T_{BL}}{T_{SAT} - T_{BL}}$$

$$\text{For } J > 1 \qquad \Phi_{J,0} = 0$$

Numerical Solution for Heat Diffusion in the Heated Plate

Equation 3.17 is

$$\frac{\partial \Phi'}{\partial t'} = \frac{\alpha_p}{4\alpha} \frac{(DIA)^2}{(A_{MAX})^2} \left(\frac{\partial^2 \Phi'}{\partial a'} + \frac{1}{a'} \frac{\partial \Phi'}{\partial a'} \right) + \frac{\alpha_p}{4\alpha} \frac{(DIA)^2}{Z^2} \frac{\partial^2 \Phi'}{\partial z'^2} \qquad \text{(B.28)}$$

$$+ \frac{Q(DIA)^2}{4\alpha \rho_p C'_p (T_{DROP} - T_{INV})}$$

The numerical solution to this equation was obtained by dividing the a′ coordinate and the z′ coordinate into equal increments, Da′ and Dz′, respectively. The subscripts I and J refer to the a′ and z′ directions, respectively. The numerical approximations to the derivatives are as follows:

$$\frac{\partial \Phi'}{\partial t'} = \frac{\Phi'_{I,J,n+1} - \Phi'_{I,J,n}}{Dt'} \qquad \text{(B.29)}$$

$$\frac{\partial \Phi'}{\partial a'} = \frac{\Phi'_{I+1,J,n} - \Phi'_{I-1,J,n}}{2Da'} \tag{B.30}$$

$$\frac{\partial^2 \Phi'}{\partial a'^2} = \frac{\Phi'_{I+1,J,n} - 2\,\Phi'_{I,J,n} + \Phi'_{I-1,J,n}}{Da'^2} \tag{B.31}$$

$$\frac{\partial^2 \Phi'}{\partial z'^2} = \frac{\Phi_{I,J+1,n} - 2\,\Phi_{I,J,n} + \Phi_{I,J-1,n}}{Dz'^2} \tag{B.32}$$

These equations were substituted into B.28 and rearranged. The resulting expression for $\Phi'_{I,J,n+1}$ is:

$$\Phi_{I,J,n+1} = \Phi_{I,J,n}\left(1 - 2\,\frac{\alpha_p (DIA)^2}{4\alpha\, A_{MAX}^2}\,\frac{Dt'}{Da'^2} - 2\,\frac{\alpha_p (DIA)^2}{4\alpha Z^2}\,\frac{Dt'}{Dz'^2}\right) \tag{B.33}$$

$$+ \Phi_{I+1,J,n}\left(\frac{\alpha_p (DIA)^2}{4\alpha\, A_{MAX}^2}\,\frac{Dt'}{Da'^2} + \frac{\alpha_p}{4\alpha}\,\frac{(DIA)^2}{A_{MAX}^2}\,\frac{1}{a'^2}\,\frac{Dt'}{Da'}\right)$$

$$+ \Phi_{I-1,J,n}\left(\frac{\alpha_p (DIA)^2}{4\alpha\, A_{MAX}^2}\,\frac{Dt'}{Da'^2} - \frac{\alpha_p}{4\alpha}\,\frac{(DIA)^2}{A_{MAX}^2}\,\frac{1}{a'^2}\,\frac{Dt'}{Da'}\right)$$

$$+ \Phi_{I,J+1,n}\left(\frac{\alpha_p (DIA)^2}{4\alpha Z^2}\,\frac{Dt'}{Dz'^2}\right) + \Phi_{I,J-1,n}\left(\frac{\alpha_p (DIA)^2}{4\alpha Z^2}\,\frac{Dt'}{Dz'^2}\right)$$

$$+ \frac{Q(DIA)^2}{4\alpha\, \rho_p\, C'_p\, (T_{DROP} - T_{INV})}$$

Equation B.33 is good for $1 \leq I \leq NR$ and $2 \leq J \leq NP$ where NR corresponds

to a distance in the a′ direction beyond which the heated plate was assumed unaffected; NP corresponds to the thickness of the heated plate. Also, Q refers to the heat generation rate which was constant. However, for J = 1, this term was composed of the sum of the constant rate of heat generation and the equivalent value of the heat sink due to the latent heat of vaporization corresponding to the particular value of I. The boundary conditions for B.33 were that $\frac{\partial \Phi'}{\partial a'}$ and $\frac{\partial \Phi'}{\partial z'}$ were zero for a′ = 0 and 1 and for z′ = 0 and 1 (the 1 indicates A_{MAX} and Z, respectively). To provide these conditions, fictitious mesh cells were assumed along the boundaries for which

$$\Phi_{0,J} = \Phi_{1,J}$$

$$\Phi_{NR+1,J} = \Phi_{NR,J}$$

$$\Phi_{I,0} = \Phi_{I,1}$$

$$\Phi_{I,NP+1} = \Phi_{I,NP}$$

The above relations together with equation B.33 (with the change of Q for J = 0 which was noted above) yielded the numerical equations for the boundary mesh cells. The initial condition was $\Phi_{I,J,0} = 0$ for all I, J.

Mass and Energy Balance in the Control Volume

The mass and energy balance for this case is similar to the previous case. The exception is the mass input. In the previous case, this is a constant, whereas in this case the mass input varies with time.

The first step in calculating the mass input from a surface mesh cell was to obtain the value of $\Phi_{I,0,n}$ and, thus the actual surface temperature. Next, the saturation vapor density corresponding to this surface temperature was obtained by using an approximating polynomial for ρ_{sat} as a function of temperature. This value, together with the known bubble vapor density was then used in the equation:

$$MP = \left(\frac{R_{GAS}\, T_{SUR}}{2\Pi M} \right)^{\frac{1}{2}} \left(\rho_{sat} - \rho_{vap} \right) \qquad (B.34)$$

Next, this value was multiplied by the increment of time under consideration and the total surface area of the mesh cell being considered. This procedure was followed for all the surface mesh cells and the total mass input was found by addition. The new total mass, the new density, and the new vapor state were then calculated in a manner similar to that in the previous case.

Next, the latent heat associated with MP was obtained by multiplying MP by the latent heat of vaporization. The latent heat was obtained from an approximating polynomial which gave this value as a function of the saturation density corresponding to the surface temperature. Next, the latent heat was transformed into an equivalent heat generation rate by dividing by the thickness $Z \cdot Dz'$. This equivalent heat sink was used in the plate heat diffusion calculation as previously mentioned. Also, the decrease in thickness of the thin liquid film was calculated as:

$$DEOU = MP \cdot Dt/\rho_1 \qquad (B.35)$$

As the bubble radius, R, was usually not an integral number of mesh steps, I·Da, the last cell was only partly covered with the thin liquid film. The remainder of that cell was still covered with cooling fluid. For this case, an equivalent mass removal rate was calculated based on the total surface area of the cell rather than just the fraction covered with thin liquid film. The criterion for calculating the equivalent rate was that the total mass removed would be the same. This same procedure was applied to the latent heat removal in this cell and to the thin liquid film thickness.

APPENDIX C

COMPUTER CODES

The procedures just described in Appendix B were programmed in ALGOL for use on the Burroughs B5500 at the Georgia Institute of Technology. With these codes, an unacceptably large amount of computer time was required to solve a complete case. This situation was partially alleviated with two modifications. The first was to use the average value of the bubble mass to advance the solution an increment of time. This value was one-half the sum of the known present value of the bubble mass and the unknown future value. A guess was made at first and iterations were performed until the assumed value was reasonably close to the actual value. The second modification involved restricting the number of mesh points in the y, a, and z directions to a value above which the bubble growth had not affected the corresponding plate or fluid temperature. Here the initial number of mesh cells in these directions was set at a minimum number of three. Next, as the dimensionless temperature difference in the outer most cell in a particular direction became greater than 0.001, the total number of cells in that direction was increased by one. The upper limit of cells in the y direction was 100 and that in the a and z directions was 50. Implementing these two modifications reduced the run time down to a level which was tolerated.

The comments at the beginning of these codes should provide enough

information for their execution. The single bubble experimental code begins on page 182 and the real boiling code begins on page 189. Also, sample data input numbers are given.

```
%                          BUBBLE  DYNAMICS FOR THE EXPERIMENTAL CASE
% INPUT NUMBERS  ***
%   M          MOLECULAR WEIGHT OF FLUID
%   RHOL       DENSITY OF LIQUID IN LB/FT*3
%   SPHEL      SPECIFIC HEAT OF LIQUID IN BTU/LB F
%   ALPHAL     EFFECTIVE THERMAL DIFFUSIVITY OF LIQUID IN FT*2/HR
%   PINF       ABSOLOUTE PRESSURE NEAR THE BUBBLE SITE  PSIA
%   TSAT       SATURATION TEMPERATURE AT PINF     F
%   RIN        INITIAL RADIUS  INCHES
%   TINV       INITIAL STEAM TEMPERATURE  F
%   MIN        MASS RATE OF VAPOR INPUT LB/HR
%   TBL        TEMPERATURE OF LIQUID IN WHICH BUBBLE GROWS  F
%   DIA        HYDRAULIC DIAMETER OF CHANNEL INCHES
%   DTR        INITIAL TIME INCREMENT  MICROSECONDS
%   DY         INCREMENT IN  Y DIRECTION
%   U          STREAM VELOCITY
%   IM         NUMBER OF DIVISIONS IN MU DIRECTION
%   NL         NUMBER OF DIVISIONS IN Y DIRECTION
%   RHO0 TO RHO4 ARE CONSTANTS IN 5 DEGREE POLYNOMIAL FOR SATURATION
%   VAPOR    DENSITY     AS FUNCTION  OF  TEMPERATURE
%   PSA0 TO PSA4  ARE CONSTANTS IN 5 DEGREE POLYNOMIAL FOR SATURATION
%   PRESSURE AS FUNCTION OF VAPOR DENSITY
%   LSA0 TO LSA4  ARE CONSTANTS IN 5 DEGREE POLYNOMIAL FOR LATENT HEAT
%   AS FUNCTION OF VAPOR DENSITY
%
%
% OUTPUT NUMBERS ***
%   MTOT   MASS CONDENSED                  LB
%   MOT    MASS CONDENSING RATE                LB/HR
%   TL[1]  LIQUID SURFACE TEMPERATURE  FOR  I=1     F
%   TL[5]  LIQUID SURFACE TEMPERATURE FOR I=5       F
%   TIME(2) RELATED TO PROCESSOR TIME
%   TIME(3) RELATED TO I/O TIME
%   TL[IM]  LIQUID SURFACE TEMPERATURE FOR  I=IM     F
%   PG       BUBBLE PRESSURE PSIA
%   R        BUBBLE RADIUS  INCHES
%   BM         BUBBLE MASS  LB
%   TI       TIME  MICROSECONDS
%      THE ABOVE APPEARS IN 11 COLUMNS  LEFT TO RIGHT
%   ALSO AT VARIOUS TIMES THE FOLLOWING APPEASR IN A SINGLE COLUMN
%        I,J,THL[I,J] FOR I=1,IM/2-0.5,IM     TEMP DISTRIBUTION IN LIQ
%        I,TL[I]   TEMP DISTRIBUTION ON BUBBLE SURFACE
%********
%  CARD NUMBER 1190  IS  IN AND NUMBER 840  IS OUT FOR FIRST RUN TO
%   MAKE FIRST TAPE AND REVERSE FOR SUCCESSIVE RUNS
%*************
BEGIN
        REAL MIN,M,RHOV,LL,R,QTOT,QOT,MTOT,MOT,RNEW,RR,RRR,RRNEW,
             RRRNEW,DTR,PG,PINF,RHOL,BVOL,BM,IBM,GA,GAD,DT,DY,DMU,MU,
             Y,QTF,RHO0,RHO1,RHO2,RHO3,RHO4,PSA0,PSA1,PSA2,PSA3,PSA4,
             LSA0,LSA1,LSA2,LSA3,LSA4,RIN,TBL,TINV,ALPHAL,SPHEL,DIA,
             TI  ,PGIN,RHOVIN,TSAT,BMIN,P1,P2,P3,P4,P5,P6,P7,P8,P9,P10
 ,UR,UC      ,P11,U1,U2,U3,U4,U5,PE,U,K1,K2,K3,K4 ,A,B,C,D,E,F,G,H   ;
        SAVE ARRAY   THL,TT[0:30,0:100],RHOEL,MOUT,QOUT, TL,
             HOLD, HIG [0:100]                                      ;
        INTEGER I,J,K,IM,NL,T,S,V;
        LABEL L4A,LAB,LAC,LAD,LAE,LAG;
        FILE IN FL5 (1,10);
        FILE OUT FL6 6(2,15);
        FORMAT FMT1(E12.5),
               FMT2(I6),
```

```
          FMOU22(I6,X5,E10.3),                                                    620
                 FMOU1(E10.3,10(X1,E10.3)),                                       630
                 FMOU2 (2(I6),X5,E10.3)};                                         640
          LIST LIST1(M,RHOL,SPHEL,ALPHAL,RH00,RH01,RH02,RH03,RH04,PSA0,           650
                       PSA1,PSA2,PSA3,PSA4,LSA0,LSA1,LSA2,LSA3,LSA4,PINF,         660
                       TSAT,RIN,TINV,MIN,            TBL,DIA,     DTR,DY,       670
                       U),                                                        680
               LIST2(IM,NL),                                                      690
               LISTOU1(MTOT,MOT,TL[1  ],TL[5  ],TIME(2),TIMF(3),  TL[IM           700
                        ],PG,R,BM ,TI  ),                                         710
          LISTOU22(J,TL[J]),                                                      720
               LISTOU2(I,J,THL[I,J])};                                            730
          LIST L1(                                                                740
               MIN,M,RHOV,LL,R,QTOT,QOT,MTOT,MOT,RNEW,RR,RRR,RRNEW,               750
               RRRNEW,DTR,PG,PINF,RHOL,BVOL,BM,IBM,GA,GAD,DT,DY,DMU,MU,           760
               Y,QTF,RH00,RH01,RH02,RH03,RH04,PSA0,PSA1,PSA2,PSA3,PSA4,           770
               LSA0,LSA1,LSA2,LSA3,LSA4,RIN,TBL,TINV,ALPHAL,SPHEL,DIA,            780
               TI  ,PGIN,RHOVIN,TSAT,BMIN,P1,P2,P3,P4,P5,P6,P7,P8,P9,P10          790
,UR,UC         ,P11,U1,U2,U3,U4,U5,PE,U,K1,K2,K3,K4 ,A,B,C,D,E,F,G,H              800
                , I,J,K,IM,NL,T,S,V     )};                                       810
          FILE TAPE1 "TR1"(2,110),                                                820
              TAPE2 "TR1"(2,110,SAVE 30)};                                        830
          INTEGER TIM};                                                           840
          GO TO LAG;   %IN SUCCESSIVE RUNS                                        850
          READ(FL5,/,LIST1) ;                                                     860
          READ(FL5,/,LIST2) ;                                                     870
          CLOSE(FL5,RELEASE)};                                                    880
          WRITE(FL6,FMI1,LIST1) ;                                                 890
          WRITE(FL6,FMI2,LIST2) ;                                                 900
          WRITE(FL6 [PAGE])};                                                     910
          FOR J←0 STEP 1 UNTIL 100 DO                                             920
          FOR I←0 STEP 1 UNTIL 30  DO                                             930
          TT[I,J]←THL[I,J]←0};                                                    940
          FOR J←0 STEP 1 UNTIL 100 DO                                             950
                              HIG[J]←RHOEL[J]←MOUT[J]←QOUT[J]←HOLD[J]←0};         960
          FOR J←0 STEP 1 UNTIL IM DO                                              970
          BEGIN                                                                   980
               TL[J]←TINV};THL[J,1]←(TINV-TBL)/(TSAT-TBL)};                       990
          END};                                                                  1000
          MTOT←0};                                                               1010
          QTOT←0};                                                               1020
          TI  ←0};                                                               1030
          PE←DIA×U×300/ALPHAL};                                                  1040
          DMU←2/(IM-1)};                                                         1050
          QTF←3×DIA/(3.14159265×DY×DMU×RHOL×SPHEL×ALPHAL×(TSAT-TBL))};           1060
          RRR←0};                                                                1070
          R←RIN};                                                                1080
          I←1};                                                                  1090
               RHOV     ←RH00+RH01×TL[I  ]+RH02×TL[I  ]↑2+RH03×                  1100
               TL[I  ]↑3 +RH04×TL[I  ]↑4  };                                     1110
          PG← PSA0 + PSA1× RHOV +PSA2×RHOV↑2 + PSA3×RHOV↑3                       1120
             + PSA4×RHOV↑4};                                                     1130
          RR←(SQRT(((PG  -PINF)×32.2     ×288)/(RHOL×3)))×12 };                  1140
          BVOL← 4× 3.14159265 ×((R/12)↑3)/3};                                    1150
          BM←RHOV×BVOL};                                                         1160
          FOR J←2 STEP 1 UNTIL IM-1 DO HIG[J]←DMU};                              1170
          HIG[1]←HIG[IM]←DMU/2};                                                 1180
          NL←3};                                                                 1190
          GO TO LAC;  % IN FIRST RUN BEFORE 100                                  1200
LAG;       READ(TAPE1,*,L1                 )};                                  1210
           READ(TAPE1,101,RHOEL[*]         )};                                  1220
           READ(TAPE1,101,MOUT[*]          )};                                  1230
           READ(TAPE1,101,QOUT[*]          )};                                  1240
           READ(TAPE1,101,TL[*]            )};                                  1250
           READ(TAPE1,101,HOLD[*]          )};                                  1260
           READ(TAPE1,101,HIG[*]           )};                                  1270
          FOR J←0 STEP 1 UNTIL 30 DO  READ(TAPE1,101,THL[J,*])};                 1280
          FOR J←0 STEP 1 UNTIL 30 DO  READ(TAPE1,101,TT[J,*])};                  1290
```

```
          LOCK(TAPE1,RELEASE);                                                    1300
          GO TO LAA;                                                              1310
LAC:      DTR←0.1        ;                                                        1320
          DT←ALPHAL×DTR×16/((DIA+2)×100000000)  ;                                 1330
          UC←RR;                                                                  1340
               LL←LSA0 + LSA1×RHOV + LSA2 × RHOV*2 +LSA3×RHOV*3                   1350
               +LSA4×RHOV*4   ;                                                   1360
          FOR I←1 STEP 1 UNTIL IM DO                                              1370
          BEGIN                                                                   1380
               RHOEL[I]←RH00+RH01×TL[I  ]+RH02×TL[I  ]*2+RH03×                    1390
               TL[I  ]*3 +RH04×TL[I  ]*4  ;                                       1400
               MOUT[I]←SQRT( 49690 × (TL[I  ]+459.69)/( M× 2 ×                    1410
               3.14159265))× (RHOV-RHOEL[I]) × 2 × 3.14159265 ×                   1420
               (R/12)*2 × HIG[I] × 3600 ;                                         1430
               QOUT[I]←MOUT[I] ×LL                                                1440
          END;                                                                    1450
          MOT←0;                                                                  1460
          QOT←0;                                                                  1470
          FOR I←1 STEP 1 UNTIL IM DO BEGIN                                        1480
          MOT←MOT+MOUT[I];                                                        1490
          QOT←QOT+QOUT[I]  END;                                                   1500
          RNEW←R+RR×  DTR/1000000 +RRR×(  DTR/1000000)*2/2;                       1510
          IBM←BM+(MIN-MOT)× DTR   /3600000000 ;                                   1520
          H←(G+IBM)/2;                                                            1530
          RHOV←H/BVOL;                                                            1540
          IF ABS(BM/H-1)>0.0001 THEN      BEGIN BM←H; GO TO LAC END ;             1550
          BEGIN                                                                   1560
          INTEGER XX2;                                                            1570
          RRNEW← RR +RRR ×  DTR /1000000 ;                                        1580
          RRRNEW←(((PG -PINF) × 667160/RHOL) -3×(RR*2)/2)/R;                      1590
          GA← 2×R/DIA;                                                            1600
          GAD← RR×DIA × 3600/(ALPHAL × 288);                                      1610
          K1←DT/DMU;                                                              1620
          K2←DT/DMU*2;                                                            1630
          K3←DT/DY ;                                                              1640
          K4←DT/DY*2 ;                                                            1650
          Y←DY/2;                                                                 1660
               P1←1+Y/GA;                                                         1670
               P2←P1*2;                                                           1680
               P3←P1×P2 ;                                                         1690
               P6← GAD×(1-1/P2);                                                  1700
               P7←PE×(1-1/P3)/2;                                                  1710
          UR← -UX      (1-R*3/((DIA×Y/2)+R)*3)×12                                1720
                                        +RR×R*2/((DIA×Y/2)+R)*2;                  1730
     IF (UR-UC)<0 THEN S←2 ELSE S←1;                                              1740
        TT[1,1]←THL[1,1]×(1-2×K4)              +(THL[1,S]-THL[1,1])×K3×          1750
      (P6+P7)+2×QTF×QOUT[1]×DT/R*2 +THL[1,2]×(K4+K3/(GA×P1)) +                    1760
          THL[1,1]×(K4-K3/(GA×P1));                                               1770
          UR←  UX      (1-R*3/((DIA×Y/2)+R)*3)×12                               1780
                                        +RR×R*2/((DIA×Y/2)+R)*2;                  1790
     IF (UR-UC)<0 THEN S←2 ELSE S←1;                                              1800
          TT[IM,1]←THL[IM,1]×(1-2×K4)                +(THL[IM,S]-THL[IM,1]      1810
    )×K3×(P6-P7)+QTF×QOUT[IM]×DT×2/R*2 +THL[IM,2]×(K4+K3/(GA×P1))+THL[IM,1       1820
          ]×(K4-K3/(GA×P1));                                                      1830
          Y←(NL-0.5)×DY;                                                          1840
               P1←1+Y/GA;                                                         1850
               P2←P1*2;                                                           1860
               P3←P1×P2 ;                                                         1870
               P6← GAD×(1-1/P2);                                                  1880
               P7←PE×(1-1/P3)/2;                                                  1890
```

```
    UR← -UX      (1-R*3/((DIA×Y/2)+R)*3)×12                                    1900
                                        +RR×R*2/((DIA×Y/2)+R)*2;               1910
    IF (UR-UC)<0 THEN V←NL ELSE V←NL-1;                                        1920
    TT[1,NL]←THL[1,NL]×(1-2×K4)+THL[1,NL-1]×(K4-K3/(GA×P1))+                   1930
    THL[1,NL]×(K4+K3/(GA×P1))+(THL[1,NL]-THL[1,V])×K3×(P6+P7);                 1940
    UR←  UX      (1-R*3/((DIA×Y/2)+R)*3)×12                                    1950
                                        +RR×R*2/((DIA×Y/2)+R)*2;               1960
    IF (UR-UC)<0 THEN V←NL ELSE V←NL-1;                                        1970
    TT[IM,NL]←THL[IM,NL]×(1-2×K4)+THL[IM,NL-1]×(K4-K3/(GA×P1))+THL             1980
   [IM,NL]×(K4+K3/(GA×P1))+(THL[IM,NL]-THL[IM,V])×K3×(P6-P7);                  1990
    FOR J←2 STEP 1 UNTIL NL-1 DO                                               2000
    BEGIN                                                                      2010
         Y←(J-1/2)×DY ;                                                        2020
         P1←1+Y/GA;                                                            2030
         P2←P1*2;                                                              2040
         P3←P1×P2 ;                                                            2050
         P6← GAD×(1-1/P2);                                                     2060
         P7←PE×(1-1/P3)/2;                                                     2070
    UR← -UX      (1-R*3/((DIA×Y/2)+R)*3)×12                                    2080
                                        +RR×R*2/((DIA×Y/2)+R)*2;               2090
IF (UR-UC)<0 THEN BEGIN S←J+1;V←J END ELSE BEGIN S←J;V←J-1 END;                 2100
         TT[1,J]←THL[1,J]×(1-2×K4)+THL[1,J+1]×(K4+K3/(GA×P1))                  2110
         +THL[1,J-1]×(K4-K3/(GA×P1))+(THL[1,S]-THL[1,V])×K3×(P6+P7)            2120
         ;                                                                     2130
    UR←  UX      (1-R*3/((DIA×Y/2)+R)*3)×12                                    2140
                                        +RR×R*2/((DIA×Y/2)+R)*2;               2150
IF (UR-UC)<0 THEN BEGIN S←J+1;V←J END ELSE BEGIN S←J;V←J-1 END;                 2160
         TT[IM,J]←THL[IM,J]×(1-2×K4)+THL[IM,J+1]×(K4+K3/(GA×P1))               2170
         +THL[IM,J-1]×(K4-K3/(GA×P1))+(THL[IM,S]-THL[IM,V])                    2180
         ×K3×(P6-P7);                                                          2190
    END;                                                                       2200
    FOR I←2 STEP 1 UNTIL IM-1 DO                                               2210
    BEGIN                                                                      2220
    MU←-1+(I-1  )×DMU;                                                         2230
         Y←DY/2;                                                               2240
         P1←1+Y/GA;                                                            2250
         P2←P1*2;                                                              2260
         P3←P2×P1;                                                             2270
         P4←GA*2×P2;                                                           2280
         P5←(1+1/(2×P3))×PE/(2×GA×P1);                                         2290
         P6← GAD×(1-1/P2);                                                     2300
         P7←PE×(1-1/P3)/2;                                                     2310
         P10←1-MU*2;                                                           2320
    UR←  UX  MU×(1-R*3/((DIA×Y/2)+R)*3)×12                                     2330
                                        +RR×R*2/((DIA×Y/2)+R)*2;               2340
IF (UR-UC)<0 THEN S←2 ELSE S←1;                                                2350
         TT[I,1]←THL[I,1]×(1-2×K4-2×K2×P10/P4-P5×P10×K1)                       2360
                 +THL[I+1,1]×(K2×P10/P4-K1×MU/P4)                              2370
      +THL[I-1,1]×(P5×P10×K1+K2×P10/P4+K1×MU/P4)+THL[I,2]×(K4+K3/(             2380
    GA×P1))+THL[I,1]×(K4-K3/(GA×P1))                                           2390
     +(THL[I,S]-THL[I,1])×K3×(P6-MU×P7)+QTF×QOUT[I]×DT/R*2;                    2400
         Y←(NL-1/2)×DY;                                                        2410
    UR←  UX  MU×(1-R*3/((DIA×Y/2)+R)*3)×12                                     2420
                                        +RR×R*2/((DIA×Y/2)+R)*2;               2430
    IF (UR-UC)<0 THEN V←NL ELSE V←NL-1;                                        2440
         P1←1+Y/GA;                                                            2450
         P2←P1*2;                                                              2460
         P3←P2×P1;                                                             2470
         P4←GA*2×P2;                                                           2480
         P5←(1+1/(2×P3))×PE/(2×GA×P1);                                         2490
         P6← GAD×(1-1/P2);                                                     2500
         P7←PE×(1-1/P3)/2;                                                     2510
         TT[I,NL]←THL[I,NL]×(1-2×K4-2×K2×P10/P4-P5×P10×K1)                     2520
                 +THL[I+1,NL]×(K2×P10/P4-K1×MU/P4)                             2530
    +THL[I,NL]×(K4+K3/(GA×P1))                                                 2540
      +THL[I-1,NL]×(P10×P5×K1+K2×P10/P4+K1×MU/P4)                              2550
                 +THL[I,NL-1]×(K4-K3/(  GA×P1))+ (THL[I,NL]-THL[I,V]           2560
```

```
     )×K3×(P6-MU×P7)};                                                    2570
     END};                                                                2580
     FOR J←2 STEP 1 UNTIL NL-1 DO                                         2590
     BEGIN                                                                2600
          Y←(J-1/2)×DY;                                                   2610
          P1←1+Y/GA;                                                      2620
          P2←P1×P1;                                                       2630
          P3←P2×P1;                                                       2640
          P4←GA*2×P2;                                                     2650
          P5←(1+1/(2×P3))×PE/(2×GA×P1);                                   2660
          P6← GAD×(1-1/P2);                                               2670
          P7←PE×(1-1/P3)/2;                                               2680
          FOR I←2 STEP 1 UNTIL IM-1 DO                                    2690
          BEGIN                                                           2700
     MU←-1+(I-1  )×DMU;                                                   2710
               P10←1-MU*2;                                                2720
     UR←  Ux  MU×(1-R*3/((DIA×Y/2)+R)*3)×12                               2730
                                        +RR×R*2/((DIA×Y/2)+R)*2};         2740
IF (UR-UC)<0 THEN BEGIN S←J+1;V←J END ELSE BEGIN S←J;V←J-1 END;           2750
               TT[I,J]←THL[I,J]×(1-2×K4-2×K2×P10/P4-P5×P10×K1)            2760
                      +THL[I-1,J]×(MU×K1/P4+P10×K2/P4+P5×P10×K1)          2770
                      +THL[I+1,J]×(K2×P10/P4-MU×K1/P4)                    2780
                      +THL[I,J+1]×(K4+K3/(GA×P1))                         2790
                      +THL[I,J-1]×(K4-K3/(GA×P1))                         2800
                     +(THL[I,S]-THL[I,V])×K3×(P6-MU×P7);                  2810
          END                                                             2820
      END;                                                                2830
     END;                                                                 2840
     R←RNEW;                                                              2850
     RR←RRNEW;                                                            2860
     RRR←RRRNEW;                                                          2870
     BVOL← 4× 3.14159265 ×((R/12)*3)/3;                                   2880
     BM←IBM;                                                              2890
     RHOV←BM/BVOL;                                                        2900
     PG← PSA0 + PSA1× RHOV +PSA2×RHOV*2 + PSA3×RHOV*3                     2910
         + PSA4×RHOV*4;                                                   2920
     G←BM;                                                                2930
     FOR I←1 STEP 1 UNTIL IM DO                                           2940
     BEGIN                                                                2950
          TL[I]←TT[I,1]×(TSAT-TBL)+TBL  ;                                 2960
          FOR J←1 STEP 1 UNTIL NL DO                                      2970
               THL[I,J]←TT[I,J]  ;                                        2980
     END;                                                                 2990
     V←0;                                                                 3000
     IF NL<100 THEN                                                       3010
     FOR I←1 STEP 1 UNTIL IM DO IF THL[I,NL]≥0.001  THEN V←1;             3020
     NL←NL+V;                                                             3030
     TT  ←TI    +  DTR ;                                                  3040
     QTOT←QTOT+QOT×DTR   /3600000000;                                     3050
     MTOT←MTOT+MOT×DTR  /3600000000;                                      3060
     WRITE(FL6,FMOU1,LISTOU1);                                            3070
     RHOV←(BM+BM-H)/BVOL;                                                 3080
     IF (TIME(2)     )/60>1700 THEN                                       3090
     BEGIN                                                                3100
     FOR I←1 ,IM/2-,5,IM DO                                               3110
     BEGIN                                                                3120
          FOR J←1 STEP 1 UNTIL NL DO                                      3130
               WRITE(FL6,FMOU2,LISTOU2)                                   3140
     END;                                                                 3150
     FOR J←1 STEP 1 UNTIL IM DO WRITE(FL6,FMOU22,LISTOU22);               3160
     WRITE(TAPE2,*,L1                    );                               3170
```

```
        WRITE(TAPE2,101,RHOEL[*]          );                          3180
        WRITE(TAPE2,101,MOUT[*]           );                          3190
        WRITE(TAPE2,101,QOUT[*]           );                          3200
        WRITE(TAPE2,101,TL[*]             );                          3210
        WRITE(TAPE2,101,HOLD[*]           );                          3220
        WRITE(TAPE2,101,HIG[*]            );                          3230
        FOR J←0 STEP 1 UNTIL 30 DO WRITE(TAPE2,101,THL[J,*]);         3240
        FOR J←0 STEP 1 UNTIL 30 DO WRITE(TAPE2,101,TT[J,*1);          3250
        LOCK(TAPE2,SAVE);                                             3260
        GO TO LAD;                                                    3270
        END;                                                          3280
        IF ABS(TI-2.0)<DTR THEN GO TO LAA;                            3290
        IF ABS(TI-8.0)<DTR THEN GO TO LAA;                            3300
        IF ABS(TI  -100)<DTR/2    THEN GO TO LAA;                     3310
        GO TO LAB;                                                    3320
LAA:    FOR I←1 ,IM/2-.5,IM DO                                        3330
        BEGIN                                                         3340
             FOR J←1 STEP 1 UNTIL NL DO                               3350
                  WRITE(FL6,FMOU2,LISTOU2)                            3360
        END;                                                          3370
        FOR J←1 STEP 1 UNTIL IM DO WRITE(FL6,FMOU22,LISTOU22);        3380
LAB:    IF TI   >500 OR  R<RIN THEN GO TO LAD;                        3390
        GO TO LAC;                                                    3400
LAD:                    END.                                          3410
```

```
          SAMPLE DATA FOR EXPERIMENTAL MODEL
18,62.4,.99,3.00,0,00521523,-.000150218,1.8677@-6,-9.51383@-9,
3.49736@-11,-.407283,387.365,557.6267,-2134.4521,3635.4166,1016.69115,
-1652.18326,13500.555,-69648.146,146296.29,
      20.6,228,.0130,230,1.69, 80,.375,.1,.00075,25.5,
13,40,
```

```
%                          BUBBLE DYNAMICS IN REAL BOILING                    10
% INPUT NUMBERS ****                                                         20
%   M          MOLECULAR WEIGHT OF FLUID                                     30
%   RHOP       DENSITY OF PLATE MATERIAL   LB/FT*3                           40
%   RHOL       DENSITY OF LIQUID        LB/FT*3                              50
%   KP         THERMAL CONDUCTIVITY OF PLATE   BTU/HR FT F                   60
%   KL         THERMAL CONDUCTIVITY OF LIQUID   BTU/HR FT F                  70
%   SPHEP      SPECIFIC HEAT PLATE MATL   BTU/LB F                           80
%   SPHEL      SPECIFIC HEAT LIQUID      BTU/LB F                            90
%   ALPHAP     THERMAL DIFFUSIVITY OF PLATE MATL   FT*2/HR                  100
%   ALPHAL     EFFECTIVE  THERMAL DIFFUSIVITY OF   FT*2/HR                  110
%   PINF       PRESSURE NEAR THE BUBBLE SITE    PSIA                       120
%   TSAT       SATURATION TEMPERATURE AT PINF  F                           130
%   RIN        INITIAL RADIUS  INCHES                                      140
%   TINV       INITIAL STEAM TEMPERATURE      F                            150
%   TDROP      LOWEST VALUE FOR PLATE TEMPERATURE  F                       160
%   Q          HEAT GENERATION RATE  BTU/HR FT*3                           170
%   Z          THICKNESS OF HEATING PLATE INCHES                           180
%   TBL        TEMP OF LIQ IN WHICH BUBBLE GROWS  F                        190
%   DELTAIN    INITIAL  THICKNESS OF THIN LIQUID FILM  INCHES              200
%   DIA        HYDRAULIC  RADIUS OF CHANNEL INCHES                         210
%   RM         MAXIMUM RADIUS  ON PLATE SURFACE CONSIDERED                 220
%   DTR        INITIAL TIME INCREMENT                                      230
%   DY         INCREMENT IN Y DIRECTION                                    240
%   NL         MAX  J  IN LIQUID                                           250
%   NP         MAX  J  IN Z DIRECTION                                      260
%   NR         MAX  I  IN R DIRECTION ON PLATE SURFACE                     270
%      RHO0 TO RHO4 ARE  CONSTANTS IN 5 DEGREE POLYNOMIAL FOR SATURATION   280
%      VAPOR DENSITY AS A FUNCTION OF TEMPERATURE                          290
%      PSA0 TO PSA4  ARE CONSTANTS IN 5 DEGREE POLYNOMIAL FOR SATURATIO    300
%      PRESSURE AS FUNCTION OF VAPOR DENSITY                               310
%      LSA0 TO LSA4 ARE CONSTANTS IN 5 DEGREE POLYNOMIAL FOR LATENT HEAT   320
%      AS FUNCTION OF VAPOR DENSITY                                        330
%                                                                          340
%                                                                          350
% OUTPUT NUMBERS ****                                                      360
%   RM         BUBBLE MASS  LB                                             370
%   PG         BUBBLE PRESSURE  PSIA                                       380
%   R          BUBBLE RADIUS INCHES                                        390
%   TL[1]      LIQUID SURFACE TEMPERATURE  F                               400
%   RHOV       BUBBLE VAPOR DENSITY  LB/FT*3                               410
%   TP[1]      PLATE TEMPERATURE AT BUBBLE CENTER   F                      420
%   TIME(3)    RELATED TO I/O TIME                                         430
%   TIME(2)    RELATED TO PROCESSOR TIME                                   440
%   DELTA[1]   THIN LIQUID FILM THICKNESS AT BUBBLE CENTER  INCHES         450
%   QTOT       AMOUNT OF HEAT REMOVED FROM PLATE   BTU                     460
%   TI         TIME MMICROSECONDS                                          470
%   THE ABOVE NUMBERS APPEAR IN 11 COLUMNS LEFT TO RIGHT                   480
%   ALSO AT VARIOUS TIMES THE FOLLOWING APPEARS IN A SINGLE COLUMN         490
%                      TL[J]    TEMP DISTRIBUTION IN LIQUID                500
%                      THP[1,J]  DIMENSIONLESS TEMP DIFFERENCE IN PLATE   510
%                      TP[J]     PLATE SURFACE TEMP DISTRIBUTION           520
%                      DELTA[J]  THICKNESS OF THIN LIQUID FILM             530
%*******                                                                   540
%  CARD NUMBER            IS  IN AND NUMBER          IS OUT FOR FIRST      550
%  RUN TO MAKE FIRST TAPE AND REVERSE FOR SUCCESIVE RUNS                   560
%************                                                             570
     BEGIN                                                                580
         REAL MIN,MOUT,M,RHOV,LL,R,QIN,QOUT,RNEW,RR,DZ,  RRR,RRRNEW,DTR,  590
         COMMENT ROBIN T;                                                 600
         PG,PINF,RHOL,BVOL,BM,GA,GAD,DU,DDU,DT,DY,DDD,DD,KU,QP,RHOEL,    610
```

```
RHO0,RHO1,RHO2,RHO3,RHO4,PSA0,PSA1,PSA2,PSA3,PSA4,LSA0,LSA1,
LSA2,LSA3,LSA4,RIN,TBL,TINV,TDROP,ALPHAL,ALPHAP,KP,KL,RHOP,
SPHEP,SPHEL,DIA,      QTOT,DELTAIN ,TI   ,QTF,Z,PGIN,RHOVIN,
RA,DR,RHO,KUA,RM,MTOT,    CAN,    IRHOV,
A1,A2,A3,B1,B2,B3,C1,C2,C3,DTO,     A4,B4,
Q,TSAT,BMIN,QPP,RRNEW,IBM;
INTEGER N,J,NL,NP,S,V,I,K,CON,NR,NUZ ,RNU,ZNU                    ;
SAVE ARRAY TP,TL,THL,AAA,MP,D   ,RHOEP,DELTA,DEOU,QINP[0:100];
 SAVE ARRAY THP,DS[0:50,0:50];
LABEL LAA,LAB,LAC,LAD,LAE    ,LAF,LAG;
FILE IN FLA (1,10);
FILE OUT FLB 6(2,15);
FORMAT FMI1(E12.5),
       FMI2(I6      ),
       FMOU1(E10.3,10(X1,E10.3)),
       FMOU2(E10.3);

FILE  TAPEA "TRA" (2,110),
      TAPER "TRA" (2,110,SAVE 30);
INTEGER TIM;
LIST L1(
     MIN,MOUT,M,RHOV,LL,R,QIN,QOUT,RNEW,RR,DZ,  RRR,RRRNEW,DTR,
PG,PINF,RHOL,RVOL,RM,GA,GAD,DU,DOU,DT,DY,DDO,OD,KU,QP,RHOEL,
RHO0,RHO1,RHO2,RHO3,RHO4,PSA0,PSA1,PSA2,PSA3,PSA4,LSA0,LSA1,
LSA2,LSA3,LSA4,RIN,TBL,TINV,TDROP,ALPHAL,ALPHAP,KP,KL,RHOP,
SPHEP,SPHEL,DIA,      QTOT,DELTAIN ,TI   ,QTF,Z,PGIN,RHOVIN,
RA,DR,RHO,KUA,RM,MTOT,    CAN,    IRHOV,
A1,A2,A3,B1,B2,B3,C1,C2,C3,DTO,     A4,B4,
Q,TSAT,BMIN,QPP,RRNEW,IBM,
        N,J,NL,NP,S,V,I,K,CON,NR,NUZ,RNU,ZNU       )         ;
LIST L2(DTR);
LIST LISTI1(M,RHOP,RHOL,KP,KL,SPHEP,SPHEL,ALPHAP,ALPHAL,
             RHO0,RHO1,RHO2,RHO3,RHO4,PSA0,PSA1,PSA2,PSA3,
             PSA4,LSA0,LSA1,LSA2,LSA3,LSA4,
             PINF,TSAT,RIN,TINV,TDROP,Q              ,Z,TBL,
             DELTAIN,DIA,          RM ,
             DTR,DY),
     LISTI2(NL,NP,NR)   ,
 LISTOU1(BM,PG,R,TL[1],RHOV  ,TP[1],     TIME(3)  ,TIME(2),
   DELTA[1], QTOT,TI  ),
LISTOU22(FOR J←1 STEP 1 UNTIL NR DO TP[J], FOR J←1 STEP 1 UNTIL
NR DO DELTA[J]),
     LISTOU2(FOR J←1 STEP 1 UNTIL NL DO TL[J],FOR J←1 STEP 1
             UNTIL NP DO THP[1,J]);
GO TO LAG;   %IN SUCCESSIVE RUNS
READ(FLA,/,LISTI1);  READ(FLA,/,LISTI2);
CLOSE(FLA,RELEASE);
 WRITE(FLB,FMT1,LISTI1); WRITE(FLB,FMI2,LISTI2);
WRITE(FLB [PAGE]);
FOR J←0 STEP 1 UNTIL 100 DO
     TP[J]←TL[J]←D[J]←AAA[J]←MP[J]←QINP[J]←RHOEP[J]←DELTA[J]
     ←DEOU[J]←THL[J]←D[J]←0;
 FOR K←1 STEP 1 UNTIL 50 DO TP[K]←TINV;
 FOR I←1 STEP 1 UNTIL 50 DO
 FOR J←1 STEP 1 UNTIL 50 DO   BEGIN
 THP[I,J]←0;     DS[I,J]←0     END       ;
TL[1]←TINV ;THL[1]←(TL[1]-TBL)/(TSAT-TBL);
 RRR←0;
 R←RIN;
 RNU←NR;    ZNU←NP;
 J←1;
```

```
          RHOV     ←RH00+RH01×TP[J] +RH02×TP[J]*2 +RH03×TP[J]*3          1240
          +RH04×TP[J]*4;                                                 1250
        IRHOV←RHOV;                                                      1260
        PG← PSA0 + PSA1 × RHOV +PSA2×RHOV*2 + PSA3× RHOV* 3+PSA4×RHOV    1270
            *4 ;                                                         1280
        RR←(SQRT(((PG  -PINF)× 32.2 × 288 )/(RH0L×3)))×12;               1290
        BVOL←2×3.14159265×((R/12)*3)/3;                                  1300
        BM←RHOV×BVOL;                                                    1310
        B1←BM;                                                           1320
        DZ←1/NP        ;                                                 1330
        DR←1/NR;                                                         1340
        QP←Q×(DIA/24)*2/(RH0P×SPHEP×ALPHAL×(TDROP-TINV));                1350
        QPP←(DIA*2)/(48×Z×DZ×RHOP×SPHEP×ALPHAL×(TDROP-TINV));            1360
        QTF←  3×DIA/(  3.14159265×DY×RH0L×SPHEL×ALPHAL×(TSAT-TBL));     1370
        TI  ←0;                                                          1380
        QTOT←0;                                                          1390
        FOR J←1 STEP 1 UNTIL 50 DO DELTA[J]←DELTAIN;                     1400
        FOR J←1 STEP 1 UNTIL 50 DO AAA[J]←1;                             1410
        NP←NL←NR←3;                                                      1420
        GO TO LAC;  % IN FIRST RUN BEFORE 100                            1430
LAG:    READ (TAPEA,*,L1                )!                               1440
        READ (TAPEA,101,TP[*]           )!                               1450
        READ (TAPEA,101,TL[*]           )!                               1460
        READ (TAPEA,101,THL[*]          )!                               1470
        READ (TAPEA,101,AAA[*]          )!                               1480
        READ (TAPEA,101,MP[*]           )!                               1490
        READ (TAPEA,101,D[*]            )!                               1500
        READ (TAPEA,101,RHOEP[*]        )!                               1510
        READ (TAPEA,101,DELTA[*]        )!                               1520
        READ (TAPEA,101,DEDV[*]         )!                               1530
        READ (TAPEA,101,QINP[*]         )!                               1540
       FOR J←0 STEP 1 UNTIL 50 DO READ (TAPEA,51,THP[J,*1)!              1550
       FOR J←0 STEP 1 UNTIL 50 DO READ (TAPEA,51, DS[J,*1)!              1560
        LOCK (TAPEA,RELEASE)!                                            1570
        GO TO LAA;                                                       1580
LAC:    FOR J←1 STEP 1 UNTIL NR DO IF DELTA[J]≤0 THEN AAA[J]←0;          1590
        DTR←R;                                                           1600
        FOR J←CON+1 STEP 1 UNTIL NR DO MP[J]←QINP[J]←0;                  1610
        CON←ENTIER(R/(DR×RM))+1;                                         1620
        DT←ALPHAL×DTR×16/((DIA*2)×100000000);                            1630
        FOR J←1 STEP 1 UNTIL CON DO                                      1640
        BEGIN                                                            1650
          RHOEP[J]←RH00+RH01×TP[J] +RH02×TP[J]*2 +RH03×TP[J]*3          1660
          +RH04×TP[J]*4;                                                 1670
          MP[J]←SQRT(49690×(TP[J]+459.69)/(M×2×3.14159265))×(            1680
         RHOEP[J]-IRHOV)×3600×AAA[J];                                    1690
          LL←LSA0+LSA1×RHOEP[J] +LSA2×RHOEP[J]*2 +LSA3×RHOEP[J]*3        1700
          +LSA4×RHOEP[J]*4;                                              1710
          QINP[J]←MP[J]×LL;                                              1720
        END;                                                             1730
        CAN←CON-1;                                                       1740
        QINP[CON]←QINP[CON]×(R*2-(CAN×DR×RM)*2)/((CON*2-CAN*2)×(DR×RM)*  1750
      2);                                                                1760
        MP[CON]←MP[CON]×(R*2-(CAN×DR×RM)*2)/((CON*2-CAN*2)×(DR×RM)*2);   1770
        MIN←0;                                                           1780
        QIN←0;                                                           1790
        FOR J←1 STEP 1 UNTIL CON DO                                      1800
        BEGIN                                                            1810
          MIN←MIN+MP[J]×  3.14159265×((J×DR)*2-((J-1)×DR)*2)×RM*2        1820
        /144;                                                            1830
          QIN←QIN+QINP[J]×  3.14159265×((J×DR)*2-((J-1)×DR)*2)×RM*2      1840
        /144;                                                            1850
```

```
        END;                                                                    1860
        RHOEL←RHO0+RHO1×TL[1]  +RHO2×(TL[1]*2)+                                 1870
              RHO3×(TL[1]*3)+ RHO4×(TL[1]*4) ;                                  1880
        MOUT←  SQRT(  49690×(TL[1]+459.69)/(M×2×3.14159265))×                   1890
              (IRHOV-RHOEL)× 2×3.14159265×(R/12)*2 ×3600 ;                      1900
        LL←LSA0+ LSA1×IRHOV + LSA2×IRHOV*2 + LSA3×IRHOV*3+                      1910
           LSA4×IRHOV*4 ;                                                       1920
        QOUT←MOUT ×LL ;                                                         1930
        RNEW←R+RR× DTR /1000000  + RRR ×(DTR/1000000)*2/2 ;                     1940
      IRM← BM +(MIN-MOUT)×DTR / 3600000000 ;                                    1950
        RRNEW ←RR + RRR × DTR /1000000 ;                                        1960
        RRRNEW ←((( PG-PINF)× 667160     /RHOL)-3× (RR*2)/2 )/R;                1970
        B2←(IRM+B1)/2;                                                          1980
      IRHOV← B2/(2×3.14159265×((RNEW/12)*3)/3);                                 1990
        IF ABS(RM/B2-1)>0.0001 THEN BEGIN BM← B2;GO TO LAC END;                 2000
        FOR J←1 STEP 1 UNTIL CON-1 DO                                           2010
        BEGIN                                                                   2020
             DEQU[J]←MP[J]×DTR/(3600000000×RHOL);                               2030
             DELTA[J]←DELTA[J]-DEQU[J]                                          2040
        END;                                                                    2050
        DEQU[CON]←MP[CON]×DTR/(3600000000×RHOL);                                2060
        DELTA[CON]←DELTA[CON]-DEQU[CON];                                        2070
BEGIN                                                                           2080
      INTEGER XXXXX;                                                            2090
        GA←2×R/DIA ;                                                            2100
        GAD← RR×DIA×15/(ALPHAL×288) ;  GAD←GAD×3600/15  ;                       2110
        DD← DT/(DY*2) ;                                                         2120
        DDD←  DT/DY   ;                                                         2130
        IF GAD≥0 THEN S←2 ELSE S←1 ;                                            2140
        D[1]←              THL[1]×(1-2×DD)+QTF×QOUT ×DT/R*2+                    2150
        THL[2]×(DD+DDD/(GA+DY/2))+THL[1]×(DD-DDD/(GA+DY/2))+                    2160
        GAD×(1-1/((1+DY/(2×GA))*2))×DDD×(THL[S]-THL[1]);                        2170
        IF GAD≥0 THEN V←NL ELSE V←NL-1;                                         2180
        D[NL]←THL[NL]×(1-2×DD)+  THL[NL-1]×(DD-DDD/(GA+(NL-0.5)×DY))            2190
        +THL[NL]×(DD+DDD/(GA+(NL-0.5)×DY))+GAD×(1-1/((1+(NL-0.5)×DY/            2200
     GA)*2))×DDD×(THL[NL]-THL[V]);                                              2210
        FOR J←2  STEP 1  UNTIL  NL-1  DO                                        2220
        BEGIN                                                                   2230
            IF GAD≥0 THEN BEGIN S←J+1; V←J END ELSE BEGIN S←J;V←J-1             2240
        END ;                                                                   2250
             DU← GAD ×(1-1/((1 +(J× DY-DY/2) /GA) *2))  ×(DDD  );               2260
             DDU← DDD/(1×  (GA +(J× DY-DY/2)))  ;                               2270
             D[J]← THL[J-1] ×(    DD  -DDU) + THL[J] × (1-2×DD)                 2280
                   +THL[J+1] × (    DD  +DDU)+DU×(THL[S]-THL[V])                2290
        END;                                                                    2300
        FOR J←NL   STEP -1 UNTIL 1 DO                                           2310
        THL[J]←D[J]  ;                                                          2320
        IF NL< 99 THEN                                                          2330
        IF THL[NL]≥0.001 THEN NL←NL+1;                                          2340
KU←DT×DIA     *2 ×ALPHAP   /(4×(Z*2)×ALPHAL×DZ*2);                              2350
        KUA←DT×DIA*2×ALPHAP/(4×RM*2×ALPHAL×DR*2);                               2360
        FOR J←1 STEP 1 UNTIL NP DO BEGIN THP[0,J]←THP[1,J];                     2370
        THP[NR+1,J]←THP[NR,J]  END;                                             2380
        FOR I ← 1 STEP 1 UNTIL NR DO BEGIN THP[I,0]←THP[I,1];                   2390
        THP[I,NP+1]←THP[I,NP] END;                                              2400
        FOR J←2 STEP 1 UNTIL NP DO                                              2410
        FOR I←1 STEP 1 UNTIL NR DO                                              2420
        DS[I,J]←THP[I,J]×(1-KUA×2-KU×2)+THP[I+1,J]×(KUA+KUA/(2×(I-1/2))        2430
        ))+THP[I-1,J]×(KUA-KUA/(2×(I-1/2)))+THP[I,J+1]×(KU)+THP[I,J-1]          2440
        ×KU+QP×DT;                                                              2450
        J←1;                                                                    2460
        FOR I←1 STEP 1 UNTIL NR DO                                              2470
```

```
      DS[I,J]←THP[I,J]×(1-KUA×2-KU×2)+THP[I+1,J]×(KUA+KUA/(2×(I-1/2)
      ))+THP[I-1,J]×(KUA-KUA/(2×(I-1/2)))+THP[I,J+1]×(KU)+THP[I,J-1]
      ×KU+QP×DT  - QINP[I]×DT×QPP;                                        2500
END;                                                                      2510
      R←RNEW;                                                             2520
      RR←RRNEW;                                                           2530
      RRR←RRRNEW;                                                         2540
      BM←IBM     ;                                                        2550
      B1←BM;                                                              2560
      BVOL←2×3.14159265×((R/12)*3)/3;                                     2570
      RHOV←IRHOV;                                                         2580
      PG← PSA0 + PSA1 × RHOV +PSA2×RHOV*2 + PSA3× RHOV* 3+PSA4×RHOV       2590
          *4 ;                                                            2600
      FOR J←1 STEP 1 UNTIL NP DO                                          2610
      FOR I←1 STEP 1 UNTIL NR DO                                          2620
      THP[I,J]←DS[I,J] ;                                                  2630
      NUZ←0;                                                              2640
      IF NP<ZNU THEN BEGIN                                                2650
      FOR I←1 STEP 1 UNTIL NR DO IF THP[I,NP]≥0.001 THEN NUZ←1;           2660
      IF NUZ=1 THEN FOR I←1 STEP 1 UNTIL NR DO THP[I,NP+1]←0;             2670
      NP←NP+NUZ;                                                          2680
      END;                                                                2690
      V←0;                                                                2700
      IF NR<RNU THEN BEGIN                                                2710
      FOR J←1 STEP 1 UNTIL NP DO IF THP[NR,J]≥0.001 THEN V←1;             2720
      IF V=1 THEN FOR J←1 STEP 1 UNTIL NP DO THP[NR+1,J]←0;               2730
      NR←NR+V;                                                            2740
      END;                                                                2750
      TI  ← TI   +DTR  ;                                                  2760
      QTOT← QTOT + QIN ×DTR/3600000000   ;                                2770
      MTOT←MTOT+MIN×DTR/3600000000;                                       2780
      FOR J←1 STEP 1 UNTIL NR DO                                          2790
    TP[J]←THP[J,1]×(TDROP-TINV)+TINV;                                     2800
      TL[1]←THL[1]× (TSAT- TBL)  + TBL ;                                  2810
      WRITE(FLB,FMOU1,LISTOU1);                                           2820
      IRHOV←(BM+BM-B2)/BVOL;                                              2830
      IF ABS(TI  -.001)<DTR/2 THEN GO TO LAA;                             2840
      IF ABS(TI  -050)<DTR/2  THEN GO TO LAA;                             2850
      IF ABS(TI  -100)<DTR/2  THEN GO TO LAA;                             2860
      IF ABS(TI  -2.7)<DTR    THEN GO TO LAA;                             2870
      IF ABS(TI  -10 )<DTR    THEN GO TO LAA;                             2880
      IF ABS(TI  -200)<DTR/2  THEN GO TO LAA;                             2890
      IF ABS(TI  -300)<DTR/2  THEN GO TO LAA;                             2900
      IF ABS(TI  -500)<DTR/2  THEN GO TO LAA;                             2910
      IF ABS(TI  -800)<DTR/2  THEN GO TO LAA;                             2920
      IF (TIME(2)    )/60>800 THEN                                        2930
      BEGIN                                                               2940
      FOR J←2 STEP 1 UNTIL NL DO                                          2950
      TL[J]← THL[J]×(TSAT-TBL) +TBL ;                                     2960
      WRITE(FLB,FMOU2,LISTOU2);                                           2970
      WRITE(FLB,FMOU2,LISTOU22);                                          2980
     WRITE (TAPEB,*,L1                 );                                 2990
     WRITE (TAPEB,101,TP[*]            );                                 3000
     WRITE (TAPEB,101,TL[*]            );                                 3010
     WRITE (TAPEB,101,THL[*]           );                                 3020
     WRITE (TAPEB,101,AAA[*]           );                                 3030
     WRITE (TAPEB,101,MP[*]            );                                 3040
     WRITE (TAPEB,101,O[*]             );                                 3050
     WRITE (TAPEB,101,RHOEP[*]         );                                 3060
     WRITE (TAPEB,101,DELTA[*]         );                                 3070
     WRITE (TAPEB,101,DEOU[*]          );                                 3080
     WRITE (TAPEB,101,QINP[*]          );                                 3090
```

```
        FOR J←0 STEP 1 UNTIL 50 DO WRITE (TAPE8,51,THP[J,*1)};                3100
        FOR J←0 STEP 1 UNTIL 50 DO WRITE (TAPE8,51, DS[J,*1)};                3110
         LOCK (TAPE8,SAVE)};                                                  3120
         GO TO LAD;                                                           3130
         END};                                                                3140
         GO TO LAB};                                                          3150
LAA:     FOR J←2 STEP 1 UNTIL NL DO                                           3160
         TL[J]← THL[J]×(TSAT-TBL) +TBL ;                                      3170
         WRITE(FLB,FMOU2,LISTOU2)};                                           3180
         WRITE(FLB,FMOU2,LISTOU22)};                                          3190
LAB:     IF II   > 1000  OR  R < RIN  THEN  GO TO LAD;                        3200
         GO TO LAC ;                                                          3210
LAD:                        END.                                              3220
```

```
          SAMPLE DATA FUR REAL BOILING MODEL
18.0,487,62.4,25.0,0.38,0.113,0.994,0.452,.087,0.005215232,-1.502183@-04,
1.8676965@-06,-0.9513834@-08,3.4973606@-11,-.407283,387.365,557.6267,-2134.4521,
3635.4166,1016.69115,-1652.18326,13500.555,-69648.146,146296.29,
14.15,212,0.001,287,212,4.389,0.004,122,
                                        3.5@-4,0.167,0.0500,.01,.00100,
50,10,50,
```

APPENDIX D

SAMPLE CALCULATION USING RUN NO. 5

Power into Steam Generator

$$V = 29.59 \pm 0.1\% \text{ volts}$$

$$I = [2.58 \text{ mv} \pm (0.1\% + 25\ \mu\text{volts})][3\ \frac{\text{amps}}{\text{millivolts}} \pm 1\%]$$

$$= 7.74 \pm 2.1\% \text{ amps}$$

$$P_{IN} = 229.03 \pm 2.2\% \text{ watts}$$

$$= 229.03 \pm 5.00 \text{ watts}$$

Heat Loss from Steam Generator

The voltage output of the steam generator was 6.050 ± 0.002 millivolts. From Figure 85, the temperature was 141 ± 2°C and the room temperature was 22.0°C ± 0.5°C. Therefore, $T_{GEN} - T_R = 119 \pm 2.5$°C. Thus, from Figure 16, page 66, the maximum heat loss was 50.5 ± 1.0 watts and the minimum was 37.5 ± 1.0 watts. Therefore, the average heat loss was (50.5 + 37.5) ÷ 2 = 44.0 watts in a possible range of 50.5 + 1 to 37.5 - 1 or the error was ± (51.5 - 36.5) ÷ 2 = 7.5 watts. Thus, the heat loss was 44.0 ± 7.5 watts.

Energy Associated with Steam Flow

The energy associated with the steam was equal to the power in minus the heat loss:

$$Q_{IN} = (229.03 \pm 5.00 \text{ watts}) - (44.0 \pm 7.5 \text{ watts})$$

$$= 185.03 \pm 3 \text{ watts} = 631.51 \pm 46.00 \text{ BTU/hr} = 631.51 \pm 7.3\%$$

Bubble Frequency

A plot of the bubble area (as magnified) versus frame number for this run is shown in Figure 83. The time associated with one bubble seems to vary from bubble to bubble. Some amount of variation was certainly expected; however, one point should be mentioned. The bubble frequency for these runs was in the range of 4000 bubbles per second while the framing rate was about 8000 frames per second. Thus, the change in area of the observed bubble from frame to frame depended on whether the bubble rate and the framing rate were "in phase" or "out of phase." This terminology is illustrated in Figure 84. It is believed that this effect is observed in Figure 83. In any case, using a high value for the number of bubbles per second yields a low value for the amount of heat associated with one bubble; this tends to minimize the mass transfer effect. Therefore, the conservative value (which is also thought to be the most accurate value) for the bubble frequency will be the one calculated on the basis of the shortest observed bubble lifetime. In this case, it is two times the time interval between frames.

Now the framing rate is

$$\frac{130 \text{ frames}}{1/60 \text{ sec}} = 7800 \text{ frames/sec}$$

or the time between frames is

$$\frac{1}{7800} = 1.28 \times 10^{-4} \text{ sec} = 128 \ \mu\text{sec}$$

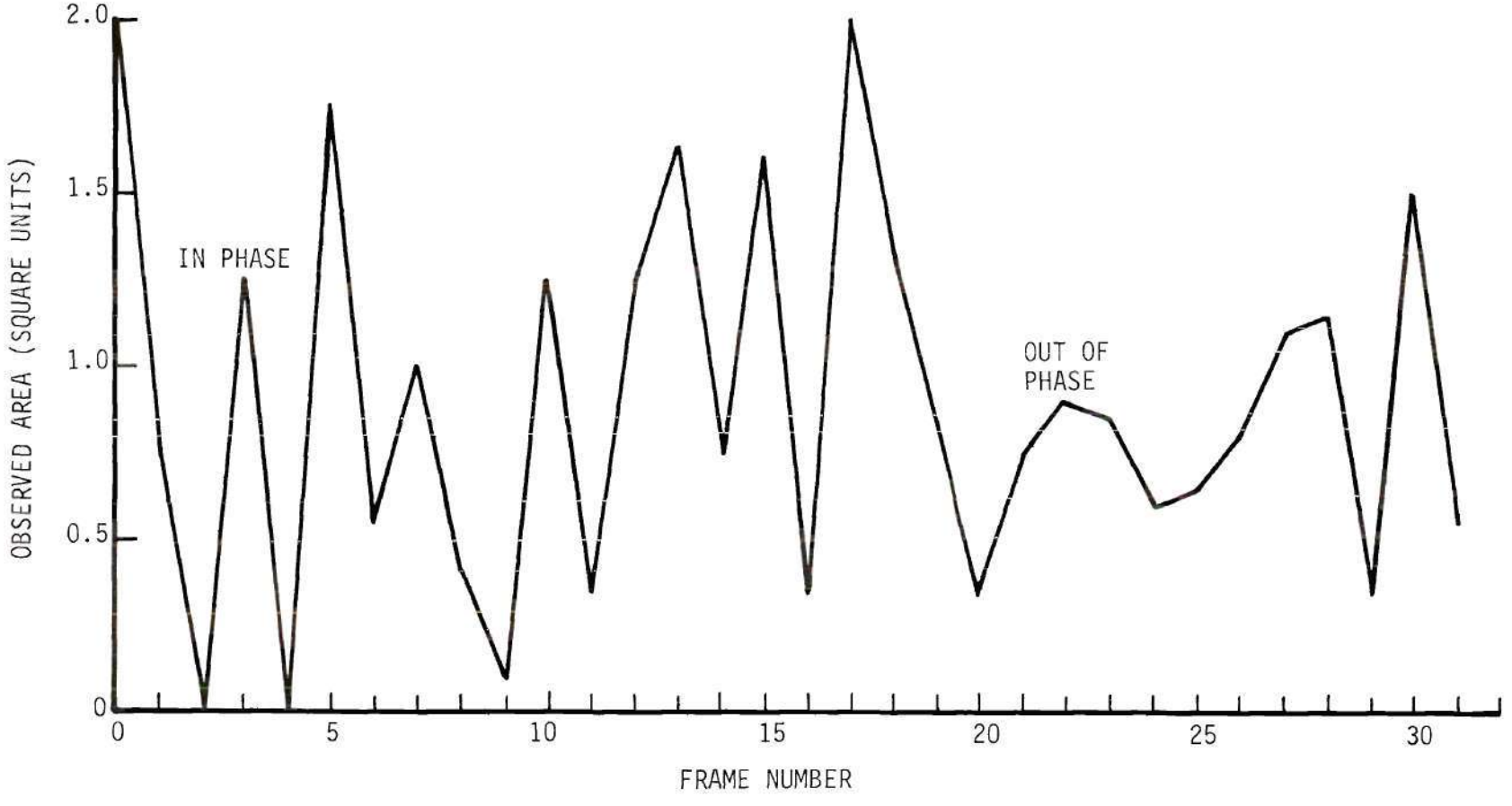

Figure 83. Observed Bubble Area (1 Unit = 0.108 Inch) Versus Frame Number for Run No. 5.

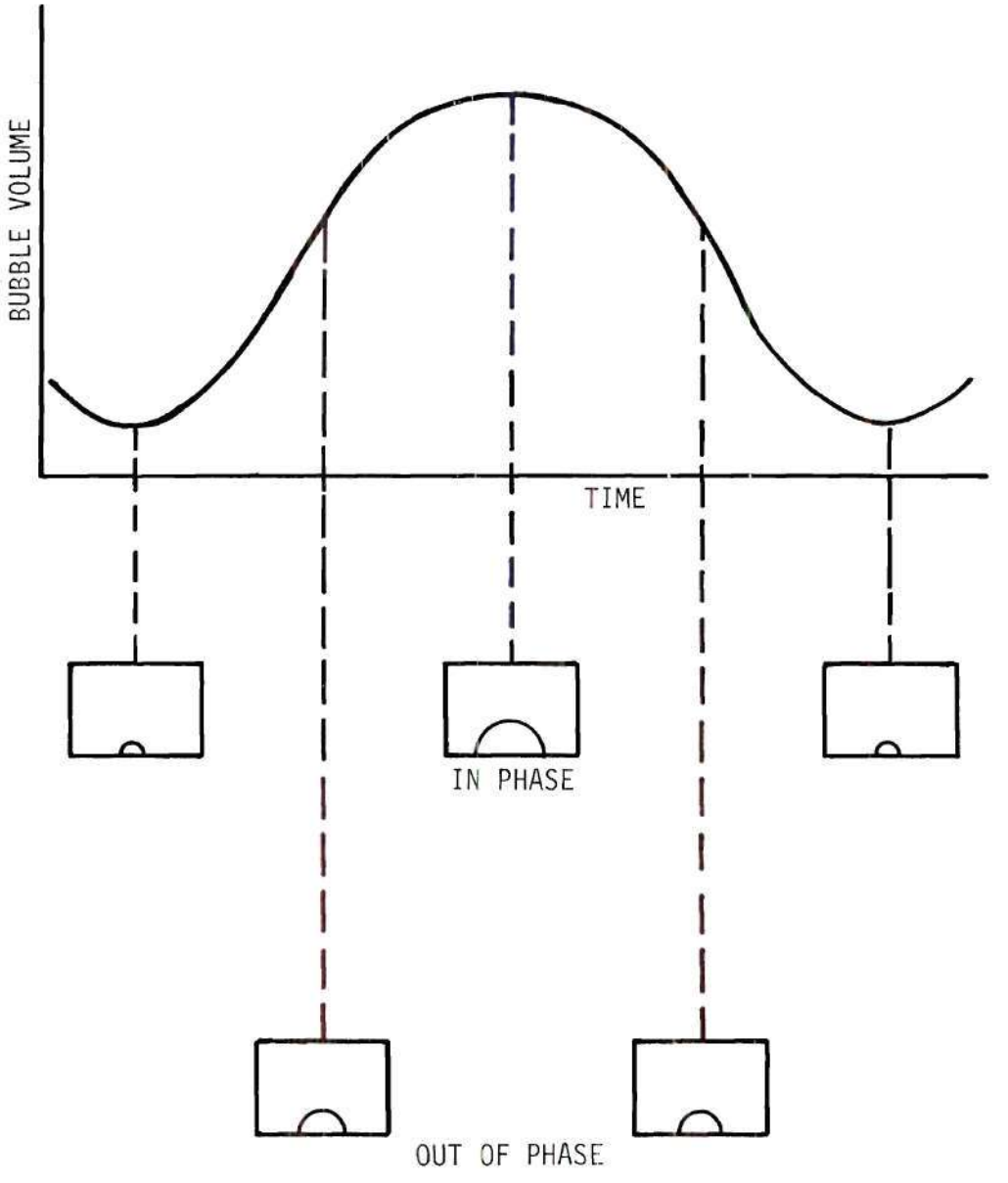

Figure 84. Phase Relation Between Bubbles Per Second and Frames Per Second.

Thus, the bubble lifetime is $2 \times 128 = 256$ μsec. Also, since the time during which the Fastax camera accepts light on one frame is

$$\frac{1}{3 \text{ (frames/sec)}} = 42.6 \text{ μsec}$$

and, since two frames were observed in determining the bubble lifetime, the error in bubble lifetime is ± 43 μsec. Now the bubble frequency is

$$\frac{1}{256 \pm 43 \text{ μsec}} = \frac{1}{256 \pm 17\%} = 3906 \pm 17\% \text{ bubble/sec}$$

Energy per Bubble

The amount of energy associated with one bubble is equal to the energy rate associated with the steam flow divided by the bubbles per second.

$$H_b = \frac{(631.51 \pm 7.3\%) \text{ BTU/hr}}{(3906 \pm 17\%) \text{ bubbles/sec}} \left(\frac{1 \text{ hr}}{3600 \text{ sec}} \right) = 4.49 \times 10^{-5} \pm 25\% \text{ BTU/bubbles}$$

$$= 4.49 \times 10^{-5} \pm 1.03 \times 10^{-5} \frac{\text{BTU}}{\text{bubble}}$$

Maximum Bubble Radius

The bubble radius was obtained by first projecting the film onto a sheet of graph paper. In each frame a marker (made of stainless steel and placed in the stream close to the bubble) was visible and its dimension was known. Thus, linear distance could be determined by comparison with the

marker.

Approximately 100 frames were observed and for those with large size bubbles present, the outline of the bubble was traced on a sheet of paper. The area was then determined using a planimeter. Using the largest area obtained, an equivalent radius was calculated assuming the bubble to be in the shape of a hemisphere. For this case, the largest area was 3.2 square units, thus

$$R_b = \sqrt{\frac{2}{\pi} 3.2} = 1.415 \text{ units}$$

and since 7.6 units represented 0.108 inch,

$$R_b = .0201 \text{ inch} = 0.00168 \text{ foot}$$

Bubble Volume

$$\text{Vol} = \frac{2}{3} \pi R_b^3 = \frac{2}{3} \pi (0.00168)^3 \text{ ft}^3 = 0.985 \times 10^{-8} \text{ ft}^3$$

The error in the volume of steam was estimated to be of the order of ± 10 percent. The main source of error was due to the necessary assumption about the dimension of the bubble in the direction perpendicular to the cross section obtained from the photograph.

Heat per Bubble (One Volume of Vapor)

The energy associated with the latent heat of vaporization of a volume of vapor equal to the maximum bubble volume may be calculated once

the thermodynamic state of the vapor is known. Rohsenow and Clark (31) suggested that the vapor state within the bubble is at a saturation condition corresponding to the pressure of the liquid.

The pressure indicated by gauge A was 8.6 psi ± 0.5 psi and that by gauge B was 3.0 psi ± 0.5 psi. Thus, from the calibration curve (Figure 87) the true pressures were 8.1 ± 0.5 psi for gauge A and 3.0 ± 0.5 psi for gauge B. Assuming the pressure drop from A to B to be linear, the pressure at the bubble site may be calculated

$$P_S = P_A - \frac{(\text{distance from A to site})}{(\text{distance from A to B})} (P_A - P_B)$$

$$= 8.1 \pm 0.5 - \frac{16.5 \pm 1\%}{18.0 \pm 1\%} (4.1 \pm 24\%)$$

$$= (8.1 \pm 0.5) - (3.8 \pm 1.0)$$

$$= 4.34 \pm 1.50 \text{ psi}$$

Since the atmospheric pressure was 74.36 cm Hg or 14.35 psia ± 0.01 psia, the absolute pressure at the site was 18.7 ± 1.5 psia. Using linear interpolation in the steam tables, the corresponding specific volume was found to be 21.41 ft^3/lb and the heat of vaporization was 962.4 BTU/lb. Now the heat per bubble is

$$H_b' = (962.4 \text{ BTU/lb})(0.985 \times 10^{-8} \text{ ft}^3)/(21.41 \text{ ft}^3/\text{lb})$$

$$= 4.43 \times 10^{-7} \text{ BTU}$$

An upper bound to this value may be obtained by using a pressure of 21 psia and a volume of 0.985×10^{-8} ft^3 + 10% or 1.08×10^{-8} ft^3. This yields a heat per bubble of 5.63×10^{-7} BTU. The lower bound may be obtained by using a pressure of 17 psia and a volume of 1.985×10^{-8} ft^3 - 10% or 0.887×10^{-8} ft^3. This yields an energy per bubble of 3.67×10^{-7} BTU. Thus, the maximum error is ± 29%. Therefore,

$$H_b' = 4.43 \times 10^{-7} \pm 1.30 \times 10^{-7} \text{ BTU}$$

Bubble Heat Transfer Coefficient

The bubble heat transfer coefficient is defined as the energy associated with the steam flow in BTU/hr divided by the maximum surface area of the bubble and the difference between the saturation temperature and the liquid inlet temperature.

$$h_b = \frac{Q_{IN} \text{ (BTU/hr)}}{2\pi \, (R_b/12)^2 \text{ ft}^2 \, (T_{SAT} - T_{IN}) \text{ °F}}$$

For this case, the energy rate was 631.5 ± 7.3% BTU/hr. The area was $2\pi \, (0.020/12)^2 = 1.76 \times 10^{-5}$ ft^2 and the error in this number was estimated to be of the order of ± 10% which was largely due to the irregular surface shape. Since the pressure in the system was 18.7 ± 1.5 psia, the saturation temperature was calculated by linear interpolation in the steam tables to be 224.39 °F. Using an upper limit of 22.5 psia on the pressure, the upper saturation temperature limit was 231.75 °F and, using a lower limit of 17.0 psia, the lower temperature was 219.44 °F. Thus,

the maximum deviation was 7.36 °F and the saturation temperature was 224.40 ± 7.4 °F. Since the liquid temperature was 110.0 °F ± 2.5 °F, the subcooling was 114.39 °F ± 9.9 °F or 114.39 °F ± 8.62%. Thus

$$h_b = \frac{631.5 \text{ BTU/hr} \pm 7.3\%}{[(1.76 \times 10^{-5} \text{ ft}^2) \pm 10\%][114.39 \text{ °F} \pm 8.6\%]}$$

$$= (3.14 \times 10^5) \frac{\text{BTU}}{\text{hr ft}^2 \text{ °F}} \pm 26\%$$

$\underline{Q_{IN}/A_b}$

$$Q_{IN}/A_b = \frac{631.5 \text{ BTU/hr} \pm 7.3\%}{1.76 \times 10^{-5} \text{ ft}^2 \pm 10\%} = 3.59 \times 10^7 \frac{\text{BTU}}{\text{hr ft}^2} \pm 17\%$$

$$= 69.25 \text{ BTU/in}^2 \text{ sec} \pm 17\%$$

$\underline{[U/0.2]^{\frac{1}{2}} \Delta T_{sub}}$

This number was used by Gunther (15) to correlate his burnout data. The significance of the velocity divided by 0.2 is that this corresponds to an effective steam velocity. Gunther observed that the bubbles moved upstream while attached to the plate with a velocity of 0.8 times the main stream velocity. Thus, the relative velocity between the bubble surface and the main stream was 0.2 times the main stream velocity. In this experiment, the relative velocity was equal to the main stream velocity, since the bubble base was attached to the hole in the heated plate. Thus, U/0.2 corresponds to an effective main stream

velocity.

Thus, since DP = 4.0 ± 0.1, the velocity was 25.5 ft/sec. For DP = 4.1, U = 26 ft/sec and for DP = 3.9, U = 25.0 ft/sec. Thus, U = 25.5 ft/sec ± 2%. Now

$$\left[\frac{U}{0.2}\right]^{\frac{1}{2}}\Delta T_{sub} = \left[\frac{25.5 \pm 2\%}{0.2}\right]^{\frac{1}{2}}[114.39\ ^{\circ}F \pm 8.6\%]$$

$$= 1.28 \times 10^{3}\ (ft/sec)^{\frac{1}{2}}\ ^{\circ}F \pm 11\%$$

APPENDIX E

DETAILS OF EXPERIMENTAL EQUIPMENT

Pump

A centrifugal Goulds' pump was provided for the loop. It was a single stage pump and was close-coupled. The construction was all bronze and the motor was three phase, five horsepower. The impeller diameter was 6-3/8 inches. The model number was 3655 - 1-1/4 x 1-1/2 - 7.

Storage and Distilling Tanks

These tanks were obtained from a Scanlan-Morris Sterilizer unit, Model A410E. Each contained a thermometer and a resistance heater (7.5 kw). The one selected for the storage tank had a copper cooling coil. This one had to be provided with three extra pipe inlets and outlets connecting the flow system.

Filter

A Pall Trinity Filter was provided for the loop and could remove 98 percent of the particles of 10 microns diameter and 100 percent of the particles of 30 microns diameter. The model number was MCS-1001 EE 16 and it had a stainless steel housing.

Heat Exchanger

An American-Standard "BCF" heat exchanger was obtained for the loop. The model number was 503D5 and it had bronze bonnets.

Ion Exchanger

An Illco-Way research model ion exchanger was used on the fill line

of the flow system.

DC Power Supply

The DC power supply consisted of a combination of a modified Christie electric Model A28-1000T24 DC power supply and a General Radio W50 adjustable autotransformer.

The Christie unit was modified by:*

1. Lines 22A and 22B were disconnected from L1; lines 25A and 25B were disconnected from L2. A single phase 208 volt line was connected to the terminal board at 23 and 24.

2. The fuse was removed from the control rectifier power supply.

3. The fan motor was removed and the mounting was reconstructed to accommodate a single phase 115 volt motor which was mounted and connected to an outside single phase 115 volt line.

4. The three-phase Variac was connected to L1, L2, and L3. The W50 Variac had a maximum power rating of 20 kw and this was the maximum power for the combination. This system had a voltage ripple of 12 percent peak to peak.

Pressure Gauges

Two types were used. The first was an aluminum test gauge with an accuracy of 1/2 of one percent and had an 8-1/2 inch diameter face. This was Model AC 10812 with a range of 0 to 100 psi. The second was Model AC 10712 with a range of 0 to 100 psi and with a 3-1/2 inch diameter face. Both were made by the Crosby Valve and Gage Company.

---

*Nomenclature refers to the wiring diagram on the unit.

Flow Meter

A Meriam Model 30ED25, type H, indicating flow meter was used. This consisted of a 13 inch manometer and stainless steel orifice flanges and orifice plates.

Potentiometer

A model 8686 Leeds and Northrup millivolt potentiometer was used.

Thermocouples

The thermocouple indicating bulk fluid temperature was a Conax K-T1 chromel-alumel thermocouple. The thermocouple assembly for the steam generator consisted of copper-constantan thermocouple wires passing through a T6-20-2 Conax transducer gland.

Oxygen Meter

The oxygen meter was made by the Yellow Springs Instrument Company. Its designation was YSI Model 51 and had an accuracy of ± 0.25 parts per million.

Differential Voltmeter

This unit was a Model 823A AC/DC differential voltmeter made by the John Fluke Manufacturing Company, Inc. For alternating current, its accuracy was ± 0.1 percent + 25 microvolts for voltages from 0.001 to 0.5 volt. For direct current, the accuracy was ± 0.01 percent in the range 0.5 to 500 volts and ± 0.01 percent + 10 microvolts for voltages below 0.5 volt.

Current Shunts

Three precision Weston shunts were used. The one used for measuring current to the heated strip was rated at 50 millivolts for 2000 amperes. The one used for calibrating the heated strip was rated at 50 millivolts

for one ampere; for the steam generator, 50 millivolts for 150 amperes.

High Speed Motion Picture Equipment

A 16 millimeter Fastax Camera was used. The number of frames per second was controlled by a Model J-515 (Goose) control unit made by Industrial Timer Corporation. The Lens was a 152 millimeter Bell and Howell, used with a bellows extension and shot at f/11. The light was provided by Sylvania ff-33 flood flash high speed flash bulbs with a 1.75 second flash duration. The film used was Dupont 931A-reversal, which was perforated for the Fastax camera. The projector used to view these films was an Industrialist (Model SFDR, W-W Photo, Inc.).

Power Regulator: Steam Generator

The power applied to the steam generator was controlled by a General Radio W20 adjustable autotransformer.

Schlieren System

The strobe light used in the schlieren system was a General Radio type No. 1530-A which produced a five microsecond flash. The camera was a 35 millimeter Nikon. The lenses were type I Kodak Aero-Ektar (306 millimeter). A razor blade was used as the knife edge.

APPENDIX F

CALIBRATION CURVES

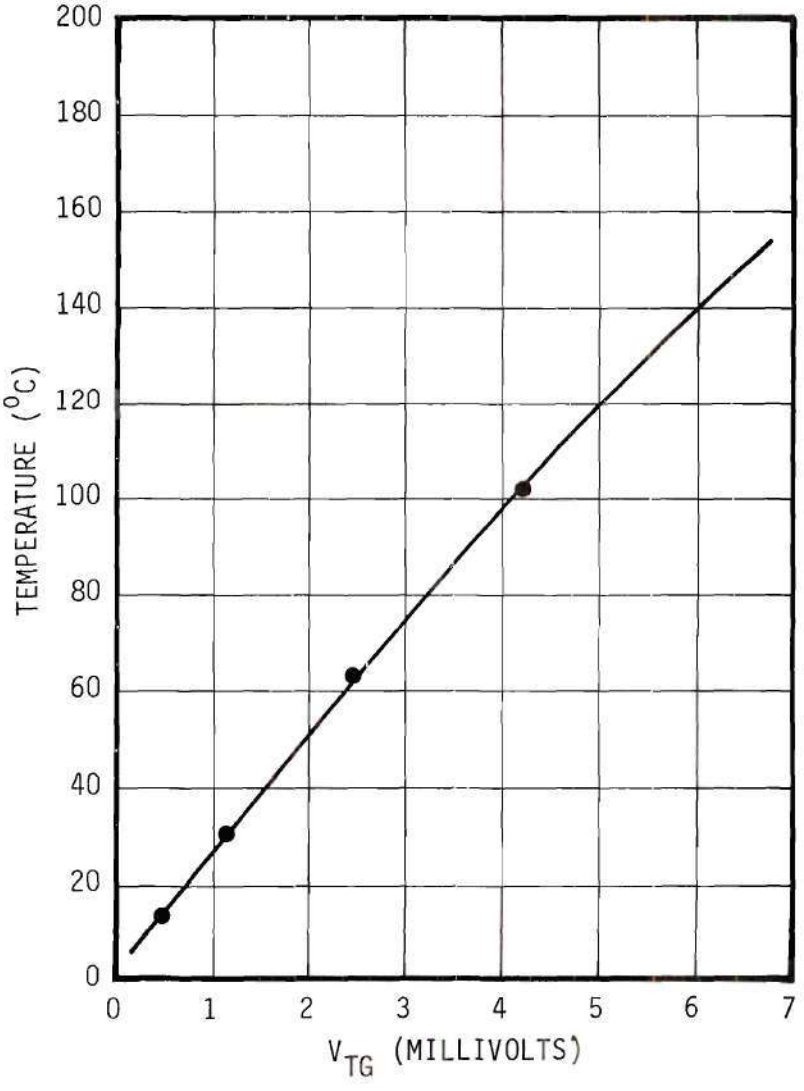

Figure 85. Steam Generator Thermocouple Calibration.

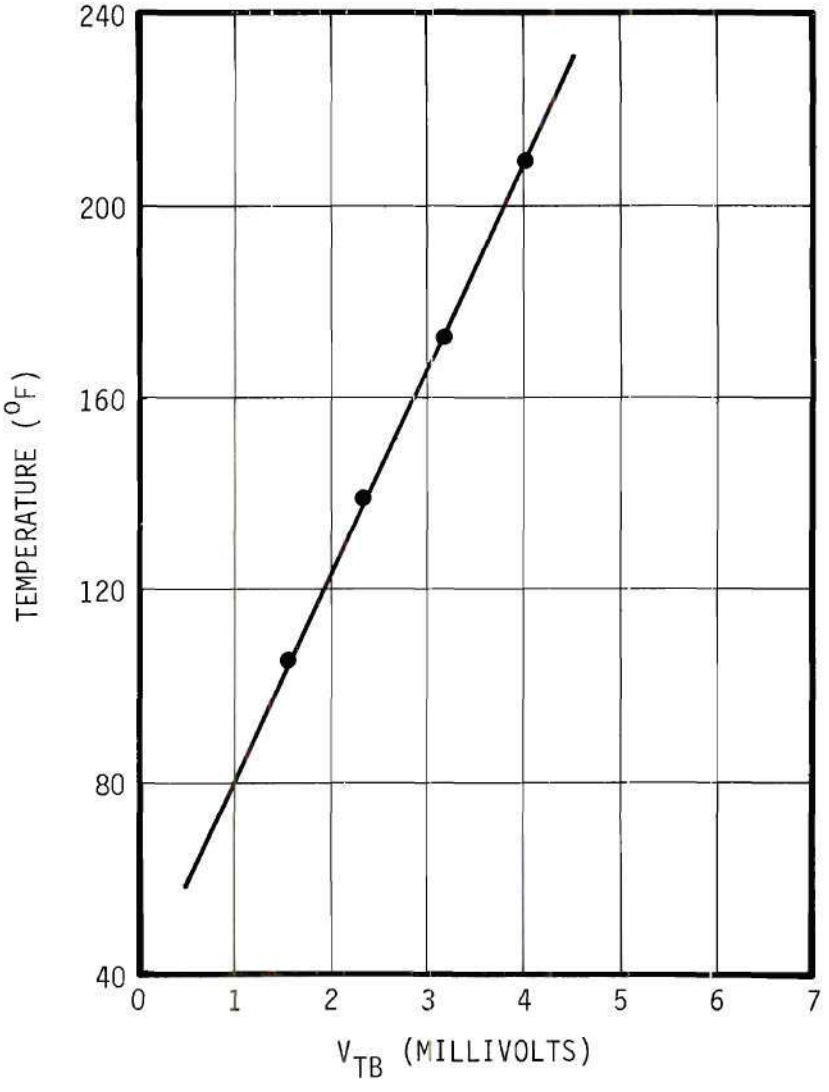

Figure 86. Fluid Bulk Thermocouple Calibration.

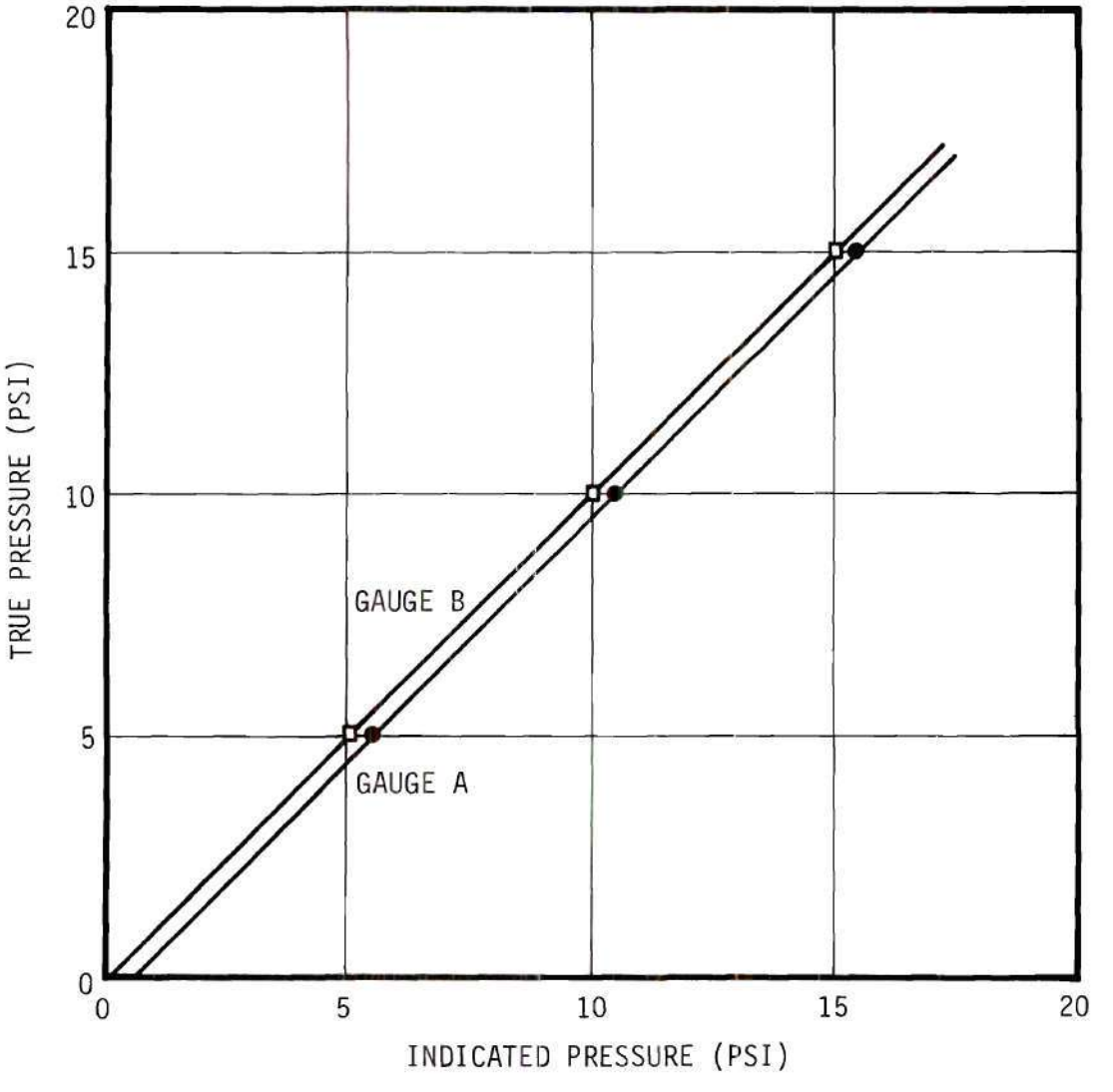

Figure 87. Pressure Gauge Calibration.

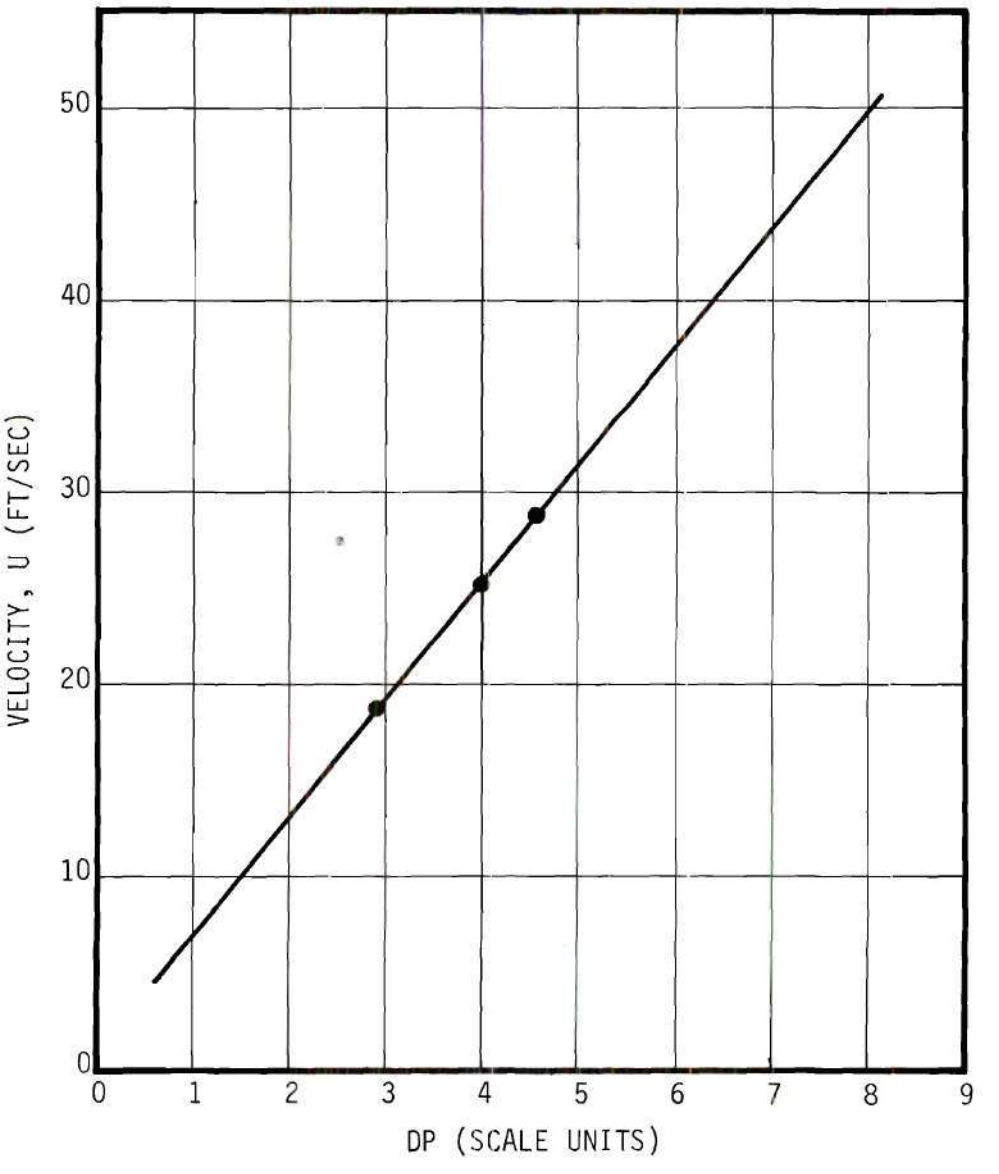

Figure 88. Flow Meter Calibration for Orifice Plate No. Y63691.

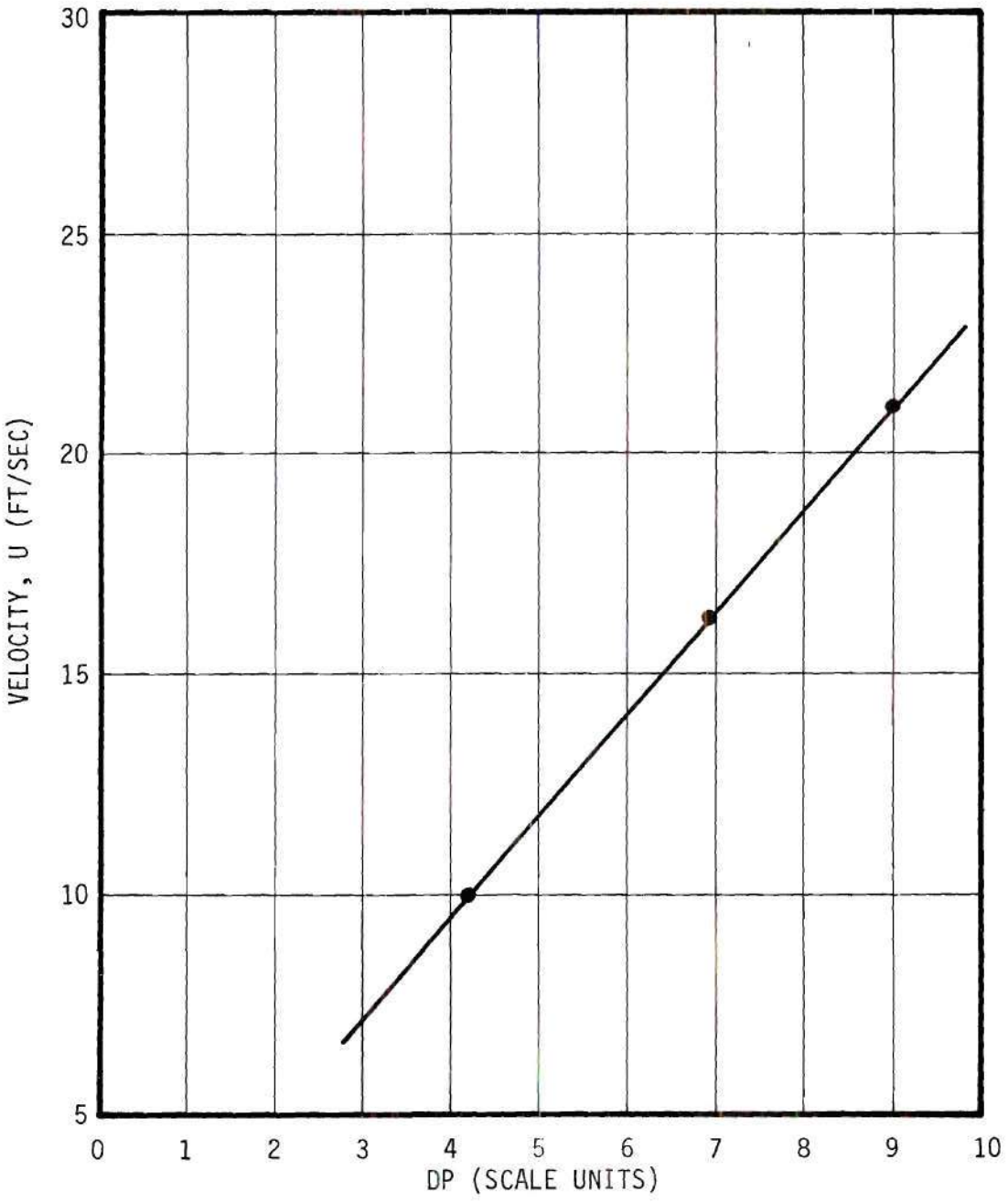

Figure 89. Flow Meter Calibration for Orifice Plate No. Y63692.

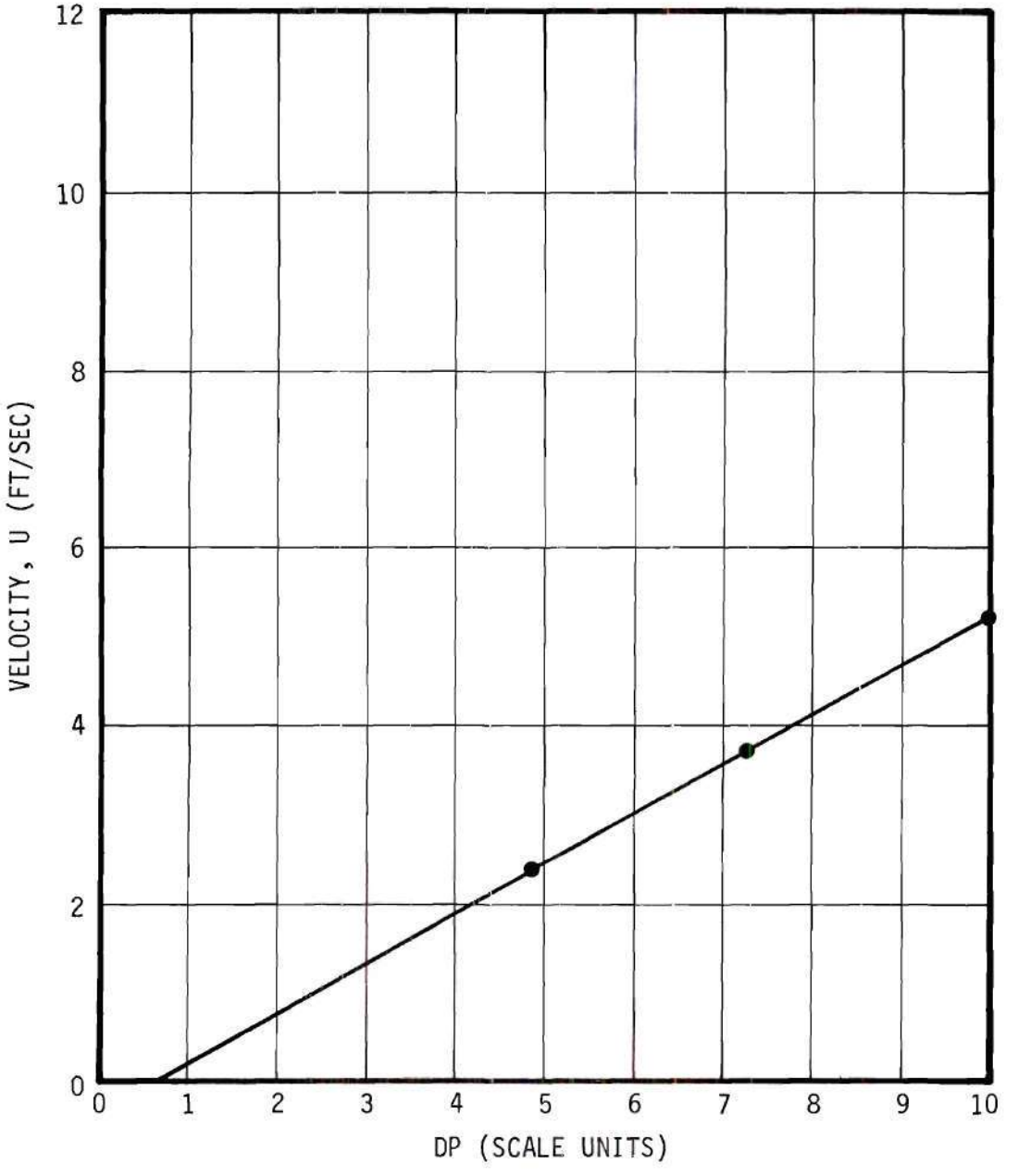

Figure 90. Flow Meter Calibration for Orifice Plate No. Y63693.

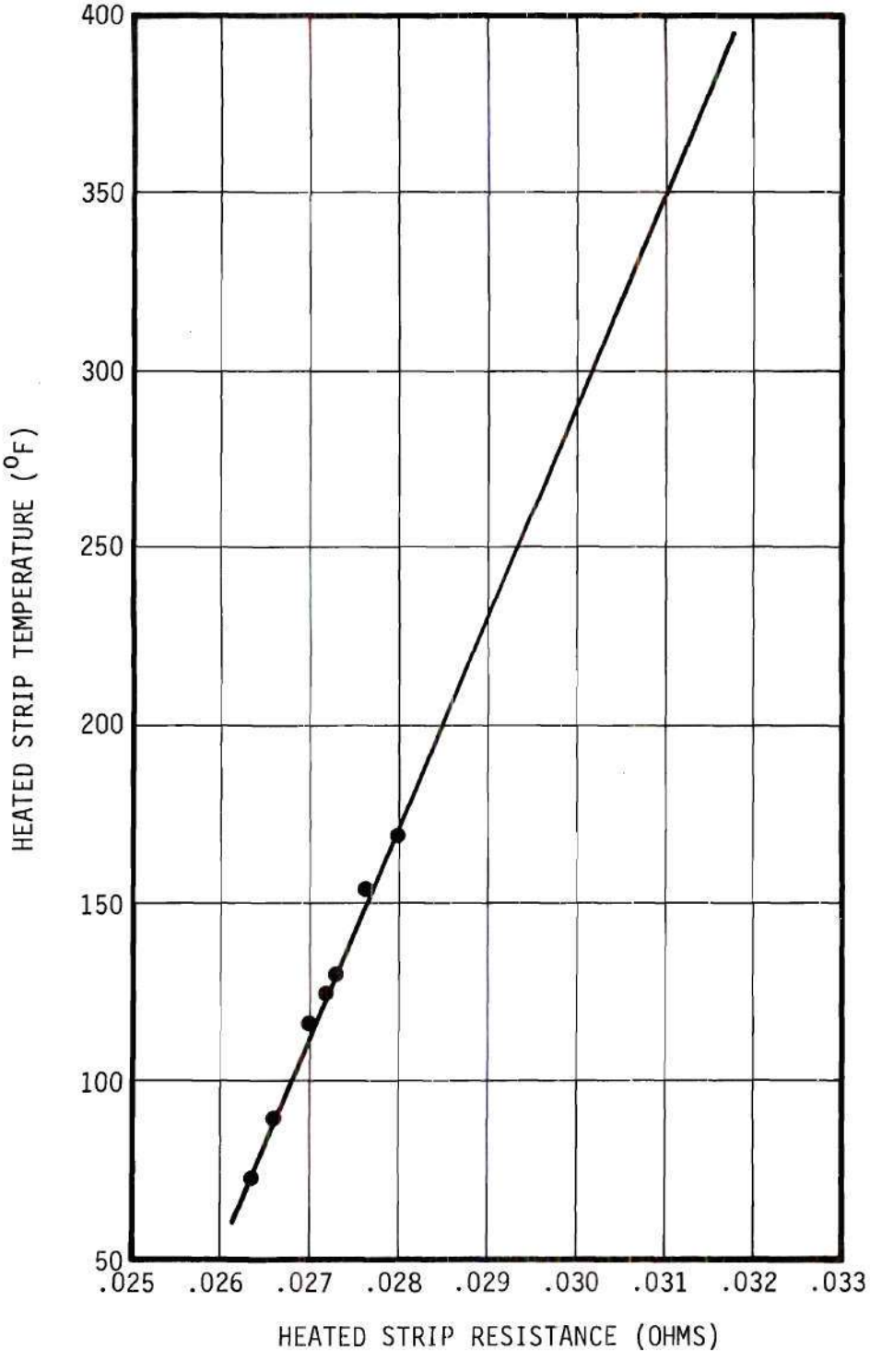

Figure 91. Heated Strip Calibration.

APPENDIX G

POSSIBLE ERRORS

Four possible errors are considered below.

(A) In the real boiling model, the temperature drop across the thin liquid film was neglected. To investigate the magnitude of this inaccuracy, consider a heat flux equal to the total heat removed from the plate divided by the product of the maximum exposed area of the thin liquid film and the bubble lifetime.

$$\frac{1.844 \times 10^{-6} \text{ BTU}}{\pi\left(\frac{0.01098}{12}\right)^2 \text{ ft}^2 \left(\frac{230}{3.6 \times 10^9}\right)\text{hr}} = 1.1 \times 10^7 \frac{\text{BTU}}{\text{hr ft}^2}$$

(These are the approximate figures for curve number 4, page 112. Thus, with an average film thickness of $1/2 \times 10^{-6}$ feet, the temperature drop would be approximately:

$$\Delta T = \frac{1.1 \times 10^7 \frac{\text{BTU}}{\text{hr ft}^2} \times \frac{1}{2} \times 10^{-6} \text{ ft}}{0.390 \frac{\text{BTU}}{\text{hr ft } ^\circ\text{F}}} = 14.1 \ ^\circ\text{F}$$

The magnitude of this number does not seem to be large enough to cause undue concern over any conclusions reached through use of the assumption in question. However, the temperature drop was not truly negligible and

thus, the magnitude of the numbers obtained in the theoretical investigation would probably shift slightly as a result of using a more precise solution to the model.

(B) A second questionable assumption was that the vapor entering the bubble in the single bubble experiment was saturated. If this vapor were wet, the droplets of water would deposit on the bubble surface; however, they would not deposit a corresponding amount of latent heat. Their presence would result in an overestimate of the amount of heat transferred to the wall by the condensation of vapor.

To determine the magnitude of this effect, consider an isentropic drop from the pressure in the steam generator to that of the cooling liquid near the bubble site. This isentropic drop would result in a six percent moisture content in the input steam. This amount of liquid would not appreciably affect the results.

Secondly, the time required for the steam to leave the exit of the hypodermic needle and enter the bubble (see Figure 9, page 53) was approximately two minutes. Thus, it seems probable that the effect of gravity would keep any small liquid droplets from entering the bubble.

(C) A third possible error in the theoretical models was the assumption that the state of the vapor in the bubble at any time was saturation corresponding to the present value of the density. As a rough check on this assumption, consider the known amount of mass added to the experimental bubble for run No. 7 as compared to the amount condensed. For the solution of the model, the mass input rate was 1.34 pounds per hour. Thus, after 130 microseconds, the mass put into the bubble was 4.85×10^{-8} pounds and the amount condensed by that time was 4.773×10^{-8}

pounds. Also, after 220 microseconds the mass input was 8.2×10^{-8} pounds while the amount condensed was 8.138×10^{-8} pounds. The agreement seems to be quite good and indicates that the simplifying assumption provides an acceptable approximation to reality.

(D) A fourth questionable point was the thickness of the mesh cell in the cooling liquid. To determine the effect of changes in Dy on the solution of the model during the initial phases of the bubble growth, a second run under the conditions of curve No. 5 of Figure 48 (see page 114) was made with Dy only half as large as the original value. Figure 92 indicates the effect of the change in Dy on the radius and the liquid surface temperature. The new radius was approximately three percent larger than the old one and the new temperature was approximately 2 °F hotter than the old temperature. These differences do not seem to be large enough to significantly change the results.

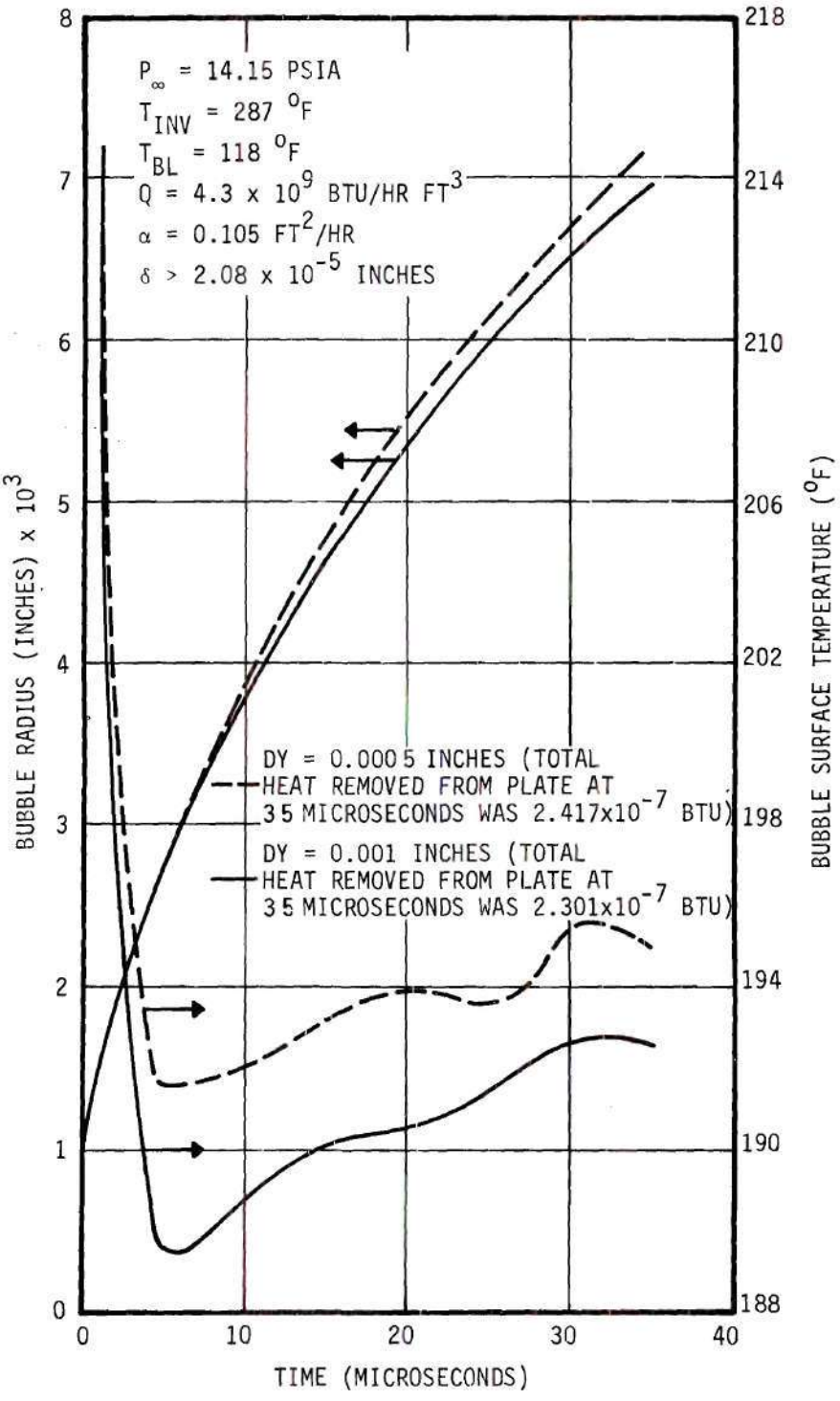

Figure 92. Effects of Dy on Bubble Radius and Bubble Surface Temperature as Functions of Time for the Real Boiling Model.

APPENDIX H

NOMENCLATURE

A_{av}	average surface area of bubble
A_b	maximum surface area of bubble
A_{cs}	observed maximum area of bubble cross section
A_{MAX}	radial distance in the plate beyond which the plate temperature was assumed unaffected by the bubble
a	radial distance in heated plate
BM	mass of vapor in bubble
C_P	specific heat of liquid
C'_P	specific heat of heated plate material
Da	increment of a
Da′	increment of a′
DIA	hydraulic diameter of channel
Dμ	increment of μ
DP	pressure drop across orifice
Dr	increment of r
Dr′	increment of r′
Dt	increment of t
Dt′	increment of t′
Dy	increment of y
Dz	increment of z
Dz′	increment of z′

f_{60} number of high speed motion picture frames taken in 1/60 second

f_b number of frames per bubble

H_b heat input to one bubble as measured

H_b' heat input to one bubble based on the observed maximum bubble volume and system pressure

h_b bubble heat transfer coefficient

IBM mass of vapor in bubble at time t + Dt

LL latent heat

M molecular weight of fluid

M_{IN} mass rate of vapor input for the single bubble case

MP mass rate of evaporation or condensation

MOT total mass output rate for the single bubble case

P_A pressure indicated by gauge A

P_{ATM} atmospheric pressure

P_B pressure indicated by gauge B

P_E Peclet number

P_{IN} power input to steam generator

P_{VAP} absolute pressure of the vapor in the bubble

P_S absolute pressure of the fluid near the bubble site

P_∞ ambient liquid pressure

Q volume heat generation rate in heater strip

Q′ volume heat generation rate associated with condensation or evaporation

Q_{IN} latent heat associated with M_{IN}

r radial distance in liquid

r′ dimensionless radial distance in liquid

R	bubble radius
R_b	maximum bubble radius
$\dot{R}$	time derivative of R
$\ddot{R}$	time derivative of $\dot{R}$
R_{GAS}	universal gas constant
R_{MAX}	a value of r beyond which the liquid temperature is assumed unaffected by the bubble
t	time
t'	dimensionless time
T	temperature
T_{BL}	initial temperature of cooling fluid near bubble
T_{DROP}	lowest temperature to which the plate drops
T_{GEN}	steam generator temperature
T_{IN}	cooling water inlet temperature
T_{INV}	initial plate temperature
T_R	room temperature
T_{SAT}	saturation temperature based on P_∞
T_{SUR}	liquid surface temperature
U	velocity of cooling stream
V_G	voltage across steam generator heater
V_{IG}	voltage across steam generator shunt
V_{IR}	voltage across heated strip shunt
V_R	voltage across heated strip
V_{TB}	voltage output of fluid bulk thermocouple
V_{TG}	voltage output of steam generator thermocouple
VOL	maximum bubble volume

$\bar{V}$ velocity vector

y dimensionless distance from bubble surface

Y_{MAX} largest value of y considered

z distance into plate (perpendicular to surface)

z' dimensionless form of z

Z thickness of heated strip

α equivalent thermal diffusivity of the liquid

α' accommodation coefficient defined as the ratio of the actual amount of condensation (or evaporation) to that predicted by kinetic theory

α_p thermal diffusivity of the heated plate material

γ dimensionless bubble radius

$\dot{\gamma}$ dimensionless derivative of γ with respect to t'

δ initial thickness of thin liquid film

ΔT_{sub} $T_{SAT} - T_{IN}$

θ bubble lifetime; angle

μ cos θ

ρ_l liquid density

ρ_p density of heated plate material

ρ_{sat} saturated vapor density at T_{SUR}

ρ_{vap} vapor density

σ surface tension

τ time

Φ dimensionless temperature difference in liquid

Φ' dimensionless temperature difference in heated plate

Ψ angle

BIBLIOGRAPHY

1. Alty, T. and Mackay, C. A., "The Accommodation Coefficient and Evaporation Coefficient of Water," Royal Society Proceedings (London), A 149, p. 104, 1935.

2. Bankoff, S. G., "On the Mechanism of Subcooled Nucleate Boiling," Jet Propulsion Laboratory Memo. 30-8, 1959.

3. Bankoff, S. G., "On the Mechanism of Subcooled Nucleate Boiling, Part I: Preliminary Considerations," Chemical Engineering Progress Symposium Series No. 32, Vol. 57, p. 156, 1961.

4. Bankoff, S. G., "On the Mechanism of Subcooled Nucleate Boiling, Part II: Sequential Rate Process Model," Chemical Engineering Progress Symposium Series No. 32, Vol. 57, p. 164, 1961.

5. Bankoff, S. G., "A Note on the Latent Heat Transport in Nucleate Boiling," American Institute of Chemical Engineers Journal, Vol. 8, No. 1, p. 63, 1962.

6. Bankoff, S. G., Colahan, W. J., Jr., and Bartz, D. R., "Summary of Conference on Bubble Dynamics and Boiling Heat Transfer Held at the Jet Propulsion Laboratory, June 14 and 15, 1956," Jet Propulsion Laboratory Memo. 20-137, 1956.

7. Bankoff, S. G. and Mason, J. P., "Heat Transfer from the Surface of a Steam Bubble in Turbulent Subcooled Liquid Stream," American Institute of Chemical Engineers Journal, Vol. 8, No. 1, p. 30, 1962.

8. Bankoff, S. G. and Mikesell, R. D., "Bubble Growth Rates in Highly Subcooled Nucleate Boiling," Chemical Engineering Progress Symposium Series No. 29, Vol. 55, p. 95, 1959.

9. Bonnet, C., Macke, E., and Molin, R., "Visualisation de L'ébullition nucléée de l'eau à pression atmosphérique et mesure simultanée des variations de température," European Atomic Energy Community--EURATOM, EUR 1622f, 1964.

10. Cichelli, M. T. and Bonilla, C. F., "Heat Transfer to Liquids Boiling Under Pressure," American Institute of Chemical Engineers, Vol. 41, pp. 755-787, 1945.

11. Dusinberre, G. M., Numerical Analysis of Heat Flow, McGraw-Hill, 1949.

BIBLIOGRAPHY (Continued)

12. Edwards, D. K., "The Role of Interphase Mass Transfer in the Mechanism of Nucleate Boiling," Masters Thesis, University of California, 1954.

13. Ellion, M. E., "A Study of the Mechanism of Boiling Heat Transfer," Jet Propulsion Laboratory Memo. 20-88, 1954.

14. Frenkel, J., Kinetic Theory of Liquids, Oxford, 1946.

15. Gunther, F. C., "Photographic Study of Surface-Boiling Heat Transfer to Water with Forced Convection," Transactions of the American Society of Mechanical Engineers, Vol. 73, No. 2, pp. 115-124, 1951.

16. Hendricks, R. C. and Sharp, R. R., "Initiation of Cooling due to Bubble Growth on a Heating Surface," NASA TN D-2290, Lewis Research Center, 1964.

17. Hickman, K. C. D., and Trevoy, D. J., "Evaporation from Liquids in High Vacuum," Chemical Engr. Prog., Vol. 49, No. 2, pp. 105-109, 1953.

18. Hickman, K., "Evaporation Coefficients of Liquids," First International Symposium on Water Desalination, SWD/27, 1965.

19. Hospeti, N. B. and Mesler, R. B., "Deposits Formed Beneath Bubbles During Nucleate Boiling of Radioactive Calcium Sulfate Solutions," American Institute of Chemical Engineers Journal, Vol. 11, No. 4, p. 662, 1965.

20. Jakob, M., "Heat Transfer in Evaporation and Condensation," Mechanical Engineering, Vol. 58, p. 643, 1936.

21. Jakob, M., Heat Transfer, Vol. I, John Wiley, New York, 1949.

22. Lamb, H., Hydrodynamics, Sixth Edition, Cambridge, p. 122, 1932.

23. McAdams, W. H., et al., "Heat Transfer at High Rates to Water with Surface Boiling," Industrial and Engineering Chemistry, Vol. 41, p. 1945, 1949.

24. Marcus, B. D., "Experiments on the Mechanism of Saturated Nucleate Pool Boiling Heat Transfer," Ph.D. Thesis, Cornell University, Ithaca, N. Y., 1963.

25. Mesler, R. B. and Banchero, J. T., "Effect of Superatmospheric Pressures on Nucleate Boiling of Organic Liquids," American Institute of Chemical Engineers Journal, Vol. 4, No. 1, p. 102, 1958.

BIBLIOGRAPHY (Concluded)

26. Moore, F. D. and Mesler, R. B., "The Measurement of Rapid Surface Temperature Fluctuations During Nucleate Boiling of Water," American Institute of Chemical Engineers Journal, Vol. 7, No. 4, p. 620, 1961.

27. Plesset, M. S., "Note on the Flow of Vapor Between Liquid Surfaces," Journal of Chemical Physics, Vol. 20, No. 5, pp. 790-793, 1952.

28. Poppendiek, H. F., "Progress Report No. 1 on Boiling Studies," Ch. 8, Department of Engineering, University of California, August, 1949.

29. Rogers, T. F. and Mesler, R. B., "An Experimental Study of Surface Cooling by Bubbles during Nucleate Boiling of Water," American Institute of Chemical Engineers Journal, Vol. 10, No. 5, p. 656, 1964.

30. Rohsenow, W. M., "Heat Transfer with Boiling," Modern Developments in Heat Transfer, edited by Ibele, W., p. 85, 1963.

31. Rohsenow, W. M. and Clark, J. A., "A Study of the Mechanism of Boiling Heat Transfer," Transactions of the American Society of Mechanical Engineers, Vol. 73, No. 5, pp. 609-620, 1951.

32. Rust, J. H. and Sesonske, A., "Turbulent Temperature Fluctuations in Mercury and Ethylene Glycol in Pipe Flow," International Journal of Heat and Mass Transfer, Vol. 9, pp. 215-227, 1966.

33. Snyder, N. W., Lecture Notes on Diffusion and Mass Transfer, University of California, 1952.

34. Snyder, N. W., Comments on pp. 13, 14, 15, 20, 21, 38, and 39 of reference 6.

35. Snyder, N. W., Personal Communication, 1966.

36. Sharp, R. R., "The Nature of Liquid Film Evaporation during Nucleate Boiling," NASA TN D-1997, Lewis Research Center, 1964.

37. Tong, L. S., Boiling Heat Transfer and Two-Phase Flow, John Wiley, New York, 1965.

38. Wittke, D. D., "Collapse of Vapor Bubbles with Translatory Motion," Ph.D. Thesis, University of Illinois, 1965.

39. Zwick, S. A., Report #21-19, Pasadena: Hydrodynamics Laboratory, California Institute of Technology, 1954.

VITA

Theodore Tydings Robin, Jr. was born in New Orleans, Louisiana, on August 29, 1939. He attended elementary school at Bay High in Bay St. Louis, Mississippi. Also, his first two years of high school were spent at Bay High. His last two years of high school were spent at Marion Military Institute in Marion, Alabama. In 1957 he entered the Georgia Institute of Technology and received the Bachelor of Mechanical Engineering degree in 1961. He completed requirements for a Master of Science in Nuclear Engineering in 1962, at which time he began work toward the Doctor of Philosophy in Nuclear Engineering.

Mr. Robin was married in 1963 to the former Helen Beatrice Jones. They have two daughters, Helen Corbin and Curry Jones.